



Laboratory-based study of viscoelastic, viscoplastic and fatigue damage of asphalt concrete

Mequanent Mulugeta Alamnie

Mequanent Mulugeta Alamnie

Laboratory-based Study of Viscoelastic,
Viscoplastic and Fatigue Damage of
Asphalt Concrete

Doctoral Dissertation for the Degree *Philosophiae Doctor (Ph.D.)*
at the Faculty of Engineering and Science, Specialisation in Engineering Sciences,
Scientific field of Civil and Structural Engineering

University of Agder
Faculty of Engineering and Science
2024

Doctoral Dissertations at the University of Agder 466
ISSN: 1504-9272
ISBN: 978-82-8427-183-5

©Mequanent Mulugeta Alamnie, 2024

Printed by Make!Graphics
Kristiansand

Preface

The work presented in this thesis was carried out at the Department of Engineering Sciences at University of Agder in Grimstad. The project received funding from the University of Agder. The work was supervised by Associate Professor Ephrem Taddesse from the Department of Engineering Sciences (UiA) and Professor Inge Hoff from the Department of Civil and Environmental Engineering (NTNU) as the main and co-supervisors, respectively. The thesis consists of a thorough background, theoretical overview and experimental approaches (chapters 1 to 3) followed by the discussion of results (chapter 4 and 5). Four of the appended papers are published in international journals and the other two papers are conference articles.

Acknowledgments

Many individuals have contributed to making the completion of this study possible in various ways. First, I would like to thank my principal supervisor, Associate Professor Ephrem Tadesse for his guidance and supporting me during these years. I also thank my co-supervisor, Professor Inge Hoff, for his guidance and facilitating the laboratory at NTNU.

I would like to convey my gratitude to Rein Terje Thorstensen, Paul R. Svennevig and Emma Elizabeth Horneman for their constant support with administrative and financial matters. My sincere gratitude also goes to Bent who greatly helped me in the laboratory work at NTNU. The lab engineers Rita and Anette at UiA also deserve special thanks for their support. I also wish to thank Dr. Rabbira Garba and Dr. Tatek Fekadu from Staten vegvesen, Dr. Milliyon Woldekidan and Dr. Abubeker Ahmed for the constructive discussions related to my research.

Many other colleagues positively contributed to my academic activities at the University of Agder. I have special thanks to fellow PhDs Solomon, Ingrid, Una, Mehrdad, and Otto. It was memorable sharing office with you and thank you for the good times.

My special thank also goes Haimanot, Tigist, Blen (and their families) for the comforting times in Agder. I am also grateful to Hana, Zewdie, Dr. Tesfaye, and Dr. Abel for their encouragement and support.

Lastly, my sincere thank and heartfelt appreciation goes out to my parents, brothers and sisters. Thank you for the love, support, prayers and continuous encouragement.

Mequanent Mulugeta Alamnie

Grimstad, Norway, 2024

Dedication

TO MY PARENTS!

Publications

- A) Alamnie, M.M.; Taddesse, E.; Hoff, I., 2022. Advances in Permanent Deformation Modeling of Asphalt Concrete—A Review. *Materials*, 15, 3480. [doi:/10.3390/ma15103480](https://doi.org/10.3390/ma15103480)
- B) Alamnie, M.M.; Taddesse, E.; Hoff, I., 2022. Thermo-piezo-rheological characterization of asphalt concrete. *Construction and Building Materials*, 329, 127106. [doi:/10.1016/j.conbuildmat.2022.127106](https://doi.org/10.1016/j.conbuildmat.2022.127106)
- C) Alamnie, M. M.; Taddesse, E.; Hoff, I., 2021. Viscoelastic characterization and comparison of Norwegian asphalt mixtures using dynamic modulus and IDT tests. *Eleventh International Conference on the Bearing Capacity of Roads, Railways and Airfields, Vol.1*. CRC Press. [doi:/10.1201/9781003222880-12](https://doi.org/10.1201/9781003222880-12)
- D) Alamnie, M.M.; Taddesse, E.; Hoff, I., 2022. Permanent deformation and fatigue damage interaction in asphalt concrete using energy approach. *Eleventh International Conference on the Bearing Capacity of Roads, Railways and Airfields, Vol.3*. CRC Press. [doi:/10.1201/9781003222910-12](https://doi.org/10.1201/9781003222910-12)
- E) Alamnie, M.M.; Taddesse, E.; Hoff, I., 2023. A study on Permanent Deformation and Fatigue Damage Interaction in Asphalt Concrete. *Construction and building materials*, 407, 133473. [doi:/10.1016/j.conbuildmat.2023.133473](https://doi.org/10.1016/j.conbuildmat.2023.133473)
- F) Chen, H.; Alamnie, M.M.; Barbieri, D.M.; Zhang X.; Gang, L.; Hoff I., 2023. Comparative Study of Indirect Tensile Test and Uniaxial Compression Test on Asphalt Mixture: Dynamic Modulus and Stress-Strain State. *Construction and building materials*, [doi:/10.1016/j.conbuildmat.2022.130187](https://doi.org/10.1016/j.conbuildmat.2022.130187)

Summary

Asphalt concrete is one of the most important road building materials worldwide. This material exhibits unique chemical, physical and mechanical properties. The most well-known mechanical properties are the viscoelastic, viscoplastic-viscodamage (deformability), fatigue cracking, and fracture under different environmental and loading scenarios. The investigation of bituminous mixtures focuses on four main properties; stiffness and stiffness change, fatigue and damage law evolution, permanent deformation and accumulation at high temperatures, and cracks and crack propagation at low temperatures. Every mechanistic-empirical (ME) and mechanistic pavement design method attempts to model and simulate these four properties for an accurate performance prediction.

The main contributions of this research project are focused on the linear viscoelastic and damage responses of asphalt concrete mixtures. This thesis presents the uniaxial and triaxial viscoelastic responses and the interaction between the permanent deformation and uniaxial cyclic fatigue responses of asphalt concrete mixtures. To achieve these objectives, extensive laboratory investigations were performed using the latest mechanistic asphalt testing equipment.

The linear viscoelastic (LVE) properties of asphalt concrete are crucial for mechanistic pavement design. The rutting and fatigue cracking properties of asphalt concrete are directly correlated with the LVE stiffness. In the first phase, the research emphasized the LVE response in both uniaxial and triaxial states, as well as the axial and indirect tensile (IDT) testing modes. Three of the appended papers extensively addressed these properties. The important conclusions from this phase were the triaxiality of the LVE properties at intermediate and high temperatures,

and the good correlation of the IDT and axial mode of the stiffness tests at low and intermediate temperatures but not at high temperatures.

The second phase of the study was devoted to the damage responses of asphalt concrete. Permanent deformation (viscoplastic-viscodamage) was investigated at high temperatures (both uniaxial and triaxial), and the cyclic fatigue damage was studied at lower temperatures. The results are reported in three appended papers. A thorough investigation of the inherent damage interaction in asphalt concrete has been conducted in this thesis, which has not been done before. Based on the extensive literature review and our observations and experiments, the permanent deformation - fatigue damage interaction sequence dominates the asphalt concrete damage mechanism. This study applied both continuum damage mechanics (CDM) and dissipated energy (DE) approaches to assess the interaction. The existing prediction models have missed the interaction damage mechanism. It is observed that the myth of rutting-fatigue interaction is interrelated. This research confirms that rutting, apart from thermal cracking, is the cause of surface cracking. This observation further confirms the need for a unified damage model for accurate pavement performance prediction.

Keywords: Asphalt concrete; Linear viscoelastic; Permanent deformation; fatigue damage; Damage interaction; Sequential Method; Triaxiality Ratio

Sammendrag

Asfaltbetong er et av de viktigste vegbyggematerialene på verdensbasis. Dette materialet viser unike kjemiske, fysiske og mekaniske egenskaper. De mest kjente mekaniske egenskapene er de viskoelastiske, viskoplastiske-viscoskade (deformerbarhet) og utmatting og sprekkebruddsegenskaper under forskjellige miljø- og belastningsscenarier. Forskning på bituminøse masser fokuserer på fire hovedegenskaper: stivhet og stivhetsendring, utvikling av utmatting- og skadeloven, permanent deformasjon og akkumulering ved høye temperaturer, og sprekker og sprekkeforplantning ved lave temperaturer. Hver mekanistisk-empirisk (ME) og mekanistisk dimensjoneringsmetode forsøker å modellere og simulere disse fire egenskapene for en nøyaktig beregning av dekkets levetid.

Hoved bidragene fra dette forskningsprosjektet er den lineære viskoelastiske og skaderesponsen til asfalt masser. Denne avhandling presenterer de uniaksiale og triaksiale viskoelastiske responsene, og kobling mellom permanent deformasjon og enaksial syklisk utmattingsrespons av asfalt masser. For å nå disse målene ble det utført omfattende laboratorieundersøkelser med det nyeste utstyret for mekanisk asfalttesting.

De lineære viskoelastiske (LVE) egenskapene til asfaltbetong er avgjørende for mekanistisk dimensjoneringsmetoder. Spor- og utmattingsegenskapene til asfaltbetong er direkte korrelert med LVE-stivheten. I den første fasen la forskningen vekt på LVE-responsen i både uniaksiale og triaksiale tilstander, samt test modusene for aksial og indirekte strekk (IDT). Tre av de vedlagte papirene tok for seg disse egenskapene. De viktige konklusjonene fra denne fasen var '*triaxiality*' til LVE-egenskapene ved middels og høye temperaturer og den gode korrelasjonen mellom

IDT og aksial test modus for stivhetstestene ved lave og middels temperaturer, men ikke ved høye temperaturer.

Den andre fasen av denne studien var om skaderesponsen til asfaltbetong. Permanent deformasjon (viskoplastisk-viscoskade) ble undersøkt ved høye temperaturer (både uniaksiale og triaksiale), og sykliske utmattelseskader ble studert ved lave temperaturer. Resultatene er rapportert i tre vedlagte artikler. Det særegne ved skadeanalysedelen av denne oppgaven er basert på intensjonen om å undersøke skadesamspillet i asfaltbetong, som ikke har vært grundig undersøkt tidligere. Basert på en omfattende litteraturgjennomgang og våre observasjoner og eksperimenter, dominerer interaksjonssekvensen permanent deformasjon - utmattingskade skademekanismen for asfaltbetong. Denne studien brukte både 'continuum damage mechanics' (CDM) og 'dissipated energy' (DE) tilnærminger og konkluderte med at myten om spor-utmattelsesinteraksjon henger sammen, mens eksisterende prediksjonsmodeller har savnet interaksjonsskademekanismen. Denne forskningen bekrefter at spordannelse, bortsett fra termisk sprekkdannelse, er årsaken til overflatesprekker. Denne observasjonen bekrefter ytterligere behovet for en enhetlig skademodell for nøyaktig beregning av dekkets levetid.

Contents

1	Introduction	1
1.1	Background	1
1.2	Asphalt concrete damages	3
1.2.1	Permanent Deformation Damage	4
1.2.2	Fatigue Damage	6
1.2.3	Permanent deformation and Fatigue damage interactions	7
1.3	Objectives	8
1.4	Research Program	9
1.5	Organization of the thesis	9
1.6	Contributions	10
2	Theoretical Overview	15
2.1	Preliminaries	15
2.2	Linear viscoelasticity	18
2.2.1	Time-temperature superposition	19
2.3	Viscoplasticity	20
2.3.1	Model based on mechanical analog	21
2.3.2	Perzyna-type viscoplastic model	22
2.3.3	The PANDA model	23
2.4	Damage modeling approaches	23
2.4.1	Energy approach	24
2.4.2	Continuum damage approach	24

3	Experimental Program	29
3.1	Test Materials	29
3.2	Specimen Fabrication	30
3.3	UTM-130 Testing System	31
3.3.1	Dynamic Modulus Test	32
3.3.2	Indirect Tensile Test	35
3.3.3	Cyclic Creep-Recovery Test	36
3.3.4	Uniaxial Fatigue Test	37
3.4	The proposed Sequential Test procedure	38
3.4.1	The PD-F sequence	39
3.4.2	The F-PD sequence	40
4	Viscoelastic Response	43
4.1	Linear Viscoelastic Response	43
4.1.1	Uniaxial Viscoelastic Response	46
4.1.2	Stress-dependent viscoelastic response	48
4.1.2.1	Triaxial Master curve	49
4.1.2.2	Triaxiality ratio	52
4.2	Comparison of Uniaxial Compression and IDT modes of Dynamic Modulus tests	53
4.3	Comparison of dynamic and resilient modulus	56
4.3.1	Resilient Modulus versus storage modulus	58
4.3.2	Resilient Modulus versus Relaxation modulus	59
5	Viscoplastic and Damage Response	61
5.1	Asphalt Concrete Damage Characterization	61
5.2	Permanent deformation characterization	62
5.2.1	Permanent deformation dissipated energy	62
5.2.2	Effect of Confining Stress	65
5.3	Fatigue damage characterization	65

5.4	Interaction between fatigue and permanent deformation damage . . .	69
5.4.1	Sequential damage	70
5.5	Unified damage model	75
5.6	Summary	76
6	Concluding Remarks	79
6.1	Conclusions	79
6.1.1	Viscoelastic analysis	79
6.1.2	Viscoplastic and fatigue cracking damage analyses	80
6.2	Limitations	82
6.3	Further research	82
	Bibliography	85
	Appended Papers	99

List of Figures

1.1	Stress components caused by moving loads	4
1.2	Typical a repeated load test and strain response	5
1.3	Schematic representation of repeated (cyclic) compression load test (a) uniaxial (b) triaxial	6
1.4	Research program overview	10
1.5	Thesis contributions	11
2.1	Strain components of typical creep–recovery cycle - the stress history and strain response	16
2.2	Schematic response of an elastic-plastic material	17
2.3	Schematic of a viscoelastic-viscoplastic material response	17
2.4	Generalized Maxwell Model	19
2.5	Burger’s Model	21
3.1	Aggregate particle distribution for mixtures (AC, AGB and SMA) produced at mixing Plant and in laboratory	30
3.2	Specimen fabrication	31
3.3	(a) The Universal testing machine (b) IMACS and PC	32
3.4	Dynamic modulus tests (a) Uniaxial test setup (b) IDT test setup	33
3.5	Schematic of sinusoidal Stress and strain response in dynamic modulus	35
3.6	(a) Haversine loading pulse (b) Block loading pulse	36
3.7	Triaxial testing system	37
3.8	(a) sample plate gluing jig (b) fatigue test setup for T-T and T-C	38
3.9	Sequential Test instrumentation	39

3.10	Schematic of Permanent deformation - Fatigue sequence (PD-F)	40
3.11	Schematic of Fatigue - Permanent deformation sequence(F-PD)	41
4.1	Representation of the introduced general model “2S2P1D” for both bituminous binders and mixes, h and k are two parabolic creep elements	44
4.2	Dynamic modulus Master curves of different asphalt concrete mix- tures (adapted from Paper E)	47
4.3	Uniaxial, Isothermal shift factors ($\log \alpha_T$)	47
4.4	Effect of one year storage - aging at room temperature on the dynamic modules of AC-11 and SMA-11 mixtures	48
4.5	Triaxial master curves at 21°C (a) Isobaric master curves (b) vertical or triaxial master curves (adapted from Paper B)	49
4.6	Effect of confining pressure on the Long-term relaxation modulus (Paper B)	51
4.7	Effect of confining pressure on the Long-term relaxation modulus (Paper B)	51
4.8	Triaxial master curves using the proposed models (adapted from Pa- per B)	52
4.9	The relationship between Triaxiality ratio (η), Temperature, and con- fining pressure (from Paper B)	53
4.10	Stress distribution in Indirect tensile loading	55
4.11	Comparison of dynamic modulus Master curves using IDT and UC (a) AC-L (b) SMA-L (from Paper F)	56
4.12	Master curves of dynamic modulus and resilient modulus - AC or AB mixture (Paper C)	57
4.13	Master curves of dynamic modulus and resilient modulus - AGB Mix- ture (Paper C)	58
4.14	Master curves relaxation modulus and resilient modulus - AC/AB mixture (Paper C)	59

5.1	Schematic stress-strain hysteresis loops (a) permanent deformation (b) cyclic fatigue (c) fatigue-creep interaction	61
5.2	Permanent deformation and DER	64
5.3	DER versus permanent strain	64
5.4	Correlation between flow number and shear endurance life	64
5.5	Effect of Stress on permanent deformation properties (from Paper E)	65
5.6	Fatigue damage characteristics of new and per-deformed samples (T-T at $10^{\circ}C$ and $300\mu\epsilon$) (PD-F)	66
5.7	Development of viscoplastic strain during controlled-strain cyclic fatigue tests	66
5.8	Fatigue damage characteristics of new and per-deformed samples (T-T at $10^{\circ}C$ and $300\mu\epsilon$) (PD-F) (Paper E)	68
5.9	Fatigue damage Using DER T-C fatigue test at different control-strain (a) $10^{\circ}C$ (b) $15^{\circ}C$	68
5.10	Dissipated energy of PD-F sequence (F10 and PD40 for different mixtures in T-T mode)	71
5.11	Dissipated energy of different samples PD-F sequence (DE_{PD} versus DE_{Tot})	71
5.12	Effect of pre-deformation on fatigue damage responses in PD-F sequence (a) parameter b (b) total fatigue dissipated energy until failure (Paper E)	72
5.13	Damage variable S and dissipated energy DEF on new samples– AC-P1-X (Paper E)	72
5.14	Dissipated energies of pre-fatigued samples in F-PD sequence (a) AC-P1-X fatigue at $10^{\circ}C$ and PD at $30^{\circ}C$ and 2 MPa (b) SMA-P2-X fatigue at $10^{\circ}C$ and PD at $40^{\circ}C$, 0.65MPa (Paper E)	73
5.15	Correlation of total dissipated energy and flow numbers in F-PD sequence (a) AC-P1-X, PD at $30^{\circ}C$ (b) SMA-P2-X, PD at $40^{\circ}C$ - (Paper E)	74

5.16 Schematic of Creep and fatigue interaction damage depending on temperature and sequence 76

List of Tables

3.1	Tested asphalt concrete mixtures properties (produced at mixing plant	30
3.2	Sample conditioning time at different temperatures	33
3.3	Confined and unconfined dynamic modulus test conditions	34
3.4	Test parameters used in the IDT testing mode	35
3.5	Uniaxial and Triaxial Compression creep-recovery test parameters . .	36
3.6	Summary of Uniaxial fatigue test Parameters	37

Abbreviations

AASHO American Association of State Highway Officials. [1](#)

AASHTO American Association of State Highway and Transport Officials. [33](#)

AC Asphalt Concrete. [1](#)

CDM Continuum damage mechanics. [23](#)

DE Dissipated Energy. [24](#)

DMR Dynamic Modulus ratio. [27](#)

EN European Norm. [35](#)

LVDT Linear Variable Differential Transformer. [33](#)

LVE Linear viscoelastic. [3](#)

ME Mechanistic-Empirical. [2](#)

NCHRP National Cooperative Highway Research Program. [2](#)

NMAS Nominal Maximum Aggregate Size. [29](#)

PMB Polymer modified Binder. [29](#)

SHRP Strategic Highway Research Program. [2](#)

STP sequential test procedure. [38](#)

UTM Universal Testing Machine. [31](#)

VD Viscodamage. [2](#)

VE Viscoelastic. [2](#)

VECD viscoelastic continuum damage. [3](#)

VP Viscoplastic. [2](#)

Symbols

The following list describes several symbols that are used within the body of the document and published articles included in this dissertation.

α_T temperature shift factor

$\Gamma(p)$ pressure shift factor

Γ^{vp} viscosity fluidity parameter

ν angular frequency

ω angular frequency

ϕ damage density variable

ρ_i relaxation time

σ stress

σ_c confining stress

σ_{ij} stress tensor

ε strain

$\dot{\varepsilon}$ strain rate

ε^R pseudo strain

ε_{ij} strain tensor

ε_{vp} viscoplastic strain

SYMBOLS

φ	phase angle
$C(S)$	pseudo stiffness
$D(t)$	creep compliance modulus
$E(t)$	relaxation modulus
E''	loss modulus
E'	storage modulus
E^*	dynamic modulus
E_{oo}	Long-term relaxation modulus
E_R	reference modulus
f_R	reduced frequency
S	damage quantity
t_R	reduced time
W^R	pseudo strain energy

SYMBOLS

Chapter 1

Introduction

This chapter presents the general background, overview, research gaps and the objectives of the study. The research approach and the organization of this dissertation are also briefly described.

1.1 Background

Asphalt pavements comprise more than 90 percent of paved road networks worldwide. According to the IRF World Road Statistics (2017), the total length of continuous asphalt roads spanned more than three times the diameter of the sun by 2017 [1]. This implies that asphalt concrete is one of the most important road building materials. Asphalt concrete (AC), also known as asphalt mixture, is a man-made material that exhibits variable properties depending on environmental conditions (mainly temperature) and loading rates. Asphalt is a complex material. Asphalt concrete exhibits viscoelastic, viscoplastic and plastic behaviors under normal operating conditions. These unique properties of AC, along with the nonlinearity of the unbound materials, renders asphalt pavements intuitively indeterministic.

The design of asphalt concrete has traditionally been based on empirical and trial-and-error methods using field data and experience [2]. The AASHO road test (1958 - 1960) has become the foundation for the latest generations of mechanistic-empirical (ME) and mechanistic pavement design methods [3]. It is well understood that pavement design has not been scientifically sound from early times. This is partly because gradually roads lose their functionality, and show signs of damage

over a longer time (i.e., they do not fail dramatically like bridges and other elevated structures) [4]. A paradigm shift in asphalt concrete (pavement structure) design occurred after some comprehensive researches were conducted. The Strategic Highway Research Program (SHRP) in the early 1990s [5, 6], European Commission projects (COST 1999) [7], and National Cooperative Highway Research Program (NCHRP) projects such as NCHRP 1-37A and NCHRP 9-19 [8] have made notable progress in this regard. These research projects led to Mechanistic-Empirical (ME) test methods, and later to pure mechanistic. State-of-the-art methods for the design and performance prediction of asphalt concrete still depend on empirical and/or mechanistic-empirical data. Empirical principles are becoming inadequate owing to the incorporation of new pavement materials and growing axle loads. Moreover, a warranty- and performance-based construction specifications have become more attractive than end result and performance-related specifications. Thus, the ability of asphalt pavements to deliver the required level of service is governed by the pavement life. Most importantly, service life is mainly related to the performance of the asphalt concrete layer. Most studies have focused on the application of ME design methods, the formulation of mechanistic performance prediction models, and the utilization of different materials in asphalt pavements [9, 10, 11]. The experimentation and modeling of the viscoelastic (VE), viscoplastic (VP), viscodamage (VD), and fracture responses, and the combination of these properties are the focus of AC research. Several theories and principles have been applied to model the *VE-VP-VD* responses of AC under certain loading and environmental conditions. In general, bituminous mixtures have four main properties of interest when analyzing pavement behavior [12]: (1) stiffness and stiffness change, (2) fatigue and damage law evolution, (3) permanent deformation and accumulation, and (4) crack and crack propagation at low temperatures. The evolution of these four properties is interrelated depending on the domains of the AC response, such small strain and large strain response, uniaxiality and triaxiality, time-temperature-pressure dependent (thermo-piezo-rheological) properties, viscoplasticity and cracking.

This project can be divided into two parts. The first part of the investigation is an extensive study of asphalt concrete at small strain responses using the theories of linear viscoelasticity (LVE). The common principles applied in viscoelastic analysis are time-temperature superposition and elastic-viscoelastic correspondence [13, 14], and method of interconversion between linear viscoelastic material functions (relaxation and creep moduli) [15]. The linear viscoelastic (LVE) model is widely used for bituminous material characterization under stress, strain, and time-temperature-controlled conditions at a small strain level [16, 17]. However, the LVE behavior is not adequate for characterizing asphalt concrete responses. Moreover, asphalt concrete materials have different properties under tensile and compressive loads and exhibit a strong nonlinear stress-strain relationship.

The second part of the study involved damage characterization and modeling of asphalt concrete under tension and compression loads. Viscoplastic deformation is a type of damage caused by compression at elevated temperatures. The theory of viscoplasticity (VP) has been widely used [18, 19]. Viscodamage at intermediate temperatures is a damage phenomenon in asphalt concrete under tensile and compressive loads. Another investigation focused on the cyclic fatigue properties of AC performance at low and intermediate temperatures. Viscoelastic continuum damage (VECD) theory and dissipated energy approaches have been extensively applied for fatigue life prediction and modeling [20].

1.2 Asphalt concrete damages

Asphalt concrete is affected by two dominant damage modes: rutting and fatigue cracking. European research [7] has reported that rutting in asphalt concrete layers is the number-one distress mechanism, followed by surface cracking. Figure 1.1 shows the stress components of the tire-pavement contact. The most damaging stress condition occurred near the load area, and all stresses were compressive within the contact area. The vertical stress remains compressive with increasing depth, and the horizontal stress changes from compression to tension. The shearing condition

prevailed under the rim of the load, and the shear stress changed sign, leading to a rotation of the principal stresses. Shear stress causes permanent deformation and top-down cracking usually develops in the longitudinal direction both within and outside the wheel path [21]. Vertical stress is main cause of rutting in the substructure and bottom-up fatigue cracking. Myers et al. [22] showed that near-surface stress includes both tension and compression stresses and the overall effect is transverse tensile stress on the pavement surface under the outer rib of the radial tire.

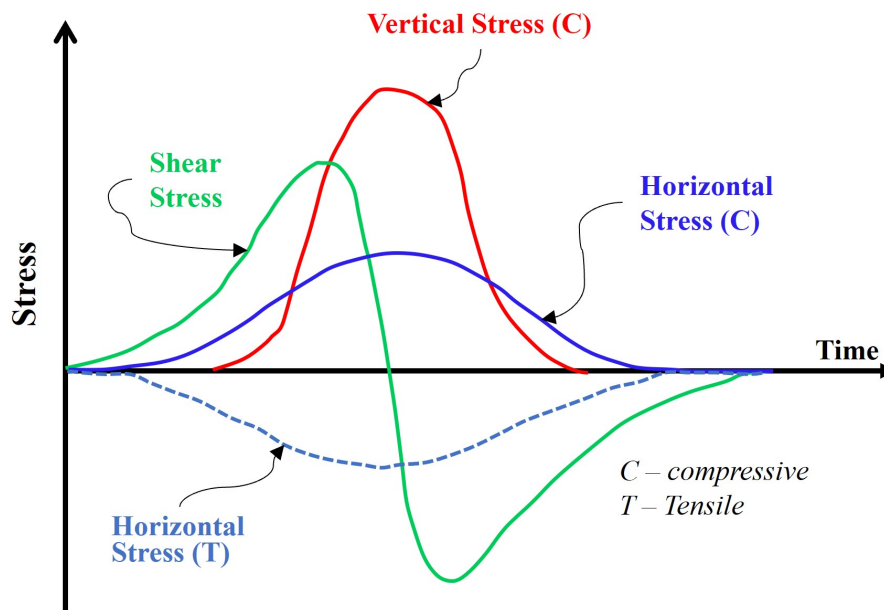


Figure 1.1: Stress components caused by moving loads

1.2.1 Permanent Deformation Damage

Permanent deformation or rutting damage in asphalt concrete is generally related to three mechanisms: (1) viscoplastic deformation in the asphalt layer (densification and shear flow) [23], (2) substructural (subbase and subgrade) failure [24], (3) studded tire abrasion in the wheel path [25]. The simultaneous densification (short term), shearing (long term), and dilation mechanisms cause permanent deformation [26, 27]. The Rut depth ($R_D = \sum \varepsilon_{vp,i} h_i$) is the sum of the deformations in each layer of the pavement (h_i and $\varepsilon_{vp,i}$ are the thickness and viscoplastic strain of the i^{th} layer, respectively). The evolution of permanent deformation at the macroscopic

level was described in three distinct stages (*primary, secondary, and tertiary*) [28], as shown in Figure 1.2. The primary stage is characterized by the rapid accumulation of permanent deformation at a decreasing rate, the secondary phase with steady-state deformation (strain-hardening) at a nearly constant rate and the tertiary stage with a rapid shear deformation rate due to micro-cracks. Permanent deformation behavior is stress dependent in uniaxial or triaxial repeated load compression performance. Several mechanistic-empirical (M-E) models have been proposed to predict these three creep stages (**Paper A**). Repeated creep and recovery with a haversine load pulse is considered the most realistic test for permanent deformation characterization [29, 30]. Moreover, confined tests are selected in lieu of unconfined tests to better simulate field conditions and quality permanent deformation data [31, 32, 33], as shown in Figure 1.3.

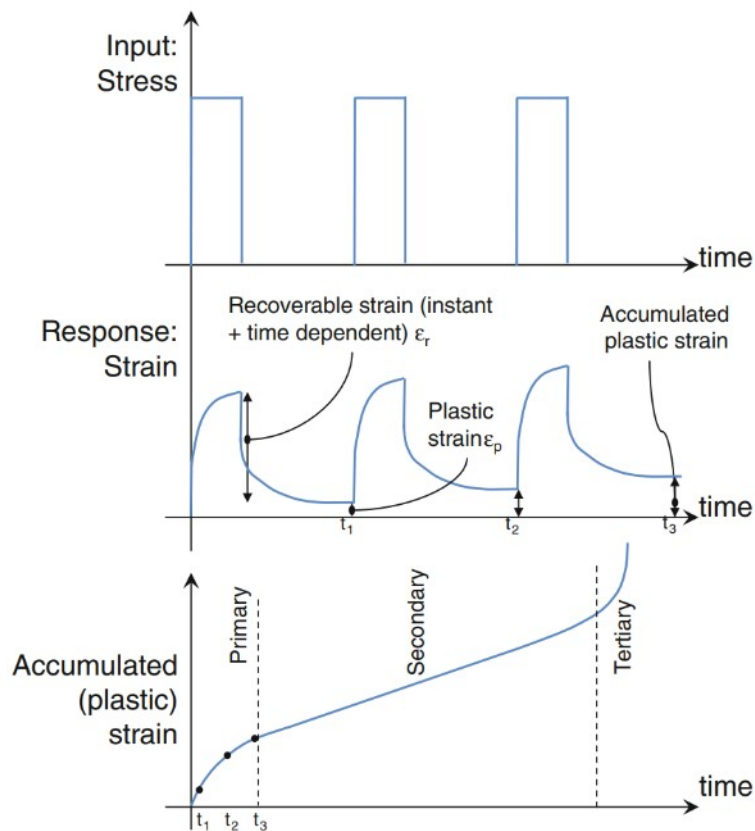


Figure 1.2: Typical a repeated load test and strain response [34]

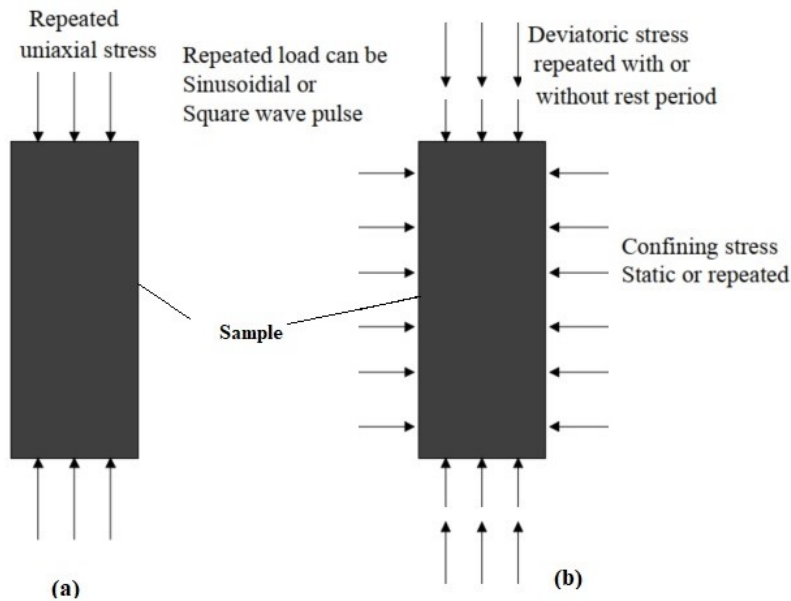


Figure 1.3: Schematic representation of repeated (cyclic) compression load test (a) uniaxial (b) triaxial

The constitutive modeling of viscoplastic strain generally uses a phenomenological and Micromechanics-based approaches. Phenomenological models are widely used owing to their simplicity and different failure criteria (Drucker Prager and Mohr-Coulomb) [29, 19, 35, 36]. The micromechanical approach can account for the effects of individual mixture constituents using imaging technologies (X-rays) [26, 37, 38, 39].

1.2.2 Fatigue Damage

Fatigue is a fracture phenomenon caused by the repeated application of tensile or tensile-compression stress that is less than the strength of the material. The critical tensile strain at the bottom of the asphalt layer is the design criterion for fatigue damage in asphalt concrete. Fatigue cracks are thought to initiate and propagate upward (bottom-up) to the surface because of repeated traffic loads. However, studies have shown that fatigue cracks also propagate from top to bottom (top-down) owing to tensile stresses from tire-pavement interaction. Top-down cracking (TDC) is prevalent in stiff asphalt mixture with a thick layer [40]. Several test types have been developed to characterize the fatigue damage. Zhou et al.[41] summarized vari-

ous fatigue cracking test candidates. The 50 percent criterion of stiffness reduction is the most common fatigue failure criterion in bending beam fatigue tests [42]. Other fatigue failure criteria have recently been developed [43, 44]. The major factors contributing to bottom-up fatigue cracking are an inadequate structural thickness and weak or brittle asphalt mixtures. One of the most comprehensive constitutive models for fatigue cracking is the viscoelastic continuum damage method based on thermodynamic principles and state variables [45, 46]. Moreover, the dissipated energy approach was used to predict the fatigue damage mechanisms of asphalt concrete [47]. In this study, both continuum and energy approaches were applied for fatigue characterization (**Paper D and E**).

1.2.3 Permanent deformation and Fatigue damage interactions

The interaction of permanent deformation and fatigue damage for asphalt concrete has not been studied in detail existing literature. Traditionally, these two types of damage modes have been modeled separately. Temperature is often considered as a distinguishing variable. Fatigue cracking is a low- and intermediate-temperature damage (with negligible viscoplastic strain), whereas permanent deformation occurs at high-temperature. This distinction is related to the relaxation behavior of asphalt concrete. Asphalt concrete relaxes faster at elevated temperatures and become more fatigue crack resistant [48, 49]. By contrast, viscoplastic deformation is sensitive to viscous flow at high temperatures. Similarly, permanent deformation is minimal at low temperatures owing to the high elasticity of AC. However, Localized tensile stress is the likely cause of top-down cracking, which is always accompanied by permanent deformation based on field and laboratory observations [40, 50, 51, 52]. Molenaar[50] reported that top-down cracking is critical on surface wearing course with a depth of around 40 – 50 mm and the bottom-up cracking (BUC) only appears as disintegrated zones. Moreover, the author said that fatigue damage is somehow a myth, which implies that the permanent deformation and fatigue damage modes should be interrelated in asphalt concrete. Mun et al.[51] also found that both the

BUC and TDC may develop, co-join and coalesce. Therefore, traditional fatigue criteria overestimate the fatigue life of asphalt concrete. For this reason, existing prediction models cannot predict real pavement conditions, and pavement life has never been accurately predicted [53].

1.3 Objectives

The objective of this study was to investigate the viscoelastic, viscoplastic, and fatigue responses of asphalt concrete by proposing test protocols and prediction models. Different viscoelastic and viscoplastic models are available in the literature; however, these models are either too complex to calibrate or too simple to capture the triaxial viscoelastic-viscoplastic response of asphalt concrete. As discussed previously, asphalt concrete is a viscoelastic-viscoplastic material that requires complete investigation and modeling in the viscoelastic and viscoplastic (damage) domains (**Paper A**). To this end, this study has two main aims among other specific objectives.

- The first objective was to analyze the linear viscoelastic responses of asphalt concrete using different test methods and loading conditions such as uniaxial and triaxial stresses, uniaxial compression and indirect tensile modes.
- The other objective of this study was to investigate extensive asphalt concrete damage mechanisms, particularly the permanent deformation and fatigue cracking responses of asphalt concrete under various loading conditions.

Specifically,

- To investigate the stress-dependent linear viscoelastic response of asphalt concrete using a triaxial dynamic modulus test (**Paper B**).
- To investigate the correlation between the IDT and axial compression loading modes for the linear viscoelastic properties of asphalt concrete (both dynamic and resilient moduli)(**Paper C and F**)

- To investigate the interaction between permanent deformation and fatigue damage of asphalt concrete by proposing a new test protocol (**Papers D and E**).

1.4 Research Program

The methodology adopted to achieve the objectives of this study involved a literature review and an extensive laboratory investigation of different asphalt mixtures. A literature study was performed to identify important gaps in the permanent deformation modeling of asphalt concrete materials and to assess the existing prediction models and their theoretical foundations. A discussion is presented in **Paper A**. The test campaign consisted of different performance tests in both undamaged and damaged states. The linear viscoelastic response was presented in **Papers B, C, and F**. Similarly, the investigation regarding the damage (viscoplastic and fatigue damage) responses was presented in **Papers D and E**. The interaction between the permanent deformation and fatigue was the main focus of the damage study (**Paper E**). The research approach is illustrated in Figure 1.4.

1.5 Organization of the thesis

This thesis is organized into six chapters. The general background and objectives are presented in Chapter 1. The theoretical background of this study is summarized in Chapter 2. In this section, the viscoelastic, viscoplastic, and fatigue damage theories and models are briefly explained. Section 3 discusses the experimental program, specimen fabrication, testing setup, and test parameters used in this study. The research outcomes are summarized in the following two sections. The viscoelastic responses of different AC mixtures, a comparison of different test methods, and the proposed model are discussed in Section 4. Section 5 discusses the damage (permanent deformation and fatigue damages) responses, and interaction between fatigue and permanent deformation. Finally, concluding remarks, recommendation, and limitations of this study are outlined in Chapter 6.

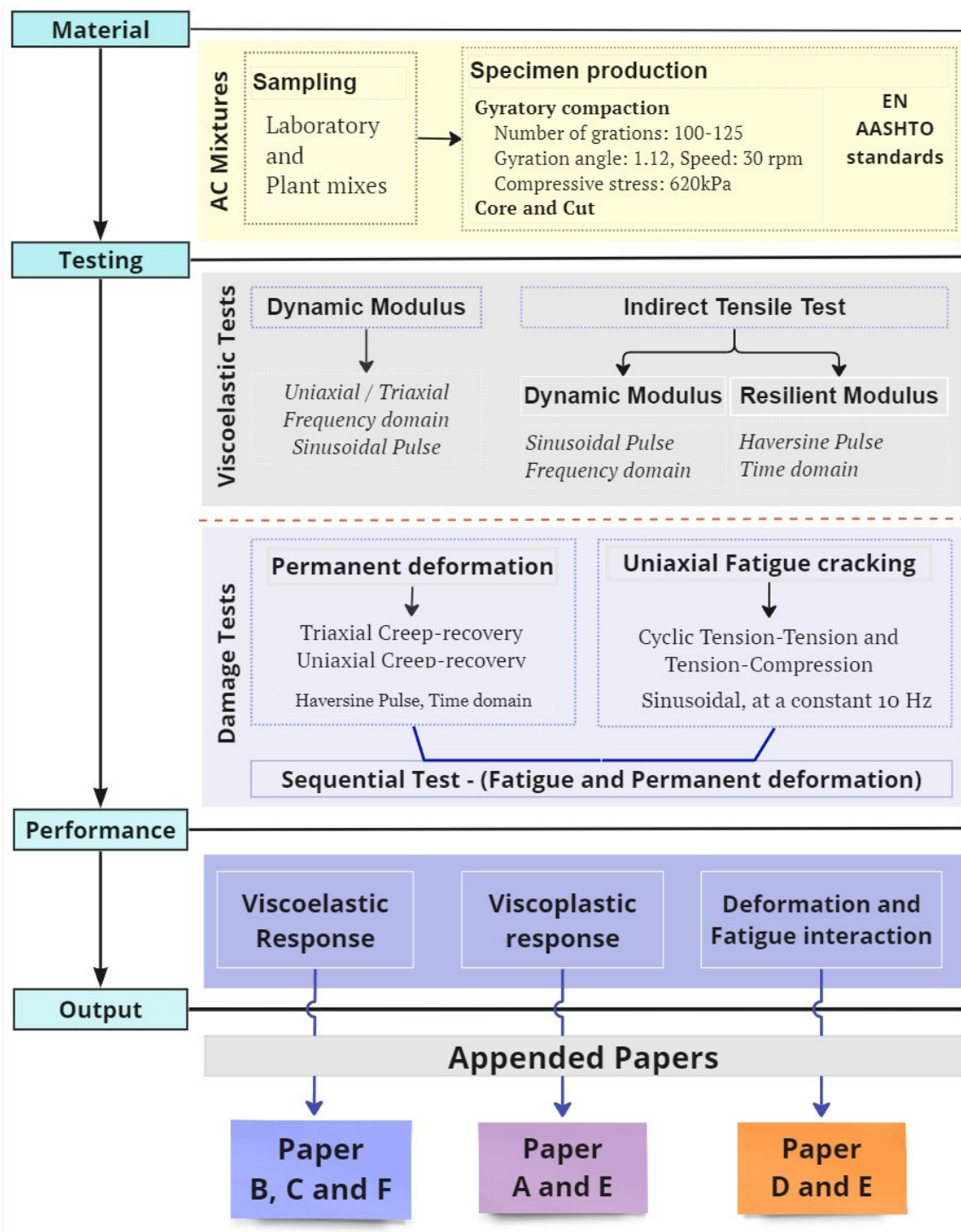


Figure 1.4: Research program overview

1.6 Contributions

The contributions of this project are organized based on four important AC material properties, as illustrated in Figure 1.5. The themes explored in this project are the viscoelastic response over wider thermodynamic variables and loading periods,

viscoplastic (deformation) behavior at high temperatures, fatigue cracking and crack growth mechanisms at lower temperatures, and the possible mutual (interactive) evolution of damage mechanisms. The strain- and stress-dependent properties of asphalt concrete in viscoelastic and viscoplastic domains were investigated in this study. Excerpts of the contributions from the appended papers are summarised as follows:

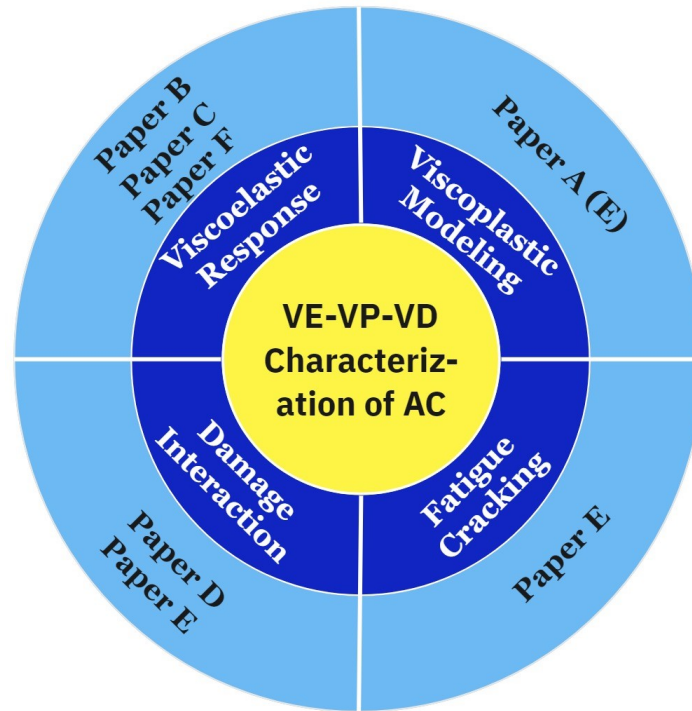


Figure 1.5: Thesis contributions

Paper A - Advances in permanent deformation modeling of asphalt concrete - a review

This paper presents a study on state-the-art of advancements in permanent deformation modeling for bituminous materials. Permanent deformation is the major mechanism of asphalt concrete damage. This paper discusses the robustness of existing models while also discussing the pertinent theories applied to model the viscoplastic strain and the governing constitutive models at both macro- and micro-structural levels. The interaction between permanent deformation and fatigue damage was also explored, and the gap in the modeling of damage interaction and coupling was highlighted.

Paper B - **Thermo-piezo-rheological characterization of asphalt concrete**

The linear viscoelastic response of asphalt concrete is the primary focus of mechanistic-empirical design approaches. This paper presents the experimental investigation and modeling of the stress-dependent (piezo rheological) linear viscoelastic response of asphalt concrete. This study employed a triaxial dynamic modulus test over a wide ranges of temperatures, pressures and frequencies to explain the thermo-piezo-rheological responses. It proposes a new triaxial shift model and a stress ratio function - triaxiality ratio function for the stress-dependent linear viscoelastic response of asphalt concrete mixtures.

Paper C - **Viscoelastic characterization and comparison of Norwegian asphalt mixtures using dynamic modulus and IDT tests**

The time- or frequency domain stiffness characterization of asphalt concrete is the most important design variable. The uni-axial compression dynamic modulus (in the frequency domain) and the bi-axial indirect tensile resilient modulus (in the time-domain) are common test candidates. This study employed two master curve function, the *sigmoid and the rheological 2S2P1D model*, and the time-temperature superposition principle. Regardless of the inherent differences between the two test modes, this study observed a closer comparison between the storage modulus (E') or relaxation modulus $E(t)$, and M_r particularly at intermediate temperatures. It was also observed that the rheological models have difficulty fitting the M_r data compared to the mathematical sigmoid function. This study also contributes to the material database of Norwegian asphalt mixtures.

Paper D - **Permanent deformation and fatigue damage interaction in asphalt concrete using energy approach**

The interaction between fatigue and permanent deformation is a complex phenomenon, and little effort has been devoted to this topic. Damage is quantified using various approaches, such as continuum damage, dissipated energy,

stiffness exhaustion, fracture, and crack length. This study investigates the fatigue and permanent deformation damage in asphalt concrete using the dissipated energy quantity and the dissipated energy ratio (DER). We focused on the interactions between the two damage. However, because the two damage modes are distinct, there are no laboratory test setups for simultaneously investigating both fatigue and permanent deformation. Therefore, a sequential test procedure was applied for fatigue and permanent deformations. The proposed criterion for permanent deformation provided additional damage indicator than the conventional flow number/strain rate criterion. This study shows that strain hardening (pre-deformation) accelerates fatigue cracking. Similarly, the highly fatigued samples were more prone to permanent deformation than the new samples.

Paper E - **A study on permanent deformation and fatigue damage interaction in asphalt concrete**

This study further explored the interaction between permanent deformation and fatigue damage of asphalt concrete using the sequential test procedure proposed in Paper D. Energy and viscoelastic continuum damage approaches were used to model the damage. The two types of damage are traditionally modeled independently, where temperature is a variable of departure. A sequential test procedure (STP) is proposed to study the interaction of fatigue (F) and permanent deformation (PD) in two sequences: ***PD-F*** and ***F-PD***. The rationale for the PD-F sequence is based on field observations that early deformation occurs prior to fatigue cracking. Conversely, the F-PD sequence assumes that fatigue cracking develops before PD, such as in thick pavements and cold areas. Thus, extensive testing was performed using creep-recovery permanent deformation and tension-compression/tension-tension fatigue tests on each specimen in both sequences. The study found that strain-hardening significantly accelerates the fatigue damage rate, particularly on aged and laboratory produced mixes. The fatigue tests without considering the strain-

hardening effect underestimate the fatigue damage rate. Moreover, a fourth creep phase is revealed using dissipated energy ratio to estimate the remaining life of asphalt concrete after flow number. In the F-PD sequence, the effect of preexisting cracks (up to 40% modulus reduction) on the permanent deformation is found to be marginal owing to factors such as healing.

Paper F - Comparative Study of Indirect Tensile Test and Uniaxial Compression Test on Asphalt Mixture: Dynamic Modulus and Stress-Strain State

This paper deals an extensive investigation of the dynamic modulus characterisation of asphalt materials through Indirect Tensile (IDT) and Uniaxial Compression (UC) tests using sinusoidal waves. Both these tests are commonly used by different road authorities. The focus of this study was to examine the stress-strain state of the two tests and comparing the dynamic modulus and phase angle of the asphalt mixtures. For this purpose, two types of asphalt mixtures (densely graded, AC and Stone Mastic Asphalt, SMA) were tested at two different laboratories. The dynamic modulus master curves and stress-strain states obtained from the two testing procedures were compared. The viscoelastic responses (dynamic and phase angles) were almost identical for medium frequencies and temperatures, whereas the results exhibited significant discrepancies for lower and higher frequency values. Moreover, the strains measured using the IDT test were variable, whereas those obtained from the UC test were stable. The IDT test has the advantage of small sample size for sample preparation methods in both the laboratory and field, whereas the UC test has better deformation control at low and medium temperatures.

Chapter 2

Theoretical Overview

In this chapter, an overview of the fundamental theories for modeling and characterizing asphalt concrete is presented. The pertinent theories of viscoelasticity, viscoplasticity, and continuum damage mechanics are discussed. The principles such as time-temperature superposition, and different permanent deformation and fatigue damage modeling approaches are also described.

2.1 Preliminaries

Asphalt concrete is a rate-dependent thermorheological material that exhibits both recoverable and irrecoverable response components under compressive loads. Here, two important behaviors are evident. First, rate-dependent materials exhibit strong temperature-based responses. The other behavior is that the response to an input depends on the input history and the rate of change of the inputs. Several test protocols have been used to understand time-dependent behavior. The creep recovery test is a standard test that can be used to understand the rate-based behavior of bituminous materials. Figure 2.1 shows the creep recovery test using a square stress loading pulse, σ_0 , applied for time t_1 , followed by a rest period t_r ($t_2 = t_1 + t_r$). At the end of the long rest period, the deformation constitutes some remains of non-recovered strain and is called permanent deformation or viscoplastic deformation, ε_{vp} . The recoverable part of the deformation is called viscoelastic deformation, ε_{ve} and is modeled using viscoelastic theories. The nonrecoverable or permanent deformation behavior of asphalt concrete was modeled using viscoplasticity theo-

ries based on metal and polymer materials. The additive decomposition technique of the total strain in a creep recovery test has been applied in both tension and compression modes [30], such that $\varepsilon_i^{ve}(t) + \varepsilon_i^{vp}(t) = \varepsilon_{tot}(t)$.

The viscoelastic (recoverable) strain component is generally obtained from non-destructive (small strain) tests. Viscoelastic strain is determined by defining the creep compliance and/or relaxation modulus functions. After the viscoelastic strain component is separated, the viscoplastic strain is calculated by subtracting the recoverable component from the total strain. The summative decomposition approach was questioned because of the complex behavior of asphalt concrete. The first difficulty is related to the need for a long rest period to completely recover the time-dependent recoverable strain. Another difficulty is related to behaviors, such as hardening-relaxation (hardening-softening) [29, 36], microstructural healing mechanisms and other associated damage modes.

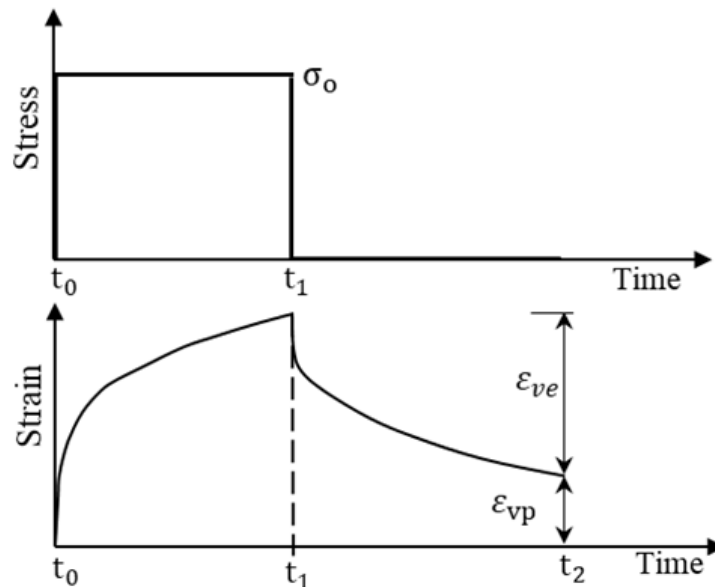


Figure 2.1: Strain components of typical creep–recovery cycle - the stress history and strain response

Figure 2.2 illustrates the stress-strain response of an elastoplastic material at a constant temperature. The strain rate is highly dependent on the applied stress, temperature, and material used. Both the rates of strain and permanent deformation

increase with the applied stress and temperature. At extremely low strain rates, the elastoplastic behavior dictates the response. With an increasing strain rate, the viscous component contributes to an increase in material stiffness. The viscoelastic-viscoplastic strain response of bituminous material in a typical loading-unloading cycle can be illustrated, as shown in Figure 2.3. The time dependent viscoplastic and viscoelastic responses depend on stress magnitude and path, rest period, loading rate, and temperature.

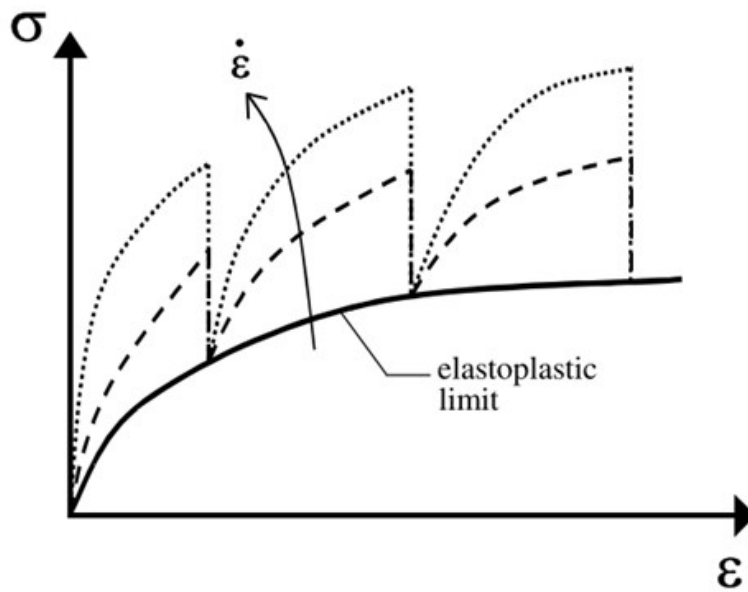


Figure 2.2: Schematic response of an elastic-plastic material

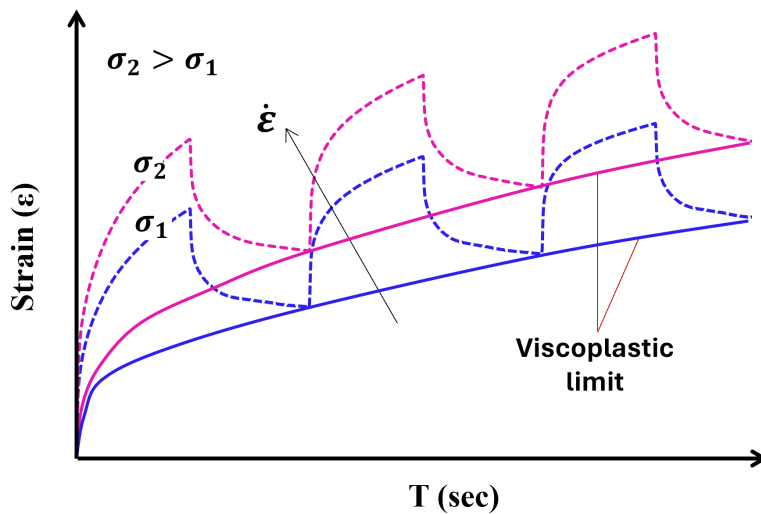


Figure 2.3: Schematic of a viscoelastic-viscoplastic material response

2.2 Linear viscoelasticity

Viscoelasticity is the constitutive behavior of a material that is neither elastic nor viscous. A class of material that responds in this manner is termed a viscoelastic material, where it is assumed that the stress is a single-valued functional of the strain, defined mathematically as follows [54]:

$$\begin{aligned}\sigma(X, t) &= E_{\tau=0}^{\tau=t}[\varepsilon(X, t)] \\ &\text{and} \\ \varepsilon(X, t) &= D_{\tau=0}^{\tau=t}[\sigma(X, t)]\end{aligned}\tag{2.1}$$

The first function in Eq. 2.1 is called the strain or modulus formulation because the strain is the input and the stress is the output variable. The second equation represents the stress (or compliance). The generic timescale, τ is used in order to clarify the meaning of the modulus functional, E and D , which map the entire history of strain into the value of the stress at the current time, t . The notation X is an index notation that has been employed as a position vector for a continuous body in either one- or three- dimensional space. The decision regarding which of the two formulations to choose normally depends on the problem to be solved and the mathematical complexity of the mechanical response of the viscoelastic materials. However, there exists a mapping or interconversion [55, 56] between functionals E and D , so that only one needs to be formulated and characterized experimentally.

The linear viscoelastic (LVE) response of asphalt concrete depends on the stress or strain magnitude. Researchers have considered different strain values for viscoelastic linearity limits. The NCHRP 9-19 reported 70 micro-strains [57], the AASHTO standard range 75 and 125 microstrains [58, 59], and Levevberg et al.[60] found 140 microstrains in compression and 80 micro-strains in tension. Other researchers [61] recommended a 50 microstrains limit for a pure linear viscoelastic response. The linear viscoelastic constitutive formulation is expressed using the effective viscoelastic stress σ_i^{ve} or the viscoelastic strain ε_i^{ve} .

$$\varepsilon_i^{ve}(t) = \int_{\tau=0}^{\tau=t} D(t - \tau) \frac{d(\sigma_i^{ve})}{d\tau} d\tau, i = 1 \dots 6\tag{2.2}$$

$$\sigma_i^{ve}(t) = \int_{\tau=0}^{\tau=t} E(t-\tau) \frac{d(\varepsilon_i^{ve})}{d\tau} d\tau, i = 1 \dots 6 \quad (2.3)$$

The generalized Maxwell model shown in Figure 2.4 is commonly used to model creep and relaxation constitutive models for viscoelastic materials. The uniaxial formulation using the Prony series forms of creep compliance $D(t)$ (1/units of stress) and relaxation moduli $E(t)$ (units of stress) is expressed as follows [55]:

$$D(t) = D_o + \sum_{i=1}^N D_i \left[1 - \exp\left(\frac{-t}{\tau_i}\right) \right] \quad (2.4)$$

$$E(t) = E_o + \sum_{i=1}^M E_i \left[\exp\left(\frac{-t}{\rho_i}\right) \right] \quad (2.5)$$

where, N and M are the total numbers of Prony terms; D_o , D_i , and τ_i are creep compliance model coefficients; and E_o , E_i , and ρ_i are relaxation model coefficients.

The interconversion between $D(t)$ and $E(t)$ is expressed as

$$\int_0^t E(t-\tau) \frac{dD(\tau)}{d\tau} d\tau \quad (2.6)$$

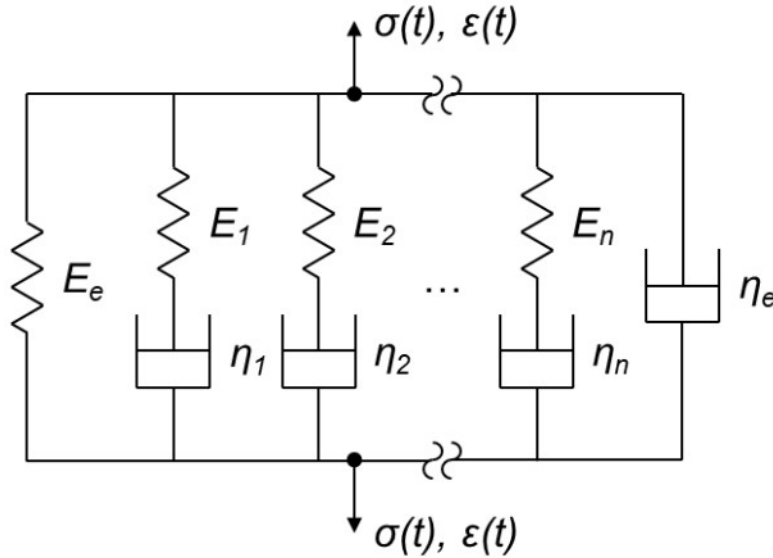


Figure 2.4: Generalized Maxwell Model

2.2.1 Time-temperature superposition

The most fundamental material property in an undamaged state is stiffness. The measurement of stiffness is the most basic piece of information required to estimate

the deformation of asphalt structures under external loads. Unlike other linear and homogeneous materials, such as steel, the stiffness of asphalt concrete is non-linear and depends on the rate of loading (time), temperature, and aging. Therefore, asphalt concrete does not exhibit a single stiffness (modulus) value. The time or rate dependency of AC is modeled using the creep compliance function $D(t)$ from creep tests, the relaxation modulus $E(t)$, or as a function of loading frequency using dynamic (complex) modulus $E^*(f)$. Thus, the LVE behavior of asphalt concrete is adequately characterized by the superposition of temperature and loading time or frequency. This unifying principle is called the time-temperature superposition principle (TTSP). The general expression is as follows:

$$E^*(T, f, \sigma_c) = E^*(T_r, f_R, P_o) \quad (2.7)$$

$$f_R = f * \alpha_{T,P}, \quad t_R = \frac{t}{\alpha_{T,P}} \quad (2.8)$$

where, f_R is reduced frequency (t_R is reduced time)

$\alpha_{T,P}$ is time-temperature- pressure shift factor

T_r and P_o are reference temperature and confining pressure (triaxial stress), respectively.

The TTSP in Equation 2.7 describes the variables that affect the dynamic modulus of asphalt concrete. The superposition principle has also been validated for viscoelastic responses in damages states [57] and also under triaxial stress conditions [62, 63].

2.3 Viscoplasticity

Viscoplasticity refers to the mechanical response of solids to time-dependent irreversible (inelastic) strain. Asphalt concrete exhibits both viscous and plastic responses and behaviors under external loading. The viscous response results in the flow of material over time, and the plastic properties are related to permanent deformation and shape changes under applied stress. The combined properties of the

viscous and plastic responses are characterized by the theory of viscoplasticity. Viscoplasticity is a constitutive model that captures the time-dependent and non-linear behavior of asphalt concrete. This behavior is essential for accurately modeling the mechanical response of asphalt pavements at large strains by considering factors such as the temperature, loading rate, and aging effects.

$$\dot{\epsilon}_{vp}(\sigma, \beta) = f(\sigma, \beta) \quad (2.9)$$

where β represents variables that affect strain rate.

Macroscopic irrecoverable deformation in asphalt concrete is commonly modeled using two approaches. The first is an analogical one that uses spring-dashpot like analogs to develop fluid-like viscoelasticity models, such as the Burgers model. The other approach uses plastic and viscoplastic models to represent the irrecoverable strain.

2.3.1 Model based on mechanical analog

Families of different analogical models have been used to model the viscoelastic-viscoplastic response of time-dependent materials. The common classic mechanical models are spring, dashpot, slip device, pot, parabolic elements, and a combination of these elements. The mechanical elements are advantageous to visualize the stress and strain responses using the analogs. The Maxwell model for viscoelastic relaxation (Figure 2.4), the Kelvin model (for creep response), and Burger's model (Figure 2.5) are used to model the viscoelastic and viscoplastic strain.

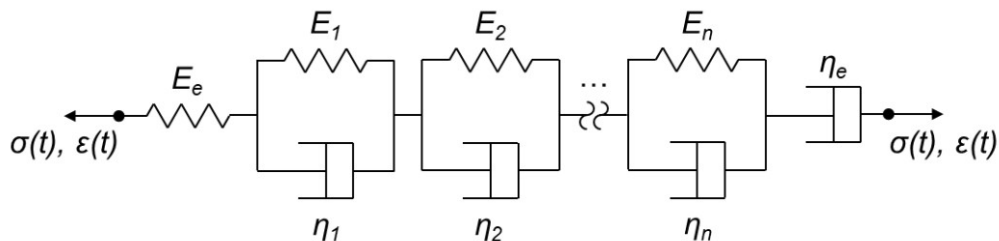


Figure 2.5: Burger's Model

Analogical models are suitable for deriving the governing mathematical formu-

lation of the stiffness modulus (creep compliance or relaxation modulus), which is important for decomposing the strain components. The viscoelastic-like model for viscoplastic strain is expressed as follows:

$$\varepsilon_{vp} = \int_0^\tau D(t - \tau) \frac{d\sigma^{vp}(\tau)}{d\tau} d\tau \quad (2.10)$$

2.3.2 Perzyna-type viscoplastic model

The classic model for the visco-plastic rate is the Perzyna hardening rule [64]. This model has been used by several researchers with Drucker-Prager type yield surfaces to predict the viscoplastic response of asphalt concrete [65]. The D-P yield surface is preferred for its efficiency in capturing the effect of the microstructure and damage propagation on the material behavior [66]. The classical viscoplastic rate is defined as follows (where $\langle x \rangle$ is the Macaulay bracket, defined as $\langle x \rangle = (x + |x|)/2$);

$$\dot{\varepsilon}_{vp} = \Gamma^{vp} \left\langle \frac{f}{\sigma_y^o} \right\rangle \frac{dF(\sigma)}{d\sigma} \quad (2.11)$$

where,

$\dot{\varepsilon}_{vp}$ is viscoplastic strain rate,

Γ^{vp} is viscoplastic fluidity parameter ($1/\Gamma^{vp}$ is a measure of viscoplastic viscosity),

$dF(\sigma)/d\sigma$ is a measure of the direction of viscoplastic strain.

σ_y^o is the yield stress quantity used to normalize the over-stress function (usually assumed as unity)

Classic Perzyna-type models have limitations in accounting for the load history effect and relaxation (softening) behavior during the rest period [66, 19, 36]. The simplest form of the strain hardening rate model is the power function, which assumes a constant hardening variable for the creep recovery load. Power law strain-hardening models for uniaxial [67] and triaxial [68] conditions have also been proposed. Schapery's viscoplastic rate model is given as;

$$\dot{\varepsilon}_{vp} = \frac{g(\sigma)}{G\varepsilon_{vp}^p} \quad (2.12)$$

where $g(\sigma)$ is the stress function, G, p are material properties.

2.3.3 The PANDA model

Pavement analysis using the nonlinear damage approach (PANDA) is the latest mechanistic pavement design approach [69, 65, 70]. The numerical-mechanistic-based PANDA method is based on three classic theories: (1) Schapery's nonlinear viscoelasticity [71], (2) Perzyna-type viscoplasticity [64] and (3) Darabi's viscodamage [66, 72] constitutive relationship. Based on these three constitutive equations, the PANDA approach has an unlimited capacity to couple different damage mechanisms (healing, aging, hardening-relaxation, and moisture-induced damage) of asphalt concrete using user-defined computer programs. The validity of TTSP with and without damage is a fundamental simplification for coupling the temperature-, rate-, and time-dependent viscoelastic and viscoplastic models of asphalt concrete. The studies conducted by Darabi et al. [72] demonstrated that viscoelastic-viscoplastic-viscodamage-healing can predict the fatigue damage responses of asphalt concrete using the PANDA approach. They conducted stress- and strain-controlled tests using repeated creep recovery, uniaxial strain rate tests, and cyclic stress- and strain-controlled tension tests to calibrate and validate the model. One of the challenges of the PANDA approach, or the mechanistic method in general, is the requirement for several tests to calibrate the model parameters.

2.4 Damage modeling approaches

Damage evolution is associated with energy dissipation or reduction of the effective area owing to crack formation and propagation, exhaustion of stiffness, and heat loss. Traditionally, damage has been estimated and modeled using two approaches. The two most common methods for quantifying damage in asphalt concrete materials under tension or compression loads are the continuum damage mechanics (CDM) and dissipated energy approaches. Both approaches have their own advantages and applications. The continuum method attempts to estimate the effective area of the material remaining after damage (cracking or deformation) to carry the applied stress. Damage criteria are often dependent on the stress direction. In contrast, the

energy method calculates the amount of energy dissipated owing to cracks or deformation under the stress-strain curve as a scale quantity, regardless of the direction of stress.

2.4.1 Energy approach

Damage is manifested in the form of dissipated energy (DE), such as heat, cracks, and deformation (shear). Thus, energy dissipation is a fundamental property of materials. The amount of DE in a cyclic load is the area under the stress-strain hysteresis curve and is expressed by the following integral [73].

$$DE = \int_0^\tau \sigma(x, t) \frac{d\varepsilon(x, \tau)}{d\tau} d\tau \quad (2.13)$$

where the integral is taken over a stabilized cycle and x denotes the point at which the field values are considered.

Different energy-based failure criteria have been previously proposed [74, 75]. Luo et al. [76] proposed the energy-based mechanistic (EBM) approach to characterize cracking and damage quantity.

2.4.2 Continuum damage approach

In continuum damage mechanics, a damaged body is represented as a homogeneous continuum on a scale that is much larger than the flaw size. Continuum theories consider a damaged body with some stiffness to be an undamaged body with reduced stiffness. The Kachanov-Robotnov (K-R) continuum damage mechanics (CDM) theory [77, 78] is a pioneer for material damage modeling using a variable or damage density ϕ , such that

$$\phi = 1 - \frac{\sigma^{(A)}}{\sigma^{(T)}} \quad (2.14)$$

where

$\sigma^{(A)}$ is apparent stress acting on the total material area, and

$\sigma^{(T)}$ is effective (true) stress acting on the intact material area.

A more accurate damage density function is expressed as follows:

$$\sigma_{ij}^- = \frac{\sigma_{ij}}{(1 - \phi)^2} \quad (2.15)$$

Where,

σ_{ij}^- is the effective stress tensor in the undamaged configuration,

σ_{ij} is the nominal Cauchy tensor in the damaged configuration.

Several continuum damage models were developed for creep and fatigue damage modes at macroscopic level [79, 80, 42]. The classical damage models are defined as a function of strain rate, stress, strain and stiffness, etc. such that, $d\phi/dt = f(\sigma, d\varepsilon/dt, \varepsilon_a, E)$.

The most convenient method available for viscoelastic materials that accounts for microstructural changes in the material is Schapery's work potential theory, which is based on the principles of thermodynamics [81, 82]. The state of damage was quantified using internal state variables (S).

The most convenient method available for viscoelastic materials, which accounts for microstructural changes in the material, is viscoelastic continuum damage (VECD). The constitutive model is based on Schapery's work potential theory [81, 82] which quantify damage as internal state variable (S) based on thermodynamics principles and elastic-viscoelastic corresponding principles [13].

The damage theory for elastic materials is generalized for viscoelastic materials using this correspondence principle. The derivation of the uniaxial VECD model begins with the assumption of damage behavior or damage evolution law, expressed as follows.

$$\frac{d(S)}{d(t)} = \left(-\frac{dW^R}{dS} \right)^\alpha \quad (2.16)$$

where

W^R is the pseudo strain energy,

S is the accumulated damage related to microstructure change,

α is a unique material property related to the rate of damage evolution [83].

The simplified VECD (S-VECD) model is formulated by considering the stiffness reduction to be defined by the pseudo-stiffness reduction [83, 84, 85, 82, 86]. Ac-

According to the correspondence principle, viscoelastic problems can be solved using elastic solutions when physical strains are replaced by pseudo-strains. The uniaxial pseudo strain ε_i^R is defined as

$$\varepsilon_i^R = \frac{1}{E_R} \int_0^t E(t - \tau) \frac{d\varepsilon}{d\tau} d\tau \quad (2.17)$$

where,

$E(t)$ is the relaxation modulus and

E_R is reference modulus (unit modulus is often taken) ($E_R = \sigma/\varepsilon^R$).

Pseudo-stiffness is expressed as the slope of the stress function and pseudo-strain.

$$C = \frac{\sigma(t)}{\varepsilon_i^R} \quad (2.18)$$

The maximum pseudo-strain energy is expressed as a function of ε_i^R and pseudo-stiffness $C(S)$.

$$W^R = \frac{1}{2} \sigma \varepsilon_i^R = \frac{1}{2} C(S) (\varepsilon_i^R)^2 \quad (2.19)$$

Substituting Equation 2.19 into Equation 2.16, and integrating, the accumulated damage after one load cycle (ΔS) can be computed in a discrete form.

$$\Delta S = \left[-\frac{DMR}{2} (\varepsilon_i^R)^2 (C_i - C_{i+1}) \right]^{\alpha/(1+\alpha)} (\Delta t_R)^{1/(1+\alpha)} \quad (2.20)$$

It is assumed that S and C are zero and one, respectively, before loading is applied. The exponent α was obtained from the slope of the relaxation modulus (m) curve [83]. The damage exponent, which is found to be a stress dependent parameter and shows a direct relationship with the long-term relaxation modulus (like $\alpha = 0.00107E_\infty + 2.62$, E_∞ in MPa) [62], is expressed as

$$\alpha = 1 + \frac{1}{m} \quad (2.21)$$

The relaxation modulus m is obtained from the double logarithmic relaxation modulus master curve.

$$m = \frac{\sum_{n=1}^N -E_n * e^{-t/\rho_n}}{E_\infty + \sum_{n=1}^N (E_n * e^{-t/\rho_n})} \quad (2.22)$$

where E_n and ρ_n are the relaxation moduli and times of Maxwell elements (Prony coefficients), respectively.

The dynamic modulus ratio DMR is a normalization parameter used to normalize specimen-to-specimen variations.

$$DMR = \frac{|E^*|_{fingerprint}}{|E^*|_{LVE}} \quad (2.23)$$

Where,

$|E^*|_{fingerprint}$ is fingerprint dynamic modulus and

$|E^*|_{LVE}$ is dynamic modulus from linear viscoelastic frequency sweep test),

Δt_R is the reduced time of a cycle.

$$\Delta t_R = \frac{1}{\alpha_T} \frac{\Delta N}{10} \quad (2.24)$$

where, α_T is time-temperature shift factor,

ΔN is the number of load cycles between two successive strain amplitudes.

Finally, the C – S relationship was fitted using the following forms:

$$\begin{aligned} C &= 1 - aS^b \\ C &= e^{aS^b} \end{aligned} \quad (2.25)$$

where a and b are model constants.

VECD theory is mostly applied to fatigue damage, and fatigue tests are primarily conducted in uniaxial modes. The three-dimensional formulation was presented by Kim et al. [82].

Chapter 3

Experimental Program

The test materials, parameters, and testing protocols for viscoelasticity, viscoplasticity, and fatigue damage responses are discussed in this chapter. The proposed sequential test procedure is also briefly explained.

3.1 Test Materials

The materials used in the experimental campaign of this study were collected from two asphalt-producing companies in Norway (P1 and P2). Some laboratory mixes were produced according to Norwegian standards. All tested mixtures had a nominal maximum aggregate size (NMAS) of 11 mm (approximately 0.43 in). The mixtures are denoted as AC (or AB), AGB, and SMA (or SKA). The mixtures were used for the surface course according to the Norwegian standard. AGB mixtures are primarily used in low-traffic roads and parking areas. The binder in the AC mixture was pure and polymer modified (PMB). The remaining mixtures contained pure binders. The detailed properties of the mixture are listed in Table 3.1, and the aggregate gradations are shown in Figure 3.1.

Table 3.1: Tested asphalt concrete mixtures properties (produced at mixing plant

S.N	Sample Code	Binder Grade	Binder Type	Binder Content
1	AC-P1	70/100	Pure	5-5.5
2	”	65/105-60	PMB	”
3	AGB-P1	160/220	Pure	5.8
4	SMA-P1	70/100	Pure	”
5	SMA-P2	70/100	Pure	”

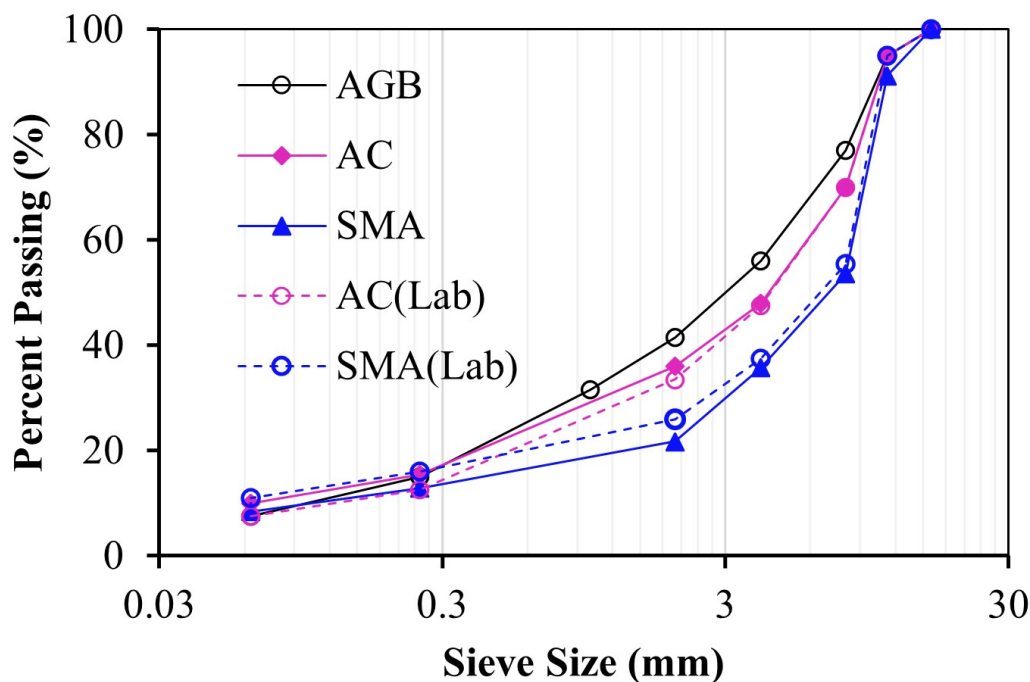


Figure 3.1: Aggregate particle distribution for mixtures (AC, AGB and SMA) produced at mixing Plant and in laboratory

3.2 Specimen Fabrication

Fresh, loose mixtures collected from the mixing plant were transported to the laboratories at NTNU and UiA to produce cylindrical samples using a gyratory compactor. The loose mix was re-heated between $135\text{ }^{\circ}\text{C}$ and $150\text{ }^{\circ}\text{C}$ before compaction. The cylindrical gyratory-compacted specimens were 150 mm in diameter and 180 mm in height. The gyratory machine applied 620 kPa axial pressure, 0.9 to 1.2 gyration angle and a speed of 20 to 30 revolutions per minute, and 100 to 115 gyrations. The final test specimens with a diameter of 100 mm and a height of 150 mm were fab-

ricated by coring and cutting the gyratory-compacted samples (as shown in Figure 3.2).



Figure 3.2: Specimen fabrication

3.3 UTM-130 Testing System

A servo-hydraulic Universal Testing Machine (UTM 130) manufactured by IPC global®¹ is used to perform different tests in this study. The machine can exert different axial loading pulses such as sinusoidal, haversine, rectangular, and creep pulses over a wide range of frequencies in controlled strain or stress modes. An integrated multiaxis control system (IMACS) and a PC were used to control and operate the machine (Figure 3.3). The IMACS is responsible for passing all commands from the UTS program running on the system PC to various hardware components to control them. It is also responsible for collecting data from all the system's sensors and transducers and transmitting it to the UTS program on the PC. The IMACS uses low-noise electronic signal conditioning technology, software-averaging techniques, and transducer response linearization algorithms, enabling a wide dynamic range and excellent accuracy, repeatability, and operator performance. The machine is

¹More information about UTM-130 and Jigs at www.controls-group.com/ipcglobal

outfitted with an environmental chamber (from $-50\text{ }^{\circ}\text{C}$ to $+100\text{ }^{\circ}\text{C}$) and confining pressure cell for confined tests. The tests performed to investigate the mechanical properties of asphalt concrete included dynamic modulus, resilient modulus, indirect tensile test, cyclic compression (creep recovery), uniaxial fatigue (S-VECD), and creep tests.

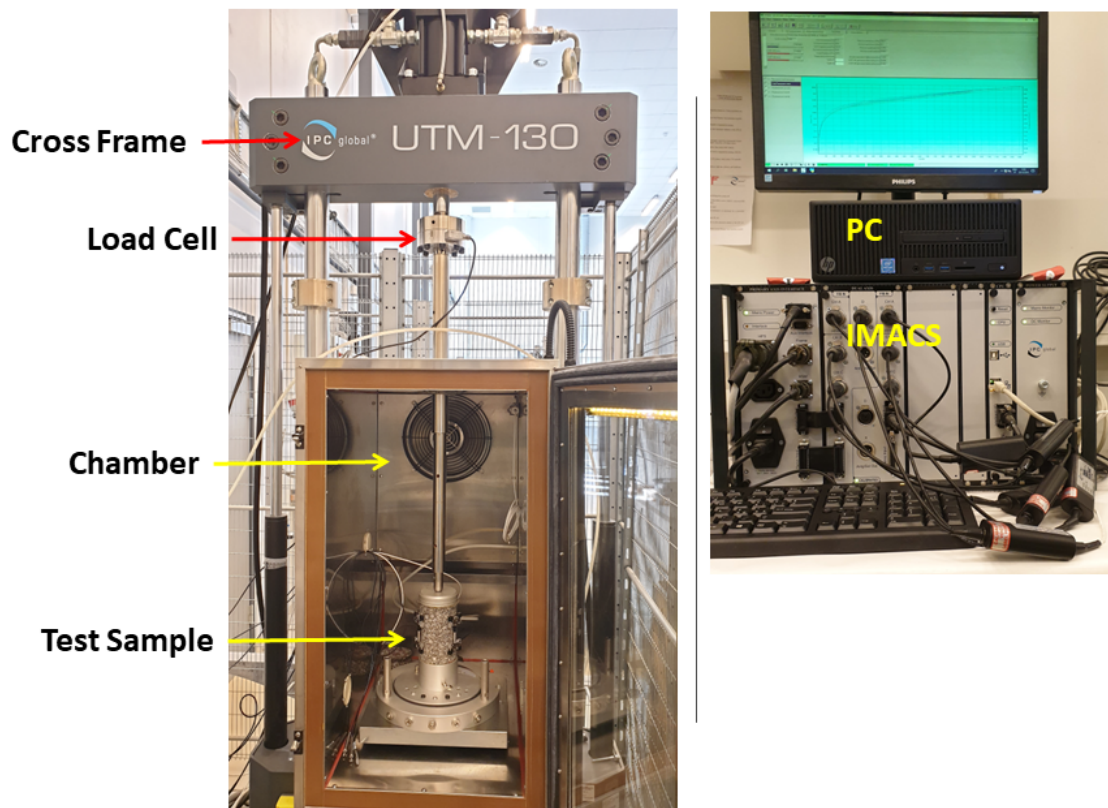


Figure 3.3: (a) The Universal testing machine (b) IMACS and PC

The tests included characterization of the linear viscoelastic (undamaged) state, damage tests such as permanent deformation, fatigue cracking, fracture strength, crosshead strain rate tests, and others at different test control conditions. The conditioning time of the test specimen depended on the test temperature and sample size (height/diameter ratio) (Table 3.2).

3.3.1 Dynamic Modulus Test

Dynamic modulus tests are commonly used to investigate the viscoelastic properties of asphalt concrete owing to their convenience in the laboratory. The tests are performed in a uniaxial or triaxial setup and in diametrical modes. The first

Table 3.2: Sample conditioning time at different temperatures

Temperature $^{\circ}C$	-10	5	21	40	55
$h/d(1.5)$	12	12	4	4	4
$h/d(0.5)$	6	6	3	2	2

mode of testing was the axial compression dynamic modulus test in accordance with AASHTO T378-17 (2017) over a wide range of frequencies (from high to low) and temperatures (from low to high). The test was performed in a controlled-strain mode with a target on-specimen strain amplitude of 50 micro-strain ($\mu\varepsilon$) to get a linear viscoelastic response. Three sets of loose core-type linear variable differential transducers (LVDTs) were mounted radially apart at 120 degrees with a 70 mm gauge length to measure the strain responses under a sinusoidal load (Figure 3.4a). The second type of dynamic modulus test was the diametrical IDT mode in accordance with EN 12697-26 (CEN, 2018) (Figure 3.4b).

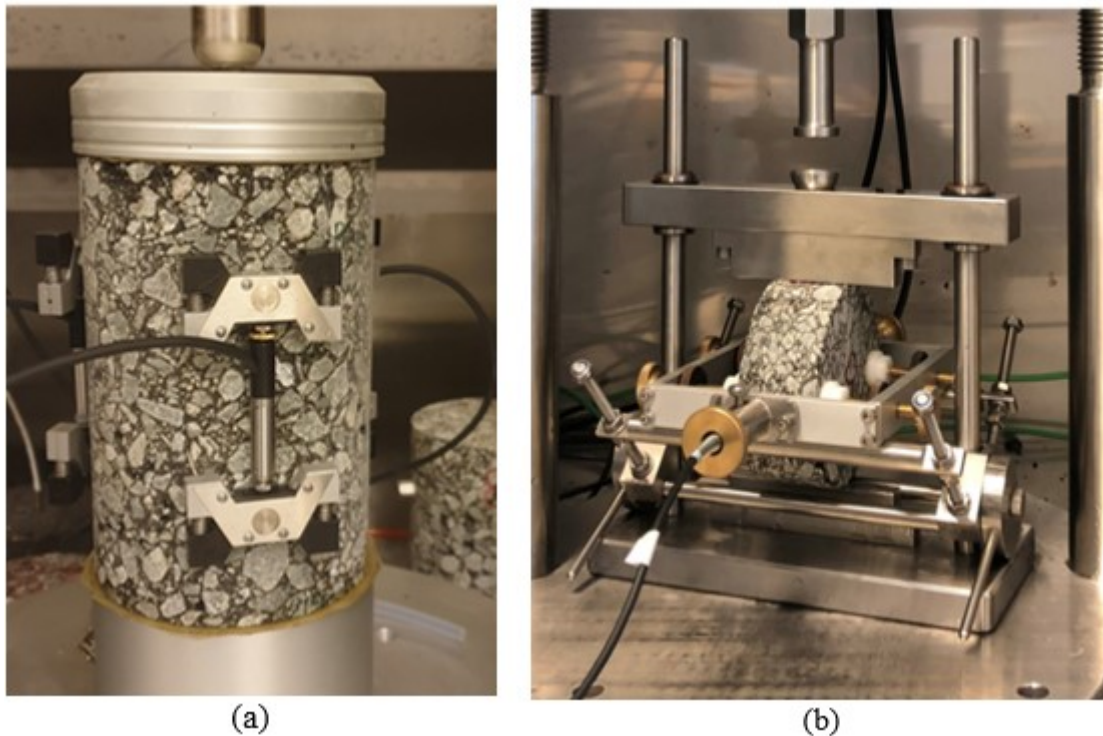


Figure 3.4: Dynamic modulus tests (a) Uniaxial test setup (b) IDT test setup

The test parameters are presented in Table 3.3. In the confined (triaxial) dynamic modulus test, confining pressures ranging from 0 to 300 kPa were applied at

each test temperature. The confining pressure was maintained constant at all the frequencies at a specified temperature.

Table 3.3: Confined and unconfined dynamic modulus test conditions

Test Mode	Axial	IDT
Frequency (Hz)	25,10,5,2,1,0.5,0.2,0.1	25,10,5,2,1,0.5,0.2,0.1
Temperature($^{\circ}C$)	-10,5,21,40,55	-10,5,10,21,30
Confining Pressure (kPa)	0,10,100,200,300	–
Control – Strain($\mu\varepsilon$)	50	50

In strain-controlled tests, the strain response always lags behind the stress in time (phase angle) for a viscous material under a sinusoidal load. (Figure 3.5).

$$\sigma(t) = \sigma_o \sin(\omega t) = \sigma_o e^{i\omega t} \quad (3.1)$$

$$\varepsilon(t) = \varepsilon_o \sin(\omega t - \varphi) = \varepsilon_o e^{i(\omega t - \varphi)} \quad (3.2)$$

Where σ_o and ε_o are, respectively, the axial stress and axial strain amplitudes, ω is the angular frequency (Hz), and ($i^2 = -1$).

The phase angle φ is a frequency-dependent measure of strain lag. The dynamic modulus, E^* , is a complex number defined by the ratio of the dynamic stress to dynamic strain, as follows:

$$E^* = \frac{\sigma_o}{\varepsilon_o} (\cos \varphi + i \sin \varphi) = E' + iE'' \quad (3.3)$$

$$|E^*| = \frac{\sigma_o}{\varepsilon_o} = \left| \sqrt{(E')^2 + (E'')^2} \right| \quad (3.4)$$

where the storage modulus, E' , and the loss modulus E'' , represent the real and imaginary components of E^* and $|E^*|$ is the norm of complex modulus. The storage and loss moduli were also related to the norms of the dynamic modulus.

$$E'(\omega) = |E^*(\omega)| \cos \varphi(\omega) \quad (3.5)$$

$$E''(\omega) = |E^*(\omega)| \sin \varphi(\omega) \quad (3.6)$$

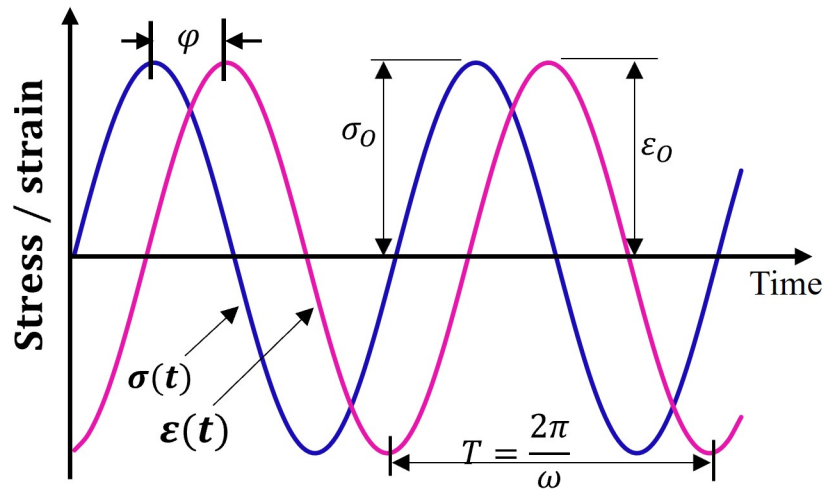


Figure 3.5: Schematic of sinusoidal Stress and strain response in dynamic modulus

3.3.2 Indirect Tensile Test

The IDT test mode was used for different tests such as resilient modulus, fracture, and strength tests. In the IDT mode, the biaxial stress and strain in the horizontal direction owing to the vertical compressive load along the specimen diameter were recorded. The dynamic modulus using the IDT mode was calculated from five cycles per test according to European Norm EN 12697-26 (CEN, 2018) (Figure 3.6). The other tests performed using the IDT mode are summarized in Table 3.4.

Table 3.4: Test parameters used in the IDT testing mode

Test Type	Temperature $^{\circ}C$	Loading (Rest) (sec)	Strain rate ($\mu\varepsilon/min$)	Displacement (mm/min)
Resilient Mod- ulus	5,10,21,30,40	0.1(0.9)	-	-
Strength	5,10,15,21,30	-	-	50
Strain rate	-	-	500,600,900, 1000,5000, 10000	-

3.3.3 Cyclic Creep-Recovery Test

Repeated creep and recovery tests were conducted in both the uniaxial and triaxial states to predict permanent deformation using haversine (Figure 3.6a) and block loading (Figure 3.6b) pulses, in accordance with the EN 12697-25 and AASHTO T378 standards. The test parameters are listed in Table 3.5. A standard triaxial cell was used for confinement test with air pressure as confining medium (Figure 3.7).

Table 3.5: Uniaxial and Triaxial Compression creep-recovery test parameters

S.N	Pulse	Temperature $^{\circ}C$	Loading (Rest) (sec)	Axial Stress (MPa)	Confining Pressure (kPa)
1.	Haversine	21,30,40,50	0.1(0.9) 0.4(1.6)	0.5 - 2	50,100,150
2.	Block	40	1.0(1.0)	0.2, 0.3	100,200

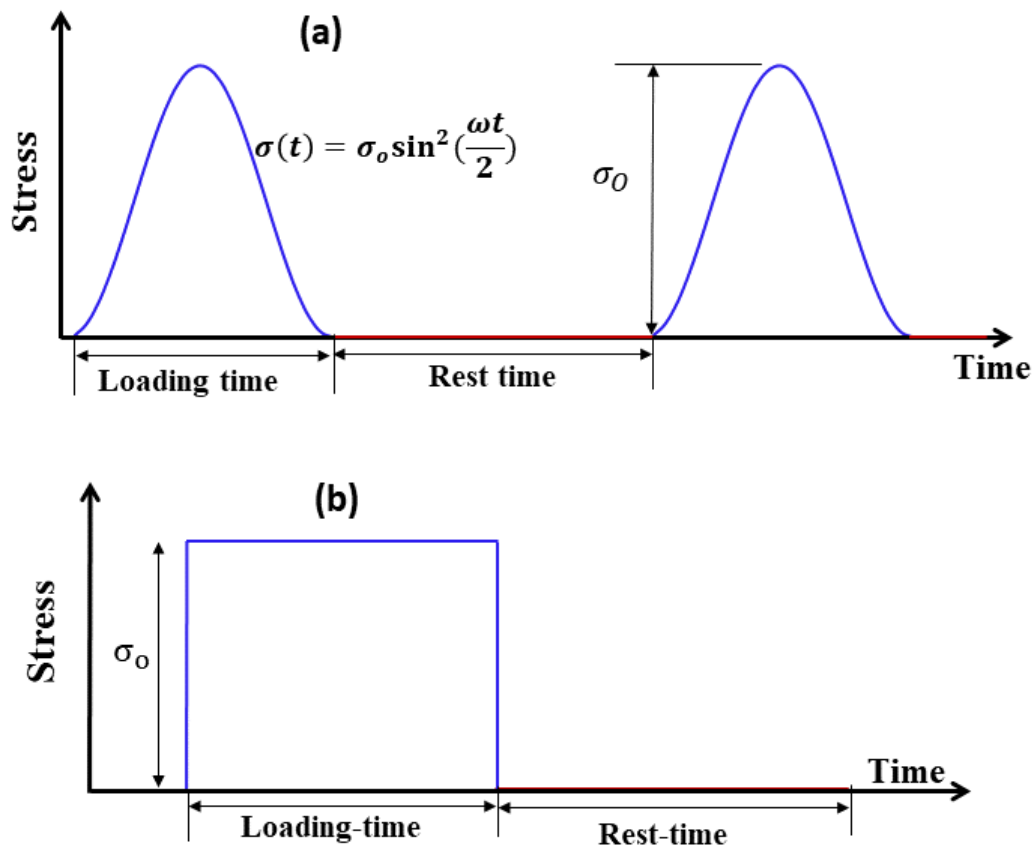


Figure 3.6: (a) Haversine loading pulse (b) Block loading pulse

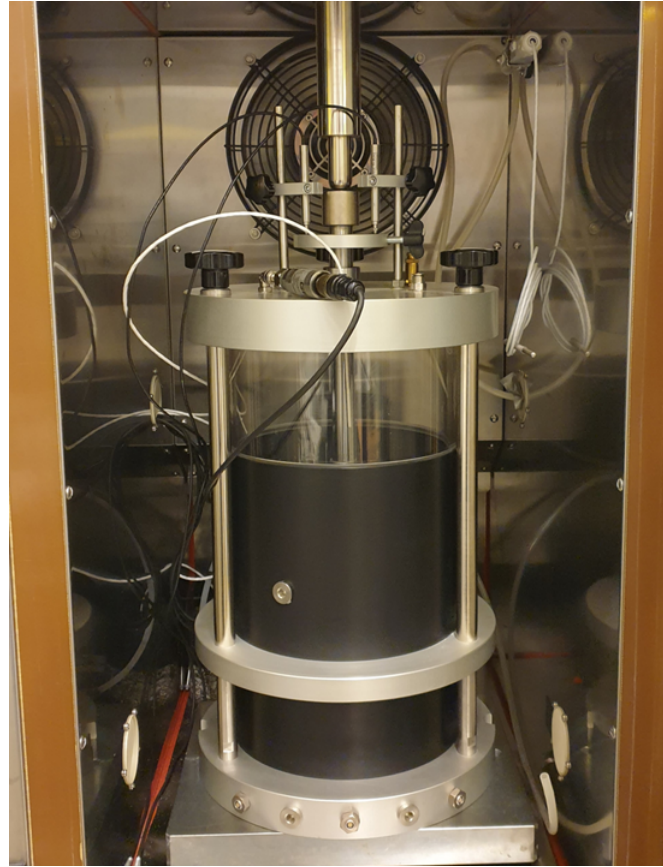


Figure 3.7: Triaxial testing system

3.3.4 Uniaxial Fatigue Test

Cyclic tension-compression or tension-tension fatigue tests were conducted to characterize the fatigue damage resistance of the asphalt concrete. The control strain tests were conducted at a constant frequency of 10 Hz (Table 3.6). The test was performed using a sinusoidal load in accordance with the AASHTO TP107 protocol (AASHTO, 2017). The uniaxial fatigue test specimen was prepared by gluing the end plates using Devcon plastic steel putty epoxy and a gluing jig (Figure 3.8). Three on-specimens and one external LVDT was used to measure the strain.

Table 3.6: Summary of Uniaxial fatigue test Parameters

S.N	Temperature $^{\circ}C$	Frequency (Hz)	Target Strain ($\mu\varepsilon$)	Mode
1.	10,15,21,30	10	100,150,200, 300,400	Tension-Tension, Tension-compression

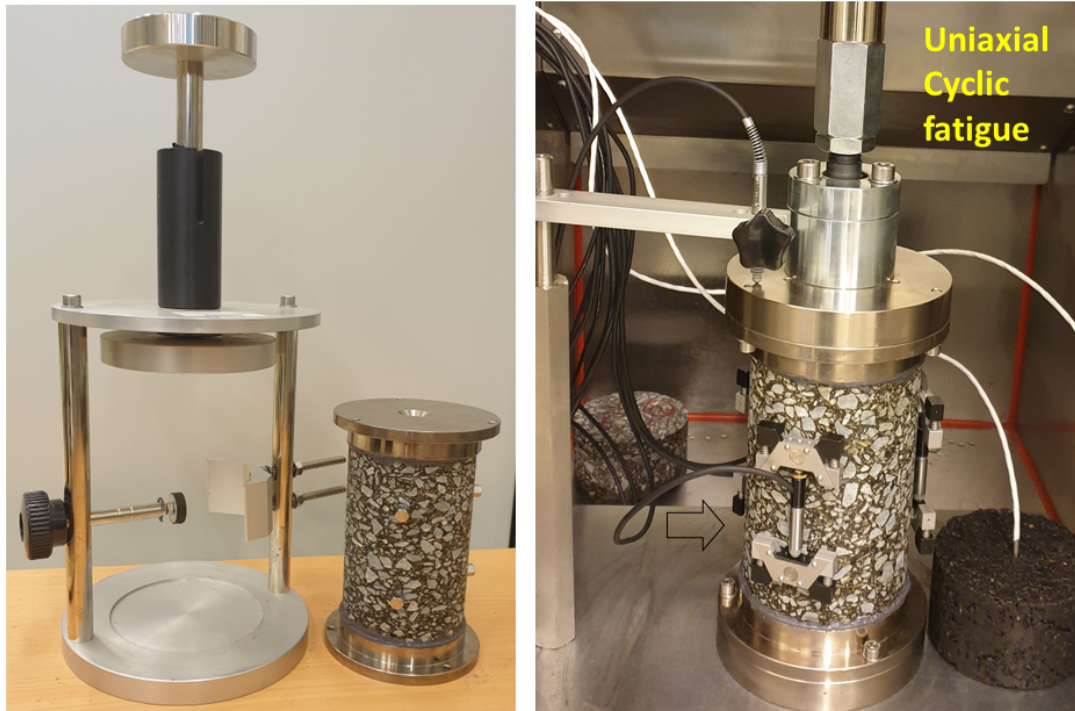


Figure 3.8: (a) sample plate gluing jig (b) fatigue test setup for T-T and T-C

3.4 The proposed Sequential Test procedure

Creep (permanent deformation) and fatigue damage interactions have been studied for homogeneous and non-rheological materials, such as steel [87, 88], rock [89]. Attempts have also been made to improve asphalt concrete. However, the interaction between creep and fatigue in thermorheological asphalt concrete materials is complex. One of the limitations of these studies is the unavailability of fatigue-rutting interaction testing protocols. A common approach to assess the influence of initial damage is to test field samples in the laboratory. The drawback of this technique is that the core samples from the field are short, and the asphalt layer contains multiple overlays. In this study, a sequential test procedure (STP) was proposed to investigate the interaction between permanent deformation and fatigue cracking damage based on the sequential damage assumption. Figure 3.9 shows the test specimen instrumentation. The STP was performed using two sequences: permanent deformation–fatigue (PD-F) and fatigue–permanent deformation (F-PD). Therefore, each specimen was subjected to fatigue and permanent deformation damage in both

sequences.

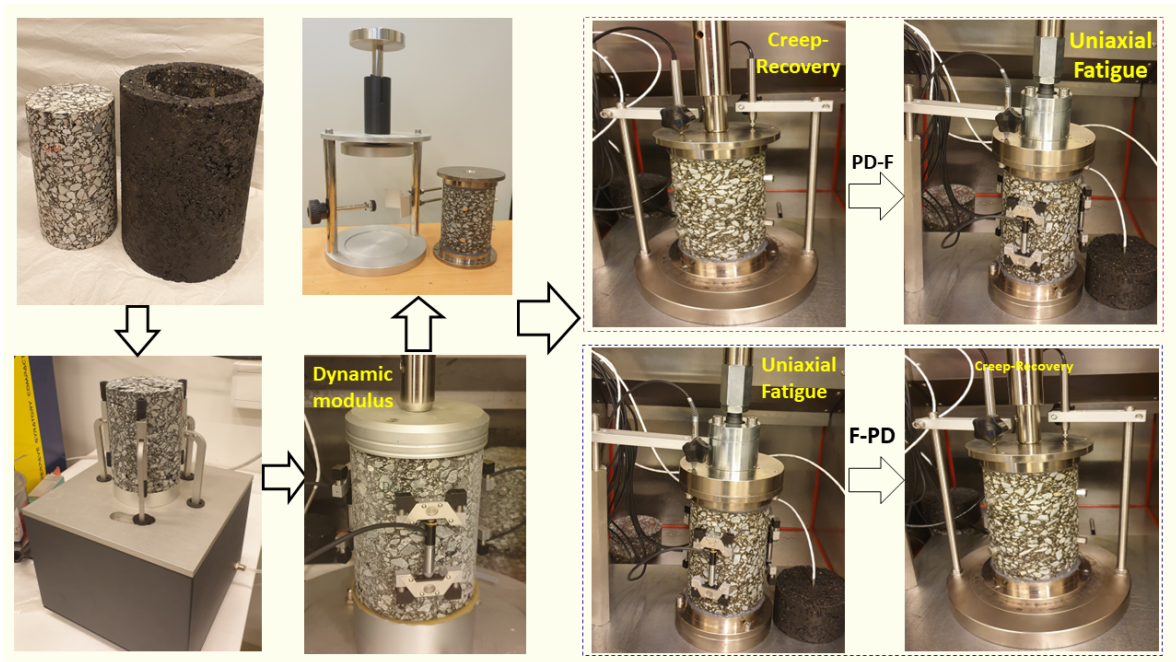


Figure 3.9: Sequential Test instrumentation

3.4.1 The PD-F sequence

The rationale for the permanent deformation-fatigue or creep-fatigue sequence is the observation that viscoplastic hardening and deformation can develop prior to fatigue cracking. This phenomenon simulates the early service life of asphalt concrete pavements, which is dominated by volumetric densification. In the PD-F sequence, a test was conducted to cause strain hardening within the steady-state stage (secondary phase) before the flow number was reached. The flow number is a common failure criterion for creep damage, and the permanent strain at the flow number is referred to as the failure strain. The permanently deformed or strain hardened specimens are then tested in cyclic Tension-Compression and/or Tension-Tension fatigue tests (in a controlled-strain mode) at intermediate temperatures of $10\text{ }^{\circ}\text{C}$ (Figure 3.10).

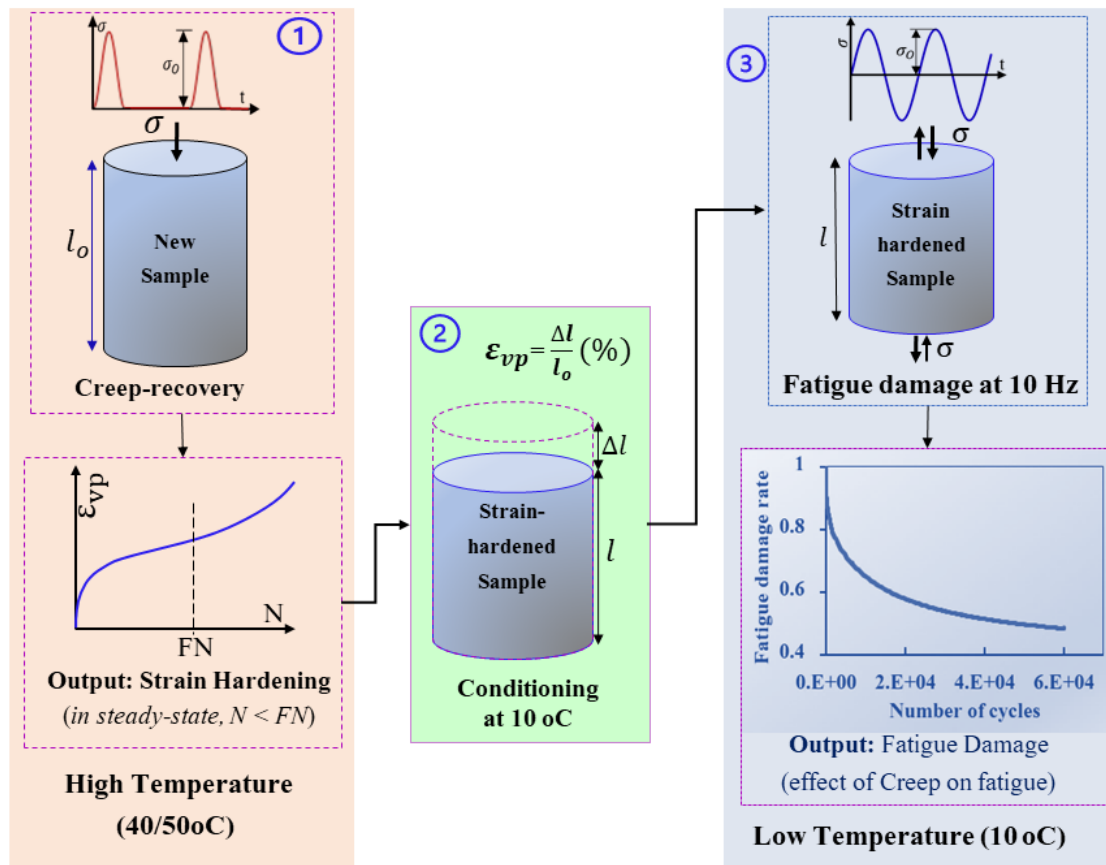


Figure 3.10: Schematic of Permanent deformation - Fatigue sequence (PD-F)

3.4.2 The F-PD sequence

The fatigue-permanent deformation (or the fatigue-creep) sequence was intended to simulate the occurrence of fatigue cracking prior to permanent deformation. This phenomenon is expected in cold-climate areas (seasons) and thick pavements. Perpetual and thick pavements can undergo surface cracking without significant viscoplastic deformation (aggregate movement and reorientation). In the F-PD sequence, the specimens are first tested for TC or TT fatigue at different target strains and intermediate temperatures. The fatigue damage level is not reached until failure (i.e., not up to 50 percent stiffness reduction). Each fatigue-damaged specimen is then tested for permanent deformation at higher temperatures of 30 or 40 °C (Figure 3.11).

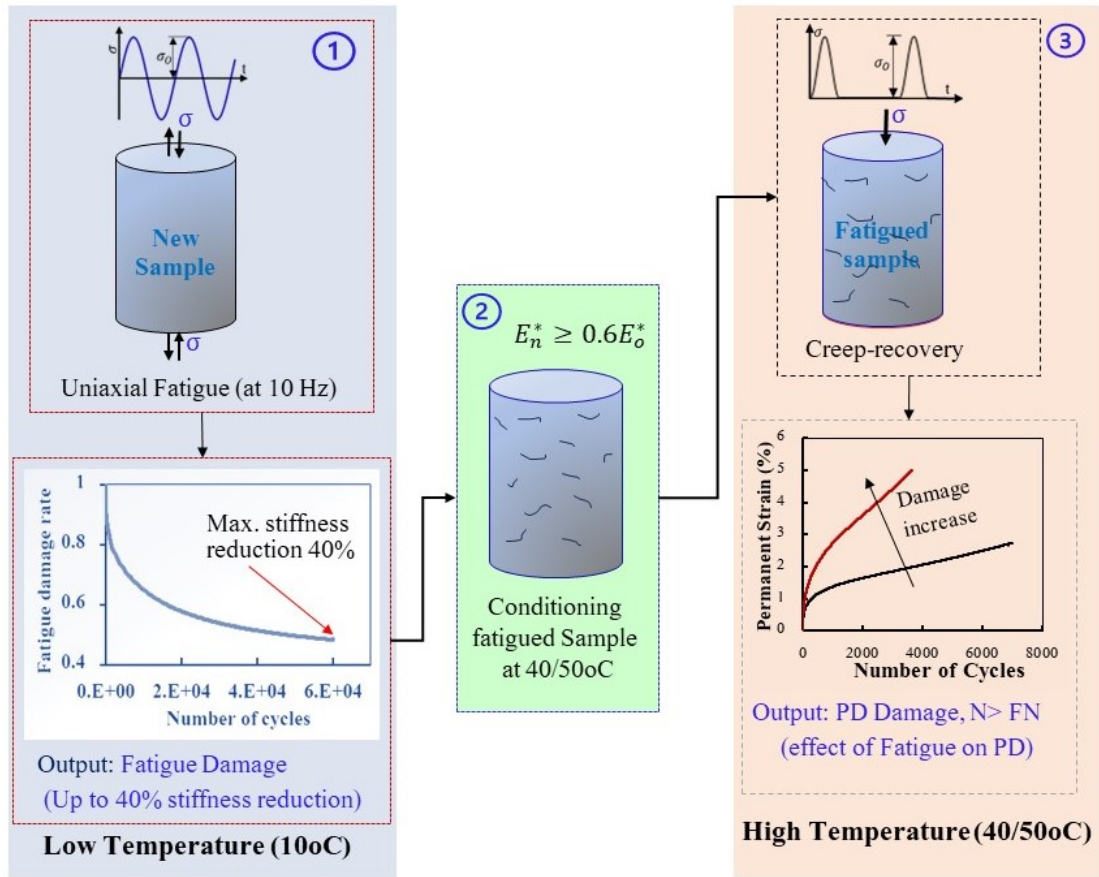


Figure 3.11: Schematic of Fatigue - Permanent deformation sequence(F-PD)

Chapter 4

Viscoelastic Response

This chapter presents the results of LVE analyses using axial compression dynamic modulus and the Indirect Tensile (IDT) test modes. The axial compression tests are performed in uniaxial and triaxial modes. Three test campaign results and modeling are briefly discussed in the frequency or time domain LVE responses of different AC mixtures.

4.1 Linear Viscoelastic Response

The viscoelastic response of asphalt concrete was investigated using small-strain frequency sweep tests. The time-temperature superposition principle (TTSP) was applied to characterize the time and temperature dependent LVE behavior of asphalt concrete, $E^*(f, T)$. Master curves of stiffness (dynamic modulus, resilient modulus) were constructed using the TTSP by ‘shifting’ the data along the loading time or frequency axis. Temperature shifts require an arbitrarily selected reference temperature (T_0). Depending on the shift factor α_T , the data shifted to the left (i.e., $\alpha_T < 1$) or right (i.e., $\alpha_T > 1$) from the reference temperature. In the triaxial tests, master curves were constructed with horizontal and vertical shifts of stiffness at a reference pressure and temperature. In this study, two master curve models were used to construct stiffness master curves. The first was a mathematical sigmoid function [90].

$$\log(E^*) = \delta + \frac{(\alpha - \delta)}{1 + \exp[\beta - \gamma * \log(f_R)]} \quad (4.1)$$

where,

δ and α are the minimum and maximum

$\log E^*$, η and γ are shape factors.

The second model was the mechanical model, referred to as the *2S2P1D* model (2-Springs, 2-Parabolic creep elements, and 1-Dashpot) [91], as shown in Figure 4.1.

The model is expressed as follows:

$$E^*_{2S2P1D}(\omega) = E_\infty + \frac{(E_o - E_{oo})}{1 + \delta(i\omega\tau)^{-k} + (i\omega\tau)^{-h} + (i\beta\omega\tau)^{-1}} \quad (4.2)$$

where,

δ , k , h are constants ($0 < k < h < 1$),

ω is the angular frequency,

E_{oo} is static modulus ($\omega \rightarrow 0$),

E_o is the glassy modulus ($\omega \rightarrow \infty$),

β is a constant that depends on the viscosity of the dashpot ($\eta = (E_o - E_{oo})\beta\tau$),

η is the Newtonian viscosity of the dashpot,

τ is the characteristic time ($\tau = \alpha_T\tau_o$), where τ_o is determined at a reference temperature.

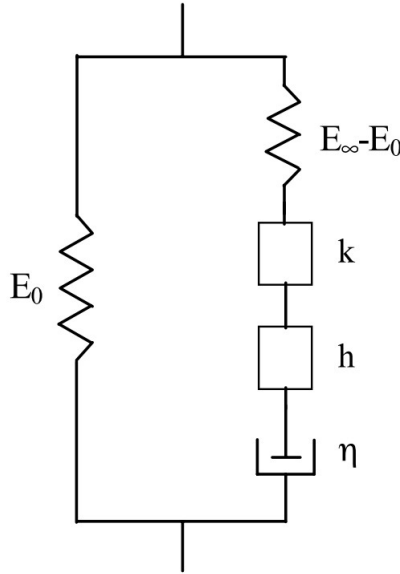


Figure 4.1: Representation of the introduced general model “2S2P1D” for both bituminous binders and mixes, h and k are two parabolic creep elements

The common Williams, Landel, and Ferry (WLF) [92] shift function was used in this study for the uniaxial LVE and isothermal conditions at a constant pressure

(mostly atmospheric).

$$\log(\alpha_T) = \frac{-C_1(T - T_{ref})}{C_2 + (T - T_{ref})} \quad (4.3)$$

where,

C_1 and C_2 are WLF constants and

T_{ref} is reference temperature.

The stress-dependent LVE properties were predicted by combining the isobaric and isothermal behaviors using triaxial tests. In this study, a modified version of the Fillers-Moonan-Tschoegl (FMT) model [93] was proposed and validated using triaxial dynamic modulus tests of different asphalt concrete mixtures. The proposed triaxial shift function takes the following form:

$$\log(\alpha_{T,P}) = \frac{-C_1[T - T_{ref} - \Gamma(p)]}{C_2(p) + [T - T_{ref} - \Gamma(p)]} \quad (4.4)$$

$$\Gamma(p) = (C_{30} + C_{31}P) \ln \frac{1 + C_4P}{1 + C_4P_o} \quad (4.5)$$

$$C_2(p) = C_{20} + C_{21}P \quad (4.6)$$

where,

P is experimental pressure,

P_0 is reference pressure (100kPa in this study),

$\Gamma(p)$ accounts for the compressibility attributed to the collapse of free volume ,

$C_{20}, C_{21}, C_{30}, C_{31}$ and C_4 are constants.

Time-domain LVE properties are more commonly used in practice and for comparison with other elastic responses, such as the resilient modulus. Thus, the relaxation modulus was obtained from the storage modulus using the following equation:

$$E'(\omega) = E_\infty + \sum_{m=1}^M \frac{\omega^2 \rho_m^2 E_m}{1 + \omega^2 \rho_m^2} \quad (4.7)$$

where,

E_m is the elastic stiffness of the General Maxwell elements

ρ_m is relaxation times of GM elements ($\rho_m = \eta_m/E_m$)

η_m is viscosity coefficients of the Maxwell elements.

4.1.1 Uniaxial Viscoelastic Response

Several asphalt concrete mixtures were investigated in the LVE domain in both uniaxial and triaxial states. LVE characterization is mostly conducted in uniaxial tests, and the dynamic modulus and phase angle data are converted to the relaxation modulus to characterize the thermo-rheological properties in the time-domain response, that is, the relaxation modulus (**Paper B, C and F**). Figure 4.2 and Figure 4.3 show the dynamic stiffness master curves and shift factors of different tested mixtures under uniaxial conditions at 21 °C reference temperature. The effects of aging at room temperature on the viscoelastic properties of two different asphalt concrete mixtures were investigated using uniaxial dynamic modulus master curves. The AC-11 and SMA-11 samples were stored at room temperature up to one year, and dynamic modulus tests were performed. As shown in Figure 4.4, both the mixtures clearly exhibited stiffness deterioration at high temperatures and low frequencies. This oxidative aging at room temperature had less of an effect on the low-temperature side of the stiffness. Furthermore, the absolute maximum slope (double log-log relaxation modulus $E(t)$ – time (t) curve) increased owing to hardening. This means that the mixtures were susceptible to both rutting (reduction in stiffness) and fatigue (increase in damage rate α) distresses.

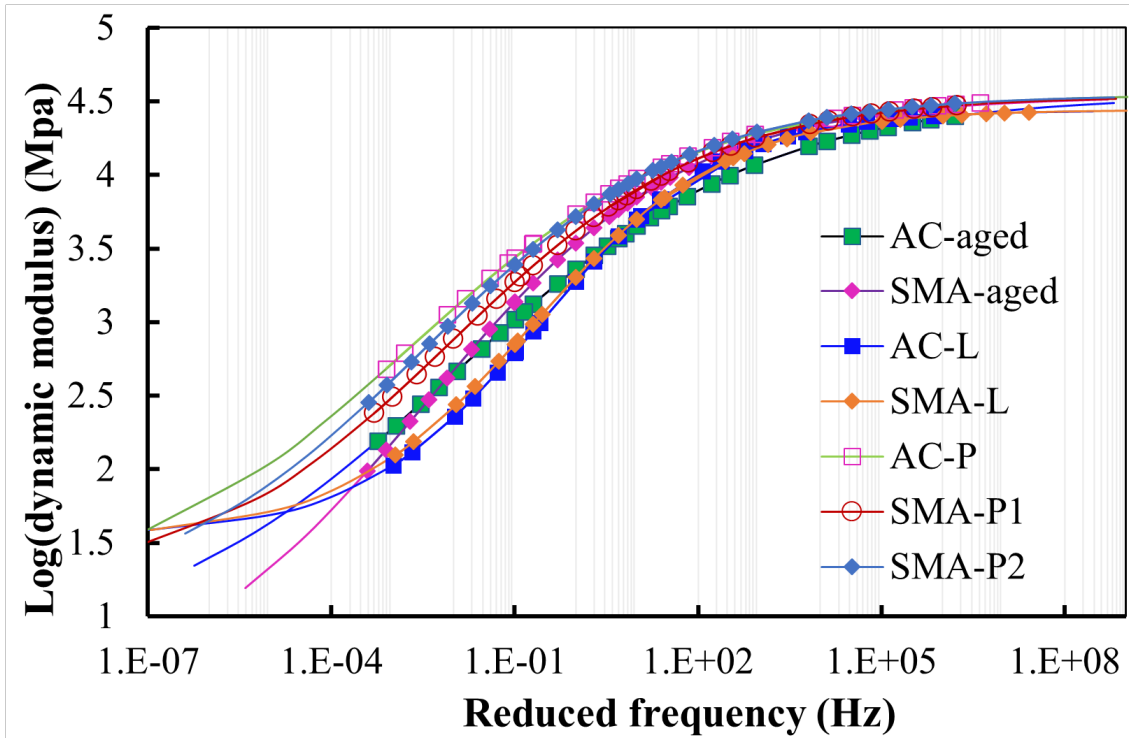


Figure 4.2: Dynamic modulus Master curves of different asphalt concrete mixtures (adapted from **Paper E**)

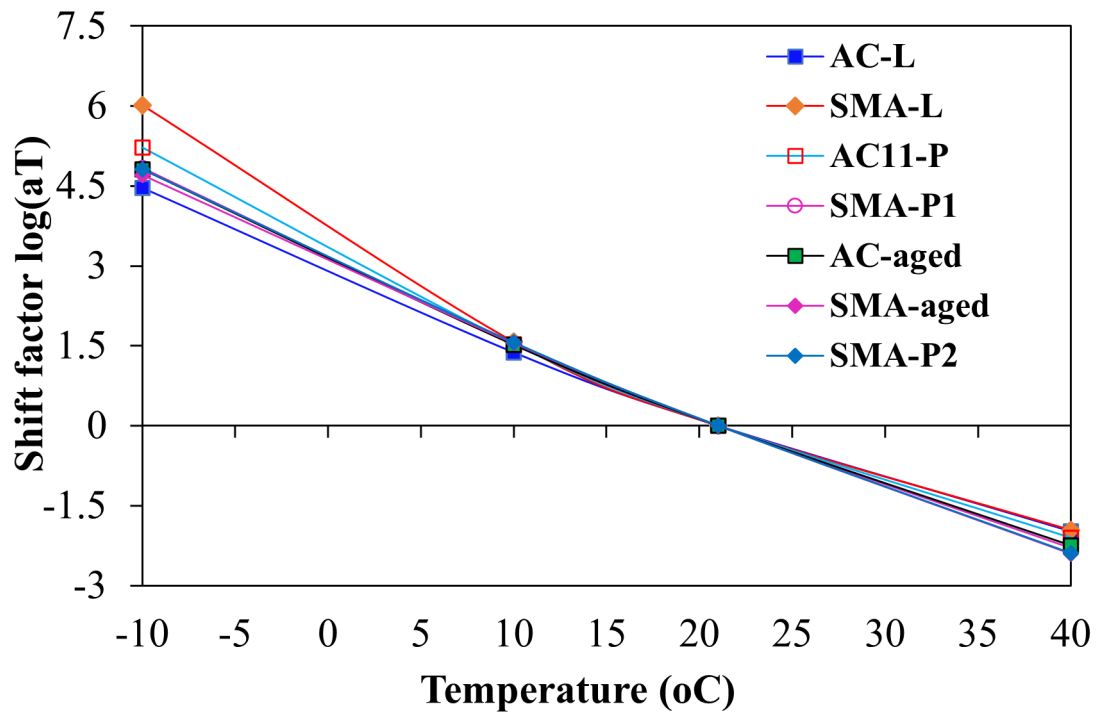


Figure 4.3: Uniaxial, Isothermal shift factors ($\log \alpha_T$)

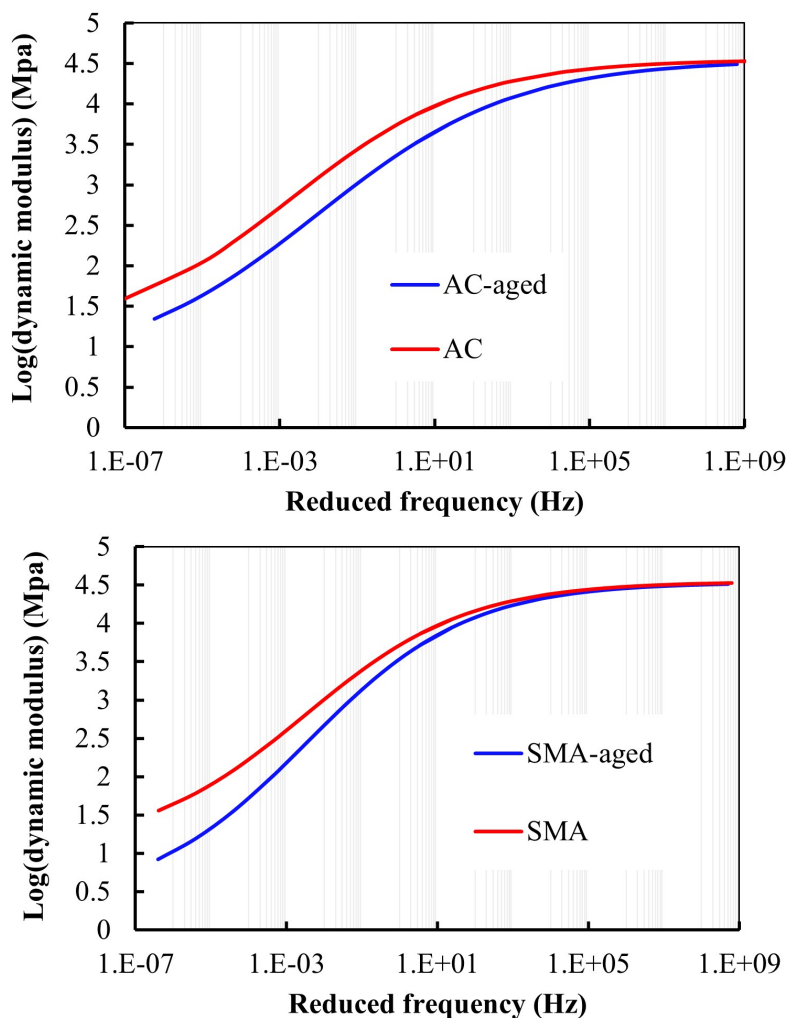


Figure 4.4: Effect of one year storage - aging at room temperature on the dynamic modulus of AC-11 and SMA-11 mixtures

4.1.2 Stress-dependent viscoelastic response

Generally, the linear viscoelastic properties of asphalt concrete mixtures are analyzed using uniaxial test methods at atmospheric pressure. The response of linear elastic materials is generally stress-path-independent. An extensive investigation was conducted to model the time-, temperature-, and pressure-dependent responses of asphalt concrete in linear viscoelastic range. The thermo-piezo-rheological simplicity of the tested mixtures was verified using the superposition principle [62]. Triaxial dynamic modulus tests were conducted over wide ranges of frequencies (times), temperatures, and pressures (confining stresses). A standard triaxial cell was used, with air as the confining medium. The confining pressure was maintained

constant during the testing. Although constant confining loading does not simulate the actual loading path in a pavement, constant confining pressure represents the residual stresses trapped in the AC layer after the load passes or a standing vehicular load on the pavement [94].

As shown in Figure 4.5, the role of confining pressure is visible on the high-temperature side of the dynamic modulus.

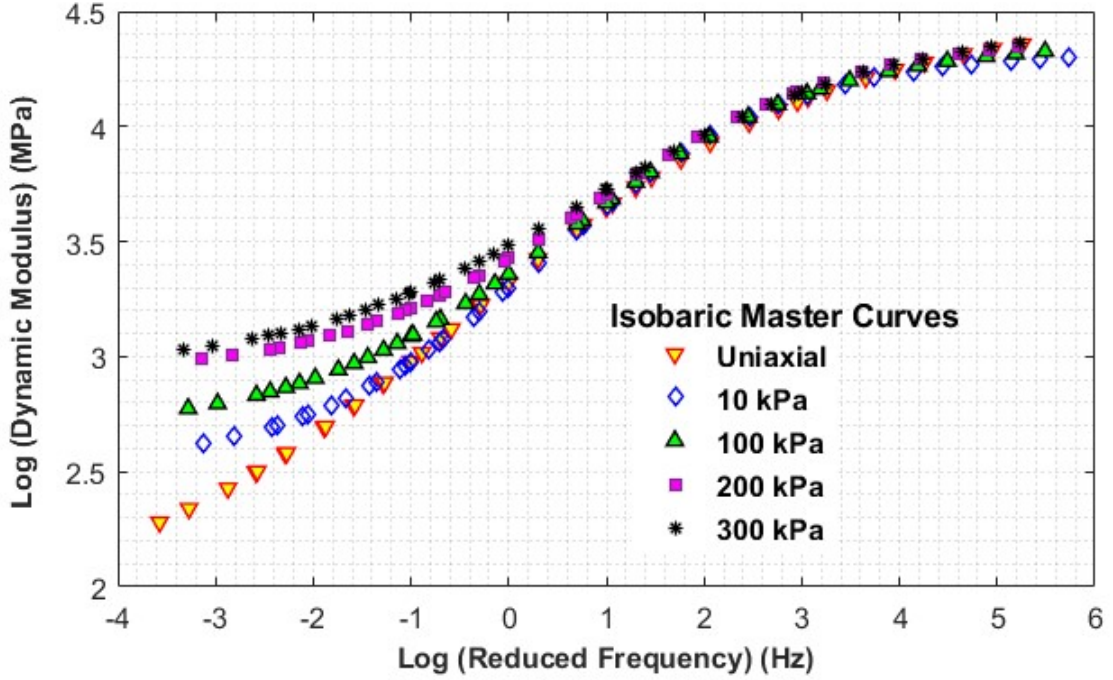


Figure 4.5: Triaxial master curves at 21°C (a) Isobaric master curves (b) vertical or triaxial master curves (adapted from **Paper B**)

Confinement increased the interlocking between aggregate particles and retarded binder flow in asphalt concrete mixtures at intermediate and high temperatures. It also decreased the flow or strain rate and increased the dynamic and relaxation moduli.

4.1.2.1 Triaxial Master curve

A new triaxial shift function was proposed [62] based on the FMT free volume theory [93, 95] and the WLF [92] function, as expressed in Equation 4.8 .

$$\log(\alpha_{T,P}) = \frac{-C_1[T - T_{ref} - \Gamma(p)]}{C_{22} + C_{23}(p) + [T - T_{ref} - \Gamma(p)]} \quad (4.8)$$

where $\Gamma(p)$ is the parameter accounting for the compressibility of the free volume, and C_{22} , C_{23} , C_1 are the model coefficients. The triaxial master curve model shifted the measured data in a two-step procedure at a pre-selected reference temperature T_{ref} and pressure P_o . The model became a uniaxial shift function at atmospheric pressure (or zero confining pressure).

1. **Horizontal Shifting:** First, the test data were shifted horizontally at the reference temperature using a time-temperature shift factor.
2. **Vertical Shifting:** The modulus was the shifted vertically at the reference confining pressure using the time-temperature-pressure shift factor.

The triaxial dynamic modulus master curve was successfully constructed using Equation 4.8, as shown in Figure 4.6.

Furthermore, the accurate construction of the triaxial master curve alone cannot provide the full viscoelastic behavior of asphalt concrete, particularly the time-domain properties. The property of interest in the time-domain is the relaxation or creep modulus which is the most widely used stiffness parameter in pavement design. Thus, the frequency-domain data were transformed into the time-domain using the Prony series. Two actions were performed. (1) The loss and storage moduli were separated from the frequency-domain dynamic modulus, and (2) The storage modulus data were smoothed using a continuous sigmoid-like function to minimize optimization difficulties for the relaxation modulus. The

The Prony method was then applied to obtain the relaxation modulus master curves from the pre-smoothed storage modulus data. The isobaric and triaxial relaxation modulus master curves are shown in Figure 4.6. From the time domain viscoelastic analyses, it was apparent that the long-term relaxation modulus, maximum slope of the relaxation modulus curve (double logarithmic), and fatigue damage rate parameter were the most sensitive to the confining stress (Figure 4.7). The long-term relaxation modulus is a stiffness that determines the recovery potential of asphalt concrete over a long loading period. As discussed in the literature section,

the confining pressure is the residual stress stored between aggregates or the trapped stress that improves the elasticity of asphalt concrete. Thus, deformability and fatigue susceptibility were reduced. Now, triaxial tests are selected in-lieu of uniaxial tests, not only for viscoplastic flow analysis, but also for LVE modeling [96, 62].

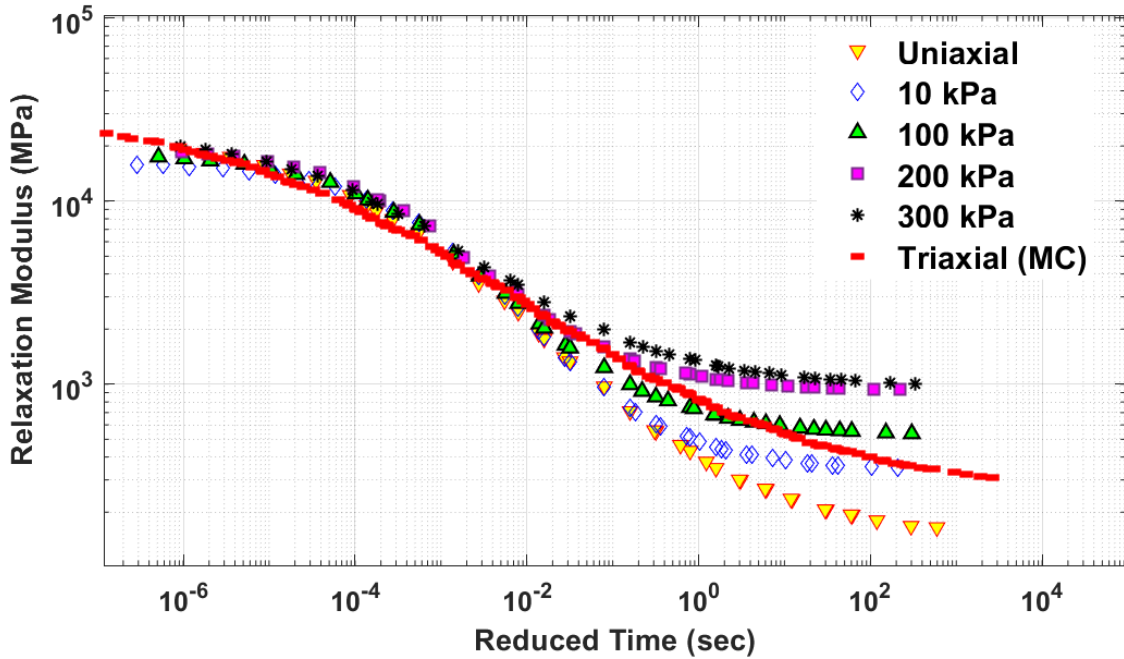


Figure 4.6: Effect of confining pressure on the Long-term relaxation modulus (**Paper B**)

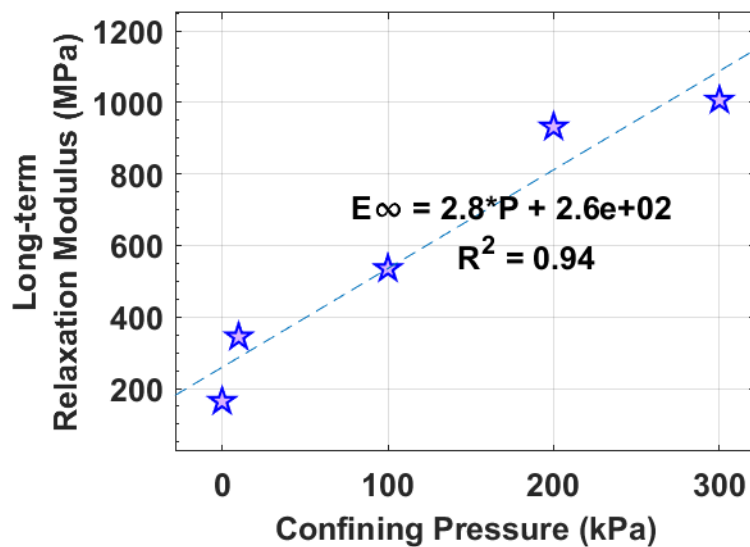


Figure 4.7: Effect of confining pressure on the Long-term relaxation modulus (**Paper B**)

4.1.2.2 Triaxiality ratio

The triaxiality ratio (η) is introduced to model the stress-dependent linear viscoelastic properties of asphalt concrete. As discussed in detail in **Paper B** [62], the stress-dependent LVE can be explained using the stress-ratio parameter in triaxial or vertical shift models. Parameter η is defined as a function of the confining stress σ_c and the deviatoric stress σ_d . The ratio is 1/3 for the unconfined stress-state.

$$\eta = \sigma_c / \sigma_d + \frac{1}{3} \quad (4.9)$$

Thus, the following model in Equation 4.10 was proposed for the triaxial shift function based on the test data:

$$\Gamma(p) = C_7 \eta \ln \left(\frac{1 + C_8 P}{1 + C_8 P_o} \right) \quad (4.10)$$

where C_7, C_8 are coefficients. Therefore, the triaxial test data were fitted using Equations 4.8 and 4.10 to construct the stress-dependent master curves. Both the models fit the data well. The strengths of the triaxiality ratio-based model are its simplicity and the fundamental theory of mechanics. Figure 4.9 shows surface plots of the triaxiality ratio, temperature and pressure. The stress sensitivity of asphalt concrete is important for high thermodynamic variables (temperature and pressure).

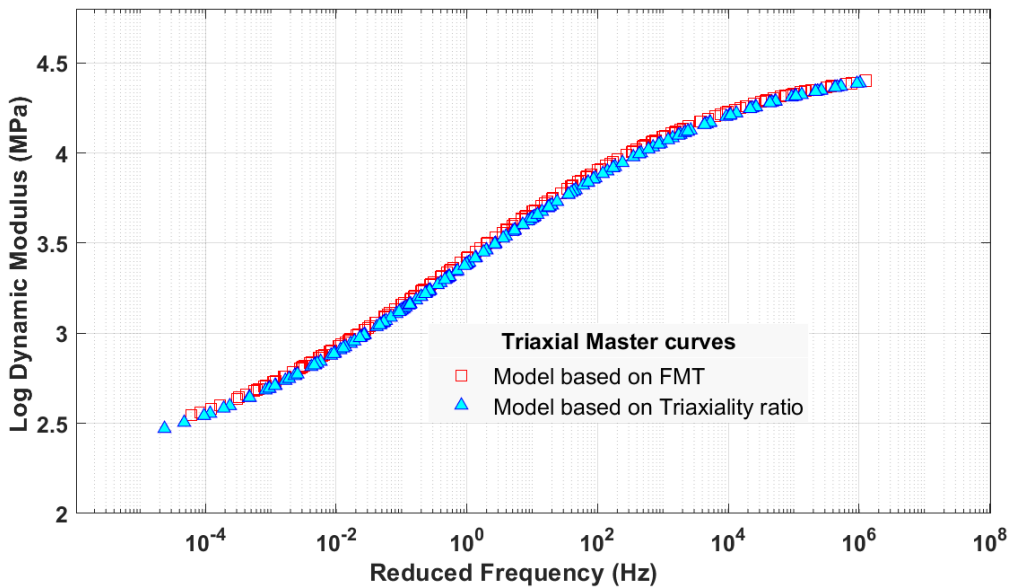


Figure 4.8: Triaxial master curves using the proposed models (adapted from **Paper B**)

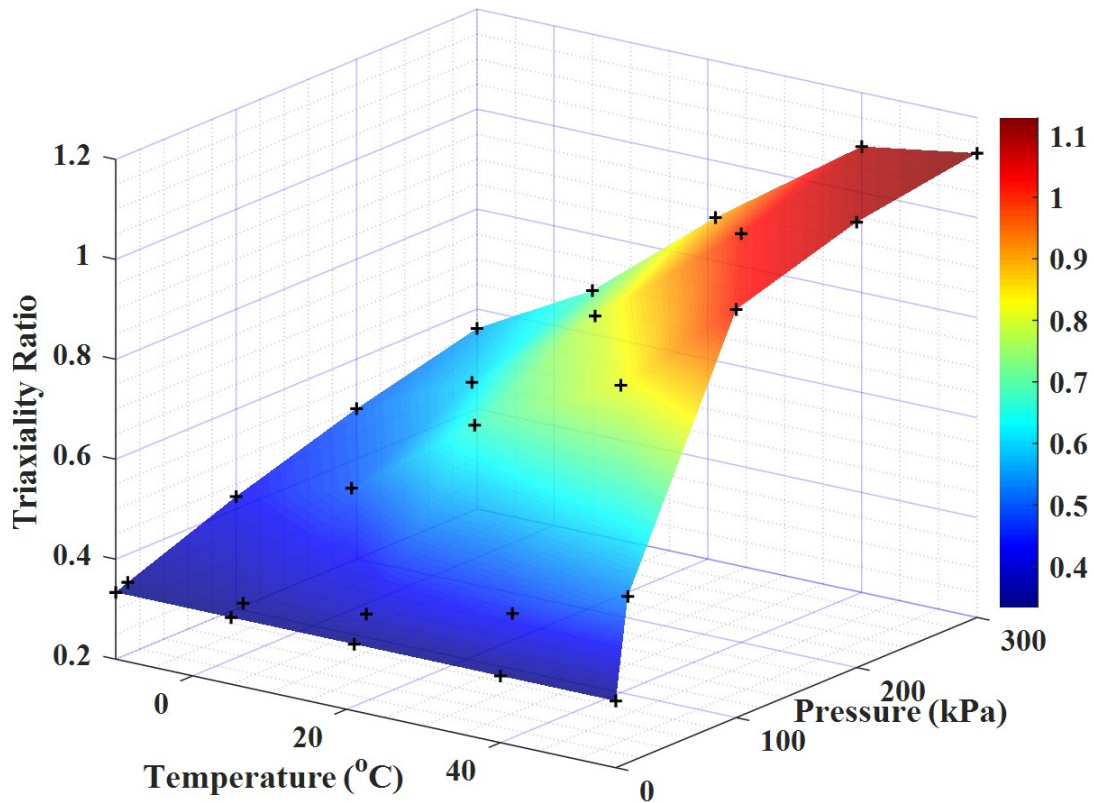


Figure 4.9: The relationship between Triaxiality ratio (η), Temperature, and confining pressure (from **Paper B**)

4.2 Comparison of Uniaxial Compression and IDT modes of Dynamic Modulus tests

The second test campaign performed in this project was a linear viscoelastic investigation of two laboratory-produced asphalt concrete mixtures (AC-L and SMA-L) using the uniaxial compression (UC) and Indirect Tensile (IDT) test methods. Both test protocols were used to characterize the stiffness properties of the asphalt mixtures. The UC mode is mainly used in the AASHTO standard, whereas the IDT is frequently used in European standards.

Kim et al. [97] compared the dynamic modulus using the UC and IDT modes and concluded that the two results were in good agreement. The mathematical formulation of the dynamic modulus in IDT mode can be simply expressed using the plane stress state for the linear elastic-like equation using the horizontal strain

ε_x and bi-axial stress components.

$$E^* = \frac{1}{\varepsilon_x}(\sigma_x - \nu\sigma_y) \quad (4.11)$$

σ_x and σ_y are the horizontal and vertical stresses and ν is the Poisson ratio. In Equation 4.11, the elastic modulus is replaced with the dynamic modulus. Similarly, the response to the sinusoidal load applied in the dynamic modulus test is expressed with an imaginary complex load, $P = P_o e^{i\omega t} = P_o(\cos \omega t + i \sin \omega t)$ where P_o and ω are amplitude and the angular frequency of the sinusoidal load, respectively. The final form of the dynamic modulus expression is obtained by re-arranging and substituting the horizontal and vertical displacements and stress states into Equation 4.11 and integrating.

$$|E^*| = 2 \frac{P_o \sin(\omega t - \phi)}{\pi a d U(t)} A \quad (4.12)$$

$$|E^*| = 2 \frac{P_o \sin(\omega t - \phi)}{\pi a d V(t)} B \quad (4.13)$$

where, a is loading strip width (m), d is specimen thickness (m), R is radius (m), x is horizontal distance from specimen center, y is vertical distance from specimen center, and α is radial angle. $V(t) = V_0 \sin(\omega t - \phi)$ and $U(t) = U_0 \sin(\omega t - \phi)$ are vertical and horizontal displacements (V_0, U_0 - constant amplitudes), respectively. The quantities A and B are expressed as follows:

$$A = (1 + \nu) \int_{-l}^l f(x) dx + (\nu - 1) \int_{-l}^l g(x) dx \quad (4.14)$$

$$B = (\nu - 1) \int_{-l}^l n(x) dy - (1 + \nu) \int_{-l}^l m(y) dy \quad (4.15)$$

with

$$\begin{aligned} f(x) &= \frac{(1 - x^2/R^2) \sin 2\alpha}{1 + 2(X^2/R^2) \cos 2\alpha + x^4/R^4} \\ g(x) &= \tan^{-1} \left(\frac{1 - y^2/R^2}{1 + x^2/R^2} \tan \alpha \right) \\ m(y) &= \frac{(1 - y^2/R^2) \sin 2\alpha}{1 + 2(y^2/R^2) \cos 2\alpha + y^4/R^4} \\ n(y) &= \tan^{-1} \left(\frac{1 - y^2/R^2}{1 + y^2/R^2} \tan \alpha \right) \end{aligned} \quad (4.16)$$

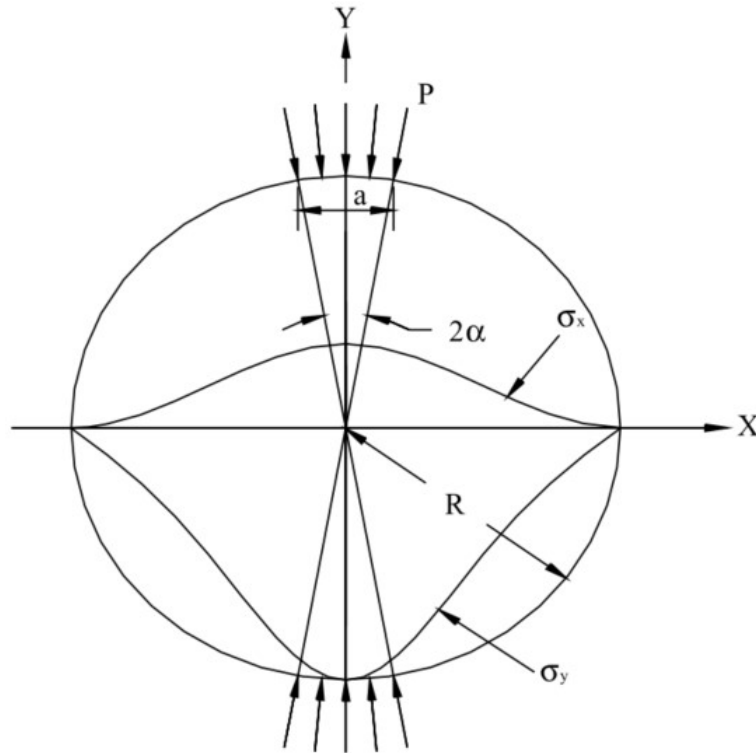


Figure 4.10: Stress distribution in Indirect tensile loading

In this study, the modeling and comparison of the uniaxial compression (UC) and IDT testing protocols were performed. An experimental study was conducted using two asphalt concrete mixtures (AC and SMA). As discussed in detail in **Paper F** [96], the two test methods exhibited comparable results at intermediate temperatures and frequencies, as shown in Figure 4.11. Otherwise, the IDT mode yielded a higher modulus than the UC mode in LVE domain. This was related to the possible bi-axial deformation in the IDT test. The stress states in the two test types differed and the modulus was calculated using the bi-axial stress and horizontal deformation in the IDT mode. It was apparent that the stress magnitude in the IDT tests was larger than that in the UC tests. Thus, a larger modulus was obtained in the IDT mode. The selection of linear viscoelastic characterization using the dynamic modulus test is dependent on several factors. Both tests have their advantages and disadvantages. The IDT test was found to be more suitable for medium- and low-temperature conditions, and has the advantage of using field samples and small-height samples (three times smaller than UC). In contrast, the UC test is more

suitable for medium- and high-temperature conditions with the benefit of a confined test for realistic modeling. Moreover, the UC test ensured the stability of the stress and strain outputs and controlled the deformation. For example, the IDT mode of testing is highly likely to induce viscoplastic strain, owing to its complex bi-axial stress state.

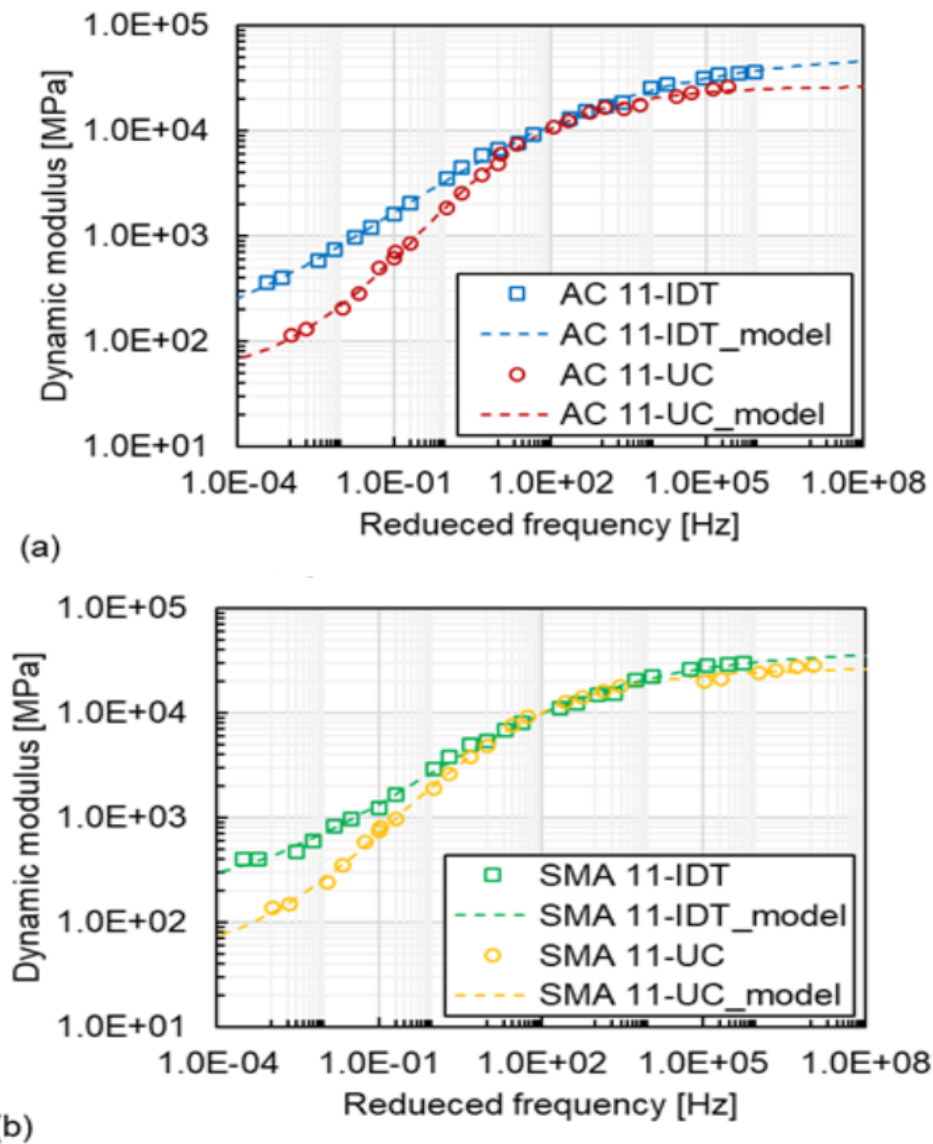


Figure 4.11: Comparison of dynamic modulus Master curves using IDT and UC (a) AC-L (b) SMA-L (from **Paper F**)

4.3 Comparison of dynamic and resilient modulus

The third campaign of viscoelastic characterization of asphalt concrete mixtures involved the investigation of the resilient modulus. A comparative study was con-

ducted using other linear viscoelastic tests (dynamic modulus E^* , storage modulus E' , and relaxation modulus $E(t)$). A resilient modulus (Mr) is computed as the ratio of stress to recoverable strain from the haversine loading pulse. Two different asphalt mixtures (AC/AB and AGB) are investigated. The AGB is a soft mixture used for low traffic roads.

The mechanistic-empirical pavement design method takes dynamic modulus (frequency domain) as an important input. However, the time-domain stiffness of asphalt concrete are usually required by the pavement community (practitioners). Resilient modulus (Mr) and relaxation modulus $E(t)$ are commonly used as fundamental material properties. In this study, a comparison was made between the resilient modulus and the moduli obtained from the sinusoidal dynamic modulus test, that is $E^* - Mr$, $E' - Mr$, and $E(t) - Mr$. The differences between the dynamic modulus and resilient modulus tests were due to the following reasons.

- The strain quantity used to calculate the modulus differed significantly between the two tests.
- The viscosity properties of asphalt concrete could not be captured using the haversine load during the remaining period of the Mr test.

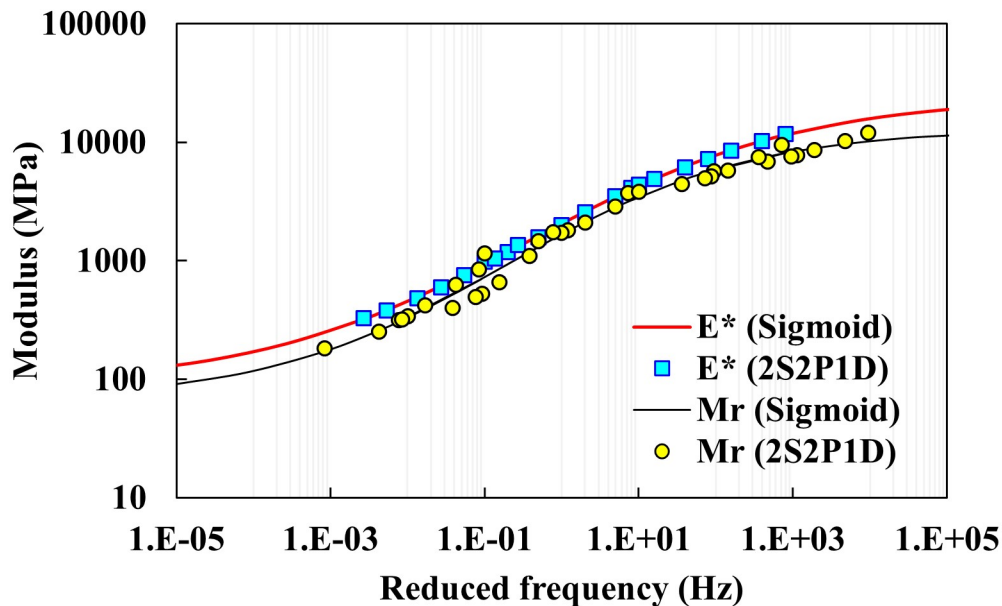


Figure 4.12: Master curves of dynamic modulus and resilient modulus - AC or AB mixture (**Paper C**)

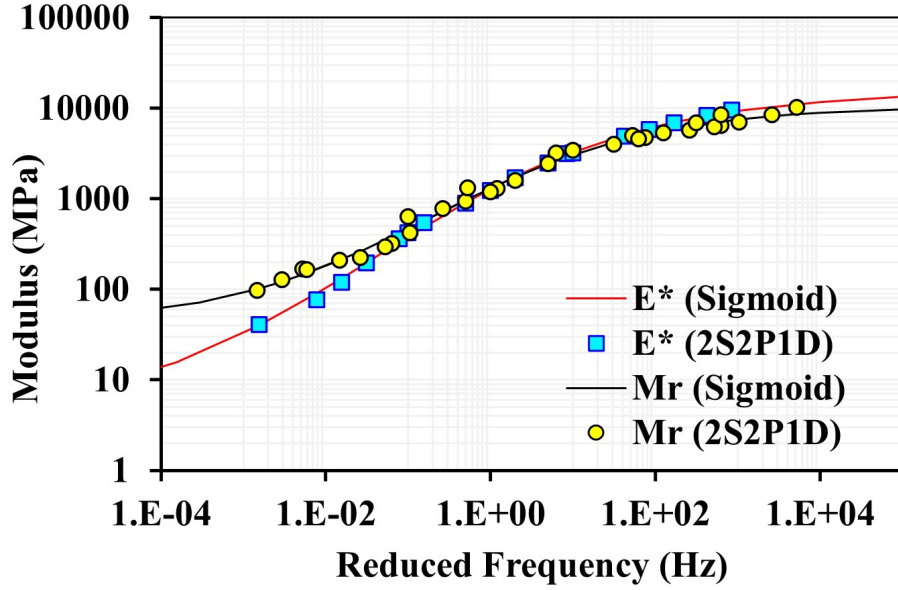


Figure 4.13: Master curves of dynamic modulus and resilient modulus - AGB Mixture (Paper C)

As shown in Figures 4.12 and 4.13, the haversine resilient modulus (Mr) and sinusoidal dynamic modulus test results are in fairly good agreement. The dynamic modulus E^* was slightly higher than Mr for stiff mixtures (Figure 4.12). However, it is notable that Mr is greater than E^* for softer mixtures because of the higher stress at high temperatures in the controlled-strain tests (Figure 4.13).

4.3.1 Resilient Modulus versus storage modulus

The deformation of a viscoelastic body dissipates energy as heat through viscous loss and elastically stored energy [98]. The maximum stored energy per cycle is $W = \sigma_o \varepsilon_o / 2$. The dissipated energy per unit volume (J/m³ per cycle) is the loss modulus expressed as $\Delta W = \pi \sigma_o \varepsilon_o \sin \varphi$. The ratio of energy loss to (or specific loss) is expressed as follows.

$$\frac{\Delta W}{W} = 2\pi \sin \varphi \quad (4.17)$$

The storage modulus ($E' = E^* \cos \varphi$) is the relevant and crucial quantity that is used to compute the time-domain viscoelastic properties of asphalt concrete (compliance and relaxation modulus). The comparison between Mr and E' shows a slightly better correlation than the dynamic modulus after the loss modulus is subtracted. The loss

modulus was more significant for soft mixtures than for stiff mixtures (**Paper C**)[99].

4.3.2 Resilient Modulus versus Relaxation modulus

The resilient modulus is determined from the storage modulus. The storage modulus data were smoothed for unevenness using a continuous function, as discussed in the previous section. Once the loss modulus was removed, the Prony function was employed to derive the relaxation modulus, $E(t)$. As shown in Figure 4.14, a more closer correlation was found between M_r and $E(t)$ than M_r and dynamic modulus. Comparison of the two moduli under similar conditions is presented in (**Paper C**).

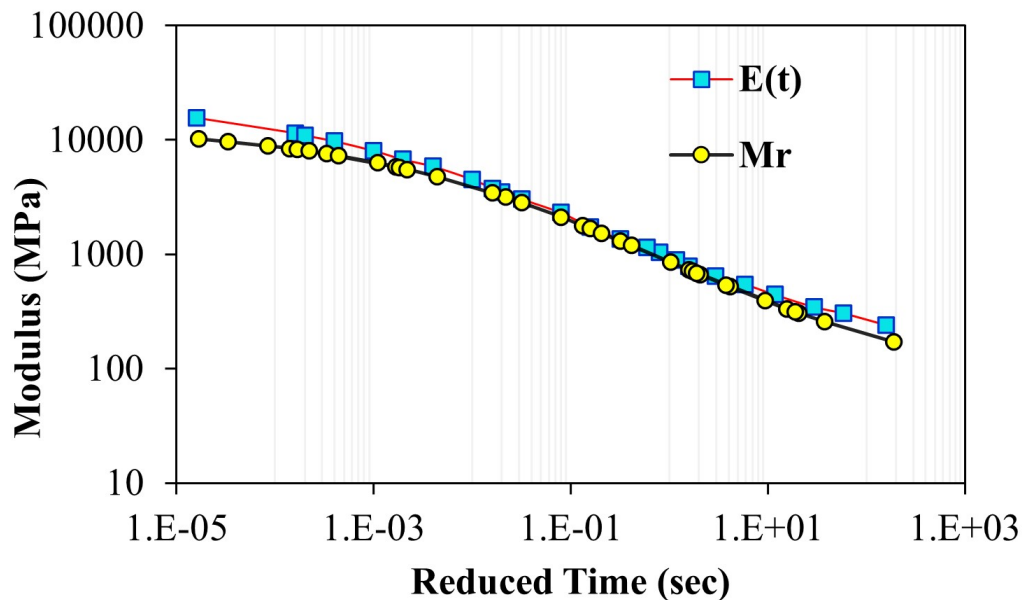


Figure 4.14: Master curves relaxation modulus and resilient modulus - AC/AB mixture (**Paper C**)

In summary, an extensive study was conducted on the various viscoelastic properties of different asphalt concrete mixtures used in high- and low- traffic roads. New models were proposed to construct triaxial master curves, and a detail comparison of the resilient modulus with the dynamic and relational moduli was presented. Moreover, the dynamic modulus test modes were investigated in the uniaxial compression and IDT modes, which showed good correlation at intermediate temperatures. The findings are presented in **Papers B, C and F**. The main highlights from these studies are:

- The stress dependent linear viscoelastic responses should be considered in the small strain asphalt concrete response, such as relaxation modulus.
- Owing to the limitations of finding long filed samples, IDT test method is commonly used. Resilient modulus, dynamic modulus, fatigue, and creep tests are performed using IDT samples (about 50 mm thickness). The IDT test has two limitations: the bi-axial (horizontal and vertical) strain state can cause permanent deformation, and the effect of confinement cannot be simulated in the IDT setup.
- The IDT test modes of resilient and dynamic moduli are comparative at intermediate temperatures (10 to 25 °C).

Chapter 5

Viscoplastic and Damage Response

This chapter presents the results and analyses of viscoplastic deformation and fatigue test results. The investigation report on the fatigue and permanent deformation interaction is also presented.

5.1 Asphalt Concrete Damage Characterization

Permanent deformation and fatigue cracking are the primary damage mechanisms in asphalt concrete. These damages evolve differently but on the same structure, with respect to the loading mode, temperature and frequency. The idealized stress-strain hysteresis for the two damage modes was distinct (Figure 5.1).

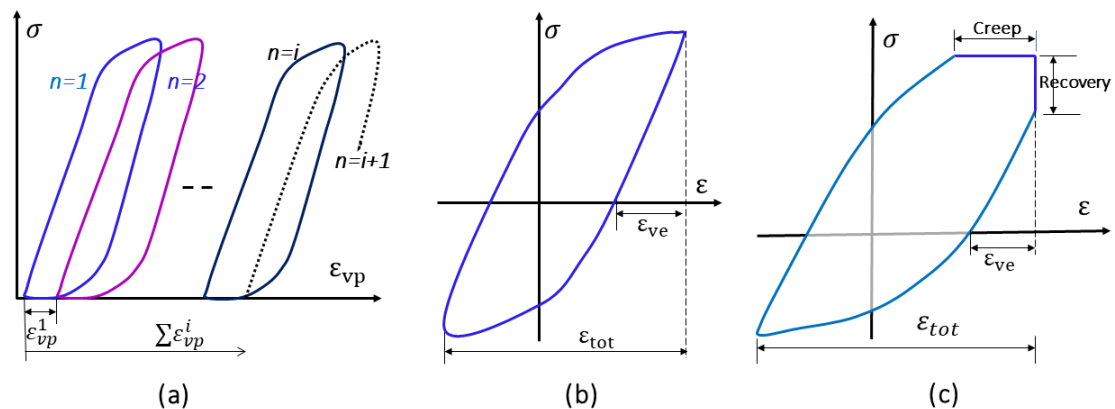


Figure 5.1: Schematic stress-strain hysteresis loops (a) permanent deformation (b) cyclic fatigue (c) fatigue-creep interaction

During creep-recovery (permanent deformation) loading, the hysteresis loops shifted horizontally owing to the accumulation of viscoplastic strain. However, in the pure cyclic fatigue test, cyclic stress caused stiffness reduction and phase angle

increment with negligible viscoplastic strain. In reality, the two types of damage are mutually related, because damage evolution is a simultaneous mechanism.

5.2 Permanent deformation characterization

The viscoplastic (VP) strain growth that causes permanent deformation depends on the loading path, stress state [100], and loading-unloading time. The classic viscoplastic failure criterion at the macroscopic level considers the strain rate during the steady-state stage of the creep-recovery test. The slope represents the hardening rate of the permanent deformation characteristics of the tested mixtures. A power law was used to approximate the rate with reasonable accuracy. The Schapery's uniaxial viscoplastic strain hardening rule (Equation 2.12) is used for steady state viscoplastic modeling. Gibson et al., [101] assumed power function for the stress and strain. For the haversine stress function $g(\sigma) = \frac{\sigma_0}{2}[1 + \sin(\omega t - \pi/2)]$, the viscoplastic strain can be expressed by substituting and integrating in the following expression.

$$\varepsilon_{vp} = \left(\frac{p+1}{G} \right)^{1/(p+1)} \left[\int g(\sigma) dt \right]^{(1/p+1)} \quad (5.1)$$

where G , p are material constants. Due to the inherent limitations of the power models, Equation 5.1 underestimates viscoplastic strain in tertiary stage. Therefore, three-stage creep models were used, such as the classic Francken model [102]. The model is expressed as follows:

$$\varepsilon_{vp} = AN^B + C(e^{DN} - 1) \quad (5.2)$$

where A , B , C , and D are model coefficients, and N is the number of cycles.

5.2.1 Permanent deformation dissipated energy

In this study, the dissipated energy ratio (DER) approach was applied to evaluate the permanent deformation properties of asphalt concrete mixtures at the macroscopic level. The dissipated energy ratio DER_{PD} criterion is expressed as follows using the dissipated energy DE_{PD} due to permanent deformation damage.

$$DER_{PD} = N \left[\frac{DE_{PD(1)}}{DE_{PD(N)}} \right] \quad (5.3)$$

where $DE_{PD(1)}$ and $DE_{PD(N)}$ are the amounts of energy dissipated during the first and N^{th} creep cycles, respectively. The amount of creep dissipated energy at each creep cycle is $DE_{cr} = \sigma_o \varepsilon_{cr}$. Using the Francken model for the dissipated energy owing to permanent deformation or creep per cycle, $DE_{PD} = \sigma_o [AN^B + C(e^{DN} - 1)]$, in Equation 5.3 gives the following expression:

$$DER_{PD} = \frac{\sigma_o [A + C(e^D - 1)]}{\sigma_o [AN^B + C(e^{DN} - 1)]} = N \frac{K}{\varepsilon_{cr}} \quad (5.4)$$

where $K = A + C(e^D - 1)$ is a parameter that depends on the stress level, temperature, and initial damage (fatigue).

Figures 5.2 and 5.3 shows the typical three-stage deformation and DER. The DER curve exhibits an additional phase change at the peak point in the tertiary creep stage. Viscoplastic deformation accumulated rapidly owing to shear at a constant volume and excess energy dissipation in the tertiary stage. The Peak Value (PV) of the DER curve marks the commencement of the fourth creep stage and formation of macro-cracks. The DER curve starts descending in the fourth stage owing to the high energy dissipation, macro-crack formation, and loss of integrity due to the external load. Flow number (FN) is a classic permanent deformation failure criterion for asphalt concrete mixtures. This marks the beginning of the micro-crack initiation and propagation. However, the pavements can be in service even after the flow number is initiated. Hence, it is essential to estimate the remaining life of asphalt concrete until macro-crack formation or failure occurs. As shown in Figure 5.2, the number of cycles between micro-crack (FN) and macro-crack formation (N_{PV}) can be referred to as the Shear Endurance Life (SEL). The number of cycles between micro-crack and macro-crack formation exhibited good consistency, as shown in Figure 5.4.

$$\begin{aligned} SEL &= N_{PV} - FN \\ \varepsilon_{SEL} &= \varepsilon_{N_{PV}} - \varepsilon_{FN} \end{aligned} \quad (5.5)$$

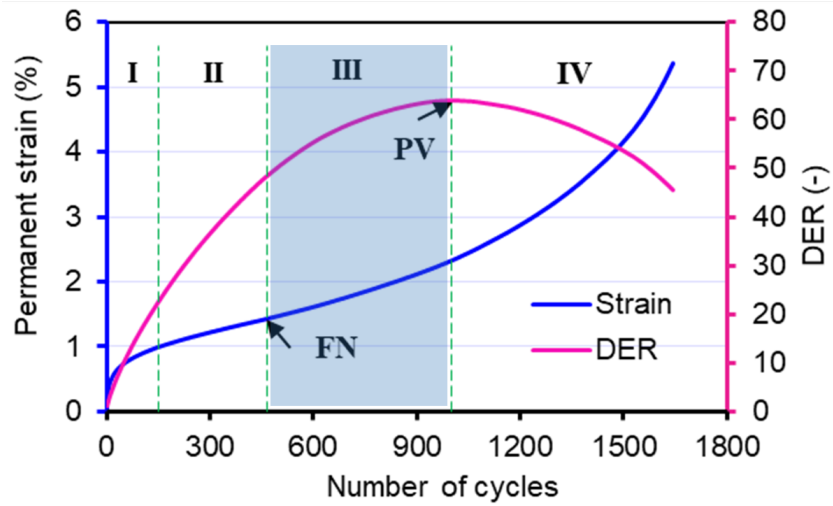


Figure 5.2: Permanent deformation and DER

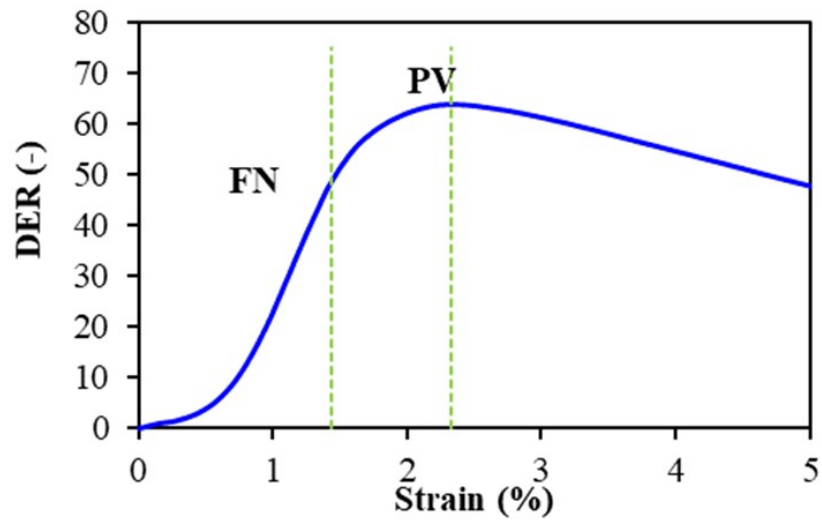


Figure 5.3: DER versus permanent strain

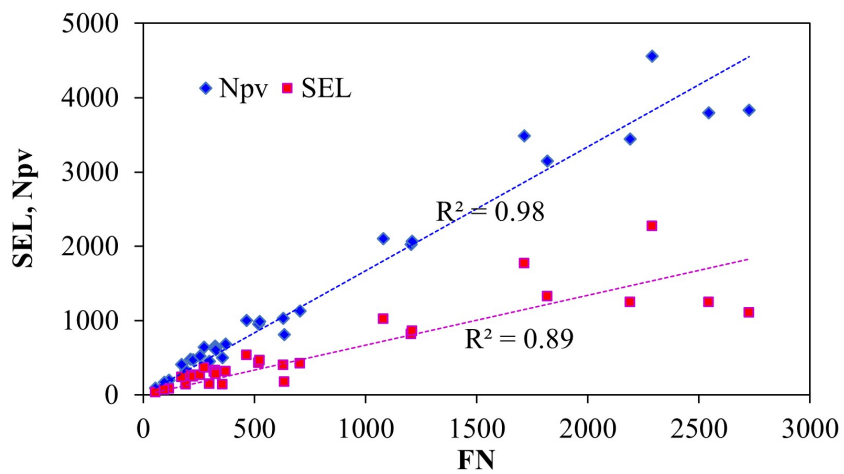


Figure 5.4: Correlation between flow number and shear endurance life

5.2.2 Effect of Confining Stress

The confining stress in the triaxial test was used to simulate the residual stress between the aggregates in the mixture morphology and the trapped stress due to stationary loads. Therefore, the triaxial test is regarded as the most realistic permanent deformation test, along with the haversine loading stress pulse and rest period between pulses. The effect of confining pressure on viscoplastic strain evolution is well documented. The test results shown in the Figure 5.5 demonstrated the effects of both axial stress and confining stress on the viscoplastic strain evolution of asphalt concrete mixtures. The role of confinement is to retard the flow rate (strain rate), in contrast to the axial stress.

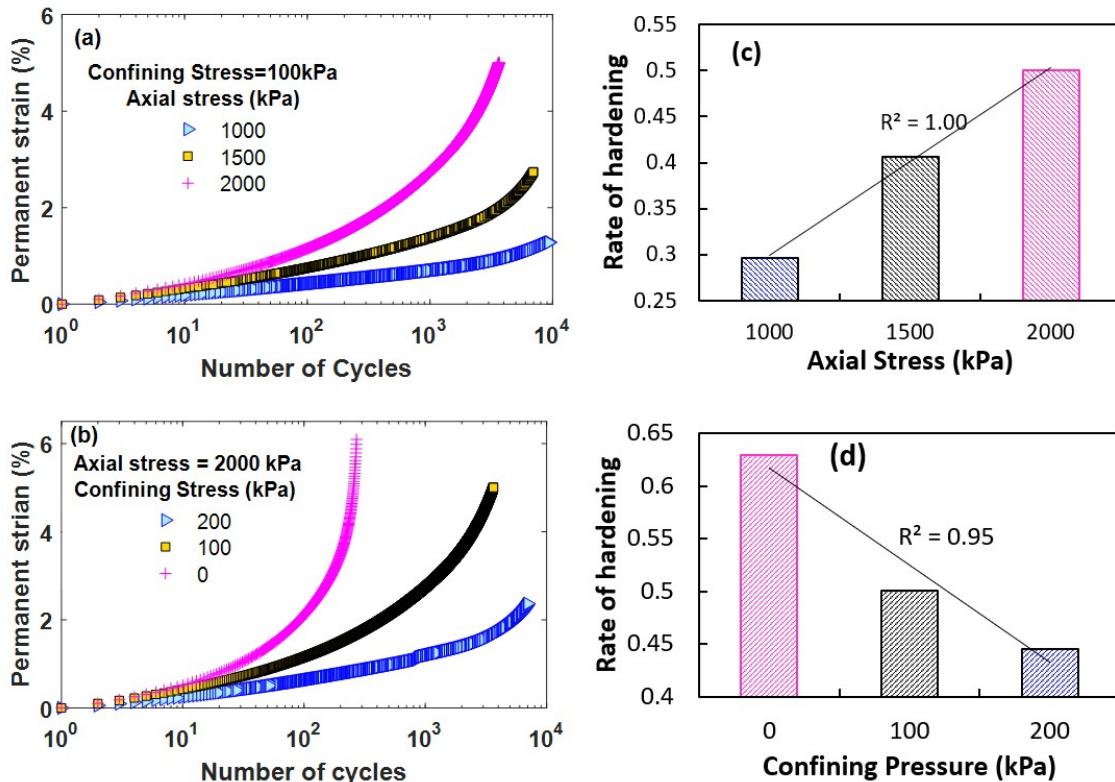


Figure 5.5: Effect of Stress on permanent deformation properties (from **Paper E**)

5.3 Fatigue damage characterization

Uniaxial fatigue tests were conducted in controlled-strain mode in both tension-tension and tension-compression cycles. Typical fatigue damage response is described using dynamic modulus deterioration curve which evolved in three stages, as

shown in Figure 5.6. A rapid reduction in the first phase, steady state in the second stage and a rapid reduction in the third stage. The viscoelastic continuum damage (VECD) model is the most comprehensive fatigue damage constitutive model that considers time-temperatures factor, rate of relaxation module change, factor for specimen-to-specimen variation and pseudo stiffness deterioration. Moreover, fatigue damage was calculated using the dissipated energy quantity. The VECD model establishes the relationship between the damage variable (S) and pseudo-stiffness (C), referred as the damage characteristic curve. The damage, S , is an internal state variable that aggregates the thermo-rheological properties, micro-crack formation and growth, and other damages such as viscoplastic deformation during fatigue.

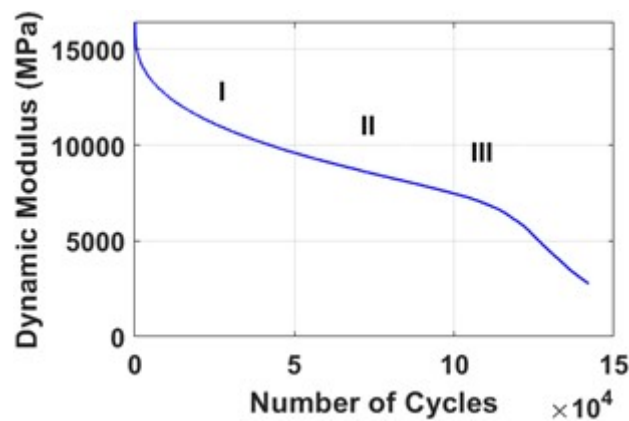


Figure 5.6: Fatigue damage characteristics of new and per-deformed samples (T-T at $10^{\circ}C$ and $300\mu\varepsilon$) (PD-F)

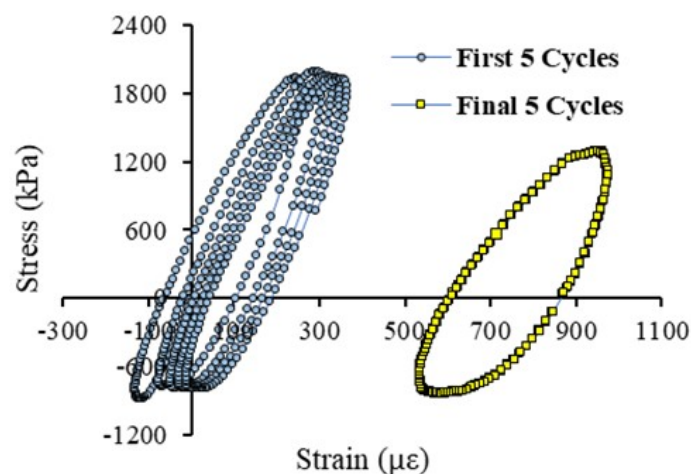


Figure 5.7: Development of viscoplastic strain during controlled-strain cyclic fatigue tests

Figure 5.7 shows the horizontal shift of stress-strain hysteresis loops. This shifting can be due to the accumulation of viscoplastic strain during the fatigue tests. It can also be observed that the hysteresis cycle has a non-zero mean stress (sum of maximum and minimum stress is non-zero or positive value), which might contribute to the accumulation of potential permanent deformation during the fatigue tests. However, the viscoplastic strain magnitude is small as compared to the viscoplastic strain in creep-recovery test. The corresponding energy dissipation is also insignificant as compared to the energy expended due to pure cyclic fatigue. Hence, a strain in the pseudo-strain space was used in the VECD model to eliminate such outliers. Furthermore, the damage characteristic curves describe the reduction in material integrity, pseudo stiffness (C) due to internal state variable or damage variable (S) in the asphalt concrete (Figure 5.8). The C – S curve is often used to classify mixtures. It should be noted that a comparison based on the C-S curve may be misleading. Several factors such as the initial void (pre-flaw) can influence damage rate. For example, from rheological viewpoint, the damage rate (alpha) is smaller for from laboratory and aged samples (**Paper E**). During the test campaign, both plant- and laboratory-produced asphalt concrete mixtures were studied. The laboratory-produced and aged specimens had higher damage rate than the plant-produced specimens.

The second method for fatigue damage characterization was evaluated using the dissipated energy quantity and the dissipated energy ratio. For a cyclic sinusoidal stress pulse, the dissipated energy per cycle, DE_F , can be expressed as:

$$DE_F = \pi E_n^* \varepsilon_n^2 \sin \varphi_n \quad (5.6)$$

where E^* is the dynamic modulus, ε_n is the strain at the n^{th} cycle, and φ_n is the phase angel. Then, the dissipated energy ratio DER_F criterion is defined as follows:

$$DER_F = n \left(\frac{E_1^*}{E_N^*} \right) \left(\frac{\sin \varphi_1}{\sin \varphi_n} \right) \quad (5.7)$$

As shown in Figure 5.9, damage (energy dissipation) rate increase with strain amplitude at intermediate temperatures (10 and 15 °C).

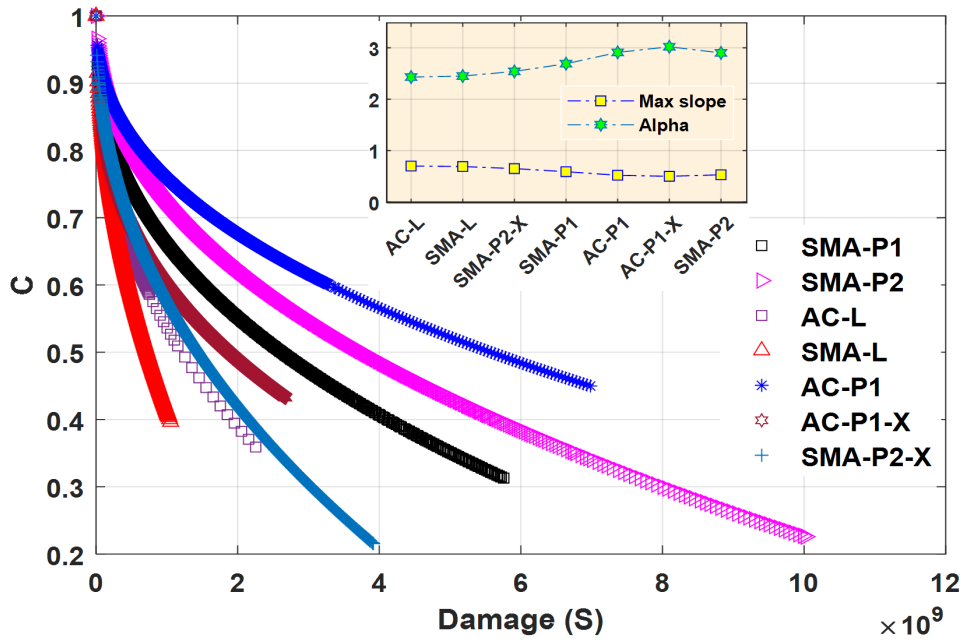


Figure 5.8: Fatigue damage characteristics of new and per-deformed samples (T-T at $10^\circ C$ and $300\mu\epsilon$) (PD-F) (Paper E)

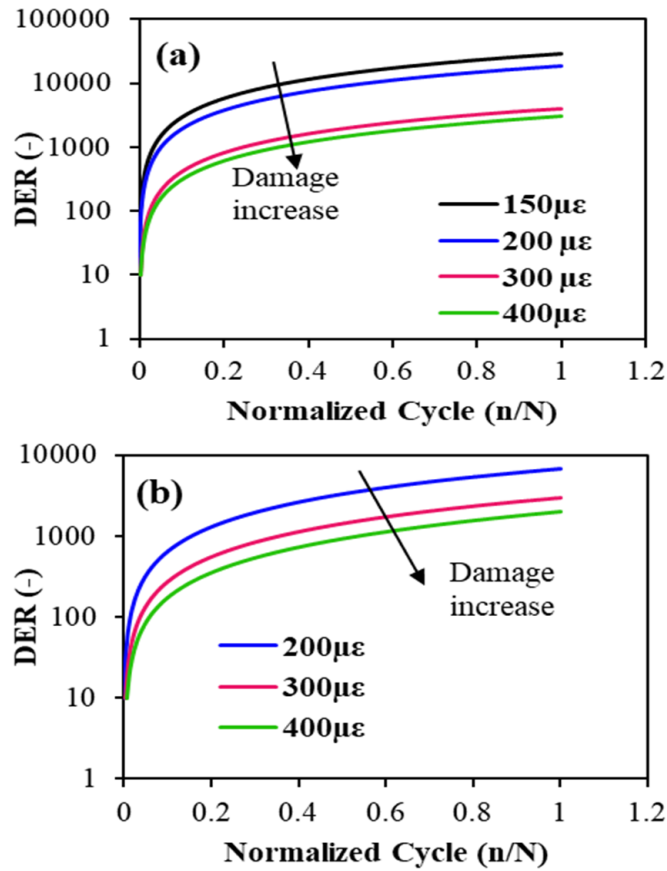


Figure 5.9: Fatigue damage Using DER T-C fatigue test at different control-strain (a) $10^\circ C$ (b) $15^\circ C$

5.4 Interaction between fatigue and permanent deformation damage

Asphalt concrete is subjected to cyclic fatigue and repeated creep-recovery during its service life. The damage inflicted on the pavement is the cumulative impact of the two dominant damage mechanisms - fatigue and permanent deformation. However, the interaction between fatigue and permanent deformation damage is a complex phenomenon in both testing and modeling. This phenomenon occurs because of the weakening of asphalt concrete caused by one type of damage, which makes it more susceptible to the other mode. For example, fatigue cracking can create localized areas of reduced stiffness in pavements, making them more prone to rutting. Similarly, rutting can induce stress concentration and strain accumulation, thereby accelerating the development of fatigue cracks. In some cases, fatigue and rutting damage can occur simultaneously, contributing to the accelerated and progressive deterioration of asphalt pavements. Fatigue cracks can act as stress concentrations, leading to accelerated rutting. Rutting provides preferential paths for water infiltration, which can exacerbate fatigue cracking. Therefore, fatigue and rutting damage must be considered in the design, construction, and maintenance of asphalt pavements. A proper mix design, adequate pavement thickness, and regular maintenance practices can help minimize the interaction between these two types of damage and extend the lifespan of the pavement. However, no comprehensive studies have been conducted to understand the inherent interactions between the two types of fundamental pavement damage. The traditional assumption of treating the two types of damage as independent mechanisms has clear limitations in the performance prediction and design of asphalt concrete. Some researchers noticed this gap and recommended for further research by stressing the inaccuracy of existing damage prediction methods. In this study, an attempt was made to investigate the effect of fatigue on permanent deformation and vice versa using a sequential testing procedure. The details were reported in **Papers D and E**. The energy approach and continuum damage mechanics theory were applied to quantify the damage.

5.4.1 Sequential damage

The evolution of creep and fatigue damage have been assumed to occur in a sequential manner, mainly for homogeneous materials like steel [87]. The respective damage can be estimated separately, and combined in different analytical forms in a continuum method. The simplest form is a linear summation of the respective damages. Based on the sequential damage assumption, the total dissipated energy (DE_{Tot}) is the sum of the energies expended on fatigue cracking (DE_F) and permanent deformation (DE_{PD}).

$$\begin{aligned}
 DE_{Tot} &= DE_F + DE_{PD} \\
 DE_{Tot} &= \pi E_n^* \varepsilon_n^2 \sin \varphi_n + \sigma_o [AN^B + C(e^{DN} - 1)]
 \end{aligned}
 \tag{5.8}$$

It should be emphasized that the total dissipated energy depends on the test or damage sequence. Thus, the damage interaction is affected the total dissipated energy in a nonlinear manner, in both the F-PD and PD-F sequences. Alternatively, the total dissipated energies in the F-PD (DE_{F-PD}) and PD-F (DE_{PD-F}) are not the same for the equal amount of fatigue and permanent deformation damage. In this study, the $PD - F$ sequence was found to be more plausible and realistic when an actual pavement was considered. Permanent deformation was most likely initiated before fatigue cracking. Moreover, the PD-F sequence is more convenient to determine using continuum damage mechanics or a dissipated energy approach. On the other hand, the F-PD sequence poses difficulty to quantify the effect of fatigue damage on permanent deformation owing to relaxation and healing effects at high temperatures during sample conditioning (as illustrated in Section 3.4).

Figures 5.10 and 5.11 show the total dissipated energy (DE_{Tot}) in the PD-F sequence. The dissipated energy due to permanent deformation or creep is much larger than that of the fatigue damage (approximately $DE_{Tot} = 1.055DE_{PD}$).

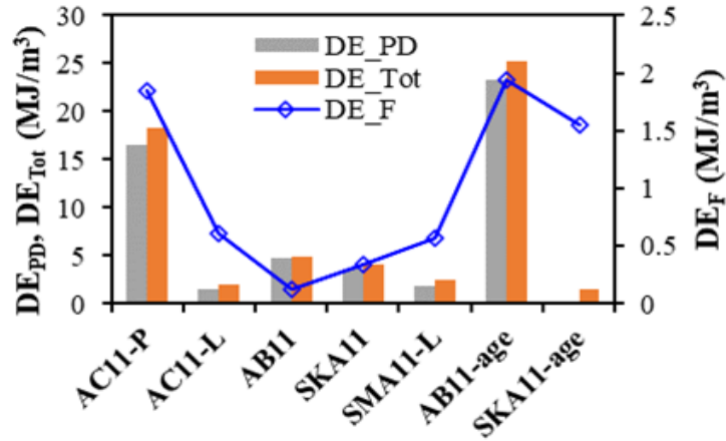


Figure 5.10: Dissipated energy of PD-F sequence (F10 and PD40 for different mixtures in T-T mode)

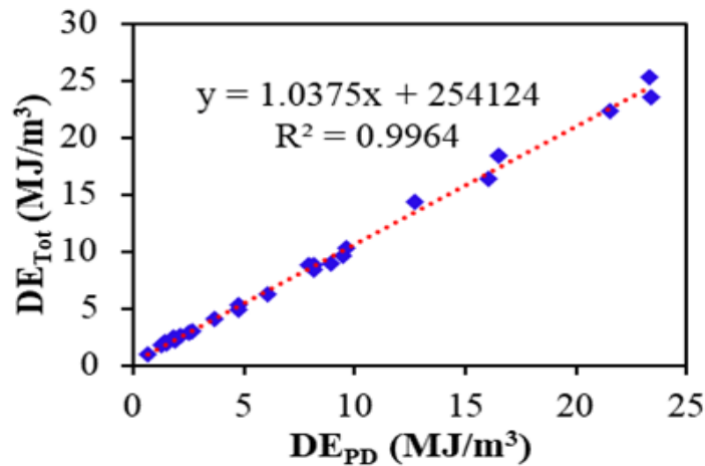


Figure 5.11: Dissipated energy of different samples PD-F sequence (DE_{PD} versus DE_{Tot})

The continuum damage (VECD) model was also applied to quantify damage in the $PD - F$ sequence. The pseudo stiffness (C) and the damage (S) were correlated as shown in Equation 2.25. The variable b indicates the rate of pseudo stiffness deterioration due damage accumulation. As shown in Figure 5.12a, strain hardening makes asphalt mixtures more susceptible to high rate of fatigue damage. Similarly, strain hardened samples require less energy dissipation to damage than new (undeformed) samples, as shown in 5.12b. Therefore, predeformation has a significant impact on the fatigue life of asphalt concrete.

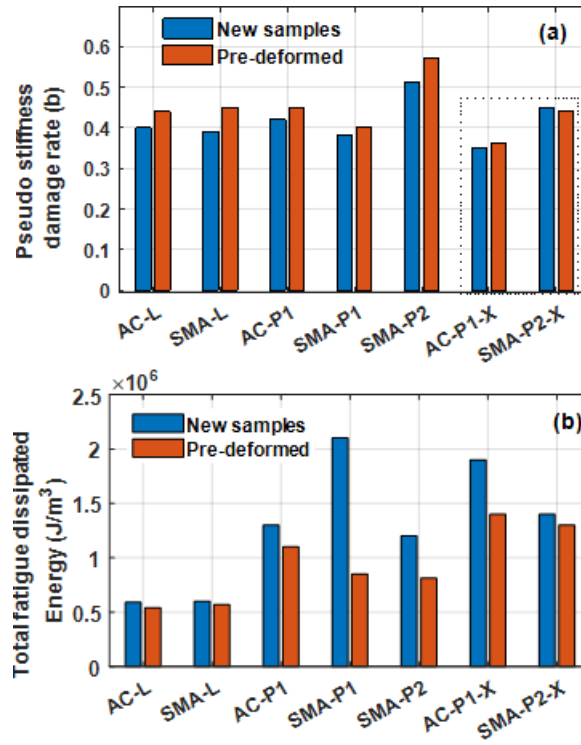


Figure 5.12: Effect of pre-deformation on fatigue damage responses in **PD-F** sequence (a) parameter b (b) total fatigue dissipated energy until failure (**Paper E**)

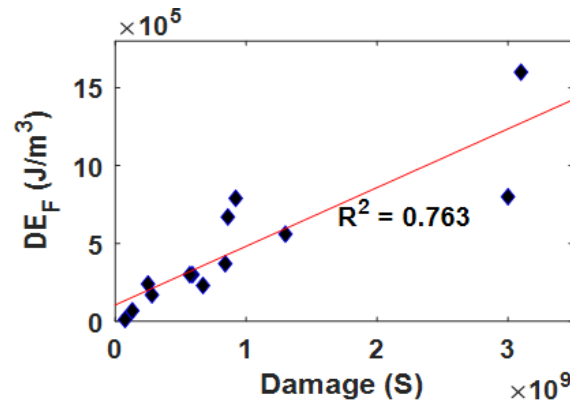


Figure 5.13: Damage variable S and dissipated energy DE_F on new samples– AC-P1-X (**Paper E**)

Furthermore, figure 5.13 shows the correlation between the amount of damage S at the failure point (that is 50 percent pseudo stiffness reduction) and the corresponding total fatigue dissipated energy at failure. Although the results showed good agreement, there were discrepancies due to the fundamental difference between the two damage prediction approaches. The continuum method considers damage as the aggregate of the internal state variables, which may include viscoplastic deforma-

tion and other phenomena. On the hand, dissipated energy is computed assuming pure sinusoidal stress and strain cycle in a viscoelastic damage. In the **F-PD** sequence, the effect of fatigue cracking on the evolution of permanent deformation was investigated. The effect of preexisting cracks on permanent deformation was analyzed using the strain rate in the steady-state stage, the flow number and the expended energy. The dissipated energy and hardening rate are strongly dependent on the deviatoric stress. High deviatoric stress result in high dissipation, rapid strain rate (small flow number). As shown in 5.14, neither the DE_{PD} nor the DE_F energy quantities are consistent with the flow number. The expended energies are dependent on mixture type, specimen, and temperature.

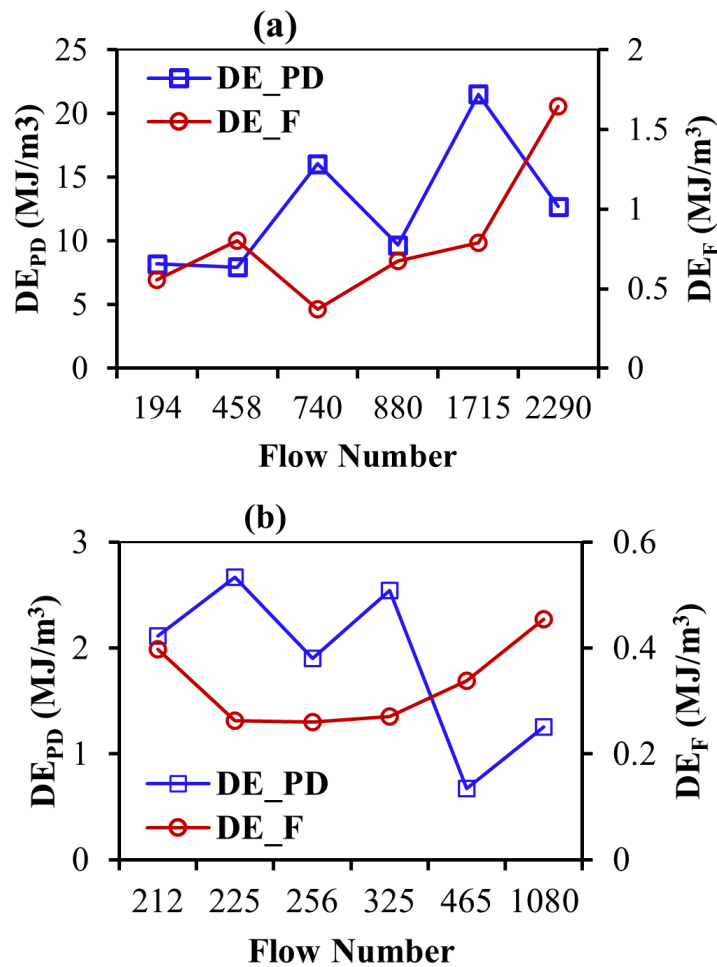


Figure 5.14: Dissipated energies of pre-fatigued samples in **F-PD** sequence (a) AC-P1-X fatigue at 10 °C and PD at 30 °C and 2 MPa (b) SMA-P2-X fatigue at 10 °C and PD at 40 °C, 0.65MPa (**Paper E**)

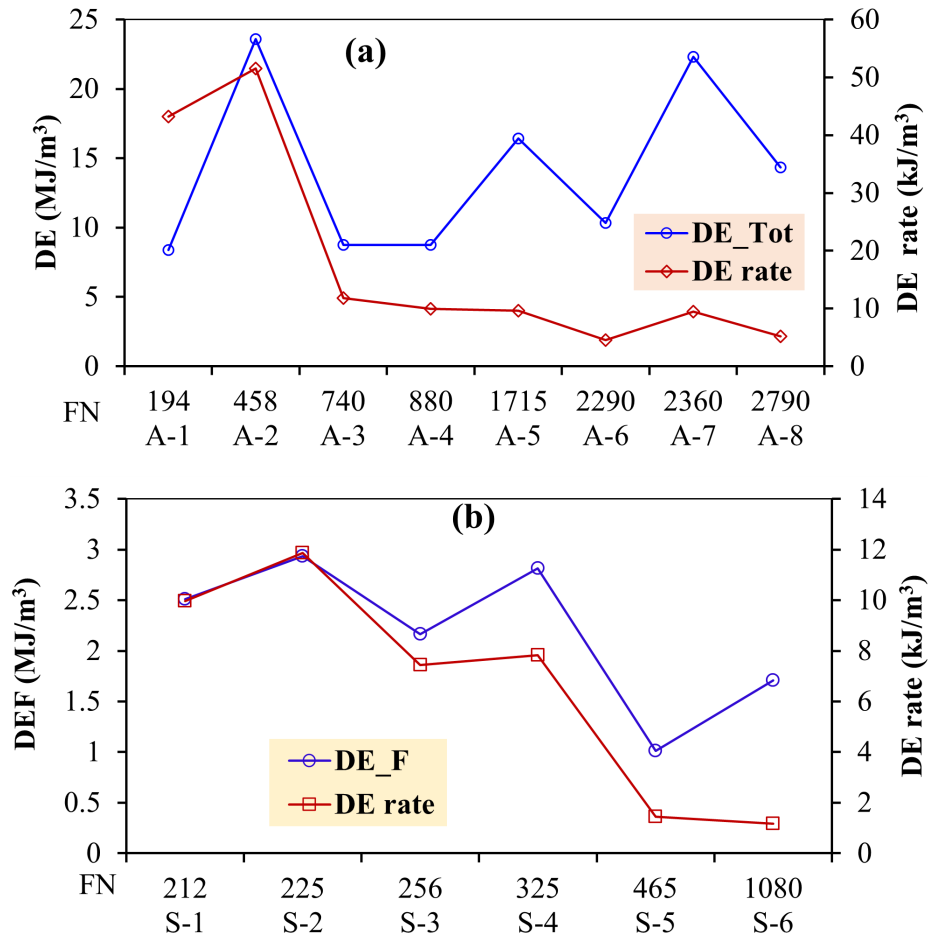


Figure 5.15: Correlation of total dissipated energy and flow numbers in **F-PD** sequence (a) AC-P1-X, PD at 30°C (b) SMA-P2-X, PD at 40°C - (**Paper E**)

Furthermore, the dissipation rate is defined as the ratio of DE_T/FN in *F-PD* sequence. As shown in 5.15 (a and b), the rate of DE_T indicates a decreasing pattern with flow number. Several phenomena can be the reasons for the inconsistency of the effect of fatigue on the subsequent permanent deformation damage.

- Firstly, the PD part of the *F-PD* sequence is performed at higher temperatures (30, 40 and 50 °C), and some of the initial fatigue cracks (at 10°C) can heal during the rest period and sample conditioning for the creep-recovery tests.
- Secondly, tension-compression or tension-tension cyclic fatigue test using cylindrical specimens requires large loading cycle. The 50 % stiffness reduction is only an approximate failure criteria. Therefore, about 20 to 40 % stiffness reduction in fatigue tests has little impact on the subsequent permanent de-

formation damage.

- The third reason could be related to potential hardening or post compaction during the tension-compression fatigue test phase. This compaction can improve deformation resistance in the early life of asphalt concrete.

Therefore, based on this study, the effect of pre-crack on the permanent deformation (F-PD sequence) is found marginal.

5.5 Unified damage model

Unified damage modeling for rheologically materials emanates from the piezo-thermo-rheological simple of asphalt concrete. The time temperature superposition principle is commonly applied to model complex modulus master curves, stress-dependent linear viscoelastic responses, and also nonlinear (with damage) viscoelastic responses of asphalt mixtures [103]. It was reported that the *viscoelastic – viscoplastic* responses are actually coupled. Medani et al. [104] proposed a ‘Unified Model’ as a tool to quantify the properties of the asphalt mixtures in relation to time temperature dependency. The model was used to describe a wide range of properties such as strain rate, stiffness, compressive strength, and tensile strength in relation to temperature and time.

As a rheologically simple material, the unified damage modeling can be formulated for creep-fatigue interaction. In literature, analytical creep-fatigue interaction models were developed for homogeneous materials like steel and rocks. The same can be applied for asphalt concrete using the two principles: *time-temperature superposition* and *sequential damage assumption*. The application of time-temperature superposition principle with damage states has been validated for asphalt concrete by researchers like Chehab et al.[57], Zhao et al.[105], Darabi et al.[66]. The simplest form of damage coupling at failure is the linear sum of the two damage rates, where n/N_f is the fatigue damage and $\varepsilon/\varepsilon_c$ is the creep damage rate.

$$\sum n/N_f + \sum \varepsilon/\varepsilon_c = 1 \quad (5.9)$$

More generally, the interaction damage ϕ can be expressed as follows:

$$d\phi = I_{fc}d\phi_c + I_{cf}d\phi_f \quad (5.10)$$

$$\phi = f_c(\varepsilon, \sigma, T, \phi_c + I_{fc}\phi_f)dN_c + f_f(\varepsilon, \sigma, T, I_{cf}\phi_c + \phi_f)dN_f \quad (5.11)$$

The interaction variables indicated in the above equation are used to incorporate effect of one damage mode on another, where I_{cf} is the interaction coefficient of creep on fatigue, and I_{fc} is the interaction of fatigue on creep damage evolution.

Figure 5.16 illustrates the domain of creep and fatigue damage, and influence of temperature on the damage evolution and the interaction. The relationship between creep and fatigue dominated damage at random values of creep-fatigue interaction coefficients is dependent on temperature, sequence of creep and fatigue (i.e., in both F-PD or PD-F).

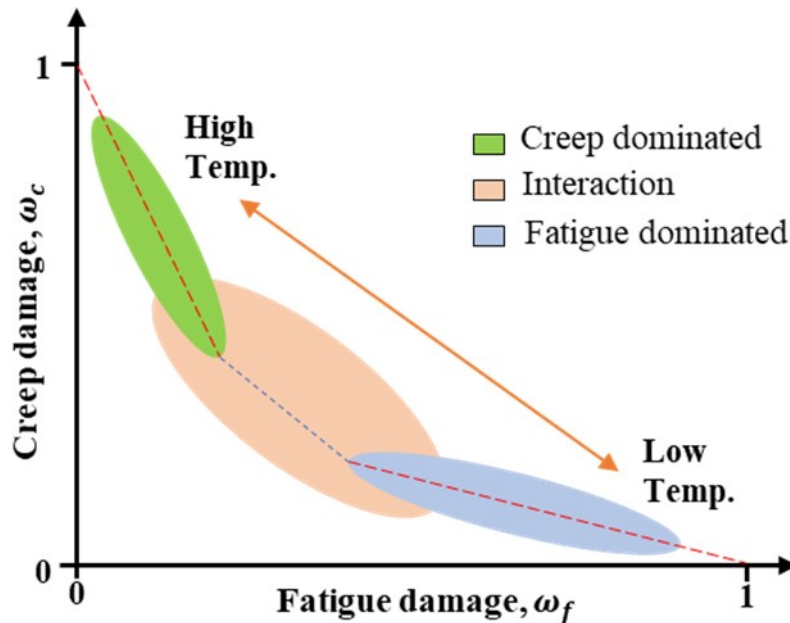


Figure 5.16: Schematic of Creep and fatigue interaction damage depending on temperature and sequence

5.6 Summary

The mechanistic prediction of damage in pavement materials has been the focus of study in recent decades. Asphalt concrete is exposed to cyclic load from traffic and

undergo a creep-recovery cycle in its service life. Fatigue cracking and permanent deformation are the two dominant damage modes, which evolve in the form of stiffness deterioration and viscoplastic flow, respectively. It was evident that the interaction between the two damage was not studied in previous research. However, field observations have shown the mutual progression of the two damage on the pavement surface along the longitudinal wheel path. In this study, for simplicity, the sequential test procedure (STP) was proposed to simulate the effect of pre-cracking on permanent deformation, and strain-hardening on the fatigue cracking evolution in asphalt concrete. In the STP, a single specimen was tested for dynamic modulus, fatigue, and creep-recovery tests, which offers saving in both material and sample preparation time. Moreover, most standard laboratory tests utilize gyratory compacted samples for fatigue and permanent deformation due to the difficulty of getting field cored samples longer than 40- or 50-mm for fatigue and permanent deformation tests. Hence, the STP can be a resolve to investigate the influence of pre-fatigue on deformation and vice versa using gyratory samples.

From the experimental observation and analyses, the PD-F sequence is more plausible and suitable for test, and the continuum method is applied conveniently to model the fatigue part of the sequence. Permanent deformation is expected before fatigue cracking initiation. The PD part of test in the PD-F sequence should be performed with attention since some asphalt mixtures may not have all the three creep phases. In the F-PD sequence, it was found a little challenging to quantify the effect of fatigue cracking on the permanent deformation due to relaxation and healing effects at high temperatures during conditioning. It was found that the effect of pre-fatigue cracking up to 40 percent of initial stiffness at low or intermediate temperatures is found marginal on permanent deformation at 30 °C and 40 °C. Furthermore, the dissipated energy method is simple and straightforward. However, the discreteness of energy quantity can be the limitation for accurate characterization of damage in continua. A nonlinear interactive damage model should be considered for accurate time-history characterization of fatigue and permanent deformation

damage interaction. A framework can be developed to investigate the sequential test procedure for various levels of pre-deformation or pre-crack as a function of material properties, temperature, stress and strain levels, etc.

Chapter 6

Concluding Remarks

In this chapter, the main contributions of the thesis are summarized. The limitations of the study and recommendations for further research related to the project are presented.

6.1 Conclusions

The main conclusions of this project can be summarized under two main domains of asphalt concrete response: undamaged and damage response. An extensive study was conducted on the viscoelastic, viscoplastic, and fatigue damage responses of asphalt concrete by using different asphalt concrete mixtures and test methods.

6.1.1 Viscoelastic analysis

The linear viscoelastic properties of asphalt concrete have been studied extensively. The experimental protocol included axial compression and indirect tensile (IDT) test modes, that is, IDT tests (in haversine and sinusoidal pulses), and both uniaxial and triaxial compression tests (sinusoidal). The thermo-piezo-rheological simplicity of asphalt concrete was validated using a stress-dependent rheological shift models. The stress-ratio concept (triaxiality ratio) was introduced to characterize the stress-dependent viscoelastic properties of asphalt concrete.

- The linear viscoelastic (LVE) properties of asphalt concrete are highly stress-dependent at intermediate and high temperatures (**Paper B**). This property is validated using the time-temperature-pressure superposition princi-

ple (TTPSP) in the LVE range, a triaxial dynamic modulus test, and a new simplified vertical shift model. The long-term relaxation modulus, maximum slope of the relaxation modulus, and viscoelastic fatigue damage parameter are strongly stress-dependent, which highlights the limitations of conventional uniaxial fatigue life prediction models particularly at intermediate temperatures (from 15 to 30 °C). Moreover, for controlled-strain dynamic modulus test, the triaxiality ratio increased with temperature and pressure, and have strong correlation with the long-term relaxation modulus. It was concluded that the triaxiality ratio can indirectly characterize the viscoelastic linearity limit of a thermo-piezo-rheological simple material.

- In **Papers C and F**, a comparative studies of the uniaxial compression (UC) dynamic modulus with IDT dynamic modulus and resilient modulus tests are presented. These studies concluded that the resilient modulus was comparable to the storage modulus at low and intermediate temperatures (**Paper C**). Furthermore, the dynamic moduli obtained using IDT and UC testing modes were comparable at intermediate temperatures (**Paper F**). One of the limitations of the IDT mode is the formation of permanent bi-axial deformation at higher temperatures. UC dynamic test have the advantages of uniform stress distribution, confinement and the possibility of avoiding permanent strains during testing. In contrast, IDT mode has the benefits a small specimen size, test simplicity, and utilization of field samples. The IDT testings have the advantages of utilizing field samples and the economical benefits.

6.1.2 Viscoplastic and fatigue cracking damage analyses

The second phase of the study began by conducting a comprehensive review of state-of-the-art permanent deformation prediction from the pure empirical methods of the 1960s to the latest mechanistic methods (**Paper A**).

- The review revealed that the latest constitutive models integrated and coupled different theories to model different types of asphalt concrete damage.

The fundamental theories and principles are continuum damage mechanics (1958), nonlinear viscoelasticity (1969), viscoplasticity (1971), and viscodamage (2011), along with the time-temperature-superposition principle. The Pavement analysis using the nonlinear damage (PANDA) model is one of the most comprehensive permanent deformation modeling approaches available in the literature (the next generation of the ME method). The inference from this study is that the coupling of different asphalt concrete damages opens up the possibility of unified asphalt damage modeling using the benefits of a mechanistic approach.

Furthermore, the interaction between fatigue and permanent deformation (rutting) is often given little attention in the existing literature, although both types of damage can evolve simultaneously, as the same load causes both damage modes. An experimental investigation was conducted following a sequential test procedure: fatigue-permanent deformation (F-PD) and permanent deformation-fatigue (PD-F) damage sequences. The following concluding remarks are made (**Paper D and Paper E**):

- First, a new criterion for independent permanent deformation and fatigue damage is proposed using an energy approach. Four creep stages were identified to mark the micro- and macro-crack phases in the creep-recovery test. The viscoelastic continuum damage (VECD) model was also applied to tension-compression (T-C) and tension-tension (T-T) fatigue tests, which have similar damage evolution effects.
- The PD-F sequence was found to be more realistic damage sequence and was suitable to analyze using both energy and continuum methods. Strain hardening (permanent deformation) was the primary cause of fatigue damage.
- The effect of pre-fatigue cracking (F-PD sequence up to 40 percent initial stiffness) on permanent deformation at 30 and 40 °C was found to be marginal. This can be related to the healing and relaxation phenomena. Moreover,

the quantity of dissipated energy alone may not be sufficiently accurate to characterize the effect of pre-cracks on permanent deformation.

6.2 Limitations

Asphalt concrete pavements undergo various mechanical and environmental loading cycles. Thus, the *viscoelastic-viscoplastic-viscodamage* response of asphalt concrete should be evaluated simultaneously under random loading and certain environmental scenarios. However, because of the complexity of this effort, the existing test protocols are designed to characterize only one mode of damage. This is a significant limitation of a mutual and realistic damage prediction method. Another limitation is that most of the mixtures tested in this study were collected from industrial mix production plants. Thus, variability and workmanship pitfalls can be assumed.

6.3 Further research

This project has opened up several research directions for future study. Potential research directions related to this study are listed .

- At the material level, the balanced mixture design approach was not addressed in this study. Improving the performance of both fatigue- and rutting- damage resistant mixtures is an ongoing challenge. At the structural level, the interaction between these two types damage is even more complex. One of the research directions is the development of unified damage model using the advantages of a mechanistic approach to achieve the coupling of damage and phenomena, such as healing, relaxation, and aging. This study presents enormous challenges in both theoretical and computational aspects.
- Conventionally, fatigue damage has been investigated in the uniaxial state. However, the triaxial nature of asphalt concrete must be considered in fatigue characterization, and viscoelastic damage constitutive models can be updated accordingly.

- Furthermore, the validity of the time-temperature-pressure superposition principle for a linear viscoelastic response can be extended in future research to assess the possibility of permanent deformation and fatigue damage interaction. Moreover, the numerical modeling of the fatigue and rutting interaction is not covered in this thesis, which can be another research direction.

Bibliography

- [1] M. N. Partl. Towards improved testing of modern asphalt pavements. *Materials and Structures*, 51(6), 2018.
- [2] Freddy L. Roberts, Louay N. Mohammad, and L. B. Wang. History of hot mix asphalt mixture design in the united states. *Journal of Materials in Civil Engineering*, 14(4):279–293, 2002.
- [3] Aleksandar S Vesic and Leonard Domaschuk. Theoretical analysis of structural behavior of road test flexible pavements. Report 0077-5614, GEORGIA INSTITUTE OF TECHNOLOGY , ATLANTA , GA., 1964.
- [4] M. N. Partl. Towards improved testing of modern asphalt pavements. *Materials and Structures*, 51(6), 2018.
- [5] Thomas William Kennedy, Gerald A Huber, Edward T Harrigan, Ronald J Cominsky, Charles S Hughes, Harold Von Quintus, and James S Moulthrop. Superior performing asphalt pavements (superpave): The product of the shrp asphalt research program. Report, National Academy of Sciences, 1994.
- [6] Robert L Lytton, Jacob Uzan, Emmanuel G Fernando, Reynaldo Roque, Dennis Hiltunen, and Shelley M Stoffels. *Development and validation of performance prediction models and specifications for asphalt binders and paving mixes*, volume 357. Strategic Highway Research Program Washington, DC, 1993.
- [7] COST 333 European Commission. *COST 333: Development of New Bituminous Pavement Design Method: Final Report of the Action*, volume 18906. European Communities, 1999. (Organization).

- [8] Matthew W Witczak. *Specification criteria for simple performance tests for rutting*, volume 580. Transportation Research Board, 2007.
- [9] Eyad Masad, Rashid Abu Al-Rub, and Dallas N. Little. Recent developments and applications of pavement analysis using nonlinear damage (panda) model. In A. Scarpas, N. Kringos, I. Al-Qadi, and Loizos A, editors, *7th RILEM International Conference on Cracking in Pavements*, pages 399–408. Springer Netherlands.
- [10] Meng Ling, Xue Luo, Yu Chen, Fan Gu, and Robert L. Lytton. Mechanistic-empirical models for top-down cracking initiation of asphalt pavements. *International Journal of Pavement Engineering*, pages 1–10, 2018.
- [11] Naresh R. Muthadi and Y. Richard Kim. Local calibration of mechanistic-empirical pavement design guide for flexible pavement design. *Transportation Research Record: Journal of the Transportation Research Board*, 2087(1):131–141, 2008.
- [12] C. Sauzeat and H. Di Benedetto. Tridimensional linear viscoelastic behavior of bituminous materials. In Shin-Che Huang and Hervé Di Benedetto, editors, *Advances in Asphalt Materials*, Woodhead Publishing Series in Civil and Structural Engineering, pages 59–95. Woodhead Publishing, Oxford, 2015.
- [13] R. A. Schapery. Correspondence principles and a generalized integral for large deformation and fracture analysis of viscoelastic media. *International Journal of Fracture*, 25(3):195–223, 1984.
- [14] Y. R. Kim, Y. C. Lee, and H. J. Lee. Correspondence principle for characterization of asphalt concrete. *Journal of Materials in Civil Engineering*, 7(1):59–68, 1995.
- [15] S. W. Park and R. A. Schapery. Methods of interconversion between linear viscoelastic material functions. part i—a numerical method based on prony series. *International Journal of Solids and Structures*, 36(11):1653–1675, 1999.

- [16] S. W. Park and R. A. Schapery. A viscoelastic constitutive model for particulate composites with growing damage. *International Journal of Solids and Structures*, 34(8):931–947, 1997.
- [17] François Olard, Hervé Di Benedetto, Bernard Eckmann, and Jean-Pierre Triquigneaux. Linear viscoelastic properties of bituminous binders and mixtures at low and intermediate temperatures. *Road Materials and Pavement Design*, 4(1):77–107, 2003.
- [18] Taeyoung Yun and Y. Richard Kim. A viscoplastic constitutive model for hot mix asphalt in compression at high confining pressure. *Construction and Building Materials*, 25(5):2733–2740, 2011.
- [19] Vijay Subramanian, Murthy N. Guddati, and Y. Richard Kim. A viscoplastic model for rate-dependent hardening for asphalt concrete in compression. *Mechanics of Materials*, 59:142–159, 2013.
- [20] I. Widyatmoko, C. Ellis, and J. M. Read. Energy dissipation and the deformation resistance of bituminous mixtures. *Materials and Structures*, 32(3):218–223, 1999.
- [21] Xue Luo, Fan Gu, Meng Ling, and Robert L. Lytton. Review of mechanistic-empirical modeling of top-down cracking in asphalt pavements. *Construction and Building Materials*, 191:1053–1070, 2018.
- [22] Leslie Ann Myers, Reynaldo Roque, Byron E. Ruth, and Christos Drakos. Measurement of contact stresses for different truck tire types to evaluate their influence on near-surface cracking and rutting. *Transportation Research Record: Journal of the Transportation Research Board*, 1655(1):175–184, 1999.
- [23] Daniel Perraton, Hervé Di Benedetto, Cédric Sauzéat, Chantal De La Roche, Wojtek Bankowski, Manfred Partl, and James Grenfell. Rutting of bituminous mixtures: wheel tracking tests campaign analysis. *Materials and Structures*, 44(5):969–986, 2011.

- [24] Hérve Di Benedetto, Thomas Gabet, James Grenfell, Daniel Perraton, Cédric Sauzéat, and Didier Bodin. *Mechanical Testing of Bituminous Mixtures*, pages 143–256. Springer Netherlands, 2013.
- [25] Joacim Lundberg, Sara Janhäll, Mats Gustafsson, and Sigurdur Erlingsson. Calibration of the swedish studded tyre abrasion wear prediction model with implication for the nortrip road dust emission model. *International Journal of Pavement Engineering*, pages 1–15, 2019.
- [26] Erdem Coleri, John T. Harvey, Kai Yang, and John M. Boone. A micromechanical approach to investigate asphalt concrete rutting mechanisms. *Construction and Building Materials*, 30:36–49, 2012.
- [27] J. Song and T. Pellinen. Dilation behavior of hot mix asphalt under triaxial loading. *Road Materials and Pavement Design*, 8(1):103–125, 2007.
- [28] Fujie Zhou and Tom Scullion. Discussion: Three stages of permanent deformation curve and rutting model. *International Journal of Pavement Engineering*, 3(4):251–260, 2002.
- [29] Wei Cao and Y. Richard Kim. A viscoplastic model for the confined permanent deformation of asphalt concrete in compression. *Mechanics of Materials*, 92:235–247, 2016.
- [30] A Sides, Jacob Uzan, and M Perl. A comprehensive viscoelasto-plastic characterization of sand-asphalt compressive and tensile cyclic loading. *Journal of testing and evaluation*, 13(1):49–59, 1985.
- [31] Juliette Blanc, Thomas Gabet, Pierre Horny, Jean-Michel Piau, and Hervé Di Benedetto. Cyclic triaxial tests on bituminous mixtures. *Road Materials and Pavement Design*, 16(1):46–69, 2014.
- [32] E. R. Brown and Kee Y. Foo. Comparison of unconfined- and confined-creep tests for hot mix asphalt. *Journal of Materials in Civil Engineering*, 6(2):307–326, 1994.

- [33] Bohdan Dołżycki and Józef Judycki. Behaviour of asphalt concrete in cyclic and static compression creep test with and without lateral confinement. *Road Materials and Pavement Design*, 9(2):207–225, 2008.
- [34] Dallas N Little, David H Allen, and Amit Bhasin. *Modeling and design of flexible pavements and materials*. Springer, 2018.
- [35] Mohammad M. Karimi, Nader Tabatabaee, Behnam Jahangiri, and Masoud K. Darabi. Constitutive modeling of hardening-relaxation response of asphalt concrete in cyclic compressive loading. *Construction and Building Materials*, 137:169–184, 2017.
- [36] Taeyoung Yun and Y. Richard Kim. Experimental investigation of rate-dependent hardening-softening behavior of hot mix asphalt in compression. *Road Materials and Pavement Design*, 12(1):99–114, 2011.
- [37] Laith Tashman, Eyad Masad, Hussein Zbib, Dallas Little, and Kamil Kaloush. Microstructural viscoplastic continuum model for permanent deformation in asphalt pavements. *Journal of Engineering Mechanics*, 131(1):48–57, 2005.
- [38] Masanobu Oda and Hideo Nakayama. Yield function for soil with anisotropic fabric. *Journal of Engineering Mechanics*, 115(1):89–104, 1989.
- [39] Huanan Yu, Balasingam Muhunthan, and Shihui Shen. Anisotropic nonlinear elastoviscoplastic model for rutting of asphalt mixtures. *Journal of Engineering Mechanics*, 140(2):242–249, 2014.
- [40] Terhi Pellinen, Geoff Rowe, and Kalapi Biswas. Evaluation of surface (top down) longitudinal wheel path cracking. Report, FHWA, 2004.
- [41] Fujie Zhou, David Newcomb, Charles Gurganus, Seyedamin Banihashemrad, Maryam Sakhaeifar, Eun Sug Park, and Robert L. Lytton. *Field Validation of Laboratory Tests to Assess Cracking Resistance of Asphalt Mixtures: An Experimental Design*. The National Academies Press, Washington, DC, 2016.

- [42] H. Di Benedetto, C. De La Roche, H. Baaj, A. Pronk, and R. Lundström. Fatigue of bituminous mixtures. *Materials and Structures*, 37(3):202–216, 2004.
- [43] M. Gajewski, W. Bańkowski, and A. C. Pronk. Evaluation of fatigue life of high modulus asphalt concrete with use of three different definitions. *International Journal of Pavement Engineering*, 21(14):1717–1728, 2020.
- [44] Yizhuang Wang and Y. Richard Kim. Development of a pseudo strain energy-based fatigue failure criterion for asphalt mixtures. *International Journal of Pavement Engineering*, 20(10):1182–1192, 2019.
- [45] Sun Woo Park, Y. Richard Kim, and Richard A. Schapery. A viscoelastic continuum damage model and its application to uniaxial behavior of asphalt concrete. *Mechanics of Materials*, 24(4):241–255, 1996.
- [46] B. Shane Underwood, Cheolmin Baek, and Y. Richard Kim. Simplified viscoelastic continuum damage model as platform for asphalt concrete fatigue analysis. *Transportation Research Record: Journal of the Transportation Research Board*, 2296(1):36–45, 2012.
- [47] Shihui Shen, Gordon D. Airey, Samuel H. Carpenter, and Hai Huang. A dissipated energy approach to fatigue evaluation. *Road Materials and Pavement Design*, 7(1):47–69, 2006.
- [48] Ibrahim Onifade, Björn Birgisson, and Romain Balieu. Energy-based damage and fracture framework for viscoelastic asphalt concrete. *Engineering Fracture Mechanics*, 145:67–85, 2015.
- [49] Boonchai Sangpetngam, Bjorn Birgisson, and Reynaldo Roque. Development of efficient crack growth simulator based on hot-mix asphalt fracture mechanics. *Transportation Research Record: Journal of the Transportation Research Board*, 1832(1):105–112, 2003.

- [50] A. A. A. Molenaar. Bottom-up fatigue cracking: myth or reality. In *In The 5th RILEM Conference: Cracking in Pavement Mitigation, Risk Assessment and Prevention*, page 275, 2004.
- [51] Sungho Mun, Murthy N. Guddati, and Y. Richard Kim. Fatigue cracking mechanisms in asphalt pavements with viscoelastic continuum damage finite-element program. *Transportation Research Record: Journal of the Transportation Research Board*, 1896(1):96–106, 2004.
- [52] Tunwin Svasdisant, Michael Schorsch, Gilbert Y. Baladi, and Suwanna Pinyosun. Mechanistic analysis of top-down cracks in asphalt pavements. *Transportation Research Record: Journal of the Transportation Research Board*, 1809(1):126–136, 2002.
- [53] R. L. Lytton, Y. Zhang, X. Luo, and R. Luo. *The fatigue cracking of asphalt mixtures in tension and compression*, pages 243–272. Woodhead Publishing, Oxford, 2015.
- [54] Dallas N. Little, David H. Allen, and Amit Bhasin. *One-Dimensional Constitutive Theory*, page 389–417. Springer International Publishing, 2018.
- [55] SW Park and YR Kim. Interconversion between relaxation modulus and creep compliance for viscoelastic solids. *Journal of materials in Civil Engineering*, 11(1):76–82, 1999.
- [56] Sungho Mun and Goangseup Zi. Modeling the viscoelastic function of asphalt concrete using a spectrum method. *Mechanics of Time-Dependent Materials*, 14(2):191–202, 2010.
- [57] GR Chehab, YR Kim, RA Schapery, MW Witzak, and R Bonaquist. Time-temperature superposition principle for asphalt concrete with growing damage in tension state. *Journal of the Association of Asphalt Paving Technologists*, 71, 2002.

- [58] G. D. Airey, B. Rahimzadeh, and A. C. Collop. Viscoelastic linearity limits for bituminous materials. *Materials and Structures*, 36(10):643–647, 2003.
- [59] Charles W. Schwartz, Nelson Gibson, and Richard A. Schapery. Time-temperature superposition for asphalt concrete at large compressive strains. *Transportation Research Record: Journal of the Transportation Research Board*, 1789(1):101–112, 2002.
- [60] E. Levenberg and J. Uzan. Triaxial small-strain viscoelastic-viscoplastic modeling of asphalt aggregate mixes. *Mechanics of Time-Dependent Materials*, 8(4):365–384, 2004.
- [61] Pierre Gayte, Hervé Di Benedetto, Cédric Sauzéat, and Quang Tuan Nguyen. Influence of transient effects for analysis of complex modulus tests on bituminous mixtures. *Road Materials and Pavement Design*, 17(2):271–289, 2016.
- [62] Mequanent Mulugeta Alamnie, Ephrem Tadesse, and Inge Hoff. Thermo-piezo-rheological characterization of asphalt concrete. *Construction and Building Materials*, 329:127106, 2022.
- [63] Eisa Rahmani, Masoud K. Darabi, Rashid K. Abu Al-Rub, Emad Kassem, Eyad A. Masad, and Dallas N. Little. Effect of confinement pressure on the nonlinear-viscoelastic response of asphalt concrete at high temperatures. *Construction and Building Materials*, 47:779–788, 2013.
- [64] Piotr Perzyna. Memory effects and internal changes of a material†. *International Journal of Non-Linear Mechanics*, 6(6):707–716, 1971.
- [65] Masoud K. Darabi, Rashmi Kola, Dallas N. Little, and Navneet Garg. Time-dependent drucker-prager-cap model coupled with panda (pavement analysis using nonlinear damage approach) to predict rutting performance of flexible pavements. *Construction and Building Materials*, 244:118326, 2020.
- [66] Masoud K. Darabi, Rashid K. Abu Al-Rub, Eyad A. Masad, Chien-Wei Huang, and Dallas N. Little. A thermo-viscoelastic–viscoplastic–viscodamage constitu-

- tive model for asphaltic materials. *International Journal of Solids and Structures*, 48(1):191–207, 2011.
- [67] R. A. Schapery. Nonlinear viscoelastic and viscoplastic constitutive equations with growing damage. *International Journal of Fracture*, 97(1/4):33–66, 1999.
- [68] Andrew C. Collop, A. Scarpas, Cor Kasbergen, and Arian De Bondt. Development and finite element implementation of stress-dependent elastoviscoplastic constitutive model with damage for asphalt. *Transportation Research Record: Journal of the Transportation Research Board*, 1832(1):96–104, 2003. (Tom).
- [69] John F. Rushing, Masoud K. Darabi, Eisa Rahmani, and Dallas N. Little. Comparing rutting of airfield pavements to simulations using pavement analysis using nonlinear damage approach (panda). *International Journal of Pavement Engineering*, 18(2):138–159, 2017.
- [70] Maryam Shakiba, Angeli Gamez, Imad L. Al-Qadi, and Dallas Neville Little. Introducing realistic tire–pavement contact stresses into pavement analysis using nonlinear damage approach (panda). *International Journal of Pavement Engineering*, 18(11):1027–1038, 2017.
- [71] R. A. Schapery. On the characterization of nonlinear viscoelastic materials. *Polymer Engineering and Science*, 9(4):295–310, 1969.
- [72] Masoud K. Darabi, Rashid K. Abu Al-Rub, Eyad A. Masad, and Dallas N. Little. Constitutive modeling of fatigue damage response of asphalt concrete materials with consideration of micro-damage healing. *International Journal of Solids and Structures*, 50(19):2901–2913, 2013.
- [73] Alexander M. Korsunsky, Daniele Dini, Fionn P. E. Dunne, and Michael J. Walsh. Comparative assessment of dissipated energy and other fatigue criteria. *International Journal of Fatigue*, 29(9):1990–1995, 2007.

- [74] Samuel H. Carpenter and Shihui Shen. Dissipated energy approach to study hot-mix asphalt healing in fatigue. *Transportation Research Record: Journal of the Transportation Research Board*, 1970(1):178–185, 2006.
- [75] Khalid A. Ghuzlan and Samuel H. Carpenter. Energy-derived, damage-based failure criterion for fatigue testing. *Transportation Research Record: Journal of the Transportation Research Board*, 1723(1):141–149, 2000.
- [76] Xue Luo, Rong Luo, and Robert L. Lytton. Energy-based mechanistic approach for damage characterization of pre-flawed visco-elasto-plastic materials. *Mechanics of Materials*, 70:18–32, 2014.
- [77] Lazar M. Kachanov. On time to rupture in creep conditions (in russian). *Izvestiya Akademii Nauk SSSR*, 8:26–31 (in Russian), 1958.
- [78] Iu N. Rabotnov. *Creep problems in structural members*, volume 7. North-Holland Publishing Company, 1969.
- [79] Lazar M. Kachanov. Rupture time under creep conditions. *International Journal of Fracture*, 97(1/4):11–18 (translated from Russian, 1958), 1999.
- [80] J. L. Chaboche and P. M. Lesne. A non-linear continuous fatigue damage model. *Fatigue and Fracture of Engineering Materials and Structures*, 11(1):1–17, 1988.
- [81] RA Schapery. A theory of mechanical behavior of elastic media with growing damage and other changes in structure. *Journal of the Mechanics and Physics of Solids*, 38(2):215–253, 1990.
- [82] Y. Richard Kim, M. N. Guddati, B. S. Underwood, T. Y. Yun, V. Subramanian, and S. Savadatti. *Development of a multiaxial viscoelastoplastic continuum damage model for asphalt mixtures*. Federal Highway Administration, 2009.
- [83] Hyun-Jong Lee, Jo Sias Daniel, and Y. Richard Kim. Continuum damage mechanics-based fatigue model of asphalt concrete. *Journal of Materials in Civil Engineering*, 12(2):105–112, 2000.

- [84] Jo Sias Daniel and Y Richard Kim. Development of a simplified fatigue test and analysis procedure using a viscoelastic, continuum damage model (with discussion). *Journal of the Association of Asphalt Paving Technologists*, 71, 2002.
- [85] B. Shane Underwood, Y. Richard Kim, Murthy Guddati, Terhi Pellinen, Wu Rongzong, Gayle King, Robert Kluttz, and Nelson Gibson. Characterization and performance prediction of alf mixtures using a viscoelastoplastic continuum damage model. In *Asphalt Paving Technology: Association of Asphalt Paving Technologists-Proceedings of the Technical Sessions*, volume 75, pages 577–636, 2006. Association of Asphalt Paving Technologists -Proceedings of the Technical Sessions 2006 Annual Meeting ; Conference date: 27-03-2006 Through 29-03-2006.
- [86] B. Shane Underwood, Y. Richard Kim, and Murthy N. Guddati. Improved calculation method of damage parameter in viscoelastic continuum damage model. *International Journal of Pavement Engineering*, 11(6):459–476, 2010.
- [87] J. Lemaitre and A. Plumtree. Application of damage concepts to predict creep-fatigue failures. *Journal of Engineering Materials and Technology*, 101(3):284–292, 1979.
- [88] R. P. Skelton and D. Gandy. Creep – fatigue damage accumulation and interaction diagram based on metallographic interpretation of mechanisms. *Materials at High Temperatures*, 25(1):27–54, 2008.
- [89] Kai Zhao, Hongling Ma, Chunhe Yang, Xiangsheng Chen, Yibiao Liu, Xiaopeng Liang, and Rui Cai. Damage evolution and deformation of rock salt under creep-fatigue loading. *Rock Mechanics and Rock Engineering*, 54(4):1985–1997, 2021.
- [90] Terhi K. Pellinen and Matthew W. Witczak. Use of stiffness of hot-mix asphalt as a simple performance test. *Transportation Research Record: Journal of the Transportation Research Board*, 1789(1):80–90, 2002.

- [91] François Olard and Hervé Di Benedetto. General “2s2p1d” model and relation between the linear viscoelastic behaviours of bituminous binders and mixes. *Road Materials and Pavement Design*, 4(2):185–224, 2003.
- [92] Malcolm L Williams, Robert F Landel, and John D Ferry. The temperature dependence of relaxation mechanisms in amorphous polymers and other glass-forming liquids. *Journal of the American Chemical society*, 77(14):3701–3707, 1955.
- [93] R. W. Fillers and N. W. Tschoegl. The effect of pressure on the mechanical properties of polymers. *Transactions of the Society of Rheology*, 21(1):51–100, 1977.
- [94] Jacob Uzan. A new approach to characterizing asphalt concrete in the linear/nonlinear small strain domain. *Mechanics of Time-Dependent Materials*, 24(1):101–127, 2020.
- [95] W. N. Findley and J. S. Y. Lai. A modified superposition principle applied to creep of nonlinear viscoelastic material under abrupt changes in state of combined stress. *Transactions of the Society of Rheology*, 11(3):361–380, 1967.
- [96] Hao Chen, Mequanent Mulugeta Alamnie, Diego Maria Barbieri, Xuemei Zhang, Gang Liu, and Inge Hoff. Comparative study of indirect tensile test and uniaxial compression test on asphalt mixtures: Dynamic modulus and stress-strain state. *Construction and Building Materials*, 366:130187, 2023.
- [97] Y. Richard Kim, Youngguk Seo, Mark King, and Mostafa Momen. Dynamic modulus testing of asphalt concrete in indirect tension mode. *Transportation Research Record: Journal of the Transportation Research Board*, 1891(1):163–173, 2004.
- [98] Nicholas W. Tschoegl. *Energy Storage and Dissipation in a Linear Viscoelastic Material*, pages 443–488. Springer Berlin Heidelberg, Berlin, Heidelberg, 1989.

- [99] M. Alamnie, E. Taddesse, and I. Hoff. *Viscoelastic characterization and comparison of Norwegian asphalt mixtures using dynamic modulus and IDT tests*, pages 118–128. CRC Press, 2021.
- [100] Juliette Blanc, Thomas Gabet, Pierre Horny, Jean-Michel Piau, and Hervé Di Benedetto. Cyclic triaxial tests on bituminous mixtures. *Road Materials and Pavement Design*, 16(1):46–69, 2014.
- [101] Nelson H. Gibson, Charles W. Schwartz, Richard A. Schapery, and Matthew W. Witczak. Viscoelastic, viscoplastic, and damage modeling of asphalt concrete in unconfined compression. *Transportation Research Record: Journal of the Transportation Research Board*, 1860(1):3–15, 2003.
- [102] L. Francken. Permanent deformation law of bituminous road mixes in repeated triaxial compression. In *4th International Conference on Structural Design of Asphalt Pavements*, volume 1, pages 483–496, 1977.
- [103] Taeyoung Yun, B. Shane Underwood, and Y. Richard Kim. Time-temperature superposition for hma with growing damage and permanent strain in confined tension and compression. *Journal of Materials in Civil Engineering*, 22(5):415–422, 2010.
- [104] Tarig O. Medani, Marinus Huurman, and André A. A. Molenaar. A unified model to describe the time-temperature dependency characteristics of several bound road materials. *Road Materials and Pavement Design*, 8(3):551–577, 2007.
- [105] Yanqing Zhao and Y. Richard Kim. Time-temperature superposition for asphalt mixtures with growing damage and permanent deformation in compression. *Transportation Research Record: Journal of the Transportation Research Board*, 1832(1):161–172, 2003.

Appendices

Appended Papers

Paper A

Advances in Permanent deformation Modeling of Asphalt concrete - A Review

Mequanent Mulugeta Alamnie, Ephrem Taddesse and Inge Hoff. Materials, 15 (3480), 2022. doi:[10.3390/ma15103480](https://doi.org/10.3390/ma15103480)

Review

Advances in Permanent Deformation Modeling of Asphalt Concrete—A Review

Mequanent Mulugeta Alamnie ^{1,*}, Ephrem Tadesse ¹ and Inge Hoff ²¹ Department of Engineering Science, University of Agder, 4879 Grimstad, Norway; ephrem.tadesse@uia.no² Department of Civil and Environmental Engineering, Norwegian Science and Technology University (NTNU), 7491 Trondheim, Norway; inge.hoff@ntnu.no

* Correspondence: mequanent.m.alamnie@uia.no

Abstract: Permanent deformation is one of the dominant asphalt concrete damages. Significant progress has been made to realistically predict the damage. In the last decade, the mechanistic approach has been the focus of research, and the fundamental theories of viscoelasticity, viscoplasticity, continuum mechanics, and micromechanics are applied to develop the material laws (constitutive equations). This paper reviews the advancement of permanent deformation models including analogical, microstructural, and continuum-based methods. Pavement analysis using the nonlinear damage approach (PANDA) is the most comprehensive and theoretically sound approach that is available in the literature. The model coupled different damages and other phenomena (such as cracking, moisture, and phenomena such as healing, aging, etc.). The anisotropic microstructure approach can be incorporated into the PANDA approach for a more realistic prediction. Moreover, the interaction of fatigue and permanent deformation is the gap that is lacking in the literature. The mechanistic approaches have the capacity to couple these damages for unified asphalt concrete damage prediction.

Keywords: permanent deformation; mechanistic; viscoplastic; viscodamage; microstructure



Citation: Alamnie, M.M.; Tadesse, E.; Hoff, I. Advances in Permanent Deformation Modeling of Asphalt Concrete—A Review. *Materials* **2022**, *15*, 3480. <https://doi.org/10.3390/ma15103480>

Academic Editor: Karim Benzarti

Received: 12 April 2022

Accepted: 9 May 2022

Published: 12 May 2022

Publisher's Note: MDPI stays neutral with regard to jurisdictional claims in published maps and institutional affiliations.



Copyright: © 2022 by the authors. Licensee MDPI, Basel, Switzerland. This article is an open access article distributed under the terms and conditions of the Creative Commons Attribution (CC BY) license (<https://creativecommons.org/licenses/by/4.0/>).

1. Introduction

A flexible pavement, the longest continuous structure, comprises an asphalt concrete layer supported by unbound compacted layers (aggregate bases and subgrade). Asphaltic materials have been used for roadway construction since the end of the nineteenth century [1]. Asphalt concrete (also called bituminous mixture or hot mix asphalt) is a complex heterogeneous and three-phase material (aggregate matrix, mastic, and the air void). Such a material's performance depends on the mixture composition, proportion, mechanical properties, and environmental conditions. It is characterized as a viscoelastic, viscoplastic, and time- and temperature-dependent material. Due to external loads and environmental factors, different distresses or damages occur in the asphalt layer. Permanent deformation or rutting is one of the primary distresses, making pavements rough and unsafe for driving, causing hydroplaning, etc. The rutting distress was noticed as a primary asphalt performance criterion [2]. The asphalt concrete's susceptibility to permanent deformation is linked to material attributes and climatic and loading factors [3–5]. Material-related factors include excessive asphalt content, fine aggregate, high natural sand percentage, rounded aggregate particles, the moisture content in the mix, or granular materials and soils. From the asphalt concrete constituent properties, the chemistry of asphalt binder is the component (if not only) that makes bituminous mixtures a complex rate-dependent, nonlinear material. This nonlinear (viscous) behavior of the binder makes the permanent deformation evolution of asphalt mixtures a nonlinear mechanism [6]. For this reason, the rheological characteristics of binder (shear modulus, G^* , and viscosity, η) are used to classify deformability properties of mixtures. The Strategic Highway Research Program (SHRP) rheological parameter, $G^*/\sin \delta$ (δ —the phase angle), is the widely used

criterion for rutting characterization [7]. The increased value of the criteria $G^*/\sin \delta$ leads to a reduced tendency to permanent deformation. However, the $G^*/\sin \delta$ showed limitations as it cannot predict modified binders. Thus, researchers have proposed modified rheological parameters for rutting [8]. Laukkanen et al. [8] conducted multiple stress creep-recovery (MSCR) tests on unmodified and modified binders. They concluded that the non-recoverable creep compliance parameter and accumulated strain at the end of the MSCR test showed a strong correlation and predicted mixture rutting performance compared to other rheological indicators. Meena et al. [9] investigated the rutting performance of asphalt mixture through the prediction of a resilient modulus (M_R) based on the $G^*/\sin \delta$ rheological model. The second major constituent of asphalt concrete mixtures is the aggregate. As the primary load-carrying component, the aggregate gradation, property, angularity, texture, etc., have direct influence on the permanent deformation resistance of asphalt concrete. Research has shown that fine aggregates are better for rutting resistance [6]. Decreasing the maximum aggregate size is also good for rut resistance [10], and a fine aggregate texture is highly correlated to rutting [11]. Two theories have been assumed related to fine aggregate's role for permanent deformation; first, fillers serve to fill the voids between aggregate particles, thereby increasing the density and strength of the compacted mixture, and secondly, the fine particles of the filler become suspended in the asphaltic binder, forming a mastic. The suspended filler particles absorb binder components, hence increasing the viscosity of the binder and, consequently, the toughness of the mixes. On the contrary, Kandhal et al. [12] reported that coarse- or fine-graded Superpave mixtures do not significantly differ in rutting resistance. In addition, the aggregate type and the chemical composition also play important roles for the creep-recovery behavior of asphalt mixtures [13]. For example, siliceous aggregate mixes show a better recovery property than do calcareous aggregates. Thus, permanent deformation is a complex phenomenon where aggregate, asphalt, and asphalt–aggregate interaction (adhesion) properties control the overall performance. These properties may change over time as a result of associated damages such as aging or moisture to the asphalt–aggregate interface and fatigue cracking. Moreover, temperature-susceptible asphalt concrete and cold weather paving, which leads to low density, are factors for permanent deformation. Other climatic factors that affect rutting are temperature, precipitation, duration, type of loading, and loading extent.

The rutting of asphalt concrete is generally related to three mechanisms. The first mechanism is related to wear rutting in the wheel path, mainly due to studded tire abrasion [14]. The second mechanism of rutting is due to the viscoplastic strain accumulation (permanent deformation) in the asphalt layer. This mechanism is caused by the densification (volume change) and shear flow at a high temperature and stress level. The third form of rutting is due to a substructural failure (subsidence) of the granular subbase, subgrade layers [15,16]. Furthermore, the development of permanent deformation is a gradual and simultaneous mechanism of densification (closing of voids), shearing (slippage due to loss of adhesion between aggregates and binder), and dilation [17] as well as the initiation and growth of micro-crack damage [18]. Again, the accumulation of permanent deformation (viscoplastic strain) within the microstructure of asphalt concrete involves three phenomena: (1) viscoplastic deformation associated with the asphalt binder, (2) rotation and slippage of aggregates (evolution of the microstructure), and (3) crack initiation and propagation (microcracks and macrocracks) [19–22]. The deformation resistance of asphalt concrete is derived from the aggregate matrix and the viscous asphalt mastic. The microstructure changes due to loading (such as air void reduction) and chemical transformation (such as aging) causes the continuous modification of aggregate matrix and asphalt mastic with time. In addition, the relaxation ability of the pavement upon load removal changes as the microstructure is continuously modified [23–25]. Furthermore, the growth of permanent deformation is highly dependent on the stress path and strain rate [26]. Excessive deviatoric stress and the environment cause a nonlinear, plastic, and viscous flow phenomenon where the stress–strain relationship shows strong nonlinearity [27] (especially at high strains where the linear thermo-rheological properties are not valid).

In the literature, both *permanent deformation* and *rutting* terminologies are used interchangeably. The term “*Rutting*” is used to describe the pavement surface roughness due to the vertical depression along the wheel path caused by the permanent deformation or wear in the asphalt layer. Permanent deformation is the accumulation of irrecoverable strain due to densification, shear deformation, and crack growth in asphalt concrete. In this paper, the term permanent deformation is used to refer to the plastic and viscoplastic strains (irrecoverable deformation). Therefore, rutting (RD, mm) is expressed as follows.

$$RD = \sum_{i=1}^i h_i \varepsilon_{vp,i} \quad (1)$$

where h_i is the i th layer’s thickness, and $\varepsilon_{vp,i}$ is the viscoplastic/permanent strain in the i th layer.

2. Objective and Scope

The aim of this review is to provide state-of-the-art information on the developments of permanent deformation modeling for asphalt concrete. In the review, the main permanent deformation modeling theories, methods, models, and calibration tests are discussed in detail. The focus of the paper is studying the advancement of constitutive modeling approaches (analogical, microstructural, and continuum-based) and synthesize the capacity of the approaches, merits, and limitations. The robustness of permanent deformation models to account for/couple simultaneous damages such as moisture, fatigue cracking, etc., were also explored. The literature studied in this paper was collected using keywords (strings) such as viscoelastic, viscoplastic, viscodamage, permanent deformation, rutting, continuum damage, microstructure or micromechanics, mechanistic methods, creep-recovery, etc. The organization of the paper is depicted in the flow chart in Figure 1.

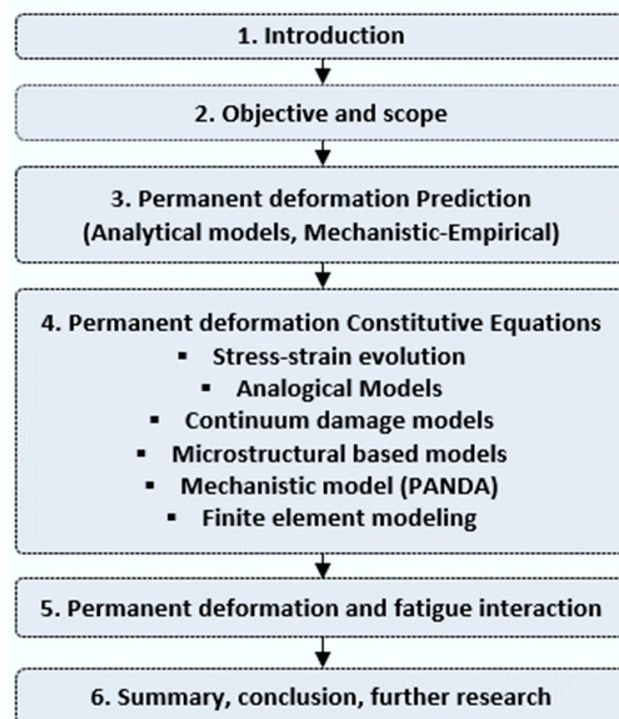


Figure 1. Flow chart of the study structure.

3. Permanent Deformation Prediction

3.1. Analytical Models

The evolution of the irrecoverable deformation of asphaltic material due to cyclic loading is described by three distinct stages, as shown in Figure 2a. The primary zone

is described by the rapid accumulation of permanent deformation at a decreasing strain rate. In the secondary zone is the constant rate of permanent deformation with strain hardening, and the tertiary stage is characterized by the increasing rate of deformation accumulate and crack formation. The flow time (FT) or the flow number (FN) is defined as the time or number of loading cycles when shear deformation under constant volume commences. Several researchers have verified that the asphalt concrete's deformation evolution showed all the three phases [28–32]. This three-stage deformation property is also regarded as asphalt concrete material property. The most common and simulative test used to characterize permanent deformation is the triaxial creep-recovery test. An example in Figure 2b shows that the creep–recovery deformation is dependent on confining stress. Confinement increases the friction between aggregates and increases the resistance to deformation. Although there is no conclusive research, the in situ confining pressure of asphalt concrete is approximated to be between 100 kPa and 225 kPa.

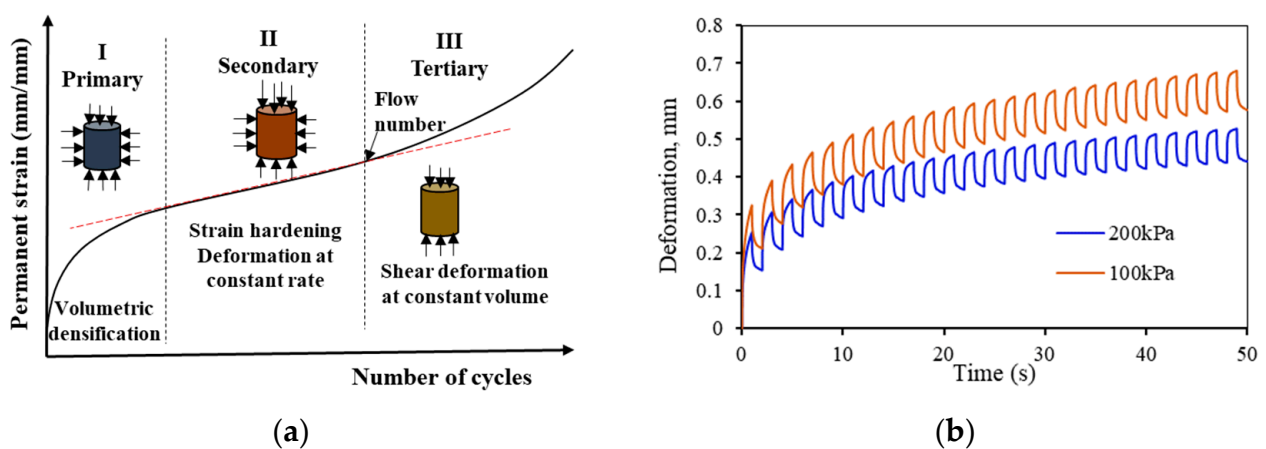


Figure 2. (a) Schematic three-stage creep deformation and (b) example of a creep–recovery test result at different confining pressures (100 kPa and 200 kPa).

Several analytical models have been proposed over several decades to predict the permanent deformation of asphalt concrete. Sousa et al. [33] gave a summary of selected analytical models. Some of the commonly used permanent deformation models and the corresponding calibration tests are summarized in Table 1. These analytical models are used to predict rutting from typical laboratory experimental data (axial stress–strain test data). The models in Table 1 can be classified as empirical and mechanistic-empirical, which are calibrated using simulative laboratory or field data. The models give the macroscopic responses of the measured data and hardly relate the fundamental material properties. Other models are regression equations to fit rutting data and lack the explicit physical or material property for the modeling parameters.

3.2. Calibration Tests

The most common laboratory test protocols used cylindrical specimens of dimensions (diameter by height) 100 mm by 150 mm for creep–recovery, or 150 mm by 50–70 mm for creep. The shear strain from simple shear tests is also used to model permanent deformation [16,34]. The coupling of shear and axial strain components in permanent deformation modeling has not been performed yet in previous studies [35]. The indirect tensile test is also used for permanent deformation with different specimen dimensions of 150 or 100 mm diameter by 50 to 70 mm thickness [36]. Moreover, the wheel tracking test is used to simulate permanent deformation [37–39].

Table 1. Some selected permanent deformation analytical models.

Model (Equation)	Variables	Description	Reference	Calibration Test
$\epsilon_p = aN^b$	a, b	Accurate for secondary stages, small stress/strain deformation		Creep, creep-recovery
$\epsilon_p = AN^B + C(e^{DN} - 1)$ Where, $A = 115(\sigma_1 - \sigma_3)E^*$ $B = 0.182 + 0.294(\sigma_{VM} - \sigma_{VL})$	A, B, C, D	Most widely used analytical model for permanent deformation in all three creep stages; the first part is a power function (for low stresses), and the second part is for high stresses (tertiary stage). (σ_{VM} —maximum stress, σ_{VL} —plastic failure threshold; σ_1, σ_3 —axial and lateral stress, E^* —stiffness)	Francken [40]	Repeated triaxial compression
$\frac{\epsilon_p}{N} = AN^{-m}, A = J\left(\frac{M_r}{\sigma_a}\right)^{-S}$	J, S, m	Analytical Power Model based on dissipated energy rate; A is a function of resilient modulus and applied stress	Khedr Safwan [41]	Multiple step dynamic test
$\epsilon_p = \epsilon_0 e^{-\left(\frac{\rho}{N}\right)^\beta}$	ϵ_0, β, ρ	Widely used analytical model to fit all creep stages	Tseng and Lytton [42]	Triaxial creep-recovery test
$\epsilon_p = \delta_1(1 - e^{\delta_2 N}) + \delta_3(e^{\delta_4 N} - 1)$	$\delta_1, \delta_2, \delta_3, \delta_4$	Analytical model for three creep stages, mainly developed for unbound materials (δ_1, δ_3 —scale primary and tertiary strain; δ_2, δ_4 —rate parameters)	Wilshire and Evans [43]	Creep tests
$\frac{\epsilon_p}{\epsilon_r} = 10^{k_1} T^{k_2} N^{k_3}$	k_1, k_2, k_3	Mechanistic-empirical (MEPDG) Model ϵ_r —resilient strain, T—temperature		Triaxial creep-recovery test
$\epsilon_p^I = aN^b$; $\epsilon_p^{II} = \epsilon_p^I + c(N_{II} - N_I)$; $\epsilon_p^{III} = \epsilon_p^{II} + d(e^{k(N - N_{II})} - 1)$	a, b, c, d, k	Three-stage rutting model (Modified Francken model) for accurate flow number identification	Zhou et al. [28]	Triaxial creep-recovery test
$\epsilon_p = A + BN - Ce^{-DN}$	A, B, C, D	Two phase, Linear exponent model (mainly for unbound granular materials)	Cerni et al. [44]	Triaxial creep-recovery test
$\epsilon_p = \frac{A+BN}{(C+N)^\alpha}$	A, B, C, α	Incremental model: mechanistic based as a function of viscoplastic hardening (H and α), loading time, deviatoric stress, and rest period (A, C contain the parameters related to initial behavior of permanent deformation)	Choi et al. [45]	Triaxial creep-recovery
$\epsilon_p = \frac{A+BN_{red}}{(C+N_{red})^\alpha}$ $N_{red} = N \times 10^{\alpha_{tot}}$ $\alpha_{tot} = \alpha_{\xi_p} + \alpha_{\sigma_d}$ $\alpha_{\xi_p} = a_1 \xi_p^{a_2} + a_3$ $\alpha_{\sigma_d} = b_1 \left(\frac{\sigma_d}{P_a}\right)^{b_2} + b_3$	$a_1, a_2, a_3, b_1, b_2, b_3, A, B, C, \alpha$	A mechanistic shift model based on the load time and stress-shift function (master curve). P_a is atmospheric pressure, ξ_p is reduced loading time, and σ_d is deviatoric stress	Choi et al. [46]	Triaxial creep-recovery
$\epsilon_p = a(N^b + e^{cN})$	a, b, c	A three-stage model modified from Francken model	Fang et al. [4]	Wheel tracking, Uniaxial cyclic compression

As shown in Figure 3, different models have different accuracy for the same permanent deformation data. It is evident that the fitting accuracy is variable especially in the primary and tertiary stages of deformation. The incremental or Choi, Tseng–Lytton, and Francken models showed close predictions of the measured data. The Francken model is the most widely used for permanent deformation modeling [30].

Each model has a different accuracy of fitting all the creep stages of permanent deformation. Some of the models presented above have clear limitations such as the implicit empiricism, being unable to model load history and hardening–relaxation behavior, a lack of capacity to couple other simultaneous damages, etc. As discussed in the next sections, mechanistic permanent deformation prediction methods are aimed to resolve the limitations of empirical/mechanistic-empirical models. The latest mechanistic models have relied on rigorous material models, which are based on fundamental theories of mechanics, stress–strain relationships, and environmental factors.

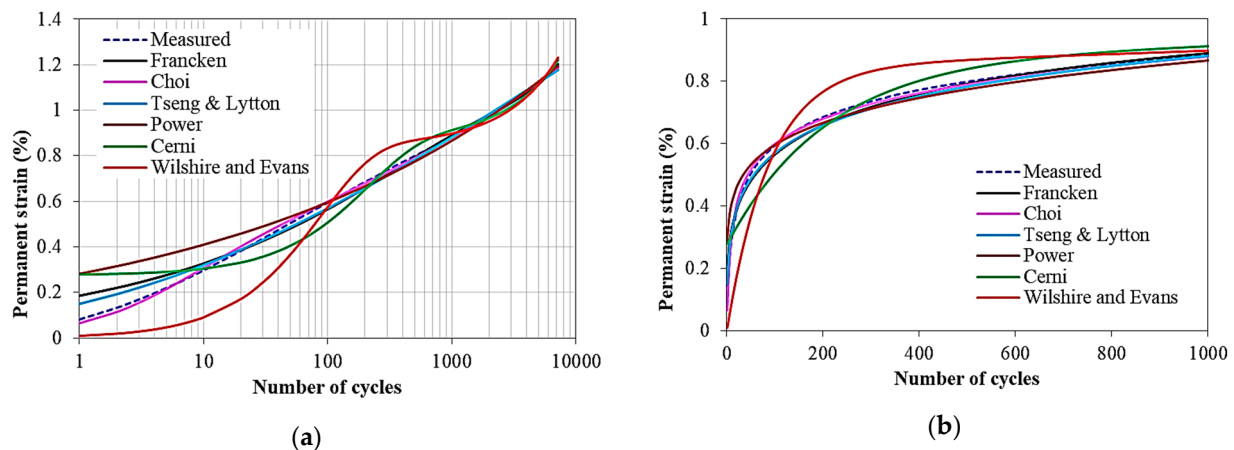


Figure 3. Example—permanent deformation prediction of some models using test data: (a) logarithmic scale and (b) normal scale.

4. Permanent Deformation Damage Modeling

4.1. Stress–Strain Response

The stress-, time-, and temperature-dependent viscoelastic, viscoplastic, and viscodamage properties of asphalt concrete material offered considerable challenges to accurately model the response under variable loading conditions. The response of asphalt concrete is stress path-dependent [26]. It is also a rate- and history-dependent material [47,48]. The linearity limits of asphalt concrete are 150 and 100 micro-strain in compression and tension, respectively [49], but others suggest 122 micro-strain as a limit for linear response [50]. Permanent deformation damage is induced on the asphalt beyond this strain limit at high temperatures. Moreover, the stress–strain evolution is highly dependent on the stress and strain levels, number of loading cycles (loading time), and temperature range. In a typical creep–recovery test, the stress–strain hysteresis loops evolve nonlinearly as shown in Figure 4a. The loop has the recovery and non-recovery (permanent deformation) parts. In each creep–recovery cycle, the deviatoric stress causes a non-recoverable strain and creates an open stress–strain hysteresis loop. Figure 4b shows the stress–strain responses of a constant rate compressive strength test (without recovery time). Asphalt concrete undergoes creep deformation during the load phase and a delayed recovery upon the load removal during the rest period. Traditionally, the additive decomposition of strain is applied to separate the permanent strain and recoverable strain from the total strain.

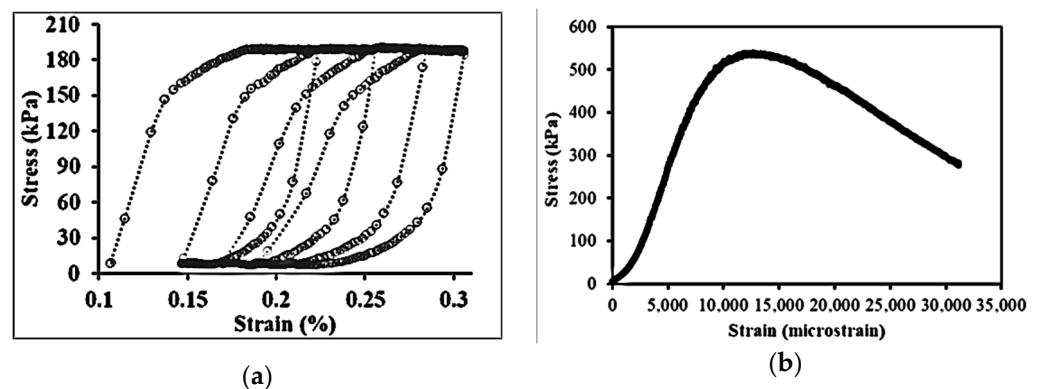


Figure 4. Stress–strain state in compression: (a) hysteresis loop under creep–recovery and (b) crosshead strain rate test.

The schematic Figure 5 shows the strain components of a single pulse creep–recovery loading. The strain components can be separated into four strain components [51,52]

(elastic ϵ^e , viscoelastic ϵ^{ve} , plastic ϵ^p , and viscoplastic ϵ^{vp}). The elastic (time-independent) and viscoelastic (time-dependent) are recoverable, while plastic (time-independent) and viscoplastic (time-dependent) strains are non-recoverable parts of total strain. The total strain is expressed as follows.

$$\epsilon_{tot} = \epsilon^e + \epsilon^{ve} + \epsilon^p + \epsilon^{vp} \tag{2}$$

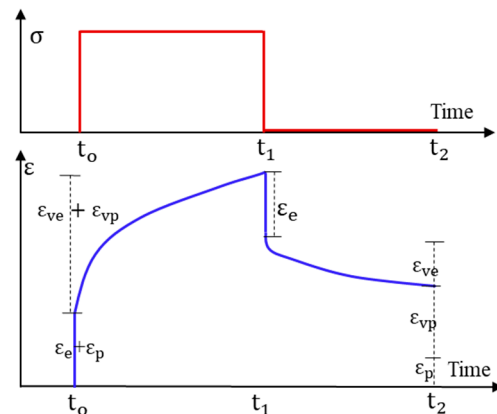


Figure 5. Schematic—typical creep-recovery strain components.

The permanent strain ($\epsilon_{vp} = \epsilon^p + \epsilon^{vp}$) is obtained by subtracting the viscoelastic strain ($\epsilon_{ve} = \epsilon^e + \epsilon^{ve}$) components from the total strain.

However, the strain decomposition approach is questioned when the hardening–relaxation mechanism of asphalt concrete is considered. In a loading–unloading cycle, the recoverable strain is dependent on the rest period. For tests with short rest periods, the computed viscoplastic strain can be overestimated [53]. The limitation of strain decomposition is from the inherent interaction between the viscoelastic and viscoplastic strain (the viscoelastic response is also a function of viscoplastic deformation history).

4.2. Constitutive Models

The computational modeling of asphalt concrete poses difficulties mainly due to the material nonlinearity, complexity to characterize under repeated and moving loads, and variable environmental conditions (temperature, moisture, etc.) [35,54]. The constitutive equations for the linear viscoelastic strain (ϵ_{ve}) in undamaged conditions is defined by the Boltzmann superposition principle.

$$\epsilon_{ve}(t) = \int_0^t D(t - \tau) \frac{d\sigma(\tau)}{d\tau} d\tau \tag{3}$$

$$\sigma(t) = \int_0^t E(t - \tau) \frac{d\epsilon_{ve}}{d\tau} d\tau \tag{4}$$

where t is time; $E(t)$ and $D(t)$ are relaxation and creep compliance moduli, respectively; and τ is the integration variable. Prony series forms of the creep compliance and relaxation moduli are expressed as follows.

$$D(t) = D_0 + \sum_{i=1}^N D_i \left[1 - \exp\left(-\frac{t}{\tau_i}\right) \right] \tag{5}$$

$$E(t) = E_\infty + \sum_{i=1}^M E_i \left[\exp\left(-\frac{t}{\rho_i}\right) \right] \tag{6}$$

where N and M are the total numbers of Prony terms; D_0 , D_i , and τ_i are creep compliance model coefficients; and E_∞ , E_i , and ρ_i are relaxation model coefficients. Often, $D(t)$ is

obtained from $E(t)$ data via the interconversion technique [55,56] ($\int_0^t E(t-\tau) \frac{dD(\tau)}{d\tau} d\tau = 1$). Once the creep compliance function is defined, the viscoelastic strain can be determined, and the viscoplastic strain is calculated from the total strain by the additive decomposition technique. A sufficient rest period is necessary to completely remove the delayed recovery strain from viscoplastic strain evolution. Cao and Kim [53] showed that 99% of viscoelastic strain is recovered for the 0.4 s pulse period and 100 s rest duration in the first cycle and 98% in cycle number 10 within 60 s. Therefore, to obtain a true viscoplastic strain, about 100 s rest period is required [45]. Experimental observations showed that the total deformation in each cycle decreases due to hardening as the number of load cycles increases. Since the viscoelastic strain is obtained from a separate dynamic modulus test (i.e., a constant viscoelastic strain), subtracting a constant cyclic viscoelastic strain from a decreasing total strain can result in a negative viscoplastic strain. That means a decreasing viscoelastic deformation model should be proposed. It is the microstructural change due to viscoplastic deformation that causes a change in viscoelastic deformation. This interaction between viscoelastic and viscoplastic deformation is referred to as *viscoelastic–viscoplastic coupling*, according to [53]. There is no available literature that couples the two deformations.

Analogical Models

The family of different analogical models has been used to model the viscoelastic–viscoplastic response of time-dependent materials [57–60]. The common classic mechanical models are spring, dashpot, slip device, pot, parabolic elements, etc., and the combination of these elements to analogs. The mechanical elements are advantageous to visualizing the stress and strain responses using the analogs. The Maxwell model (for the viscoelastic model), Kelvin model (for creep response), and the Burgers model are used to model the viscoelastic and viscoplastic strain (Figure 6a,b). The governing differential equations (viscoelastic constitutive equations) were developed from a number of springs and dashpots arranged in series and parallel. In the generalized Maxwell model, the same strain is shared across all elements, and the stress is additive, while in the generalized Burgers model the strains are additive, and the stress is the same for each element. It can be noted here that the generalized Burgers model shares the same framework as classical viscoplasticity models and allows nonlinearities based on stress to be accommodated more easily [57]. The viscoelastic and viscoplastic components can be calculated using the hereditary integral formulation as follows.

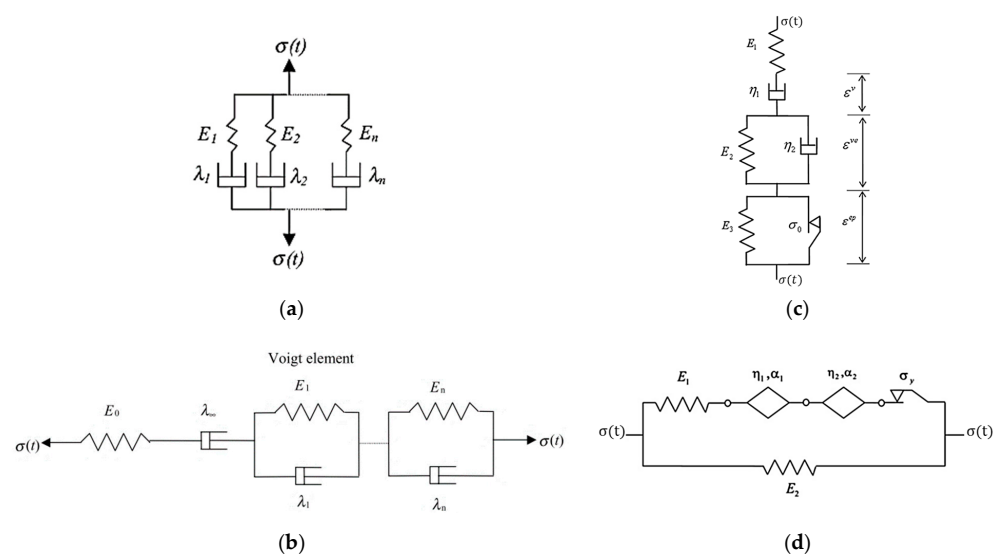


Figure 6. (a) Maxwell’s viscoelastic model, (b) Burgers viscoelastic model, (c) viscoelastic–plastic model with slider, and (d) elastic-visco-plastic nonlinear fractional (spring-pot) model.

$$\epsilon_{ve}(t) = D_{ve}(0)\sigma(t) + \int_0^t \sigma(\tau) \frac{dD_{ve}(t-\tau)}{d(t-\tau)} d\tau \tag{7}$$

$$\epsilon_{vp}(t) = D_{vp}(0)\sigma(t) + \int_0^t \sigma(\tau) \frac{dD_{vp}(t-\tau)}{d(t-\tau)} d\tau \tag{8}$$

D_{ve} and D_{vp} are viscoelastic and viscoplastic creep compliance. The hereditary integrals in Equations (7) and (8) are different from the one in Equation (3). A formulation based on stress and the rate of compliance rather than a formulation based on the rate of stress and compliance is advantageous to avoid problems due to the sudden application of a stress in which the rate of stress can be extremely high (e.g., in a creep test). The first derivatives of the viscoelastic and viscoplastic creep compliance for a generalized Burgers model are $\frac{dD_{ve}(t-\tau)}{d(t-\tau)} = \sum_{i=1}^N \frac{1}{\lambda_i} e^{-(t-\tau)/\tau_i}$ and $\frac{dD_{vp}(t-\tau)}{d(t-\tau)} = \frac{1}{\lambda_\infty}$, $D_{ve}(0) = D_{vp}(0) = 0$, $\tau_i = \lambda_i/E_i$, where λ_i is the viscosity of the i th Voigt element; E_i is the modulus of elasticity; and λ_∞ is the viscosity of viscoplastic element. A power function for creep compliance is also used for small stress cases. Moreover, the model in Figure 7c is a modified Burgers model with a plasticity element for asphalt mixture [60,61]. The additional elastoplastic network composed of the spring and slider in parallel is used. The limit stress in the slider modeling plasticity is denoted by σ_o . The authors also extended the fractional rheological model for nonlinear elastic, nonlinear viscous, and plastic properties and formulated a differential equation to characterize the viscoelastic–plastic response of asphalt concrete. Other similar analogical models such as the 2S2P1D (two springs, two parabolic. and one dashpot elements) in Figure 7a and DBN (Di Benedetto–Neifar) in Figure 7b are also frequently used to predict linear viscoelastic and creep responses (for a small number of cycles) for binders and bituminous mixtures [58,59,62]. The DBN model is a special case of the Kelvin–Voigt model where the DBN model has an elastoplastic (EP) element instead of an elastic element only.

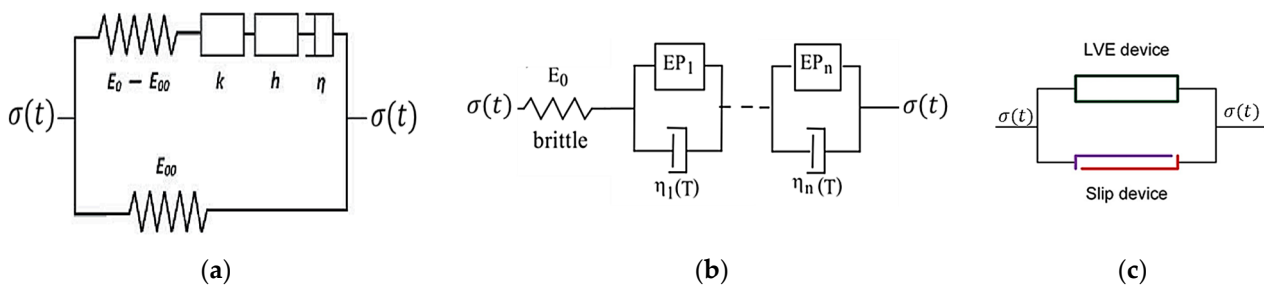


Figure 7. (a) The 2S2P1D rheological model (h and k are two parabolic creep elements), (b) DBN model for bituminous mixtures, and (c) slip device for the viscoplastic model with viscoelastic component.

From these models, the governing differential equation for creep compliance or stress and strain functions is derived to predict the permanent deformation response of asphalt concrete.

One can note that the parabolic elements (k, h) in 2S2P1D model, the slider element in (Figure 6c), and the spring-pot element in the fractional model (Figure 6d) have similar arrangements. The parabolic creep elements in 2S2P1D (Figure 7a), the elastic-plastic (EP) elements in DNB (Figure 7b) and the spring-pot elements in fractional model (Figure 6d) have also similar functions to model the elastoplastic response of asphalt concrete. The slip device shown in Figure 7c is placed in parallel with linear viscoelastic (LVE) element which has similar property as the fractional model in Figure 6c. The slip device functions as an irreversible deformation, which means that whenever the LVE device relaxes during unloading, the slip device locks, thereby disallowing strain recovery. Based on this phenomenology, the viscoelastic integrals are proposed for hardening and permanent deformation, considering that viscoelastic deformation, viscoplastic deformation, and hardening function are history dependent. Subramanian et al. [48] proposed a viscoelastic-like viscoplastic constitutive

model for the permanent deformation of asphalt concrete. The proposed model takes the following form in Macaulay brackets.

$$\epsilon_{vp}(t) = \langle \int_0^t D_1(t - \tau) \frac{d\sigma_{vp}(\tau)}{d\tau} d\tau \rangle \tag{9}$$

$$H(t) = H_0 + \langle \int_0^t D_2(t - \tau) \frac{d\sigma_H(\tau)}{d\tau} d\tau \rangle \tag{10}$$

where $H(t)$ is the material hardening variable, H_0 denotes the initial hardening state, $\sigma_H(t)$ and $\sigma_{vp}(t)$ are functions of deviatoric stress for hardening and viscoplastic deformation calculation, and $D_1(t)$ and $D_2(t)$ are compliance functions. The two stress terms are approximated by power functions, as follows.

$$\sigma_H(t) = H_1(\sigma_d(t))^{q_1} \tag{11}$$

$$\sigma_{vp}(t) = \frac{(G_1\sigma_d(t))^{p_1} + (G_2\sigma_d(t))^{p_2}}{(H(t))^\alpha} \tag{12}$$

where $\sigma_d(t)$ is the deviatoric stress history; and $H_1, q_1, G_1, G_2, p_1, p_2,$ and α are parameters. This model considers only hardening during loading pulses and ignored the softening mechanism. Based on the model in [48], Cao and Kim [53] proposed a viscoplastic model using “internal stress” as the hardening variable. They hypothesized that as soon as the deformation of the LVE device is constrained (in Figure 7c), the internal stress inside the device starts to develop due to stress relaxation. As illustrated in Figure 8, the internal stress decreases with time due to LVE device relaxation before the next load cycle but has a direction opposite to the external load. Once the applied stress rises above the level of the concurrent resisting internal stress in the LVE device, the slip device is unlocked and becomes frictionless, allowing the overall deformation of the mechanical analog to increase in a viscoelastic fashion. The proposed viscoelastic-type viscoplastic model takes the following form [53].

$$\epsilon_{vp}(t) = \langle \int_0^t D(t - \tau) \frac{d\sigma_d(\tau)}{d\tau} d\tau \rangle \tag{13}$$

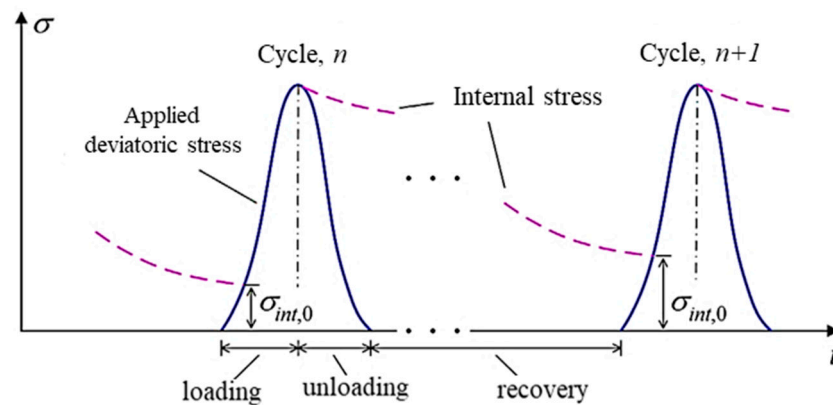


Figure 8. Schematic of representation of internal stress evolution during loading and unloading. Adapted with permission from [53]. 2016, Mechanics of Materials, Elsevier.

This model introduces the coupling of viscoelastic and viscoplastic responses using the internal stress as a hardening variable and viscoelastic-like hardening–relaxation spectrum.

4.3. Continuum Based Models

4.3.1. Damage Density

Continuum mechanics is a standalone and widely applied theory for damage formulation. The concept of continuum damage mechanics (CDM) was pioneered by Kachanov [63],

who introduced a scalar measure called damage variable or damage density ϕ , which is defined as follows.

$$\phi = 1 - \frac{A}{A_d} = \frac{A_d - A}{A_d} \quad (14)$$

where A —real (intact) area, A_d —damaged area, $A_d - A$ is the area of micro-damage, $\phi = 0$ means the initial state, and $\phi = 1$ mean complete rupture. Based on the damage density function and effective area, the effective stress concept in CDM is defined as follows.

$$\bar{\sigma}_{ij} = \frac{\sigma_{ij}}{1 - \phi} \quad (15)$$

where $\bar{\sigma}_{ij}$ is the effective stress tensor in an undamaged configuration; and σ_{ij} is the nominal Cauchy tensor in damage configuration. For more accurate modeling, the damage evolution is modified as follows [64].

$$\bar{\sigma}_{ij} = \frac{\sigma_{ij}}{(1 - \phi)^2} \quad (16)$$

The classic Kachanov–Robotnov damage models [63,65] were extensively used for creep damage (ϕ_c) modeling for different materials.

$$\text{Kachanov : } \dot{\phi}_c = G \left(\frac{\sigma}{A} \right)^r (1 - \phi_c)^{-k} \quad (17)$$

$$\text{Robotnov : } \dot{\phi}_c = \frac{C_1 \sigma^\gamma}{(1 - \phi_c)^\eta}, \quad \dot{\phi}_c = \frac{C_2 \exp(k\varepsilon)}{(1 - \phi_c)^\eta} \quad (18)$$

where A , G , r , k , and C_1 , γ , η , C_2 , k are material constants. Recently, Darabi et al. [64] developed a continuum viscodamage model using the effective total strain (ε_{ef}^T), viscoplastic hardening, and temperature coupling functions.

$$\dot{\phi}_c = \Gamma_0^\phi \left[\frac{\bar{Y}(1 - \phi_c)^2}{Y_0} \right]^q \exp(k\varepsilon_{ef}^T) G(T) \quad (19)$$

where Γ_0^ϕ is reference damage viscosity, Y_0 is reference damage force, \bar{Y} is damage driving force in effective configuration, $G(T)$ is temperature coupling term, and k and q are constants.

4.3.2. Viscoplasticity

The classic Perzyna viscoplastic hardening rule [66] assumes a constant hardening variable for a cyclic creep-recovery load, defined as

$$\dot{\varepsilon}_{vp} = \Gamma^{vp} f \frac{\partial F(\sigma)}{\partial \sigma} \quad (20)$$

where Γ^{vp} is the viscoplastic fluidity parameter such that $1/\Gamma^{vp}$ is a measure of viscoplastic viscosity; and $\frac{\partial F(\sigma)}{\partial \sigma}$ is a measure of the direction of viscoplastic strain. The classical hardening assumes that the viscoplastic strain rate decreases progressively with an increase in loading time. However, the hardening function is not constant due to the hardening–relaxation behavior [23]. Different researchers pointed out that the Perzyna-type rate models have limitations such as that the model cannot capture the load history effect, the relaxation or softening behavior during the rest period is ignored, and it assumes a constant hardening parameter [23,47,48]. As illustrated in Figure 9, the viscoplastic strain rate is no longer a decreasing function. The quantity q^{vp} is the hardening–relaxation internal state variable that memorizes the maximum experienced viscoplastic strain for which the hardening recovery has occurred.

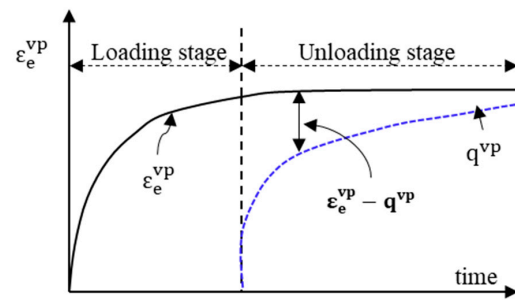


Figure 9. Schematic—the evolution of the effective viscoplastic strain and the hardening–relaxation during loading–unloading cycle. ($\epsilon_e^{vp} - q^{vp}$ the driving force for viscoplastic softening or recovery in the viscoplastic hardening). Adapted with permission from [23], 2012, International Journal of Plasticity, Elsevier.

4.4. Mechanistic Methods

4.4.1. Pavement Analysis Using the Nonlinear Damage Approach (PANDA)

Pavement analysis using the nonlinear damage approach (PANDA) is the latest generation of mechanistic pavement design approach [67]. The PANDA is a mechanistic-based pavement analysis method that is founded on three classic theories: (1) Schapery's [68] nonlinear viscoelasticity, (2) Perzyna's [66] viscoplasticity, and (3) Darabi's [64] viscodamage constitutive relationship. Based on the three constitutive equations, the PANDA approach has an unlimited capacity to couple different damage mechanisms of pavement structures. The approach coupled the temperature, rate, and time-dependent viscoelastic and viscoplastic models to predict the permanent deformation of asphalt concrete. For example, healing, aging, hardening–relaxation, moisture-induced damage, and other behaviors are conveniently incorporated into the PANDA approach [69–73]. In Figure 10, the development of the PANDA model and the constitutive equations are summarized.

- (1) First, the linear and nonlinear viscoelastic variables are obtained from dynamic modulus (for linear viscoelastic) and creep-recovery tests (nonlinear viscoelastic). The nonlinear viscoelastic strain is formulated using the well-known Schapery's viscoelastic constitutive equation [68].
- (2) Secondly, the viscoelastic strain is deducted from the total strain to extract the viscoplastic strain from the same creep-recovery test data using the strain decomposition principle. Then, the classic Perzyna's viscoplasticity [66] theory is adopted to predict the viscoplastic strain evolution. The Drucker–Prager yield surface function is often used [23,74].

$$\dot{\epsilon}_{vp} = \Gamma^{vp} \left\langle \frac{f}{\sigma_y^0} \right\rangle^N \frac{\partial F(\sigma)}{\partial \sigma} \quad (21)$$

- (3) The third foundation of the PANDA constitutive model is the viscodamage model [64] using the continuum damage mechanics (CDM) theory. The effective strain is used in effective configuration. The viscodamage model mainly predicts the permanent deformation in the tertiary creep.

Therefore, the PANDA model encompasses nonlinear viscoelastic, viscoplastic (hardening), and viscodamage responses. The thermo-piezo-rheological viscoelastic properties [75] coupled with the viscoplastic yield criteria (the Drucker–Prager yield surface) is an integral part of the PANDA method [76]. Several material parameters need to be optimized to calibrate the viscoelastic–viscoplastic–viscodamage, the hardening–relaxation, moisture damage, and healing responses of asphalt concrete. The parameters and their physical meaning are presented in Table 2. Despite the unlimited capacity of the PANDA approach, calibrating the large number of model parameters is a laborious task. Hence, a systematic procedure is followed to obtain material parameters with a smaller number of tests. Once robust mechanistic constitutive models are developed and calibrated, the numerical implementation (finite element modeling) is performed using the user-defined material

(UMAT) tool to define material laws in commercial software such as ABAQUS. Finite element modeling (FEM) is conducted at the desired modeling space (2D or 3D), and realistic tire–pavement contact [77], traffic, and full pavement structure (asphalt, base, subbase, and subgrade), etc., can be constructed [67,76,78–80]. Although the PANDA approach is still at a research stage, it is evident that advantages as well as limitations can be listed. In Table 3, some of the merits and limitations of the PANDA are described. The calibration of PANDA models used uniaxial creep, uniaxial constant stress creep-recovery, the crosshead strain rate test, and multiple stress creep tests, etc. The influence of confining pressure on the linear viscoelastic as well as nonlinear viscoelastic responses is significant [75,81]. Most studies that tried to calibrate the PANDA models used uniaxial test data, or some used a single confining pressure.

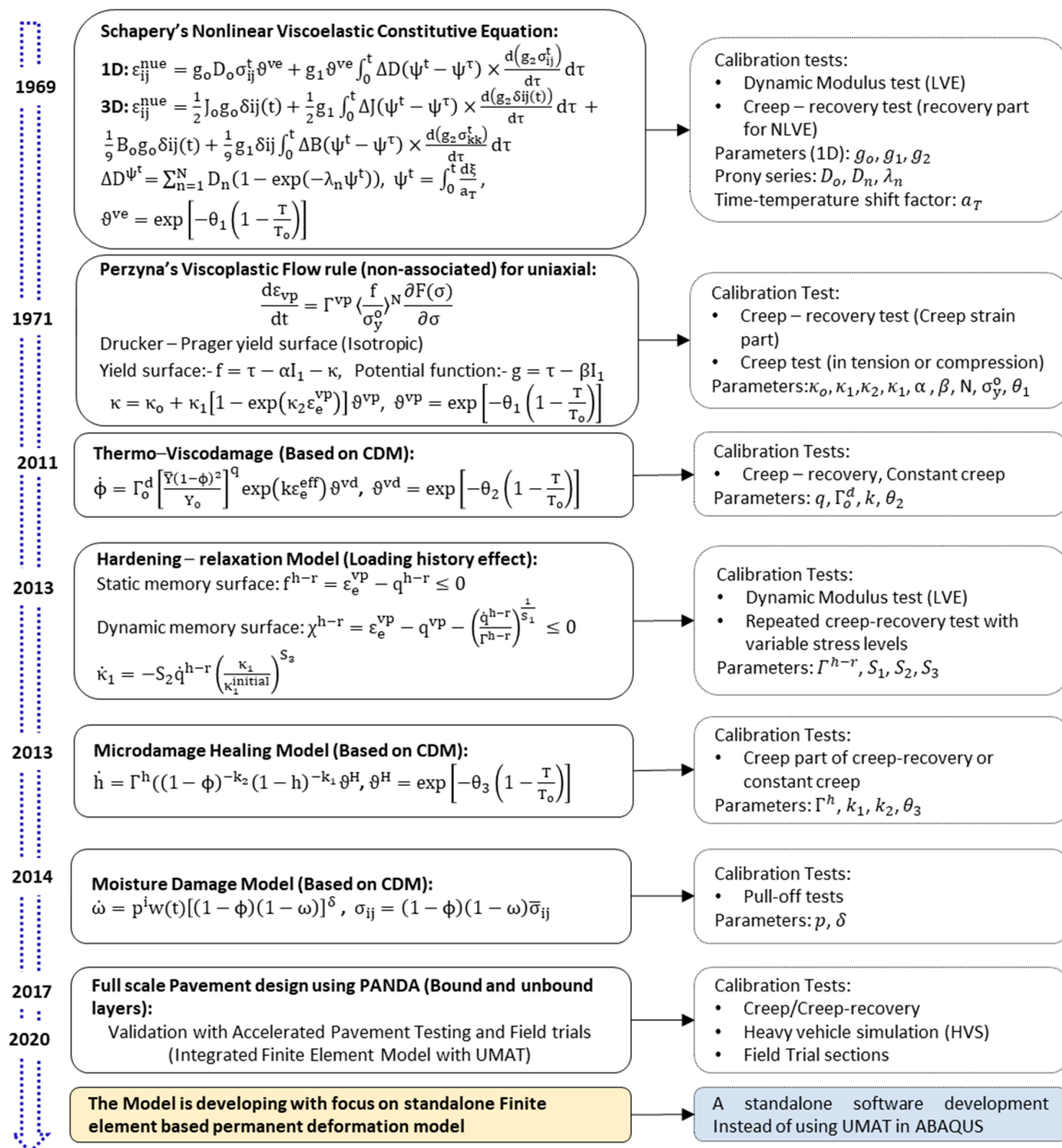


Figure 10. Development of the PANDA mechanistic permanent deformation model.

Table 2. Summary of material parameters of the constitutive equations and physical meaning in Figure 10.

Parameter	Physical Meaning	Theory/Domain	Calibration Test
<i>Viscoelastic Model Parameters [68,82]</i>			
D_0	Instantaneous creep compliance. Characterizes the instantaneous elastic part of the viscoelastic strain	Linear viscoelastic	Creep compliance or Dynamic Modulus
λ_n	nth retardation time. A measure of the required time for the viscoelastic material to relax the induced stress		
D_n	nth coefficient of the Prony series associated with the nth retardation time λ_n . These parameters characterize the transient compliance of the material		
g_0, g_1, g_2	Nonlinear viscoelastic parameters, where g_0 measures the reduction or the increase in the instantaneous compliance; g_1 defines the nonlinearity effects in the transient compliance; and g_2 is the nonlinear parameter accounting for the loading rate effects on the creep response	Schapery's Nonlinear viscoelastic	Creep-recovery
<i>Viscoplastic Model Parameters [64,66,69]</i>			
Γ^{vp}	Viscoplastic fluidity parameter, such that $1/\Gamma^{vp}$ is a measure of viscoplastic viscosity	Perzyna's Viscoplastic (with Drucker–Prager yield criteria)	Creep, creep-recovery (creep part), constrain strain rate test
$\kappa_0, \kappa_1, \kappa_2$	Isotropic hardening parameters, where κ_0 defines the initial yield strength; $\kappa_0 + \kappa_1$ defines the saturated limit of the hardening function; and κ_2 defines the hardening rate and controls the shape of the hardening function versus the effective viscoplastic strain (ϵ_e^{vp})		
N	Viscoplastic rate sensitivity exponent and describes the nonlinear rate dependency of viscoplastic response		
α, β	Govern the pressure sensitivity of the yield surface and plastic potential functions. Related to the angle of friction in the asphalt concrete		
d^{vp}	Model parameter distinguishing viscoplastic responses in extension and contraction modes of loading		
<i>Visco-damage Model Parameters [64]</i>			
Γ^{vd}	Visco-damage fluidity parameter ($1/\Gamma^{vd}$ is a measure of damage viscosity)	CDM (Tertiary creep)	Creep tests
q	Stress dependency parameter. Defines the sensitivity of the damage evolution due to stress level		
γ_0	The reference damage force obtained at a reference stress of a creep test		
k	Strain exponent parameter. Defines the sensitivity of the damage evolution due to strain level		
d^{vd}	Model parameter distinguishing visco-damage responses in extension and contraction modes of loading		
<i>Micro-damage healing model Parameters [83]</i>			
Γ^h	Micro-damage healing fluidity parameter, such that $1/\Gamma^h$ is a measure of healing viscosity	CDM for healing	
k_1, k_2	Healing model parameters that describe the effect of the damage and healing histories on the healing evolution		
<i>Temperature coupling terms parameters [64]</i>			
$\theta_1, \theta_2, \theta_3$	Temperature sensitivity model parameters for viscoplastic, viscodamage and microdamage healing, respectively	Time–temperature superposition	Dynamic Modulus, Creep compliance
T_0	Reference temperature		
<i>Hardening–relaxation Model Parameters [24,25]</i>			
Γ^{h-r}	The hardening–relaxation fluidity parameter, such that $1/\Gamma^{h-r}$ is the hardening–relaxation retardation time controlling the rate of the hardening–relaxation		Creep-recovery (at different rest periods)
S_1, S_2, S_3	Hardening–relaxation rate-sensitivity parameters that describe the relaxation behavior of viscoplastic hardening due to recoverable potential during rest period		
<i>Moisture damage Model Parameters [84]</i>			
p δ	Adhesion or cohesion moisture damage parameter Parameter that describes the moisture damage history	CDM for moisture damage	Pull-off test

Table 3. Advantages and limitations of the PANDA Model.

Advantages	Disadvantages
<ul style="list-style-type: none"> ■ The approach is based on fundamental theories of mechanics (mechanistic) ■ Unlimited modeling capacity ■ The material properties and temperature coupling are integrated ■ The approach has the capacity to couple different damage types (such as moisture, fatigue cracking, etc.) with permanent deformation ■ It enables realistic rutting prediction with full pavement structure modeling using finite element method (3D modeling) ■ Moving loads can be modeled, which was not possible in traditional methods ■ etc. 	<ul style="list-style-type: none"> ■ Complex constitutive equations ■ Large number of modeling parameters ■ It requires many different calibration tests ■ It is computationally and experimentally costly ■ It is at development stage and some theories have limitations (e.g., classic viscoplasticity theory) ■ The numerical implementation is based on user material (UMAT) model (not standalone) ■ etc.

4.4.2. Microstructural Based Models

The micromechanics approach is probably the best way to account the effects of individual mixture constituents and their interactions and the anisotropy of heterogeneous asphalt mixture. The microstructure change in asphalt concrete is mainly due to the friction between the aggregates and interlocking bond breakage. This mechanism is responsible for the accumulation of permanent deformation rather than the recoverable part of the deformation. The continuous increase in the resistance of the material due to the permanent microstructure rearrangement is physically related to the strain hardening. The hardening parameter reflects the combined effect of the cohesion of asphalt binders, the adhesion properties between binder and aggregate, and the frictional properties of the aggregate structure. The fabric of granular media refers to the size, shape, and arrangement of the solid particles and the associated voids. The scalar quantity, like void ratio, is not capable of characterizing the directional nature of fabric and describing the state of packing of granular materials [85]. The microstructure approach is necessary to consider the directional nature of granular fabric. The approach is capable of modeling nonlinearities such as heterogeneity, aggregate distribution, anisotropy, crack, and air void. The micromechanics coupled with the continuum damage approach is a powerful way to model the permanent deformation of granular asphalt concrete with an appropriate representative volume element (RVE) [19–22]. The fundamental element of the granular microstructure is a directional unit vector m and the vector magnitude Δ (Figure 11).

$$\Delta = \frac{1}{M} \left[\sum_{k=1}^M (\cos 2\theta^k)^2 + \sum_{k=1}^M (\sin 2\theta^k)^2 \right]^{\frac{1}{2}} \quad (22)$$

where M is the total number of objects analyzed in an image; and θ^k is the orientation of the unit vector n and ranges between -90 and $+90^\circ$. Theoretically, the value of Δ is between zero and unity; $\Delta = 0$ indicates that objects are completely randomly distributed, which is analogous to isotropic materials; and $\Delta = 1$ indicates that objects are entirely oriented in one direction, which is analogous to perfectly transverse anisotropic materials. Oda and Nakayama [86] introduced a symmetrical microstructure tensor F_{ij} that gives a measure of the two-dimensional anisotropy produced by the preferred orientation of non-spherical particles.

$$F_{ij} = \begin{pmatrix} (1 - \Delta)/(3 + \Delta) & 0 & 0 \\ 0 & (1 + \Delta)/(3 + \Delta) & 0 \\ 0 & 0 & (1 - \Delta)/(3 + \Delta) \end{pmatrix} \quad (23)$$

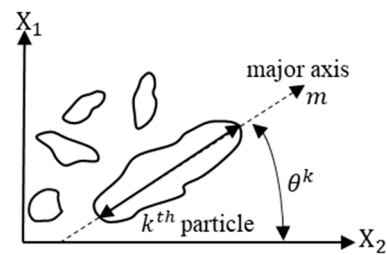


Figure 11. Two-dimensional particles orientation for micromechanics modeling (orientation, θ and vector, m).

For simplicity the anisotropy value can be taken as constant (the initial value). For isotropic elements, $F_{11} = (-4\Delta)/3(3 + \Delta)$ and $F_{22} = F_{33} = (2\Delta)/3(3 + \Delta)$.

The microstructure tensor is incorporated in the Drucker–Prager yield function by modifying the first and second invariants. The classical Perzyna’s viscoplastic and continuum damage models are then used to formulate the microstructure-based viscoplastic strain model to characterize permanent deformation of asphalt concrete. The detail derivation of the model can be found in the study [19,20,86]. The final form of the viscoplastic model in a triaxial compression test (axial strain) based on micro-structural anisotropy takes the following form.

$$\dot{\epsilon}_{vp} = \frac{[\sqrt{X} - \beta(1 - Y)]}{\sqrt{\frac{3}{2}X + 3\beta Y\sqrt{X} + 3\beta^2 + \frac{3}{2}\beta^2 Y^2}} \sqrt{\dot{\epsilon}_{ij}^{vp} \dot{\epsilon}_{ij}^{vp}} = \dot{\epsilon}_{11}^{vp} \quad (24)$$

where $X = \frac{1}{3} - \frac{4}{9}\sqrt{24}\mu\left(\frac{\Delta}{3+\Delta}\right)^2$, $Y = \frac{4}{3}\sqrt{24}\lambda\left(\frac{\Delta}{3+\Delta}\right)^2$, and λ and μ are anisotropy coefficients that reflect the effect of the aggregate anisotropic distribution on the confining and shear stresses, respectively. The viscoplastic model considers phenomena including the effect of the binder fluidity (Γ); confinement and aggregate friction (α); aggregate interlocking and dilation (β); binder cohesion and its adhesion to the aggregates (κ); anisotropy of aggregate distribution (Δ); and microstructure damage (ξ). As shown in Figure 12, the anisotropy parameter significantly contributes to compressive viscoplastic behavior and has little effect or no effect on the tensile and linear viscoelastic property [22]. In a conventional continuum method (isotropic mode), phenomenologically motivated, microstructural-based viscoplastic models have been developed, for example in [23,25] and others.

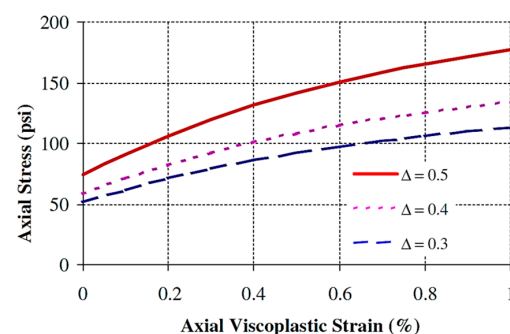


Figure 12. Effect of anisotropy on the stress–strain relationship predicted by the model. Reprinted with permission from [87]. 2005, International Journal of Plasticity, Elsevier.

Microstructure modeling is directly integrated with the utilization of digital technologies to capture the particles arrangement, deformation, etc., in the granular materials packing. Digital image correlations, X-ray chromatography, and other tools were used for asphalt concrete. Coleri et al. [88] used the X-ray computed tomography (CT) method to model asphalt concrete rutting in a full-scale heavy vehicle simulation (HVS) test site.

The object segmentation and processing procedure using a digital camera is shown in Figure 13, and an example of the discretization phases is shown in Figure 14. Using the digital technology, parts of a heterogenous mixture can be easily dissected, modeled, and analyzed into the FEM and other post processes.

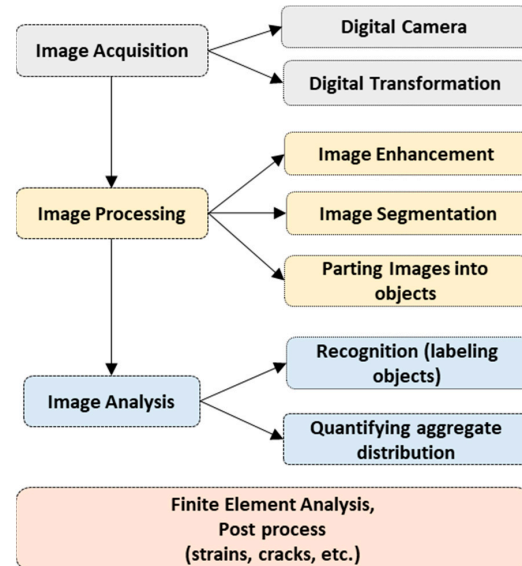


Figure 13. Digital image analysis process for microstructure modeling.

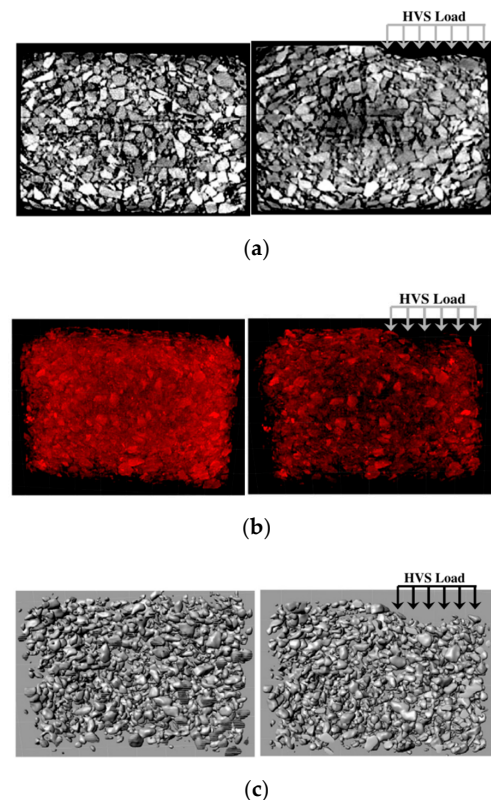


Figure 14. The procedure followed for aggregate domain creation: (a) unprocessed 2D X-ray CT image used for the development of image stacks (left: before HVS trafficking and right: after HVS trafficking), (b) 3D images developed from X-ray CT image stacks (left: before HVS trafficking and right: after HVS trafficking), and (c) 3D aggregate volumes (left: before HVS trafficking and right: after HVS trafficking). Note: direction of HVS traffic is out of the page. Reprinted with permission from [88]. 2012, Construction and Building Materials, Elsevier.

In general, the microstructural based micromechanics modeling is ideal to consider the effect of individual constituent particles in viscoplastic evolution [89]. However, this approach needs image analyzing tools, discretization, and finite element modeling. Several material behaviors such as hardening–relaxation, healing, stress history, viscodamage, etc., need to be integrated for accurate formulation. Limited literature can be found in this area. With the advancement of morphological image analyzing tools, the microstructural approach will be the next active research area to characterize permanent deformation.

4.4.3. Finite Element Simulation

Even if pavement is considered a homogeneous, isotropic, elastic, multi-layered system, the calculated stress–strain distribution in the structure under the simple action of a passing wheel is very complex. For a realistic modeling of pavements, each layer and material constituent should be modeled with the appropriate material constitutive law, and the interaction of each layer should be analyzed as a pavement system. The finite element method is the most versatile approach in the mechanistic pavement design approaches. The FEM is an integral part of the PANDA approach; the modeling space (2D or 3D), wheel loading configuration, constitutive law, etc., are of great importance [67,69,76,79]. Collop et al. [57] implemented Burgers analogical constitutive model into FEM to predict viscoplastic deformation. A comprehensive FEM study by [80] investigated the effect of loading scenario in 2D and 3D modeling spaces and implemented the PANDA constitutive law. They investigated 11 different loading modes (given in Table 4) and compared three different material constitutive equations: elasto-viscoplastic, viscoelastic–viscoplastic, and viscoelastic–viscoplastic–viscodamage or PANDA. Based on wheel tracking test data, they concluded that the 2D model significantly overestimates permanent deformation (rutting) compared to the 3D moving load case (which is the most realistic case). Moreover, they found that the viscoelastic–viscoplastic–viscodamage model gives higher rutting damage predictions compared to elasto-viscoplastic and viscoelastic–viscoplastic models. The viscoelastic–viscoplastic and elasto-viscoplastic models give close predictions, where the form gives a still higher rutting prediction. On the contrary, another study using the viscoelastic–viscoplastic–viscodamage constitutive model and 3D FEM modeling of tire–pavement interaction showed that the pulsatile and equivalent loading assumptions overestimated rutting compared to the realistic moving load [90]. The FEM simulation has been applied for different viscoelastic, viscoplastic, and crack modeling. The linear viscoelastic simulation has been modeled using the analogical models (e.g., Maxwell model), the Prony series, and time–temperature superposition principles in commercial software such as ABAQUS.

Table 4. The commonly used FEM simulation loading assumptions.

Mode	Load Configuration	Loading Approach		
		Pulse Loading	Equivalent Loading	Moving Loading
2D	Single wheel (plane strain)	✓	✓	✓
	Single wheel (axisymmetric)	✓	✓	✓
	Single wheel (moving loading)			✓
	Multiple wheel (moving loading)			✓
3D	Single wheel (rectangular)	✓	✓	✓
	Whole wheel path	✓	✓	
	Single wheel (circular)	✓	✓	
	Single wheel (moving)			✓
	Multiple wheel			✓

✓ FEM simulation applied.

5. Permanent Deformation and Fatigue Interaction Damage

Permanent deformation and fatigue cracking are the two dominant pavement damage mechanisms. Extensive research has been conducted to characterize the two damages independently. Advanced mechanistic models were proposed [64,83,84,91]. Fatigue damage occurred due to the formation and propagation of cracks due to repetitive loads. The bottom-up cracking of the asphalt concrete layer was the traditional fatigue mechanism. However, experimental and field observations showed that top-down cracking due to tire compression is also the cause of fatigue damage [92,93]. The crack initiation in compression occurs when the viscoplastic strain hardening reaches saturation at the flow number. The extra energy at maximum saturation (hardening) is consumed to initiate microcracks and increase phase angle. When asphalt with pre-existing cracks is subjected to a compressive load, wing cracks develop and propagate parallel to the load direction [94,95], contrary to tensile loading (cracks grow perpendicular to the stress direction). When pavement temperature is considered, fatigue cracking is critical at low temperatures, and permanent deformation is a high-temperature damage. At elevated temperatures, the critical energy threshold (the mixture relaxes faster) becomes more resistant to micro-cracks and needs more energy to initiate cracks [96]. On the other hand, deformation via plastic flow (aggregate re-orientation) is dominant at high temperatures. When asphalt concrete is subjected to repetitive loading, energy is dissipated by viscous flow and/or plastic flow, leading to *fatigue cracking* and/or *permanent deformation* [97], and some part of the energy is transferred into heat [50]. The energy dissipation caused material ductility exhaustion, hardening, and viscoplastic flow. The classic energy balance principle states that the decreasing rate of potential energy (stored and recoverable) during crack initiation is equal to the dissipated energy rate due to plastic/viscoplastic deformation and crack opening, and different failure criteria were proposed [98,99]. The dissipated energy (W) in a cyclic load is the area under the stress–strain hysteresis and expressed as follows.

$$W = \int_0^{\tau} \sigma(t) \frac{\partial \varepsilon(\tau)}{\partial \tau} d\tau \quad (25)$$

where τ is the integration variable, σ is the stress function, and ε is the strain function. One hysteresis cycle consists of the total strain energy, which is the sum of damage-causing dissipated energy (the hysteresis area) and the recovery strain energy (stored energy).

The classic approach considered rutting and fatigue separately (cf. Figure 15a) [100]. However, both fatigue and permanent deformation damages are caused by the same load in pavements. The difference is which damage mode dominates at different temperatures. Therefore, a realistic damage modeling should consider the simultaneous damage evolution of fatigue and permanent deformation. An interaction domain of rutting and fatigue can be shown in Figure 15b [101]. For an interaction damage condition, the dissipated energy (in Equation (26)) can be decomposed further into permanent deformation and fatigue damage-causing energies. As discussed above, the existing models for permanent deformation or fatigue damages are based on the idealized hysteresis loops of pure creep and pure fatigue. Only very few attempts can be found; for example, Luo et al. [99] investigated the permanent deformation behavior of pre-cracked asphalt concrete.

In a cyclic creep-recovery test, material hardening grows, and the hysteresis loops shift horizontally due to the accumulation of irrecoverable viscoplastic strain (open loops). On the other hand, in the idealized fatigue test (either stress- or strain-controlled), cyclic load is applied that causes stiffness reduction and a phase angle increment with a negligible viscoplastic strain (hysteresis loops do not shift horizontally or loops are closed). In simultaneous fatigue-permanent deformation damage, the material hardening contributes to initiate fatigue cracking at intermediate temperatures, and the fatigue cracks accelerate the microstructure change and contribute to viscoplastic deformation. The viscous flow creates a plastic zone (the crack initiation point), and fatigue cracking can evolve without plastic flow (aggregate movement and re-orientation). That means the simultaneous

occurrence of the two damages cannot be ignored as they are interdependent. Thus, the hysteresis loops can be modified by superposing the two loops (Figures 4a and 16a) to account for the interaction of the two damages, as shown in Figure 16b. Similar fatigue–creep interaction loops can be found elsewhere for steel [102,103]. A detailed discussion of the interaction of the two damages is presented in next sections.

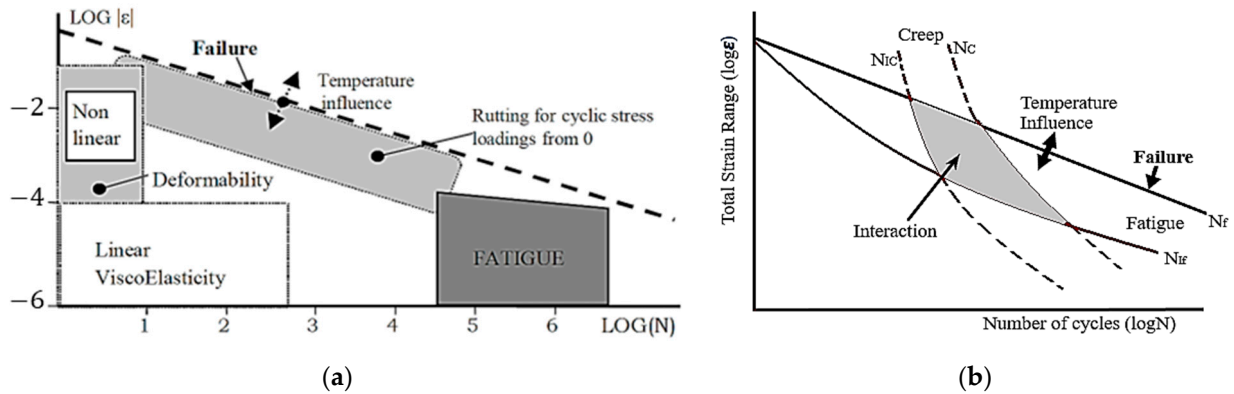


Figure 15. (a) Damage domains of bituminous mixtures (ϵ —strain amplitude and N —number of cycles) and (b) fatigue and permanent deformation interactive damage for asphalt concrete (N_C , N_{IC} , N_f , and N_{If} failure lines for creep and fatigue domains).

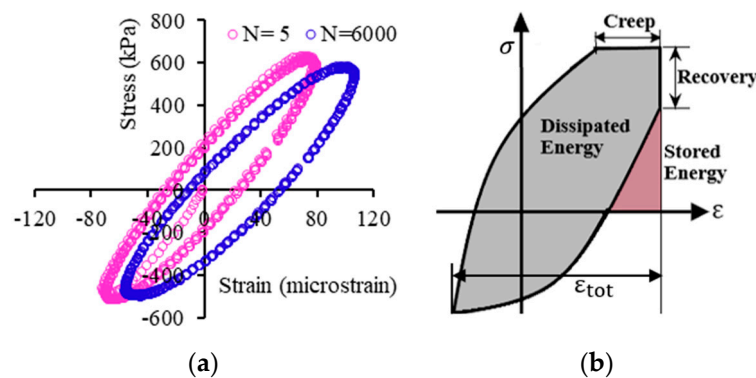


Figure 16. (a) Cyclic fatigue hysteresis and (b) creep–fatigue interaction stress–strain loop.

One of the limitations for interaction damage modeling is the lack of integrated testing protocol for permanent deformation and fatigue. Some attempts were made, such as Indirect Tension (IDT) testing for deformation and fracture and applying a haversine loading waveform in fatigue tests [104,105]. The haversine load is used with the assumption that the pulse can be decomposed into pure creep and pure sinusoidal components. However, the creep–recovery behavior cannot be captured with such approaches. In another study, Zhang et al. [106] conducted a destructive dynamic modulus test to simultaneously characterize permanent deformation and fracture properties using 16 different asphalt mixtures. In their work, they successfully modeled viscoelastic, viscoplastic, and viscofracture properties using a new destructive dynamic modulus test. Another reason for the independent treatment of fatigue and rutting damages on asphalt concrete damage is the perception that permanent deformation (creep) is expected in the early life of pavements, while fatigue is high-cycle damage after asphalt concrete accumulates sufficient hardening and age. However, this precedence is dependent on several factors such as temperature, loading range (loading time, rest period, deviatoric stress), material stiffness, number of cycles, and other climatic factors. For example, fatigue cracking can evolve before creep damage in stiff and thick pavements. The top-down cracking due to tire compression can develop without permanent deformation. Some field and laboratory observations have also

shown that fatigue cracking accompanied rutting [92]. Therefore, both the creep–fatigue and fatigue–creep damage sequences can occur in asphalt concrete pavements [99].

The main objective in the design and service life estimation of asphalt concrete is to estimate the number of cycles (N_f) to initiate fatigue cracking and/or the critical strain (ϵ_c —rupture strain) that causes the flow or rutting of asphalt concrete. The simplest way to evaluate the interaction damage of creep and fatigue is separately calculating the creep and fatigue damages and adding them together.

$$\sum \frac{n}{N_f} + \sum \frac{\epsilon}{\epsilon_c} = 1 \tag{26}$$

By the life fraction rule, the sum of fatigue damage (ϕ_f) and creep damage (ϕ_c) equals a certain damage density value, ϕ . The nonlinear summative decomposition of damage can be expressed as follows for a more general representation.

$$d\phi = d\phi_c + d\phi_f = f_c(\epsilon, \sigma, T, \phi_c + \phi_f)dN_c + f_f(\epsilon, \sigma, T, \phi_c + \phi_f)dN_f \tag{27}$$

The classic continuum damage models were used to define the damage rates for creep [63,65] and fatigue damage [107,108]. Lemaitre et al. [109] proposed sequential damage interaction, and the total damage accumulation during one cycle of creep followed by fatigue and fatigue followed by a creep sequence can be expressed as follows (respectively).

$$\phi_{c-f} = \int_0^{n_c} \frac{\delta\phi_c}{\delta N} \delta N + \int_{n_c}^{n_c+n_f} \frac{\delta\phi_f}{\delta N} \delta N \tag{28}$$

$$\phi_{f-c} = \int_0^{n_f} \frac{\delta\phi_c}{\delta N} \delta N + \int_{n_f}^{n_f+n_c} \frac{\delta\phi_f}{\delta N} \delta N \tag{29}$$

For time-dependent materials such as asphalt concrete, damage densities ϕ_{c-f} and ϕ_{f-c} will not be the same for the same number of cycles in both sequences. This is because of the different modes of damage formation in creep and fatigue and the possible interactive damage one on another. A parameter can be defined for “interactive” damage. Skelton et al. [101] presented analytical expressions to allow creep to be modified by fatigue and fatigue to be modified by creep. The combined equation for the “creep–fatigue” and “fatigue–creep” interactive damages can take the following form.

$$\frac{\phi_f}{1 - I_{cf}\phi_c} + \frac{\phi_c}{1 - I_{fc}\phi_f} = 1 \tag{30}$$

The interaction coefficients I_{cf} (creep on fatigue) and I_{fc} (fatigue on creep) can take any value between zero and unity. The damage density for fatigue and creep can be determined by rearranging terms and solving a quadratic solution. In the creep–fatigue sequence, it is assumed that pure creep is followed by fatigue damage. The fatigue damage part is modified to account for the pre-existing creep damage. Therefore, the creep–fatigue and fatigue–creep interactive damages can be expressed as follows, respectively.

$$\phi_c + \frac{\phi_f}{1 - I_{cf}\phi_c} = 1, \phi_f + \frac{\phi_c}{1 - I_{fc}\phi_f} = 1 \tag{31}$$

Re-arranging and solving for ϕ_c and ϕ_f gives the following expressions.

$$\phi_c = \frac{(1 + I_{cf}) - \sqrt{(I_{cf} - 1)^2 + 4I_{cf}\phi_f}}{2I_{cf}}, \phi_f = \frac{(1 + I_{fc}) - \sqrt{(I_{fc} - 1)^2 + 4I_{fc}\phi_c}}{2I_{fc}} \tag{32}$$

The creep–fatigue and fatigue–creep interaction coefficients I_{cf} and I_{fc} are non-zero and take any value between -1 and 1 . Figure 17 shows the relationship between creep and fatigue damage densities at random values of creep–fatigue interaction coefficients.

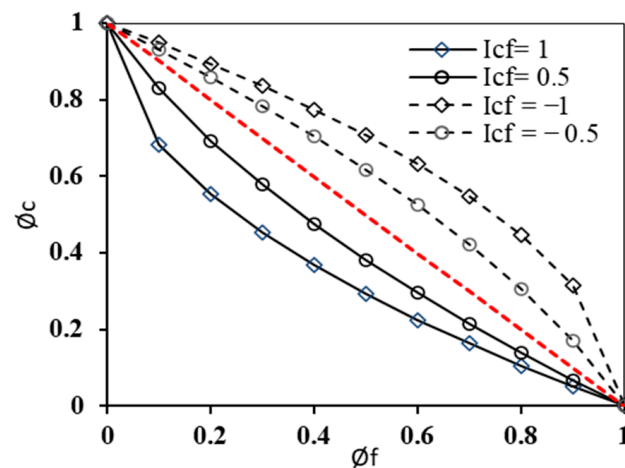


Figure 17. Parametric study of creep–fatigue damage interaction coefficient.

6. Summary, Conclusions, Further Research

6.1. Summary

The practice is always trailing the theory in pavement design, and the case of the permanent deformation prediction is no different. Many highway agencies and road administrations are practicing an empirical method of permanent deformation characterizations (for example, the Marshall test). Some progresses are being made to transition from empirical to mechanistic-empirical design methods. The primary motivation of this literature study was to explore the advancement of asphalt concrete permanent deformation characterization, constitutive modeling, and application. The current state of research is focused on the formulation of a mechanistic method that applies the fundamental theories of mechanics and materials to predict permanent deformation damage. In the last decade, promising advancements have been made in the development of comprehensive and coupled permanent deformation modeling. Pavement analysis using the nonlinear damage approach (also known as PANDA) constitutive model is one of the notable progresses that is gaining wide acceptance (as the next generation mechanistic pavement design approach). Another promising area of progress is the microstructural approach aided with 3D digital image analysis equipment and finite element modeling. This digital technology-based permanent deformation modeling is also the future prospect for accurate permanent deformation modeling and prediction of different asphalt mixtures. The mechanistic methods offer unlimited potential to expand the modeling parameters, and different damages and phenomena such as aging, healing, moisture damage, pre-crack, etc., can be coupled to unify damage prediction. The drawbacks of mechanistic models are sophistication, requiring extensive testing, and the calibration of several modeling variables. For example, the viscoelastic–viscoplastic–viscodamage model requires more than 21 model variables to be optimized using at least two different experiments and several test repetitions at different temperatures stresses and strains. The improvement of the latest models from the classic viscoplastic strain hardening model is the consideration of cyclic hardening and relaxation mechanisms and the viscodamage of asphalt concrete. Although the mechanistic method is theoretically appealing, the calibration cost and rigorous equations can be considered the limitations. The micromechanics approach considers the evolution of permanent deformation related to changes in the microstructure of asphalt concrete constituents (aggregates and mastic). Thus, the micromechanics method is regarded as the most realistic way of modeling heterogeneous materials such as asphalt concrete. Based on the extensive literature study, the permanent deformation prediction and modeling approaches can be categorized into four aspects, as shown in Table 5.

Table 5. Summary of permanent deformation modeling approaches.

Properties, Theories, Methods	Approach			
	PANDA	Microstructure	Analogical	Empirical
Continuum damage mechanics	✓	✓	-	-
Viscoelastic	✓	-	✓	✓
Viscoplasticity	✓	✓	✓	✓
Micromechanics	†	✓	-	-
Finite element simulation	✓	✓	✓	-
Time–temperature superposition	✓	✓	✓	-
Coupling (healing, moisture)	✓	✓	-	-
Coupling fatigue–rutting damage	-	-	-	-
Full pavement deformation model	✓	✓	-	-
Hardening–relaxation mechanism	✓	✓	-	-
Uniaxial and triaxial	✓	✓	✓	✓
repeated load test	✓	✓	✓	✓

✓ Incorporated, † Not yet incorporated.

6.2. Conclusions

A review study was conducted to explore the state of the art on permanent deformation prediction from the 1960s' pure empirical to latest mechanistic (from 2011) methods. The review study revealed that the latest constitutive models integrate and couple different theories, i.e., continuum mechanics (1958), nonlinear viscoelastic (1969), viscoplasticity (1971), and viscodamage (2011), along with the crucial time–temperature superposition principle. Such coupling techniques offered advantages of integrating different asphalt concrete damages and opened the possibility of a unified asphalt damage model in the future. The PANDA model is one of the most comprehensive permanent deformation modeling approaches available in the literature (the next generation to the mechanistic-empirical method). The calibration and/or validation tests are reliant upon the conventional creep or creep-recovery tests in either confined or unconfined modes. The computation and experiment cost of mechanistic methods are the limitations. The practical application of the mechanistic models is very limited at the moment. Moreover, the fatigue–permanent deformation (rutting) interaction is often ignored in the existing (studied) literature. It is inferred that both damages can evolve simultaneously as the same load caused both damages. The mechanistic approach has the potential to couple the two predominant pavement damages. From the extensive study, it can be synthesized that a unified permanent deformation damage model can be developed by integrating continuum damage and microstructure approaches and coupling fatigue, moisture, healing, aging, and other physical and chemical phenomena in asphalt concrete.

6.3. Further Research

The mechanistic method is “universally” applicable to predict damage regardless of climatic conditions, stress state, or material type. This characteristic presents wide, open research questions, for example, (1) developing a unified pavement damage performance prediction model, (2) a coupled model for fatigue and rutting damages using continuum mechanics and viscoelastic and viscoplastic theories, (3) considering (coupling) different strains such as shear and axial strains in permanent deformation prediction models, and (4) developing simplified (unified) asphalt concrete test methods to characterized different damages simultaneously (fatigue, rutting, moisture, etc.). The authors of this paper are conducting research on the simultaneous creep–fatigue damage evolution in a sequential manner.

Author Contributions: Conceptualization, M.M.A.; methodology, M.M.A.; investigation, M.M.A.; writing—original draft preparation, M.M.A.; writing—review and editing, M.M.A., E.T. and I.H.; supervision, E.T. and I.H. All authors have read and agreed to the published version of the manuscript.

Funding: This research received no external funding.

Institutional Review Board Statement: Not applicable.

Informed Consent Statement: Not applicable.

Data Availability Statement: Not applicable.

Conflicts of Interest: The authors declare no conflict of interest.

References

1. Roberts, F.L.; Mohammad, L.N.; Wang, L.B. History of Hot Mix Asphalt Mixture Design in the United States. *J. Mater. Civ. Eng.* **2002**, *14*, 279–293. [[CrossRef](#)]
2. Vesic, A.S.; Domaschuk, L. *Theoretical Analysis of Structural Behavior of Road Test Flexible Pavements*; National Academy of Science: Washington, DC, USA, 1964.
3. Archilla, A.R.; Madanat, S. Development of a Pavement Rutting Model from Experimental Data. *J. Transp. Eng.* **2000**, *126*, 291–299. [[CrossRef](#)]
4. Fang, H.; Liu, Q.; Mo, L.; Javilla, B.; Shu, B.; Wu, S. Characterization of three-stage rutting development of asphalt mixtures. *Constr. Build. Mater.* **2017**, *154*, 340–348. [[CrossRef](#)]
5. Celauro, C. Influence of the Hourly Variation of Temperature on the Estimation of Fatigue Damage and Rutting in Flexible Pavement Design. *Int. J. Pavement Eng.* **2004**, *5*, 221–231. [[CrossRef](#)]
6. Delgadillo, R.; Bahia, H.U. The Relationship between Nonlinearity of Asphalt Binders and Asphalt Mixture Permanent Deformation. *Road Mater. Pavement Des.* **2010**, *11*, 653–680. [[CrossRef](#)]
7. Kennedy, T.W.; Huber, G.A.; Harrigan, E.T.; Cominsky, R.J.; Hughes, C.S.; Von Quintus, H.; Moulthrop, J.S. *Superior Performing Asphalt Pavements (Superpave): The Product of the SHRP Asphalt Research Program*; Strategic Highway Research Program, National Research Council: Washington, DC, USA, 1994.
8. Laukkanen, O.-V.; Soenen, H.; Pellinen, T.; Heyrman, S.; Lemoine, G. Creep-recovery behavior of bituminous binders and its relation to asphalt mixture rutting. *Mater. Struct.* **2014**, *48*, 4039–4053. [[CrossRef](#)]
9. Meena, S.; Biligiri, K.P. Binder rheological predictive models to evaluate rutting performance of asphalt mixtures. *Constr. Build. Mater.* **2016**, *111*, 556–564. [[CrossRef](#)]
10. İskender, E. Rutting evaluation of stone mastic asphalt for basalt and basalt–limestone aggregate combinations. *Compos. Part B Eng.* **2013**, *54*, 255–264. [[CrossRef](#)]
11. Masad, E.; Olcott, D.; White, T.; Tashman, L. Correlation of Fine Aggregate Imaging Shape Indices with Asphalt Mixture Performance. *Transp. Res. Rec. J. Transp. Res. Board* **2001**, *1757*, 148–156. [[CrossRef](#)]
12. Kandhal, P.S.; Cooley, L. Coarse- Versus Fine-Graded Superpave Mixtures: Comparative Evaluation of Resistance to Rutting. *Transp. Res. Rec. J. Transp. Res. Board* **2002**, *1789*, 216–224. [[CrossRef](#)]
13. Singh, M.; Kumar, P.; Anupam, A.K. Effect of type of aggregate on permanent deformation of bituminous concrete mixes. *Road Mater. Pavement Des.* **2016**, *17*, 417–433. [[CrossRef](#)]
14. Lundberg, J.; Janhäll, S.; Gustafsson, M.; Erlingsson, S. Calibration of the Swedish studded tyre abrasion wear prediction model with implication for the NORTRIP road dust emission model. *Int. J. Pavement Eng.* **2019**, *22*, 432–446. [[CrossRef](#)]
15. Ahmed, A.; Erlingsson, S. Evaluation of permanent deformation models for unbound granular materials using accelerated pavement tests. *Road Mater. Pavement Des.* **2013**, *14*, 178–195. [[CrossRef](#)]
16. Deacon, J.A.; Harvey, J.T.; Guada, I.; Popescu, L.; Monismith, C.L. Analytically Based Approach to Rutting Prediction. *Transp. Res. Rec. J. Transp. Res. Board* **2002**, *1806*, 9–18. [[CrossRef](#)]
17. Song, J.; Pellinen, T. Dilation Behavior of Hot Mix Asphalt Under Triaxial Loading. *Road Mater. Pavement Des.* **2007**, *8*, 103–125. [[CrossRef](#)]
18. Park, S.W.; Richard Kim, Y.; Schapery, R.A. A viscoelastic continuum damage model and its application to uniaxial behavior of asphalt concrete. *Mech. Mater.* **1996**, *24*, 241–255. [[CrossRef](#)]
19. Tashman, L.; Masad, E.; Zbib, H.; Little, D.; Kaloush, K. Microstructural Viscoplastic Continuum Model for Permanent Deformation in Asphalt Pavements. *J. Eng. Mech.* **2005**, *131*, 48–57. [[CrossRef](#)]
20. Yu, H.; Muhunthan, B.; Shen, S. Anisotropic Nonlinear Elastoviscoplastic Model for Rutting of Asphalt Mixtures. *J. Eng. Mech.* **2014**, *140*, 242–249. [[CrossRef](#)]
21. Kim, Y.-R.; Lutfi, J.E.S.; Allen, D.H. Determining Representative Volume Elements of Asphalt Concrete Mixtures without Damage. *Transp. Res. Rec. J. Transp. Res. Board* **2009**, *2127*, 52–59. [[CrossRef](#)]
22. Underwood, S.; Heidari, A.H.; Guddati, M.; Kim, Y.R. Experimental Investigation of Anisotropy in Asphalt Concrete. *Transp. Res. Rec. J. Transp. Res. Board* **2005**, *1929*, 238–247. [[CrossRef](#)]

23. Darabi, M.K.; Abu Al-Rub, R.K.; Masad, E.A.; Huang, C.-W.; Little, D.N. A modified viscoplastic model to predict the permanent deformation of asphaltic materials under cyclic-compression loading at high temperatures. *Int. J. Plast.* **2012**, *35*, 100–134. [[CrossRef](#)]
24. Darabi, M.K.; Abu Al-Rub, R.K.; Masad, E.A.; Little, D.N. Cyclic Hardening-Relaxation Viscoplasticity Model for Asphalt Concrete Materials. *J. Eng. Mech.* **2013**, *139*, 832–847. [[CrossRef](#)]
25. Karimi, M.M.; Tabatabaee, N.; Jahangiri, B.; Darabi, M.K. Constitutive modeling of hardening-relaxation response of asphalt concrete in cyclic compressive loading. *Constr. Build. Mater.* **2017**, *137*, 169–184. [[CrossRef](#)]
26. Blanc, J.; Gabet, T.; Horny, P.; Piau, J.-M.; Di Benedetto, H. Cyclic triaxial tests on bituminous mixtures. *Road Mater. Pavement Des.* **2014**, *16*, 46–69. [[CrossRef](#)]
27. Airey, G.D.; Rahimzadeh, B.; Collop, A.C. Viscoelastic linearity limits for bituminous materials. *Mater. Struct.* **2003**, *36*, 643–647. [[CrossRef](#)]
28. Zhou, F.; Scullion, T.; Sun, L. Verification and Modeling of Three-Stage Permanent Deformation Behavior of Asphalt Mixes. *J. Transp. Eng.* **2004**, *130*, 486–494. [[CrossRef](#)]
29. Zhou, F.; Scullion, T. Discussion: Three Stages of Permanent Deformation Curve and Rutting Model. *Int. J. Pavement Eng.* **2002**, *3*, 251–260. [[CrossRef](#)]
30. Biligiri, K.P.; Kaloush, K.E.; Mamlouk, M.S.; Witczak, M.W. Rational Modeling of Tertiary Flow for Asphalt Mixtures. *Transp. Res. Rec. J. Transp. Res. Board* **2007**, *2001*, 63–72. [[CrossRef](#)]
31. Ameri, M.; Sheikhmotevali, A.H.; Fasihpour, A. Evaluation and comparison of flow number calculation methods. *Road Mater. Pavement Des.* **2014**, *15*, 182–206. [[CrossRef](#)]
32. Javilla, B.; Mo, L.; Hao, F.; An, S.; Wu, S. Systematic comparison of two-stage analytical rutting models of asphalt mixtures. *Constr. Build. Mater.* **2017**, *153*, 716–727. [[CrossRef](#)]
33. Sousa, J.B.; Craus, J.; Monismith, C.L. *Summary Report on Permanent Deformation in Asphalt Concrete*; University of California: Berkeley, CA, USA, 1991.
34. Uzan, J.; Motola, Y. Damage Evaluation in Simple Shear Tests with and without Stress Reversal of Asphalt Concrete. *Road Mater. Pavement Des.* **2006**, *7*, 71–86. [[CrossRef](#)]
35. Li, Q.; Lee, H.J.; Lee, S.Y. Permanent Deformation Model Based on Shear Properties of Asphalt Mixtures: Development and Calibration. *Transp. Res. Rec.* **2011**, *2210*, 81–89. [[CrossRef](#)]
36. Zieliński, P. Indirect tensile test as a simple method for rut resistance evaluation of asphalt mixtures—Polish experience. *Road Mater. Pavement Des.* **2020**, *23*, 112–128. [[CrossRef](#)]
37. Perraton, D.; Di Benedetto, H.; Sauzéat, C.; De La Roche, C.; Bankowski, W.; Partl, M.; Grenfell, J. Rutting of bituminous mixtures: Wheel tracking tests campaign analysis. *Mater. Struct.* **2011**, *44*, 969–986. [[CrossRef](#)]
38. Mohammad, L.N.; Elseifi, M.; Cao, W.; Raghavendra, A.; Ye, M. Evaluation of various Hamburg wheel-tracking devices and AASHTO T 324 specification for rutting testing of asphalt mixtures. *Road Mater. Pavement Des.* **2017**, *18*, 128–143. [[CrossRef](#)]
39. Ahmed, A.W.; Erlingsson, S. Evaluation of a permanent deformation model for asphalt concrete mixtures using extra-large wheel-tracking and heavy vehicle simulator tests. *Road Mater. Pavement Des.* **2014**, *16*, 154–171. [[CrossRef](#)]
40. Francken, L. Permanent deformation law of bituminous road mixes in repeated triaxial compression. In Proceedings of the 4th International Conference on Structural Design of Asphalt Pavements, Ann Arbor, MI, USA, 22–26 August 1977; pp. 483–496.
41. Khedr Safwan, A. Deformation Mechanism in Asphaltic Concrete. *J. Transp. Eng.* **1986**, *112*, 29–45. [[CrossRef](#)]
42. Tseng, K.-H.; Lytton, R.L. Prediction of Permanent Deformation in Flexible Pavement Materials. In *Implication of Aggregates in the Design, Construction and Performance of Flexible Pavements*; ASTM International: West Conshohocken, PA, USA, 1989; Volume 1016, pp. 154–172.
43. Wilshire, B.; Evans, R.W. Acquisition and analysis of creep data. *J. Strain Anal. Eng. Des.* **1994**, *29*, 159–165. [[CrossRef](#)]
44. Cerni, G.; Cardone, F.; Virgili, A.; Camilli, S. Characterisation of permanent deformation behaviour of unbound granular materials under repeated triaxial loading. *Constr. Build. Mater.* **2012**, *28*, 79–87. [[CrossRef](#)]
45. Choi, Y.T.; Subramanian, V.; Guddati, M.N.; Kim, Y.R. Incremental Model for Prediction of Permanent Deformation of Asphalt Concrete in Compression. *Transp. Res. Rec.* **2012**, *2296*, 24–35. [[CrossRef](#)]
46. Choi, Y.-T.; Kim, Y.R. Development of characterisation models for incremental permanent deformation model for asphalt concrete in confined compression. *Road Mater. Pavement Des.* **2013**, *14*, 266–288. [[CrossRef](#)]
47. Yun, T.; Kim, Y.R. A viscoplastic constitutive model for hot mix asphalt in compression at high confining pressure. *Constr. Build. Mater.* **2011**, *25*, 2733–2740. [[CrossRef](#)]
48. Subramanian, V.; Guddati, M.N.; Richard Kim, Y. A viscoplastic model for rate-dependent hardening for asphalt concrete in compression. *Mech. Mater.* **2013**, *59*, 142–159. [[CrossRef](#)]
49. Levenberg, E.; Uzan, J. Triaxial Small-Strain Viscoelastic-Viscoplastic Modeling of Asphalt Aggregate Mixes. *Mech. Time-Depend. Mater.* **2004**, *8*, 365–384. [[CrossRef](#)]
50. Di Benedetto, H.; Nguyen, Q.T.; Sauzéat, C. Nonlinearity, Heating, Fatigue and Thixotropy during Cyclic Loading of Asphalt Mixtures. *Road Mater. Pavement Des.* **2011**, *12*, 129–158. [[CrossRef](#)]
51. Perl, M.; Uzan, J.; Sides, A. Visco-elasto-plastic constitutive law for a bituminous mixture under repeated loading. *Transp. Res. Rec.* **1983**, *911*, 20–26.

52. Sides, A.; Uzan, J.; Perl, M. A comprehensive viscoelasto-plastic characterization of sand-asphalt compressive and tensile cyclic loading. *J. Test. Eval.* **1985**, *13*, 49–59.
53. Cao, W.; Kim, Y.R. A viscoplastic model for the confined permanent deformation of asphalt concrete in compression. *Mech. Mater.* **2016**, *92*, 235–247. [[CrossRef](#)]
54. Uzan, J. Permanent Deformation in Flexible Pavements. *J. Transp. Eng.* **2004**, *130*, 6–13. [[CrossRef](#)]
55. Park, S.; Kim, Y. Interconversion between relaxation modulus and creep compliance for viscoelastic solids. *J. Mater. Civ. Eng.* **1999**, *11*, 76–82. [[CrossRef](#)]
56. Mun, S.; Chehab, G.R.; Kim, Y.R. Determination of Time-domain Viscoelastic Functions using Optimized Interconversion Techniques. *Road Mater. Pavement Des.* **2007**, *8*, 351–365. [[CrossRef](#)]
57. Collop, A.C.; Scarpas, A.; Kasbergen, C.; De Bondt, A. Development and Finite Element Implementation of Stress-Dependent Elastoviscoplastic Constitutive Model with Damage for Asphalt. *Transp. Res. Rec. J. Transp. Res. Board* **2003**, *1832*, 96–104. [[CrossRef](#)]
58. Di Benedetto, H.; Mondher, N.; Sauzéat, C.; Olard, F. Three-dimensional Thermo-viscoplastic Behaviour of Bituminous Materials: The DBN Model. *Road Mater. Pavement Des.* **2007**, *8*, 285–315. [[CrossRef](#)]
59. Olard, F.; Di Benedetto, H. General “2S2P1D” Model and Relation Between the Linear Viscoelastic Behaviours of Bituminous Binders and Mixes. *Road Mater. Pavement Des.* **2003**, *4*, 185–224. [[CrossRef](#)]
60. Grzesikiewicz, W.; Wakulicz, A.; Zbiciak, A. Non-linear problems of fractional calculus in modeling of mechanical systems. *Int. J. Mech. Sci.* **2013**, *70*, 90–98. [[CrossRef](#)]
61. Zbiciak, A. Mathematical description of rheological properties of asphalt-aggregate mixes. *Bull. Pol. Acad. Sci. Tech. Sci.* **2013**, *61*, 65–72. [[CrossRef](#)]
62. Di Benedetto, H.; Olard, F.; Sauzéat, C.; Delaporte, B. Linear viscoelastic behaviour of bituminous materials: From binders to mixes. *Road Mater. Pavement Des.* **2004**, *5*, 163–202. [[CrossRef](#)]
63. Kachanov, L.M. On time to rupture in creep conditions. *Izv. Akad. Nauk SSSR* **1958**, *8*, 26–31. (In Russian)
64. Darabi, M.K.; Abu Al-Rub, R.K.; Masad, E.A.; Huang, C.-W.; Little, D.N. A thermo-viscoelastic-viscoplastic-viscodamage constitutive model for asphaltic materials. *Int. J. Solids Struct.* **2011**, *48*, 191–207. [[CrossRef](#)]
65. Rabotnov, I.N.; Rabotnov, I.U.N.; Rabotnov, I.U.r.N.; Rabotnov, J.N.; Rabotnov, Y.N.; Leckie, F.A. *Creep Problems in Structural Members*; North-Holland Publishing Company: Amsterdam, The Netherlands, 1969; Volume 7.
66. Perzyna, P. Thermodynamic Theory of Viscoplasticity. In *Advances in Applied Mechanics*; Elsevier: Amsterdam, The Netherlands, 1971; pp. 313–354.
67. Rushing, J.F.; Darabi, M.K.; Rahmani, E.; Little, D.N. Comparing rutting of airfield pavements to simulations using Pavement Analysis Using Nonlinear Damage Approach (PANDA). *Int. J. Pavement Eng.* **2017**, *18*, 138–159. [[CrossRef](#)]
68. Schapery, R.A. On the characterization of nonlinear viscoelastic materials. *Polym. Eng. Sci.* **1969**, *9*, 295–310. [[CrossRef](#)]
69. Huang, C.-W.; Abu Al-Rub, R.K.; Masad, E.A.; Little, D.N.; Airey, G.D. Numerical implementation and validation of a nonlinear viscoelastic and viscoplastic model for asphalt mixes. *Int. J. Pavement Eng.* **2011**, *12*, 433–447. [[CrossRef](#)]
70. Abu Al-Rub, R.K.; Darabi, M.K.; Kim, S.-M.; Little, D.N.; Glover, C.J. Mechanistic-based constitutive modeling of oxidative aging in aging-susceptible materials and its effect on the damage potential of asphalt concrete. *Constr. Build. Mater.* **2013**, *41*, 439–454. [[CrossRef](#)]
71. Abu Al-Rub, R.K.; Darabi, M.K.; Little, D.N.; Masad, E.A. A micro-damage healing model that improves prediction of fatigue life in asphalt mixes. *Int. J. Eng. Sci.* **2010**, *48*, 966–990. [[CrossRef](#)]
72. Shakiba, M.; Darabi, M.K.; Abu Al-Rub, R.K.; You, T.; Little, D.N.; Masad, E.A. Three-dimensional microstructural modelling of coupled moisture-mechanical response of asphalt concrete. *Int. J. Pavement Eng.* **2015**, *16*, 445–466. [[CrossRef](#)]
73. Huang, C.-W.; Abu Al-Rub, R.K.; Masad, E.A.; Little, D.N. Three-Dimensional Simulations of Asphalt Pavement Permanent Deformation Using a Nonlinear Viscoelastic and Viscoplastic Model. *J. Mater. Civ. Eng.* **2011**, *23*, 56–68. [[CrossRef](#)]
74. Darabi, M.K.; Kola, R.; Little, D.N.; Garg, N. Time-dependent Drucker-Prager-Cap model coupled with PANDA (Pavement Analysis Using Nonlinear Damage Approach) to predict rutting performance of flexible pavements. *Constr. Build. Mater.* **2020**, *244*, 118326. [[CrossRef](#)]
75. Rahmani, E.; Darabi, M.K.; Abu Al-Rub, R.K.; Kassem, E.; Masad, E.A.; Little, D.N. Effect of confinement pressure on the nonlinear-viscoelastic response of asphalt concrete at high temperatures. *Constr. Build. Mater.* **2013**, *47*, 779–788. [[CrossRef](#)]
76. Darabi, M.K.; Kola, R.; Little, D.N.; Rahmani, E.; Garg, N. Predicting Rutting Performance of Flexible Airfield Pavements Using a Coupled Viscoelastic-Viscoplastic-Cap Constitutive Relationship. *J. Eng. Mech.* **2019**, *145*, 04018129. [[CrossRef](#)]
77. Behnke, R.; Wollny, I.; Hartung, F.; Kaliske, M. Thermo-mechanical finite element prediction of the structural long-term response of asphalt pavements subjected to periodic traffic load: Tire-pavement interaction and rutting. *Comput. Struct.* **2019**, *218*, 9–31. [[CrossRef](#)]
78. Kim, S.-M.; Darabi, M.K.; Little, D.N.; Abu Al-Rub, R.K. Effect of the Realistic Tire Contact Pressure on the Rutting Performance of Asphaltic Concrete Pavements. *KSCE J. Civ. Eng.* **2018**, *22*, 2138–2146. [[CrossRef](#)]
79. You, T.; Im, S.; Kim, Y.-R.; Little, D.N. Mechanistic Modeling to Evaluate Structural Performance of Bituminous Pavements with Inelastic Deformation and Fatigue Damage of Mixtures. *J. Eng. Mech.* **2017**, *143*, 04016126. [[CrossRef](#)]
80. Abu Al-Rub, R.K.; Darabi, M.K.; Huang, C.-W.; Masad, E.A.; Little, D.N. Comparing finite element and constitutive modelling techniques for predicting rutting of asphalt pavements. *Int. J. Pavement Eng.* **2012**, *13*, 322–338. [[CrossRef](#)]

81. Mulugeta Alamnie, M.; Tadesse, E.; Hoff, I. Thermo-piezo-rheological characterization of asphalt concrete. *Constr. Build. Mater.* **2022**, *329*, 127106. [[CrossRef](#)]
82. Lai, J.; Bakker, A. 3-D Schapery representation for non-linear viscoelasticity and finite element implementation. *Comput. Mech.* **1996**, *18*, 182–191. [[CrossRef](#)]
83. Darabi, M.K.; Abu Al-Rub, R.K.; Masad, E.A.; Little, D.N. Constitutive modeling of fatigue damage response of asphalt concrete materials with consideration of micro-damage healing. *Int. J. Solids Struct.* **2013**, *50*, 2901–2913. [[CrossRef](#)]
84. Shakiba, M.; Darabi, M.K.; Abu Al-Rub, R.K.; Masad, E.A.; Little, D.N. Microstructural modeling of asphalt concrete using a coupled moisture–mechanical constitutive relationship. *Int. J. Solids Struct.* **2014**, *51*, 4260–4279. [[CrossRef](#)]
85. Yideti, T.F.; Birgisson, B.; Jelagin, D.; Guarin, A. Packing theory-based framework to evaluate permanent deformation of unbound granular materials. *Int. J. Pavement Eng.* **2013**, *14*, 309–320. [[CrossRef](#)]
86. Oda, M.; Nakayama, H. Yield Function for Soil with Anisotropic Fabric. *J. Eng. Mech.* **1989**, *115*, 89–104. [[CrossRef](#)]
87. Tashman, L.; Masad, E.; Little, D.; Zbib, H. A microstructure-based viscoplastic model for asphalt concrete. *Int. J. Plast.* **2005**, *21*, 1659–1685. [[CrossRef](#)]
88. Coleri, E.; Harvey, J.T.; Yang, K.; Boone, J.M. A micromechanical approach to investigate asphalt concrete rutting mechanisms. *Constr. Build. Mater.* **2012**, *30*, 36–49. [[CrossRef](#)]
89. Chehab, G.R.; Seo, Y.; Kim, Y.R. Viscoelastoplastic damage characterization of asphalt-aggregate mixtures using digital image correlation. *Int. J. Geomech.* **2007**, *7*, 111–118. [[CrossRef](#)]
90. Shojaeifard, M.; Baghani, M.; Shahsavari, H. Rutting investigation of asphalt pavement subjected to moving cyclic loads: An implicit viscoelastic–viscoplastic–viscodamage FE framework. *Int. J. Pavement Eng.* **2018**, *21*, 1393–1407. [[CrossRef](#)]
91. Underwood, B.S. A continuum damage model for asphalt cement and asphalt mastic fatigue. *Int. J. Fatigue* **2016**, *82*, 387–401. [[CrossRef](#)]
92. Pellinen, T.K.; Christensen, D.W.; Rowe, G.M.; Sharrock, M. Fatigue-Transfer Functions: How Do They Compare? *Transp. Res. Rec. J. Transp. Res. Board* **2004**, *1896*, 77–87. [[CrossRef](#)]
93. Ling, M.; Luo, X.; Chen, Y.; Gu, F.; Lytton, R.L. Mechanistic-empirical models for top-down cracking initiation of asphalt pavements. *Int. J. Pavement Eng.* **2018**, *21*, 464–473. [[CrossRef](#)]
94. Zhang, Y.; Luo, X.; Luo, R.; Lytton, R.L. Crack initiation in asphalt mixtures under external compressive loads. *Constr. Build. Mater.* **2014**, *72*, 94–103. [[CrossRef](#)]
95. Dyskin, A.V.; Sahouryeh, E.; Jewell, R.J.; Joer, H.; Ustinov, K.B. Influence of shape and locations of initial 3-D cracks on their growth in uniaxial compression. *Eng. Fract. Mech.* **2003**, *70*, 2115–2136. [[CrossRef](#)]
96. Onifade, I.; Birgisson, B.; Balieu, R. Energy-based damage and fracture framework for viscoelastic asphalt concrete. *Eng. Fract. Mech.* **2015**, *145*, 67–85. [[CrossRef](#)]
97. Widyatmoko, I.; Ellis, C.; Read, J.M. Energy dissipation and the deformation resistance of bituminous mixtures. *Mater. Struct.* **1999**, *32*, 218–223. [[CrossRef](#)]
98. Ghuzlan, K.A.; Carpenter, S.H. Energy-Derived, Damage-Based Failure Criterion for Fatigue Testing. *Transp. Res. Rec. J. Transp. Res. Board* **2000**, *1723*, 141–149. [[CrossRef](#)]
99. Luo, X.; Luo, R.; Lytton, R.L. Energy-based mechanistic approach for damage characterization of pre-flawed visco-elasto-plastic materials. *Mech. Mater.* **2014**, *70*, 18–32. [[CrossRef](#)]
100. Di Benedetto, H.; Partl, M.N.; Francken, L.; De La Roche Saint André, C. Stiffness testing for bituminous mixtures. *Mater. Struct.* **2001**, *34*, 66–70. [[CrossRef](#)]
101. Skelton, R.P.; Gandy, D. Creep-fatigue damage accumulation and interaction diagram based on metallographic interpretation of mechanisms. *Mater. High Temp.* **2008**, *25*, 27–54. [[CrossRef](#)]
102. Chaboche, J.L. Constitutive equations for cyclic plasticity and cyclic viscoplasticity. *Int. J. Plast.* **1989**, *5*, 247–302. [[CrossRef](#)]
103. Barbera, D.; Chen, H.; Liu, Y. On Creep Fatigue Interaction of Components at Elevated Temperature. *J. Press. Vessel Technol.* **2016**, *138*, 041403. [[CrossRef](#)]
104. Liu, H.; Yang, X.; Jiang, L.; Lv, S.; Huang, T.; Yang, Y. Fatigue-creep damage interaction model of asphalt mixture under the semi-sine cycle loading. *Constr. Build. Mater.* **2020**, *251*, 119070. [[CrossRef](#)]
105. Gupta, R.; Atul Narayan, S.P. Tensile creep of asphalt concrete in repeated loading tests and its effect on energy dissipation. *Int. J. Pavement Eng.* **2019**, *22*, 927–939. [[CrossRef](#)]
106. Zhang, Y.; Luo, R.; Lytton, R.L. Characterizing Permanent Deformation and Fracture of Asphalt Mixtures by Using Compressive Dynamic Modulus Tests. *J. Mater. Civ. Eng.* **2012**, *24*, 898–906. [[CrossRef](#)]
107. Chaboche, J.L.; Lesne, P.M. A Non-Linear Continuous Fatigue Damage Model. *Fatigue Fract. Eng. Mater. Struct.* **1988**, *11*, 1–17. [[CrossRef](#)]
108. Cheng, G. A fatigue damage accumulation model based on continuum damage mechanics and ductility exhaustion. *Int. J. Fatigue* **1998**, *20*, 495–501. [[CrossRef](#)]
109. Lemaitre, J.; Plumtree, A. Application of Damage Concepts to Predict Creep-Fatigue Failures. *J. Eng. Mater. Technol.* **1979**, *101*, 284–292. [[CrossRef](#)]

Paper B

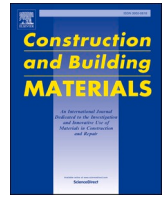
Thermo-piezo-rheological characterization of asphalt concrete

Mequanent Mulugeta Alamnie, Ephrem Taddesse and Inge Hoff. Construction and Building Materials, 329 (127106), 2022. doi: [10.1016/j.conbuildmat.2022.127106](https://doi.org/10.1016/j.conbuildmat.2022.127106)



Contents lists available at ScienceDirect

Construction and Building Materials

journal homepage: www.elsevier.com/locate/conbuildmat

Thermo-piezo-rheological characterization of asphalt concrete

Mequanent Mulugeta Alamnie^{a,*}, Ephrem Tadesse^a, Inge Hoff^b

^a Department of Engineering Science, University of Agder, 4879 Grimstad, Norway

^b Department of Civil and Environmental Engineering, Norwegian University of Science and Technology (NTNU), Høgskoleringen 7a, Trondheim, Norway

ARTICLE INFO

Keywords:

Thermo-piezo-rheology
Linear viscoelastic
Triaxial dynamic modulus
Relaxation modulus
Triaxiality ratio
Asphalt concrete

ABSTRACT

The linear viscoelastic (LVE) properties of asphalt concrete is investigated in this paper using a controlled-strain triaxial dynamic modulus test over wide frequency, temperature, and confining pressure ranges. The time–temperature–pressure superposition principle (TTPSP) is applied to validate the thermo-piezo-rheological simplicity of the tested materials using triaxial master curves. The LVE response is found highly stress-dependent at intermediate and high temperatures. The Prony series modeling of time-domain properties ascertains that confining pressure strongly correlates with long-term relaxation modulus, the absolute maximum slope of the relaxation modulus, and viscoelastic damage parameter. The stress triaxiality ratio concept is applied, and a new shift model is proposed that takes the triaxiality ratio as an internal state variable in the TTPSP. The model prediction agrees well with the experimental data. Moreover, a relationship between the long-term relaxation modulus and the triaxiality ratio is established. The triaxiality ratio coupled with TTPSP can accurately describe the stress-dependent response of asphalt concrete in the LVE domain.

1. Introduction

Asphalt concrete is a composite, time-dependent material that exhibits elements of elastic, viscous, and viscoelastic properties. The response of such materials is dependent on loading frequencies and a set of thermodynamic variables. As a fundamental thermodynamic variable, temperature and pressure significantly influence the viscoelastic and viscoplastic responses of time-dependent materials. The effect of time (frequency) and temperature is characterized using a joint parameter called reduced time (or reduced frequency) for a thermo-rheological simple material. Similarly, a time-pressure shift factor is used to analyze the joint effect of time and pressure for the piezo-rheological simple material. Several researchers have validated that the thermo-rheological simplicity (time–temperature response) of different asphalt concrete mixtures and the applicability of time–temperature superposition principle (TTSP) in both undamaged and damaged states [3,20,29,26,14]. The validity of TTSP in undamaged and damaged states yields a significant material saving for the test [5]. The combined effect of the two fundamental thermodynamic variables (temperature and pressure) on the viscoelastic response is described using the Time-Temperature-Pressure superposition principle (TTPSP). A material that satisfies the TTPSP principle is called a *thermo-piezo-rheological simple* material [23,6]. The role of confining pressure on time-

dependent materials has also been studied for several decades, such as for polymers [8,12]. As a three-phase material, asphalt concrete showed strong stress-dependent properties. Most studies on the triaxial stress response of asphalt concrete were focused on the viscoplastic properties [2,1,19,24]. Some studies such as Yun et al. [26] and Rahmani et al. [18] have investigated the role of confinement on the applicability of TTSP with growing damage and the effect of confining pressure on Schapery's nonlinear viscoelastic parameters, respectively. Other studies [28,29,21] have investigated the effect of confining pressure on linear viscoelastic (LVE) responses of asphalt concrete mixtures using triaxial master curves. Previous research focused on proposing 'vertical' shift models as a function of confining pressure and was mainly involved in constructing the 'triaxial' master curves. The triaxial stress evolution in the LVE range was not discussed in previous research. Furthermore, most standards typically use uniaxial dynamic modulus tests for asphalt concrete LVE properties, including the mechanistic-empirical pavement analysis methods. However, the triaxial (confined) dynamic modulus test is more realistic to simulate the in-situ condition and the stress-dependent LVE properties should be investigated for accurate characterization of asphalt concrete.

In this paper, strain-controlled triaxial dynamic modulus tests were conducted at wide ranges of confining pressure (0 to 300 kPa), temperature (-10 to 55 °C), and frequency (20 to 0.1 Hz). A target on-

* Corresponding author.

E-mail addresses: mequanent.m.alamnie@uia.no (M. Mulugeta Alamnie), ephrem.tadesse@uia.no (E. Tadesse), inge.hoff@ntnu.no (I. Hoff).

specimen strain magnitude of less than or equal to 50 micros is selected to ensure that the deformation due to sinusoidal stress is within the LVE domain. A test procedure was proposed in the experimental campaign, and two different asphalt mixtures were tested. The main objective of this research is to investigate the stress-dependent LVE properties of asphalt concrete using the triaxial dynamic modulus test and develop a simplified triaxial shift model. The objective is achieved; first by verifying the *thermo-piezo-rheological simplicity* of the tested materials (constructing triaxial dynamic modulus master curves using existing and new triaxial shift models), and second by investigating the stress-dependent time-domain LVE properties using the Prony method. Furthermore, the role of confinement was also explored on the maximum slope of relaxation modulus and the viscoelastic damage parameter. Finally, the triaxiality ratio concept is introduced to analyze the triaxial (3D) stress-state on the LVE responses of asphalt concrete. A new triaxial shifting model is proposed using the triaxiality ratio as an internal state variable and validated using experimental data. Moreover, a simplified model is established between the long-term relaxation modulus and the triaxiality ratio to explain the stress-dependent viscoelastic behaviors of asphalt concrete. Unless otherwise stated, the term pressure in this paper refers to confining pressure (stress).

2. Viscoelasticity

The uniaxial stress–strain constitutive relationship for linear viscoelastic (LVE) material can be expressed in a Boltzmann superposition integral form in the time domain.

$$\sigma(t) = \int_0^t E(t-\tau) \frac{d\varepsilon}{d\tau} d\tau \quad (1)$$

Where σ and ε are stress and strain, respectively; t is physical time; τ is integral variable; $E(t)$ is relaxation modulus. The one-dimensional relaxation modulus, $E(t)$ is commonly expressed using a generalized Maxwell mechanical model (GM in parallel) with the Prony series.

$$E(t) = E_\infty + \sum_{m=1}^M E_m [e^{(-t/\rho_m)}] \quad (2)$$

Where E_∞ is Long-term (equilibrium) modulus; E_m is components of the relaxation modulus; ρ_m is components of relaxation time; and M is the total number of the Maxwell elements (one Maxwell element is composed of one elastic spring and one viscous dashpot connected in series). For generalizations into 3D formulations, the deformations within a material can be decoupled into shear and volumetric components. The time-dependent stress–strain response of an isotropic LVE material in 3D can thus be described in both deviatoric ($G(t)$) and bulk or volumetric ($K(t)$) relaxation moduli, as follow.

$$G(t) = G_\infty + \sum_{m=1}^M G_m [e^{(-t/\rho_{m,G})}] \quad (3)$$

$$K(t) = K_\infty + \sum_{n=1}^N K_n [e^{(-t/\rho_{n,K})}] \quad (4)$$

Where G_∞ and K_∞ are Long term (equilibrium) shear and bulk moduli, G_m , $\rho_{m,G}$ and K_n , $\rho_{n,K}$ are Prony coefficients of relaxation modulus and time for shear and bulk, respectively. M and N are the number of Prony coefficients for shear and bulk relaxation. It is generally assumed as $\rho_{m,G} = \rho_{n,K} = \rho_m$. For the small stress LVE test, the time-dependent volumetric deformation of asphalt concrete is negligible. The reasons include (i) the hydrostatic pressure is usually less than the material's tensile strength that causes a linear elastic volumetric deformation, (ii) $K(t)$ is very high and viscous flow is assumed isochronous (linear flow). Hence, the time-dependent volume change is much smaller than the corresponding shear distortion on the same material [9] and a constant

Table 1
Aggregate gradation.

Sieve size [mm]	AB11 [%]	SKA11 [%]
16.0	100	100
11.2	95	91.2
8.0	70	53.6
4.0	48	35.7
2.0	36	21.7
0.25	15.5	12.8
0.063	10	8.4
Binder Content [%]	5.6	5.83

Poisson ratio (ν) is often assumed for asphalt concrete.

$$\begin{aligned} K(t) &= \frac{E(t)}{3(1-2\nu)}, \\ G(t) &= \frac{E(t)}{2(1+\nu)} \end{aligned} \quad (5)$$

In theory, the relationships between the three moduli ($K(t)$, $G(t)$, and $E(t)$) should be established using a time-dependent Poisson's ratio [27,17].

3. Materials and test method

3.1. Materials

In this study, two different asphalt concrete mixtures (AB11 and SKA11) collected from asphalt concrete production plants were used. The AB11 mixture is dense-graded asphalt concrete and SKA11 is a stone mastic asphalt. Both mixes have an 11 mm nominal maximum aggregate size (NMAS), where AB11 is a polymer-modified (PMB 65/105–60) while SKA11 is a 70/100 neat binder mixture. The gradation is given in Table 1. Cylindrical samples were produced by re-heating the loose mix at 150 °C for up to 4 h and compacting using a gyratory compactor according to the Superpave specification. The final test specimens (Ø100 mm and 150 mm height) were fabricated by coring and cutting from the Ø 150 mm and 180 mm height samples.

3.2. Test procedure

A triaxial dynamic modulus test was performed using a servo-hydraulic universal testing machine (IPC UTM-130). Three sets of loose core linear variable differential transducers (LVDTs) were mounted on the specimen at 120° apart radially with 70 mm gauge length. The instrumented specimens were conditioned at a target temperature for at least 2 h. A strain-controlled sinusoidal compressive load was applied axially with a target on-specimen axial strain of 50 micros or less. The test was conducted according to AASHTO T378 over a wide range of temperatures (-10, 5, 21, 40, 55 °C), pressures (0, 10, 100, 200, 300 kPa) and frequencies (20, 10, 5, 2, 1, 0.5, 0.2, 0.1 Hz). Three specimen replicates were tested at each temperature and pressure according to the following steps.

- (1). The instrumented sample is installed in the testing system at the target temperature. A sinusoidal load is applied from high to low frequencies without a rest period between sweeps. The average strain of three LVDTs should not be more than the target 50 micros.
- (2). Then, 10 kPa confining pressure is applied for about 15 min to stabilize the deformation due to confinement. Repeat step 1.
- (3). Compare dynamic modulus and phase angle values from steps 1 (unconfined or uniaxial) and step 2 (10 kPa confined). The dynamic modulus results should not vary by a significant margin.
- (4). Apply 100 kPa confining pressure (for 15 min). Repeat step 1.
- (5). Apply 200 kPa confining pressure (for 15 min). Repeat step 1.
- (6). Apply 300 kPa confining pressure (for 15 min). Repeat step 1.

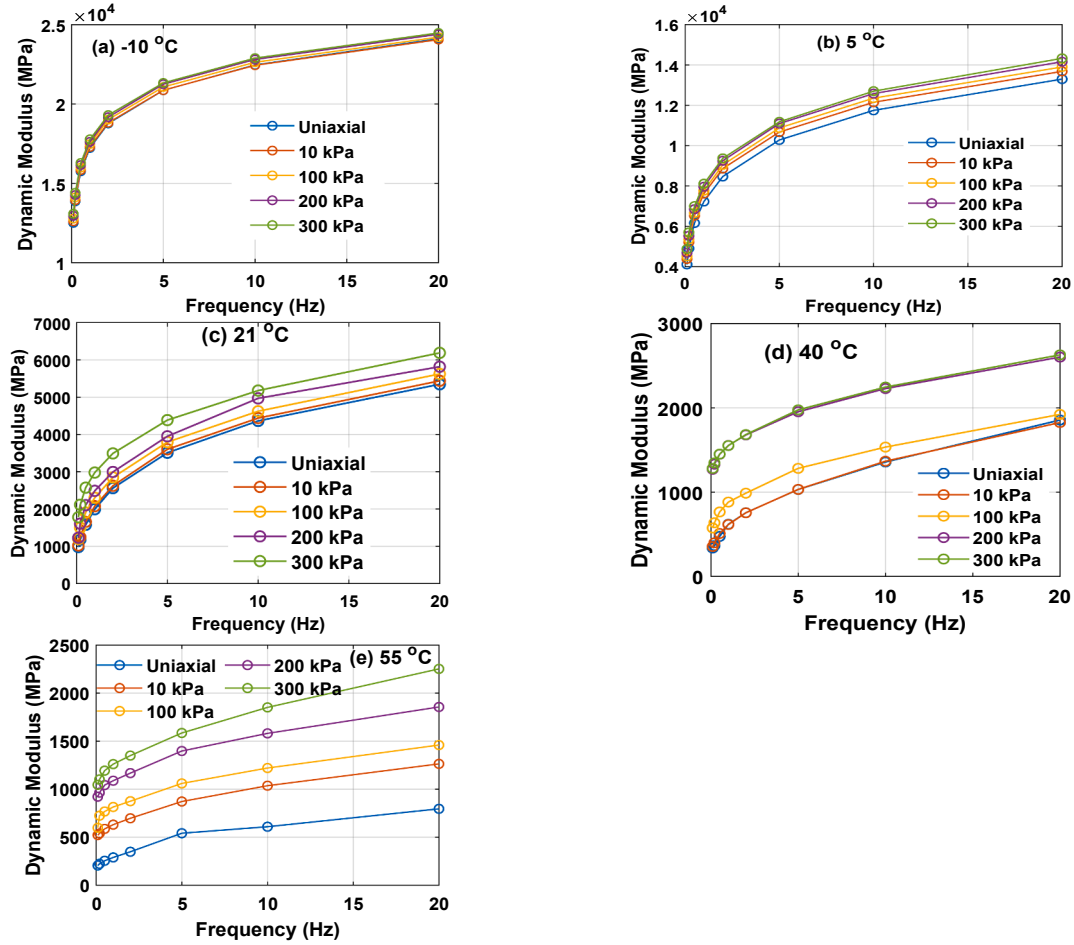


Fig. 1. Dynamic modulus at different temperatures and confining pressures - AB11 mixture.

4. Dynamic modulus test results

The response of an asphalt concrete material in a dynamic modulus test under a continuous sinusoidal loading is expressed by a complex modulus, E^* . The three measured parameters (outputs) strain $\epsilon(t)$, stress $\sigma(t)$, and dynamic modulus, E^* are expressed as follows.

$$\epsilon(t) = \epsilon_o \sin(\omega t) \quad (6)$$

$$\sigma(t) = \sigma_o \sin(\omega t + \varphi) \quad (7)$$

$$E^* = \frac{\sigma_o e^{i(\omega t + \varphi)}}{\epsilon_o e^{i\omega t}} = |E^*|(\cos\varphi + i\sin\varphi) = |E^*|e^{i\varphi} \quad (8)$$

$|E^*|$ is the norm of dynamic modulus, $E' = |E^*|\cos\varphi$ and $E'' = |E^*|\sin\varphi$ are the storage and loss moduli, respectively, σ_o and ϵ_o are stress and strain amplitudes, respectively. The phase angle, φ [0, 90°] is calculated from time lag (t_l) in strain signal and loading period (t_p) of the stress signal, $\varphi = 360^\circ \left(\frac{t_l}{t_p} \right)$. A material with a phase angle between 0° (purely elastic) and 90° (purely viscous) is a viscoelastic material. The dynamic modulus test results are the average of modulus on three specimens at each temperature, confining pressure and frequency. The average specimen-to-specimen variation for dynamic modulus value is generally less than 10% at high temperatures (40 and 55 °C). The variation is overall less than 5% for lower temperatures (21, 5 and -10 °C).

4.1. Effect of confining pressure on dynamic modulus

The effect of confining stress on the viscoelastic response of asphalt

concrete is investigated by conducting triaxial dynamic modulus tests. The triaxial dynamic modulus test results of the AB11 mixture are presented in Fig. 1 (a-e). It is clearly seen that confining pressure has a significant role on the viscoelastic response of asphalt concrete at intermediate (21 °C) and high temperatures (40 °C and 55 °C) but marginal or no effect at lower temperatures (such as 5 °C). For example, at 1 Hz frequency, the dynamic modulus at 300 kPa is 1.5 times (at 21 °C), 2.5 times (at 40 °C), and 4.4 times (at 55 °C) that of the uniaxial dynamic modulus. Moreover, the effect of confinement at 40 °C has some irregular patterns as compared to the dynamic moduli at 21 and 55 °C. The cause of such variations can be due to the increase in binder viscosity at high temperatures and low frequencies, resulting in a higher phase angle. However, the measured phase angles at higher temperatures are dictated not only by the binder but also by aggregate interactions. The binder becomes soft at high temperatures and low frequencies and the elastic aggregate structure dominates the mixture behavior, which is reflected by the reduction of phase angle. The role of confinement in such conditions is retarding the binder flow, and aggregate-to-aggregate contact is reduced. The other reason can be the transient effects during the dynamic modulus test [10], in addition to the microstructural change between 30 and 55 °C.

4.2. Isobaric master curves

The dynamic modulus test data are shifted horizontally (along the logarithmic frequency axis) to construct a master curve at a reference temperature using a sigmoidal function [16].

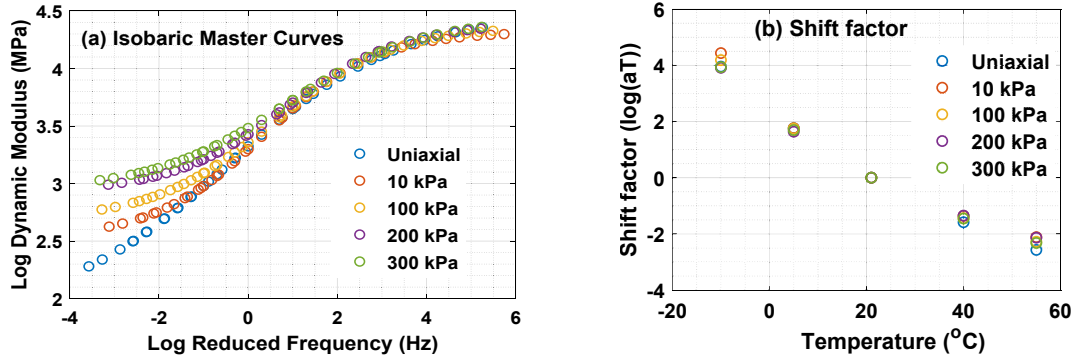


Fig. 2. Isobaric master curves and shift factors at 21 °C reference temperature – AB11 Mixture.

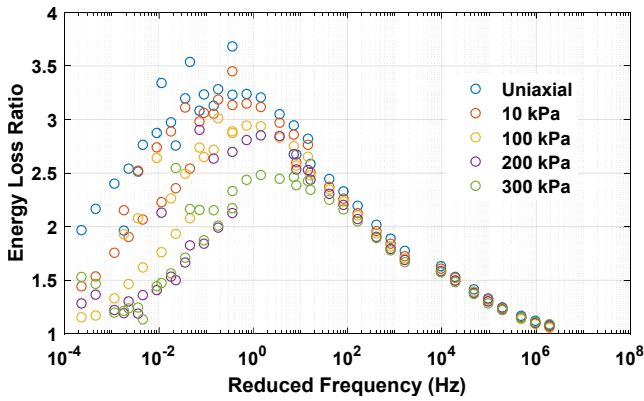


Fig. 3. Energy loss ratio (specific loss) at different confining stress levels – AB11 Mixture.

$$\log(E^*) = \delta + \frac{(\alpha - \delta)}{1 + \exp(\eta - \gamma \log f_r)} \quad (9)$$

Where E^* is the dynamic modulus, δ and α are the minimum and maximum logarithm of the dynamic modulus, respectively, η and γ are shape factors and f_r is reduced frequency.

$$f_r = a_T \times f \quad (10)$$

Where f is the frequency and a_T is time–temperature shift factor. The Williams, Landel, and Ferry (WLF) function [25] is widely used for a_T .

$$\log a_T = -\frac{C_1(T - T_0)}{C_2 + T - T_0} \quad (11)$$

Where C_1 and C_2 are WLF constants and T_0 is reference temperature. The isobaric master curves are constructed at 21 °C reference temperature using the sigmoid model and WLF shift function for the AB11 mixture, as shown in Fig. 2a. The isobaric master curves did not fall into a single curve at high temperatures (and low frequencies). The shift factors in Fig. 2b also showed a slight variation at different confining pressure levels. Moreover, the effect of confining pressure can be seen from the energy loss quantity during the dynamic modulus test. The total energy in cyclic viscoelastic deformation has a dissipated ($\Delta W = \pi \sigma_o \epsilon_o \sin \phi$) and stored ($W = \frac{\sigma_o \epsilon_o}{2}$) energy components in J/m^3 per cycle [22,9]. The ratio of dissipated energy to the maximum stored energy ($\frac{\Delta W}{W}$) is independent of stress and strain amplitudes, as shown in Eq. (12).

$$\frac{\Delta W}{W} = 2\pi \sin \phi \quad (12)$$

As shown in Fig. 3, the maximum energy loss ratio is recorded around 0.1 Hz frequency. At this point, confining pressure contributed to reducing the dissipated energy (or phase angle) and confining pressure has no significant effect on energy loss at low temperatures and

high frequencies. Therefore, confining pressure retarded energy loss and contributed to the elastic energy at high temperatures and low frequencies. These observations verify that the LVE properties of asphalt concrete are stress-dependent at intermediate and elevated temperatures. Hence, a stress-dependent shift function is necessary to generate a single, continuous master curve for LVE characterization in a triaxial stress state.

4.3. Stress-dependent master curve

In the triaxial dynamic modulus test, the confining pressure causes an increase of dynamic modulus. To construct a stress-dependent master curve, the modulus at different frequencies, confining pressures and temperatures are shifted both horizontally and vertically. The time–temperature shift factor is superposed and modified to couple pressure in the shifting function. Two models are suggested to construct and compare stress-dependent or triaxial master curves. The first model (Model-1) is the modified WLF function proposed by Fillers, Moonan, and Tschögl (FMT) model [8], expressed as follows.

$$\log \alpha_{TP} = \frac{-C_1(T - T_0 - \Gamma(p))}{C_2(P) + T - T_0 - \Gamma(p)} \quad (13)$$

$$\Gamma(p) = C_3(P) \ln \frac{1 + C_4 P}{1 + C_4 P_0} - C_5(P) \ln \frac{1 + C_6 P}{1 + C_6 P_0} \quad (14)$$

Where α_{TP} is time–temperature–pressure shift factor; P is the pressure of interest; P_0 is reference pressure; C_1 , C_4 and C_6 are constants; $C_2(p)$, $C_3(p)$ and $C_5(p)$ are pressure-dependent parameters. In the FMT model, the coefficients represent the thermal expansion of the relative free volume and the pressure-dependent parameter $\Gamma(p)$ accounts for the compressibility attributed to the collapse of free volume [7]. The FMT equation can be reduced to the WLF equation at $P = P_0 = 0$, and when $T = T_0$, the FMT function becomes a pressure shift function. A modified version of Model-1 is proposed in this paper. The pressure-dependent coefficients $C_2(P)$ and $C_3(P)$ are approximated as linear functions and the last component of Eq. (14) can be dropped.

$$\begin{aligned} C_2(P) &= C_{20} + C_{21}P, \\ C_3(P) &= C_{30} + C_{31}P \end{aligned} \quad (15)$$

Where C_{20} , C_{21} , C_{30} , C_{31} are coefficients. The proposed modified FMT model (Model-1) time–pressure or “vertical” shift factor takes the following form.

$$\Gamma(p) = (C_{30} + C_{31}P) \ln \frac{1 + C_4 P}{1 + C_4 P_0} \quad (16)$$

The second triaxial shifting model (Model-2) is a sigmoid-type Zhao’s model [30], expressed as,

$$\log \lambda = \frac{-(P - P_o)}{\exp[C_3 + C_4 \log(f_r)] + C_5(P + P_a)^{C_6}} \quad (17)$$

Table 2
Sigmoid and TTPS Shift model coefficients - AB11 Mixture.

Model	Coefficients									
	α	β	γ	δ	C_1	C_{20}	C_{21}	C_{30}	C_{31}	C_4
1	4.52	-0.06	-0.46	2.24	10.11	83.42	0.21	1.53	0.02	0.25
2	4.40	0.29	-0.68	2.61	8.92	99.11	0.99	0.96	1.50	5.17

Table 3
Sigmoid and TTPS Shift model coefficients - SKA11 Mixture.

Model	Coefficients									
	α	β	γ	δ	C_1	C_2	C_3	C_4	C_5	C_6
1	4.15	-0.81	-0.83	1.75	7.03	54.44	0.04	0.15	2.5E-03	92.27
2	4.12	-0.79	-0.85	1.77	6.85	54.5	2.0	2.0	2.2	4.9

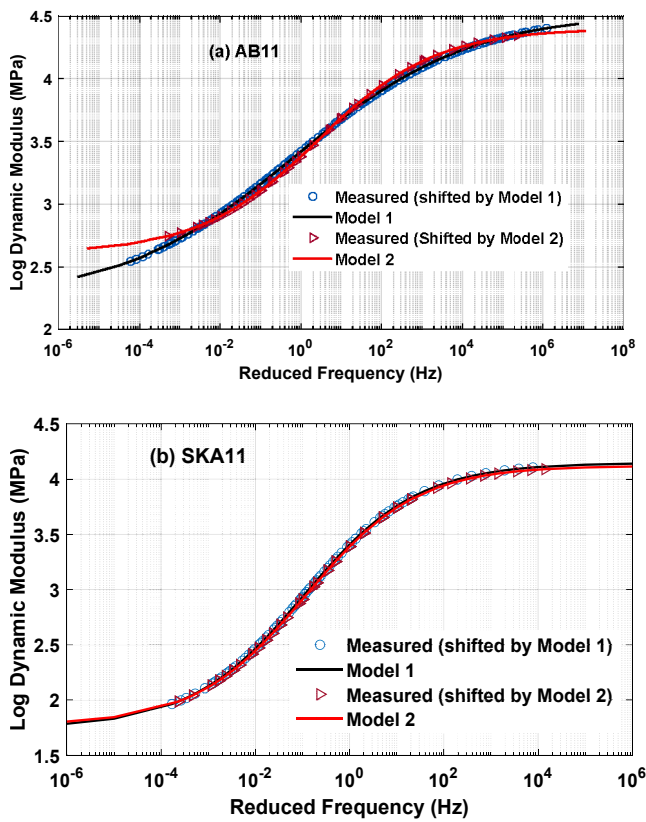


Fig. 4. Stress-dependent Master Curves at 21 °C and 100 kPa for AB11 and SKA11 Mixtures.

Where P_a is atmospheric pressure (101.3 kPa); C_3 – C_6 are regression coefficients; P , P_o are confining and reference pressures, respectively.

All stress-dependent master curves in the subsequent sections are constructed at 21 °C reference temperature and 100 kPa reference confining pressure. A total of ten parameters (including four sigmoid parameters) were optimized to construct the stress-dependent master curves (see in Table 2 and Table 3).

In Fig. 4 a-b, the triaxial master curves are presented for AB11 and SKA11 mixtures. Both Model 1 and Model-2 have good prediction accuracy ($R^2 = 0.98$ for model-1 and $R^2 = 0.95$ for Model-2 for AB11) (as shown in Fig. 5). For the SKA11 mixture, a very close prediction is observed using both models (Fig. 4 b). It is seen that both models have the advantage of simplicity while successfully shifting stress-dependent master curves. Model 1 has a wider reduced frequency range and better accuracy than Model2. In addition, Model 1 is derived based on the free

volume theory and has a sound physical and theoretical basis. On the other hand, Model 2 is a mathematical sigmoid function with a characteristic S-shaped. The vertical shift model is independently determined and added to the sigmoid model (i.e., the model is a two-step process). Hence, Model-1 is favored and proposed for further analyses in this paper with simplification. As shown in Fig. 6, the vertical shift factor $\Gamma(p)$ has an approximate linear function relationship with confining pressure.

5. Time-domain viscoelastic properties

Although the frequency domain dynamic modulus can give sufficient information about the viscoelastic properties of asphalt concrete, the time domain modulus is often used for performance prediction. Inter-conversion between frequency and time domain is performed using storage and loss modulus data. Often conversions based on the storage modulus data provide sufficient accuracy. But it is essential to evaluate the smoothness of storage modulus data before conversion to time-domain moduli. As shown in Fig. 3, the dissipated energy due to phase angle introduces noise and inconsistency to the storage modulus at high temperatures. Hence, a continuous sigmoidal function [13] in Eq. (18) is used to smoothen and avoid discreteness, wave or noise in the data. The error optimization function of $min[\log_{10}(E(f_R)) - g(f_R)]$ is used.

$$g(f_R) = a_1 + \frac{a_2}{a_2 + \frac{a_4}{\exp(a_5 + a_6 \log f_R)}} \quad (18)$$

Where a_1, a_2, \dots, a_6 are coefficients, f_R is the reduced frequency. The filtered storage modulus data (as shown in Fig. 7) is then utilized to obtain relaxation modulus using the Prony method.

5.1. Relaxation modulus

The Prony function (Eq. (19)) [15] with error minimization objective function, OF (Eq. (20)) is used to predict the relaxation modulus from pre-smoothen storage modulus data.

$$E(\omega) = E_\infty + \sum_{m=1}^M \frac{\omega^2 \rho_m^2 E_m}{1 + \omega^2 \rho_m^2} \quad (19)$$

$$OF = \frac{1}{N} \left[\sum_{i=1}^N \left(1 - \frac{|E^*(\omega_i)|_{Predicted}}{|E^*(\omega_i)|_{Measured}} \right)^2 \right] \quad (20)$$

Where E_∞ is long-term relaxation modulus (Mpa), E_m and ρ_m are Prony coefficients (relaxation modulus [MPa] and relaxation time [sec], ω is angular frequency, M is number of Prony coefficients of a generalized Maxwell model, and N is number of storage modulus data points.

The data presented in the subsequent sections are only for AB11 asphalt concrete. In Fig. 8, the isobaric and triaxial relaxation modulus

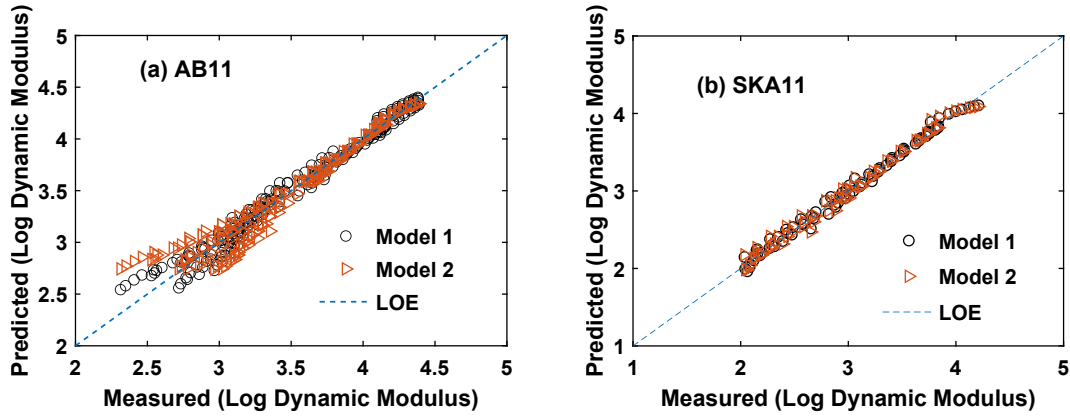


Fig. 5. Accuracy of Stress-dependent master curve predicting models for AB11 and SKA11 mixtures.

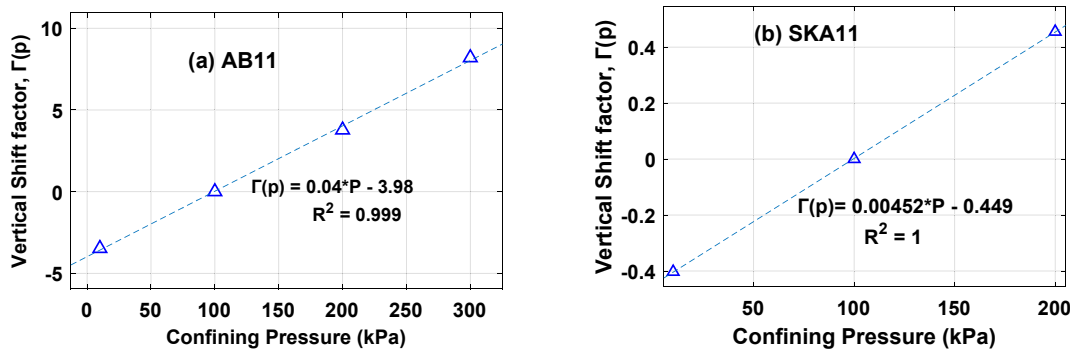


Fig. 6. Vertical shift factor versus confining Pressure (Model 1) for AB11 and SKA11 mixtures.

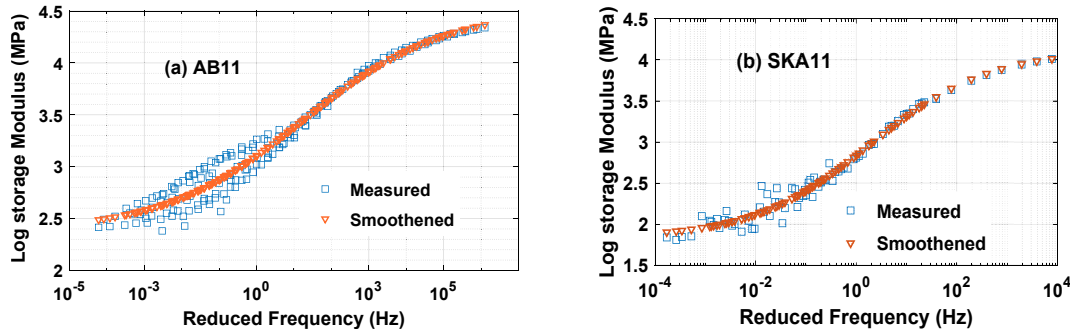


Fig. 7. Pre-smoothed Storage Modulus master curves.

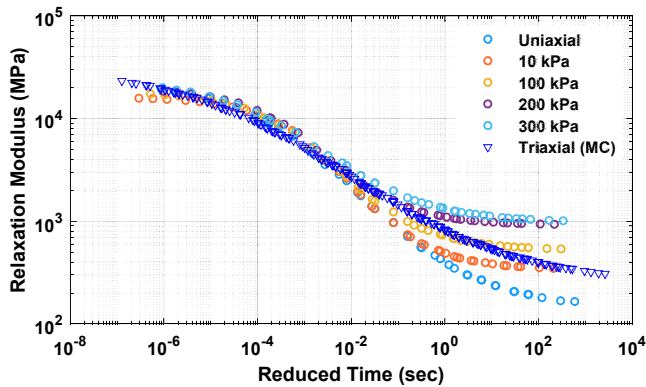


Fig. 8. Isobaric and triaxial Relaxation Modulus Master Curves – AB11 Mixture.

master curves using Model-1 are shown. It is seen that the effect of confining pressure is significant on the long-term side of the relaxation modulus. The Prony terms of a generalized Maxwell model presented in Fig. 9 and Table 4 showed a normal (Gaussian) distribution of relaxation moduli of the Prony coefficients. A total of twelve Prony coefficients were used. The coefficients (E_i) at long-time are almost the same and can be taken as independent of confining stress.

Furthermore, the bulk (volumetric) and shear moduli should be considered in the triaxial stress analysis for granular materials like asphalt concrete. From Eq. (5), it can be observed that the bulk relaxation modulus is more sensitive to change in Poisson ratio than the corresponding shear modulus. For incompressible materials (when $\nu = 0.5$), the bulk relaxation spectra (K_m) are zero or the bulk modulus $K(t)$ is infinite. To illustrate the relationship between the three moduli (E , G and K), a parametric study at different constant Poisson ratios is shown in Fig. 10. For example, as Poisson ratio increases from 0.3 to 0.35, the shear modulus increases by 3.8%, and the bulk modulus is reduced by

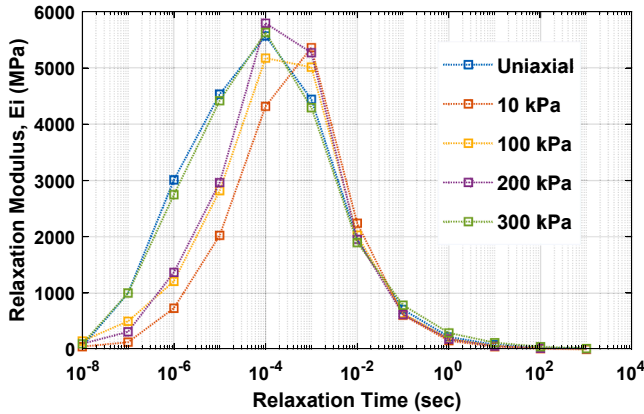


Fig. 9. Prony Coefficient Relaxation Moduli (Gaussian type distribution) – AB11 Mixture.

Table 4
Prony Coefficients of relaxation Spectrum.

m	ρ_m [sec]	Confining Pressure [kPa]				
		Uniaxial	10	100	200	300
1.	1.0E-08	49.93	50.00	148.88	99.91	99.90
2.	1.0E-07	1000.00	128.85	500.00	313.05	1000.00
3.	1.0E-06	3010.97	732.38	1210.12	1368.52	2746.72
4.	1.0E-05	4531.55	2025.15	2820.49	2962.72	4417.43
5.	1.0E-04	5566.01	4315.72	5173.00	5792.28	5628.03
6.	1.0E-03	4439.48	5359.20	5010.70	5268.25	4292.64
7.	1.0E-02	1956.16	2241.81	2027.36	1954.50	1896.97
8.	1.0E-01	708.32	607.34	638.67	621.62	786.14
9.	1.0E + 00	224.02	154.84	188.90	183.54	294.38
10.	1.0E + 01	83.97	48.50	64.21	60.77	120.83
11.	1.0E + 02	33.15	15.41	22.31	19.59	49.20
12.	1.0E + 03	18.12	0.01	1.79	9.94	18.09
E_∞ [MPa]		149.26	344.35	533.57	921.67	989.65

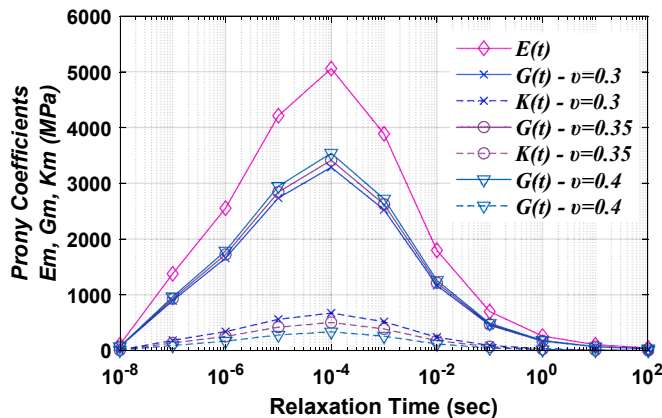


Fig. 10. Parametric study – relaxation, shear, and bulk Moduli at different Poisson ratios.

25%. Similarly, if the Poisson ratio increases from 0.35 to 0.4, the bulk modulus showed a 33% reduction and the shear component increased by 3.7%. As discussed previously, the applied confining pressure is expected to be lower than the minimum tensile strength of asphalt concrete. Thus, deformation caused by confining stress is assumed an elastic strain. Moreover, as temperature increases, tensile strength decreases contrary to the increment of the Poisson ratio. Therefore, the bulk modulus will ultimately be reduced and vanish due to high viscosity at $\nu = 0.5$ (incompressible).

5.2. The effect of confining pressure on viscoelastic damage parameter

For a viscoelastic material, the absolute maximum slope of the relaxation modulus curve is found confining stress-dependent. The maximum slope of the Log-Log relaxation modulus $E(t)$ – time (t) curve is computed using the following expression.

$$S_o = \frac{d[\log E(t)]}{dt} = \frac{\sum_{m=1}^M (-E_m \times e^{-\frac{t}{\rho_m}})}{E_\infty + \sum_{m=1}^M (E_m \times e^{-\frac{t}{\rho_m}})} \quad (21)$$

The maximum slope (S_o) is a crucial parameter for the viscoelastic damage prediction of asphalt concrete. The viscoelastic continuum damage parameter (α) is described as $\alpha = \frac{1}{S_o}$ for control-stress and $\alpha = \frac{1}{S_o} + 1$ for control-strain fatigue damage modes [4,11]. As shown in Fig. 11a, the absolute maximum slope is reduced as confining pressure increases and due to the increment of relaxation modulus at an infinite time (or when frequency approaches zero, $\omega \cong 0$) on the high-temperature side. On the other hand, the damage parameter (α) increases as confining pressure increases much faster (5.4 times) than the slope (S_o) reduction rate (Fig. 11b). Conventionally, fatigue damage tests are uniaxial and ignored the role of triaxial (3D) stress conditions. It is revealed that the triaxial stress-state affects the damage evolution parameter and subsequently impacts the fatigue life prediction of asphalt concrete. Further research is underway on this topic by the authors of this paper. The role of confinement on the permanent deformation evolution is well understood and incorporated in the strain hardening phenomenon of asphalt concrete materials.

5.3. Effect of confining Pressure on the Long-term relaxation modulus

The long-term relaxation modulus (E_∞) is a modulus at a very long time ($t \rightarrow \infty$) or when the frequency approaches zero ($\omega \rightarrow 0$). After removing the applied load, the viscoelastic material gradually recovers its deformation, and full recovery is possible given sufficient time. The long-term relaxation modulus is the modulus that governs the stress relaxation of a material in the long-time limit. The relaxation modulus is a crucial quantity for performance prediction. From the sigmoid storage modulus $[\log(E) = \delta + \frac{(\alpha-\delta)}{1+\exp(\eta-\gamma \log f_n)}]$, the long-term relaxation modulus is the minimum value as frequency closes to zero (i.e., δ or $E_\infty \cong 10^\delta$). Different models have been proposed to correlate E_∞ with confining stress [16,28]. As shown in Fig. 9 and Fig. 12, the long-term relaxation modulus is dependent on confining stress and a linear relation can be seen between the long-term relaxation modulus and confining pressure.

There is a relatively weak correlation between the long-term relaxation modulus and the absolute maximum slope of the relaxation modulus curve and the damage parameter, as shown in Fig. 13.

5.4. Triaxiality ratio in linear viscoelastic response

In this paper, the stress ratio parameter (triaxiality ratio) is introduced to investigate the linear viscoelastic (LVE) property of asphalt concrete. The triaxiality ratio (η) is defined as the ratio of hydrostatic pressure (mean stress, σ_m) and the von Mises equivalent stress (σ_{vm}) or the ratio of the first stress invariant (I_1) to the second deviatoric stress invariant (J_2). It is argued that the stress ratio factor is essential to describe the stress-dependent LVE response of asphalt concrete.

$$\eta = \frac{\sigma_m}{\sigma_{vm}} = \frac{I_{1/3}}{\sqrt{3J_2}} \quad (22)$$

Where η is triaxiality ratio; $\sigma_m = \frac{\sigma_1 + \sigma_2 + \sigma_3}{3}$; $\sigma_{vm} = \sqrt{\frac{(\sigma_1 - \sigma_2)^2 + (\sigma_1 - \sigma_3)^2 + (\sigma_2 - \sigma_3)^2}{2}}$; $\sigma_1, \sigma_2, \sigma_3$ are principal stresses. Simplifying Eq. (22) for triaxial condition, i.e., $\sigma_1 = \sigma_d + \sigma_c$ and $\sigma_2 = \sigma_3 = \sigma_c$ (σ_c is denotes confining pressure and σ_d is peak deviatoric stress) takes the following form.

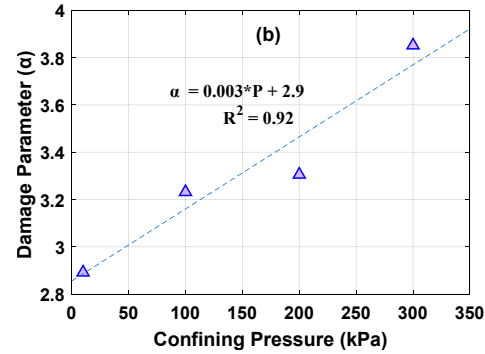
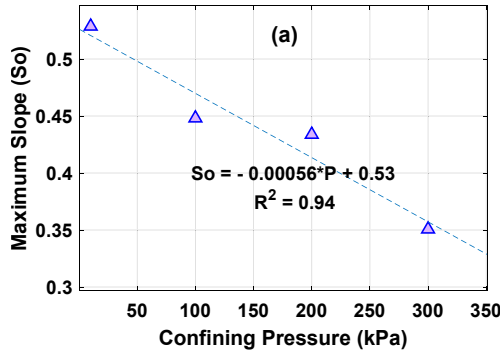


Fig. 11. Confining Pressure versus (a) Maximum slope (S_o) (b) Damage evolution Parameter (α).

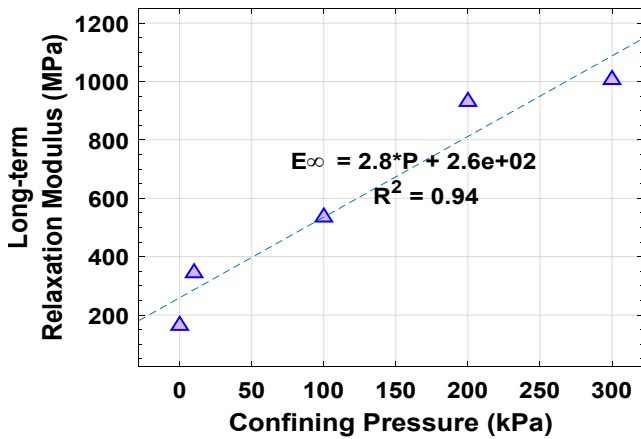


Fig. 12. Long-term relaxation Modulus at different confining pressures.

$$\eta = \frac{\sigma_c}{\sigma_d} + \frac{1}{3} \quad (23)$$

The triaxiality ratio for the uniaxial or unconfined ($\sigma_c = 0$) condition is 1/3. The ratio increases as the confinement level dominates the Mises equivalent stress. Theoretically, the maximum ratio (i.e., $\eta = \infty$) is obtained when deviatoric stress is minimum or at very high hydrostatic stress.

The peak deviatoric stress is obtained from the frequency sweep dynamic modulus test. Fig. 14 shows the peak deviatoric stress in a strain-controlled triaxial dynamic modulus test. The stress decreases as temperature increases and frequency reduces. That means maximum deviatoric stress is exerted at low temperature and high frequency to maintain the target strain limit (50 micros). As can be seen in the figure, the peak deviatoric stress does not vary much with confining pressure at a particular test temperature. This confirms the consistency of applied deviatoric stress regardless of the different volumetric stresses.

However, the slight variations observed (e.g., at 21 °C) could be due to transient effects during the sinusoidal test or due to lateral pressures. As shown in Fig. 15a-b, the triaxiality ratios are computed at each temperature and confining stress. It is clearly seen that η is both pressure and temperature-dependent, and increases with both confining pressure and temperature in a controlled-strain test. Furthermore, a power relationship (with R^2 over 0.95) is observed between η and the two thermodynamic variables (temperature and pressure). The rate of triaxiality ratio starts decreasing from and after 100 kPa confinement (Fig. 15b) and 40 °C temperature (Fig. 15a). Although the realistic confining pressure in the asphalt pavement is not accurately known, the range between 100 and 250 is generally considered as an in-situ confining stress range (average of 150 to 175 kPa). The surface plot in Fig. 16 also shows that the triaxiality ratio is critical at the combination of hot temperature and high confinement conditions. This observation indirectly implies that the linearity limit of asphalt concrete depends on the triaxiality ratio (Von Mises and mean stresses) and can be determined using different combinations of confining pressures, temperatures, and deviatoric stresses. Based on the observations from Figs. 15 and 16, the triaxiality ratio can be integrated into the time-temperature-pressure shift model to predict triaxial stress-dependent LVE response of asphalt concrete.

5.5. The proposed model

The triaxiality ratio (η) is a fundamental material parameter that can couple the stress-dependent thermo-piezo-rheology responses of viscoelastic materials. The Prony method is widely used for viscoelastic modeling of asphalt concrete. From a mechanistic viewpoint, the triaxiality ratio is a more comprehensive and efficient approach to model triaxial viscoelastic properties. As discussed in Section 5.4, the triaxiality ratio (η) is dependent on both temperature and pressure. This paper proposes a new model to integrate the triaxiality ratio with the time-temperature-pressure superposition principle. The proposed model takes the following form.

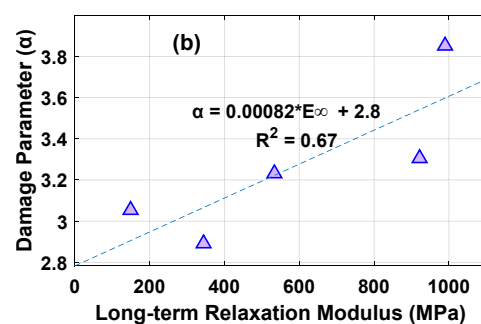
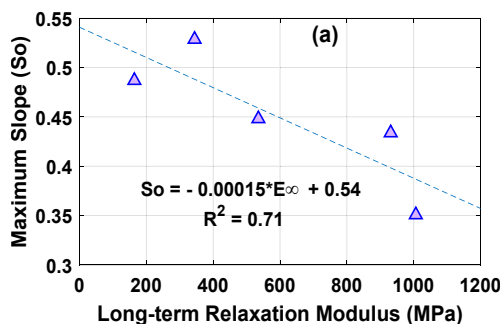


Fig. 13. Long-term relaxation Modulus versus Maximum slope and viscoelastic damage parameter.

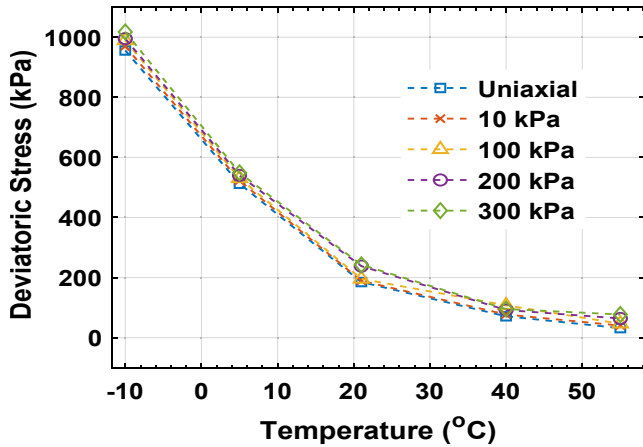


Fig. 14. Peak deviatoric stress at different Confining Pressures and temperatures.

$$\log \alpha_{TP} = \frac{-C_1[T - T_0 - \Gamma(p)]}{C_{22} + C_{23}\eta + T - T_0 - \Gamma(p)} \quad (24)$$

$$\Gamma(p) = (C_7\eta) \ln \left(\frac{1 + C_8P}{1 + C_8P_0} \right) \quad (25)$$

Where $C_1, C_{22}, C_{23}, C_7, C_8$ are temperature and pressure shift factor coefficients. A master curve is constructed using the new proposed model (Eqs. (24) and (25)) and compared with Model-1 (Eqs. (13), 15, and 16). As shown in Fig. 17, the proposed triaxiality ratio-based model fitted the measure data well. The main advantage of this model is the consideration of deviatoric stress in the LVE modeling while being concise and fewer number of model coefficients. In most dynamic modulus tests, the load control mechanism is controlled-strain modes. Limiting the strain output is more controllable than that of the stress when linear viscoelastic response is concerned. However, there are circumstances where stress-controlled responses can be more plausible. In such conditions, the proposed triaxiality ratio shift model is convenient to predict the linear viscoelastic response.

Furthermore, the relationship between the long-term relaxation modulus (E_∞) and the triaxiality ratio (η) is established.

$$E_\infty = 10^{[\kappa + \lambda \times \ln(\eta)]} \quad (26)$$

Where κ and λ are fitting parameters. The exponent in Eq. (26) is equivalent to the minimum dynamic modulus value δ of the sigmoid function i.e., $\min[\log(E^*)] = \delta = \kappa + \lambda \times \ln(\eta)$. As shown in Fig. 18, a good correlation is observed between long-term relaxation modulus (E_∞) and the triaxiality ratio (η) at high temperatures. This is because the stress ratio is more critical on the viscous side of asphalt concrete than the elastic part (as shown in Fig. 16). The fitting parameters of the model (Eq. (26)) are given in Table 5.

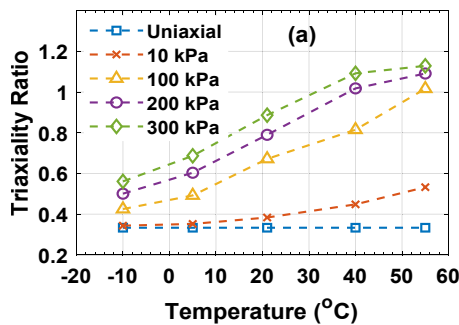


Fig. 15. Triaxiality ratio at different Confining Pressures and Temperatures.

6. Conclusion

In this paper, the effect of triaxial stress on the linear viscoelastic properties of asphalt concrete material was investigated using triaxial dynamic modulus test over a wide range of temperatures, frequencies, and confining stresses. Two different asphalt mixtures (neat and polymer-modified binder) were used and proved as thermo-piezorheologically simple material. The Fillers, Moonan, and Tschoegl (FMT) model is adopted for time-temperature-Pressure shifting and compared with another model from literature (Model 2). The stress ratio concept (triaxiality ratio) is introduced to characterize the stress-dependent viscoelastic properties of asphalt concrete. The main contributions are summarized as follows.

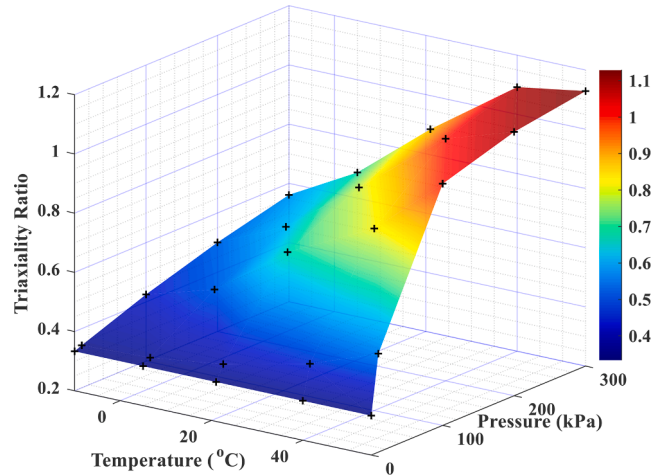


Fig. 16. Three-dimensional Surface plot of Triaxiality ratio.

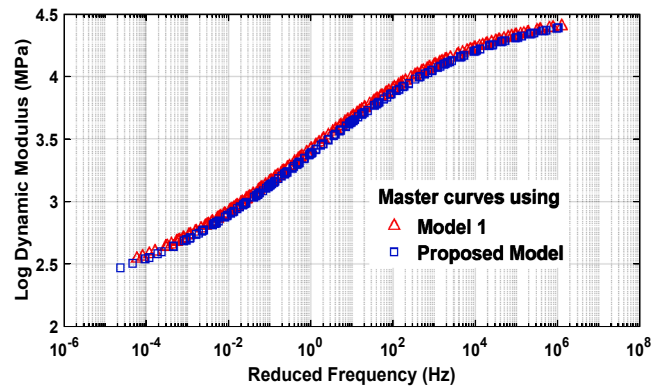
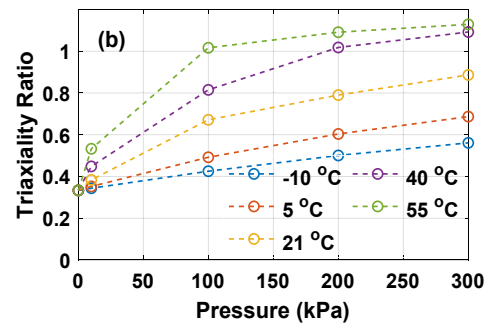


Fig. 17. Triaxial Master curves using Model-1 and the New Triaxial Ratio-based model.



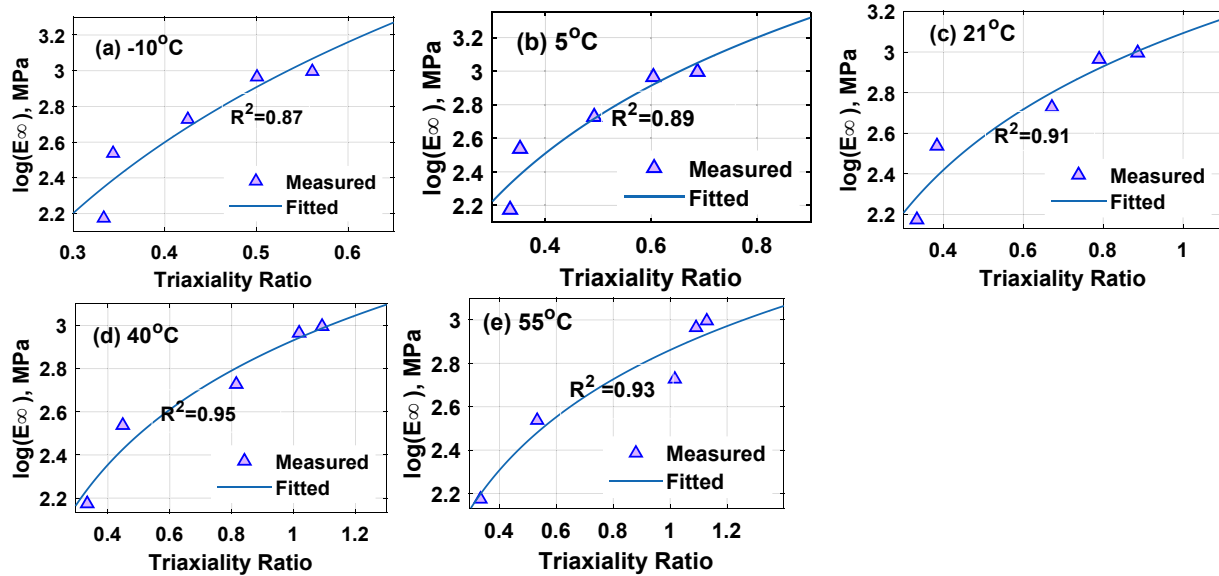


Fig. 18. Triaxiality ratio versus long-term relaxation modulus at different pressure and temperatures.

Table 5
Fitting Parameters for Eq. (26).

Coefficient	Temperature [°C]				
	-10	5	21	40	55
κ	3.87	3.42	3.09	2.93	2.86
λ	1.38	1.00	0.73	0.63	0.60

- The linear viscoelastic (LVE) property of asphalt concrete in a triaxial stress state is validated using the time-temperature-pressure superposition principle (TTPSP). The LVE properties are highly stress-dependent at intermediate and high temperatures.
- A simplified, integral (one-step), and theoretically sound vertical shift model is proposed by modifying the FMT model to construct triaxial master curves.
- A Prony method time-domain viscoelastic analysis revealed that the long-term relaxation modulus and maximum slope of a relaxation modulus curve are strongly stress-dependent. However, the Prony series coefficients (E_i) are independent of pressure at high relaxation time.
- A slight reduction of the maximum slope of relaxation modulus due to confining pressure causes more than 5.4 times increment of the viscoelastic fatigue damage parameter, highlighting the limitations of uniaxial fatigue life prediction, particularly at intermediate temperatures (from 15 to 25).
- The concept of triaxiality ratio is introduced to characterize the 3D stress effect on the linear viscoelastic responses of asphalt concrete. For a controlled-strain dynamic modulus test, the triaxiality ratio increases with temperature and pressure. In addition, the ratio has a strong correlation with the long-term relaxation modulus.
- A new triaxial TTPSP shifting model is proposed and validated. The triaxiality ratio can indirectly characterize the viscoelastic linearity limit for the thermo-piezo-rheological simple materials.

CRediT authorship contribution statement

Mequanent Mulugeta Alamnie: Conceptualization, Methodology, Data curation, Writing – original draft, Visualization. **Ephrem Taddesse:** Conceptualization, Supervision. **Inge Hoff:** Supervision.

Declaration of Competing Interest

The authors declare that they have no known competing financial interests or personal relationships that could have appeared to influence the work reported in this paper.

Appendix A. Supplementary data

Supplementary data to this article can be found online at <https://doi.org/10.1016/j.conbuildmat.2022.127106>.

References

- [1] J. Blanc, T. Gabet, P. Hornych, J.-M. Piau, H. di Benedetto, Cyclic triaxial tests on bituminous mixtures, *Road Mater. Pavement Des.* 16 (2014) 46–69.
- [2] W. Cao, Y.R. Kim, A viscoplastic model for the confined permanent deformation of asphalt concrete in compression, *Mech. Mater.* 92 (2016) 235–247.
- [3] G. Chehab, Y. Kim, R. Schapery, M. Witczak, R. Bonaquist, Time-temperature superposition principle for asphalt concrete with growing damage in tension state, *J. Assoc. Asphalt Paving Technol.* 71 (2002).
- [4] J.S. Daniel, Y.R. Kim, Development of a simplified fatigue test and analysis procedure using a viscoelastic, continuum damage model (with discussion), *J. Assoc. Asphalt Paving Technol.* 71 (2002).
- [5] M.K. Darabi, R.K. Abu Al-Rub, E.A. Masad, C.-W. Huang, D.N. Little, A thermo-viscoelastic–viscoplastic–viscodamage constitutive model for asphaltic materials, *Int. J. Solids Struct.* 48 (2011) 191–207.
- [6] EMRI, I. 2005. Rheology of solid polymers. *Rheology Reviews*, 2005, 49.
- [7] J.D. Ferry, R.A. Stratton, The free volume interpretation of the dependence of viscosities and viscoelastic relaxation times on concentration, pressure, and tensile strain, *Kolloid-Zeitschrift* 171 (1960) 107–111.
- [8] R.W. Fillers, N.W. Tschoegl, The Effect of Pressure on the Mechanical Properties of Polymers, *Trans. Soc. Rheol.* 21 (1977) 51–100.
- [9] W.N. Findley, J.S. Lai, K. Onaran, Creep and relaxation of nonlinear viscoelastic materials, North-Holland Publishing, 1976.
- [10] P. Gayte, H. di Benedetto, C. Sauzéat, Q.T. Nguyen, Influence of transient effects for analysis of complex modulus tests on bituminous mixtures, *Road Mater. Pavement Des.* 17 (2016) 271–289.
- [11] H.-J. Lee, J.S. Daniel, Y.R. Kim, Continuum Damage Mechanics-Based Fatigue Model of Asphalt Concrete, *J. Mater. Civ. Eng.* 12 (2000) 105–112.
- [12] W.K. Moonan, N.W. Tschoegl, The effect of pressure on the mechanical properties of polymers. IV. Measurements in torsion, *J. Polym. Sci.: Polym. Physics Ed.* 23 (1985) 623–651.
- [13] S. Mun, G.R. Chehab, Y.R. Kim, Determination of Time-domain Viscoelastic Functions using Optimized Interconversion Techniques, *Road Mater. Pavement Des.* 8 (2007) 351–365.
- [14] M.L. Nguyen, C. Sauzéat, H. di Benedetto, N. Tapsoba, Validation of the time-temperature superposition principle for crack propagation in bituminous mixtures, *Mater. Struct.* 46 (2013) 1075–1087.
- [15] Park, S. W. & Schapery, R. A. 1999. Methods of interconversion between linear viscoelastic material functions. Part I—a numerical method based on Prony series. 36, 1653-1675.

- [16] T.K. Pellinen, M.W. Witzczak, M. Marasteanu, G. Chehab, S. Alavi, R. Dongré, Stress dependent master curve construction for dynamic (complex) modulus. *Asphalt Paving Technology: Association of Asphalt Paving Technologists-Proceedings of the Technical Sessions, Association of Asphalt Paving Technologist*, 2002, pp. 281–309.
- [17] D. Perraton, H. di Benedetto, C. Sauzéat, B. Hofko, A. Graziani, Q.T. Nguyen, S. Pouget, L.D. Poulidakos, N. Tapsoba, J. Grenfell, 3Dim experimental investigation of linear viscoelastic properties of bituminous mixtures, *Mater. Struct.* 49 (2016) 4813–4829.
- [18] E. Rahmani, M.K. Darabi, R.K. Abu Al-Rub, E. Kassem, E.A. Masad, D.N. Little, Effect of confinement pressure on the nonlinear-viscoelastic response of asphalt concrete at high temperatures, *Constr. Build. Mater.* 47 (2013) 779–788.
- [19] N. Roy, A. Veeraragavan, J.M. Krishnan, Influence of confinement pressure and air voids on the repeated creep and recovery of asphalt concrete mixtures, *Int. J. Pavement Eng.* 17 (2016) 133–147.
- [20] C.W. Schwartz, N. Gibson, R.A. Schapery, Time-Temperature Superposition for Asphalt Concrete at Large Compressive Strains, *Transp. Res. Rec.: J. Transp. Res. Board* 1789 (2002) 101–112.
- [21] Y. Sun, B. Huang, J. Chen, X. Shu, Y. Li, Characterization of Triaxial Stress State Linear Viscoelastic Behavior of Asphalt Concrete, *J. Mater. Civ. Eng.* 29 (2017) 04016259.
- [22] N.W. Tschoegl, Energy Storage and Dissipation in a Linear Viscoelastic Material, in: N.W. Tschoegl (Ed.), *The Phenomenological Theory of Linear Viscoelastic Behavior*, Springer Berlin Heidelberg, Berlin, Heidelberg, 1989.
- [23] N.W. Tschoegl, Time Dependence in Material Properties: An Overview, *Mech. Time-Dependent Mater.* 1 (1997) 3–31.
- [24] J. Uzan, Characterization of Asphalt Concrete Materials for Permanent Deformation, *Int. J. Pavement Eng.* 4 (2003) 77–86.
- [25] M.L. Williams, R.F. Landel, J.D. Ferry, The temperature dependence of relaxation mechanisms in amorphous polymers and other glass-forming liquids, *J. Am. Chem. Soc.* 77 (1955) 3701–3707.
- [26] T. Yun, B.S. Underwood, Y.R. Kim, Time-Temperature Superposition for HMA with Growing Damage and Permanent Strain in Confined Tension and Compression, *J. Mater. Civ. Eng.* 22 (2010) 415–422.
- [27] Y. Zhang, R. Luo, L. Lytton Robert, Anisotropic Viscoelastic Properties of Undamaged Asphalt Mixtures, *J. Transp. Eng.* 138 (2012) 75–89.
- [28] Y. Zhao, H. Liu, W. Liu, Characterization of linear viscoelastic properties of asphalt concrete subjected to confining pressure, *Mech. Time-Dependent Mater.* 17 (2013) 449–463.
- [29] Y. Zhao, Y. Richard Kim, Time-Temperature Superposition for Asphalt Mixtures with Growing Damage and Permanent Deformation in Compression, *Transp. Res. Rec.: J. Transp. Res. Board* 1832 (2003) 161–172.
- [30] Y. Zhao, J. Tang, H. Liu, Construction of triaxial dynamic modulus master curve for asphalt mixtures, *Constr. Build. Mater.* 37 (2012) 21–26.

Paper C

Viscoelastic characterization and comparison of Norwegian asphalt mixtures using dynamic modulus and IDT tests

Mequanent Mulugeta Alamnie, Ephrem Taddesse and Inge Hoff. Eleventh International Conference on the Bearing Capacity of Roads, Railways and Airfields, Vol. 1:118-128, 2021. doi:[10.1201/9781003222880-12](https://doi.org/10.1201/9781003222880-12)

Viscoelastic characterization and comparison of Norwegian asphalt mixtures using dynamic modulus and IDT tests

M. Alamnie & E. Taddesse

Department of Civil and Structural Engineering, University of Agder (UiA), Grimstad, Norway

I. Hoff

Department of Civil and Transport Engineering, Norwegian University of Science and Technology, Trondheim, Norway

ABSTRACT: This paper presents the comparison of stiffnesses of two types of asphalt concrete mixes (Ab11 and Agb11) fabricated in the laboratory using two commonly used stiffness tests. (1) uniaxial compression dynamic modulus (E^*) and (2) Indirect tensile resilient modulus (M_r) tests are conducted at various temperatures, frequencies, and loading times. As expected, both E^* and M_r values decrease as temperature increases and frequency decreases. It is observed that the M_r is generally less than the E^* . However, this phenomenon is dependent on frequency, temperature, and material type. The viscoelastic property of the two mixes is characterized using the time-temperature superposition principle. Master curves are developed using the mathematical sigmoid and the rheological 2S2P1D models. It has been observed that the rheological model has shown difficulty to converge optimization error to fit M_r master curve while sigmoid function accurately fitted the measured data. M_r is compared with E^* both in frequency and time domains using master curves. A closer comparison is observed with the storage modulus (E') and time-domain relaxation modulus $E(t)$ master curves. Considering the inherent time-domain property of M_r , it is recommended to compare with E' or $E(t)$. From the master curves and data analysis and by considering inputs such as energy loss, modular ratio, frequency, temperature, and other volumetric properties, a rigorous M_r vertical shifting function can be developed. Finally, a material database is obtained for Norwegian asphalt mixes.

Keywords: Viscoelastic, Dynamic Modulus, Resilient Modulus, 2S2P1D Model

1 INTRODUCTION

Asphalt concrete (mixture) is a composite material constituted of aggregate particles embedded in a bitumen/binder. The asphalt binder firmly adheres to the aggregate particles and binds them to form asphalt concrete (a.k.a. bituminous mixture). Asphalt concrete is a viscoelastic material at small strain or stress levels, whereas it behaves in a nonlinear viscoelastoplastic manner at high temperatures and large deformations. Since the pioneering of the mechanistic-based design method, enormous research efforts are put forth towards developing more accurate and complicated testing methods. Various field and laboratory test methods are developed to characterize asphalt concrete in linear, nonlinear, viscoelastic, or viscoplastic states. A wide range of material data is needed to calibrate advanced pavement design models, which required extensive testing using advanced test equipment. However, equipment cost,

complexity equipment/test method, and requirements skilled labor/time are imminent challenges.

For this reason, asphalt material characterization still relies on simple performance indicators such as Indirect tensile, Marshall stability, and other rheological tests. The Indirect Tensile (IDT) resilient modulus test is a standard test used as a performance indicator to assess stiffness, permanent deformation, and fatigue cracking of asphalt concrete (Bennert et al., 2018). The small strain dynamic modulus test is another well-known test for linear viscoelastic characterization of asphalt concrete in the frequency domain. In essence, the IDT strength is a relative indicator of the resistance of the asphalt mixture to tensile loads. Efforts have been made to correlate the IDT resilient modulus and dynamic modulus values (Lacroix et al., 2007, Ping and Xiao, 2008, Loulizi et al., 2006).

This study aims to characterize and compare dynamic modulus and IDT resilient modulus tests using two laboratory fabricated asphalt concrete mixtures used in Norway. For the test campaign, the small strain (viscoelastic) range is considered for both test methods. The asphalt mixtures are selected based on binder stiffness (i.e., soft and relatively harder polymer-modified binder mixes). Moreover, the study investigates the correlation between E^* and M_r , and M_r with storage dynamic modulus (E') using the superposition principle and through the use of master curves. In addition, a material database is obtained for the Norwegian asphalt concrete mixes.

2 THEORETICAL BACKGROUND

The performance of asphalt concrete is dependent on the fundamental thermodynamic variables (temperature and pressure) and loading frequency. The effect of temperature has been studied with more emphasis than pressure. The superposition principle of Time and Temperature (TTSP) is used to develop viscoelastic models. Several researchers have validated the applicability of TTSP for asphalt concrete with and without damage (i.e., in linear or small strain, and nonlinear or large strain states) (Schwartz et al., 2002, Zhao and Richard Kim, 2003, Yun et al., 2010, Nguyen et al., 2013). The TTSP is used to shift experimental data (at various temperatures, stress, frequency, strain rate, etc.) to a specified reference parameter (such as temperature, stress, or strain rate). A material that satisfies the superposition principle is called a thermo-rheologically simple material. Using TTSP, the same material response can be obtained either at low temperatures and longer loading times (low frequency) or at high temperatures but short loading times (high frequency). The relationship can be described as follows (Equation 1).

$$|E^*(T, f)| = |E^*(f_R)| \quad (1)$$

Where, $f_R = f \cdot aT$ = reduced frequency; f = frequency; aT = shift factor for temperature (T).

The horizontal shifting behavior allows for the processed data to form a single curve but with a wide frequency beyond the experimental window. The curve generated by shifting experimental data is called the master curve. The Time-temperature shift factor (amount of horizontal shift to a reference temperature) and the master curve enable us to predict the linear viscoelastic (LVE) behavior over a wide range of time, frequency, stress, strain, etc. Different shift factor models are available in the literature (Yusoff et al., 2011). The Williams, Landel, and Ferry (WLF) function (Williams et al., 1955) is the commonly used model (Equation 2).

$$\log(a_T) = -\frac{C_1(T - T_r)}{(T - T_r) + C_2} \quad (2)$$

Where C_1, C_2 – WLF constants

3 EXPERIMENTAL PROGRAM

3.1 Materials and sample production

In this study, two widely used asphalt mixtures in Norway (identified as Ab11, Agb11) are used for investigation. The mixes are collected from a production plant supplied by an asphalt producer. Both mixes have a nominal maximum aggregate size (NMAS) of 11 mm, as shown in the granulometric distribution (Table 1). The Ab11 is a polymer-modified mix (70/100 binder grade and 5.6% content), and it is mainly used in high-traffic pavement. On the other hand, the Agb11 is a soft mixture mainly applied for low to medium-traffic roads and contains 5.83 % content of a 160/220 grade type binder. The sampled mix is reheated at 150°C for 4 hours before compaction in a gyratory compactor. The 150 mm diameter and 180 mm height cylindrical samples are cored and cut to get the final specimens for dynamic modulus (100 mm 150 mm height) and resilient modulus (100 mm 45 to 50 mm thickness).

Table 1. Aggregate gradation (Ab11 and Agb11).

Sieve Size (mm)	% Passing	
	Agb11	Ab11
16	100	100
11.2	95	95
8	77	70
4	56	48
2	41.5	36
1	31.5	27.5
0.25	15	15.5
0.063	7.5	10

3.2 Mechanical characterization of asphalt concrete

In the dynamic modulus (E^*) test, a uniaxial compressive sinusoidal (harmonic) load is applied on a specimen without a rest period (no delayed elastic rebound) at different frequency sweeps (Figure 1 a). The steady-state stress is applied so that it maintains an axial strain amplitude (ε_o) between 50 to 100 $\mu\text{m/m}$ and smaller (Gayte et al., 2016, Schwartz et al., 2002). A strain amplitude up to 150 $\mu\text{m/m}$ is recommended in compression (Levenberg and Uzan, 2004). However, the idealized steady-state (harmonic) condition is deviated due to transient behaviors, such as non-uniform loading, nonlinearity, or any other phenomenon (Gayte et al., 2016). A complex number (E^*) defines the stress-strain relationship under continuous sinusoidal loading. The theoretical sinusoidal evolutions of the three measured parameters with time (strain, stress, and dynamic modulus) are expressed in Equations 3 to 5.

$$\varepsilon(t) = \varepsilon_o \sin(\omega t) \quad (3)$$

$$\sigma(t) = \sigma_o \sin(\omega t + \varphi) \quad (4)$$

$$E^* = \frac{\sigma_o}{\varepsilon_o} e^{i\varphi} = |E^*| (\cos\varphi + i \sin\varphi) = |E^*| e^{i\varphi} \quad (5)$$

Where, $|E^*| = E' + iE''$, $E' = |E^*| \cos\varphi$ – storage modulus and $E'' = |E^*| \sin\varphi$ – loss modulus; ε_o , σ_o – the axial strain and stress amplitudes, respectively; i – complex number ($i^2 = -1$); φ – phase angle $[0, 90^\circ]$ which is calculated using time lag (t_l) in strain signal and loading period (t_p) of the stress signal (i.e., $\varphi = 360^\circ \frac{t_l}{t_p}$).

On the other hand, in the resilient modulus (M_r) test, a haversine compressive load is usually applied with a rest period along the vertical diametral plane of a cylindrical asphalt concrete specimen (Figure 1 b). The load should be selected to avoid damage to the sample at different pulse and rest periods. A minimum of 200N axial force and 50 microstrains target deformation are selected. The M_r is calculated using the measured recoverable strain (deformation) during the unloading and the rest period with an assumed constant Poisson ratio, $\mu=0.35$ (EN 12697-26). It should be noted that the haversine load with a rest period can be decomposed into a cycle of true sinusoidal load and a creep load.

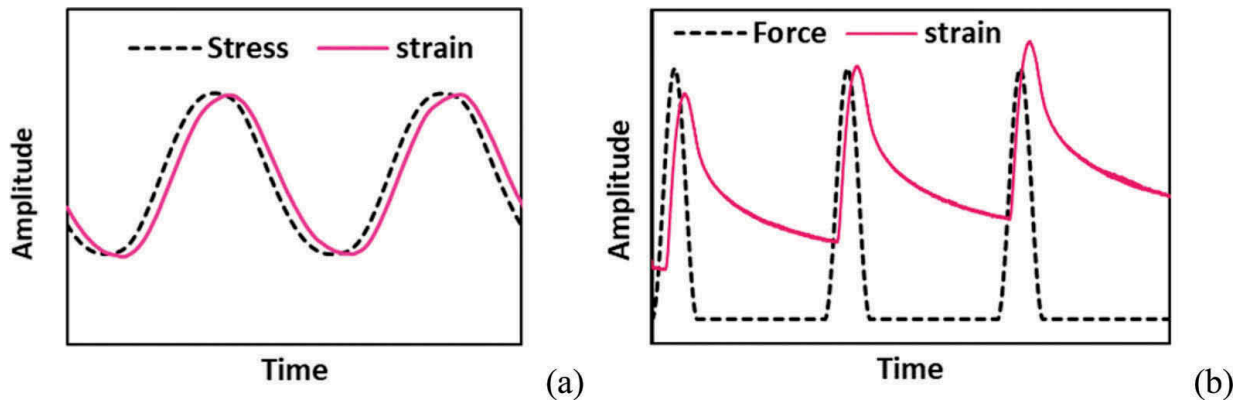


Figure 1. Stress-strain signal responses (not to scale) (a) Dynamic Modulus (b) Resilient Modulus.

Three sets of linear variable differential transducers (LVDTs) are mounted at 120 degrees apart for the dynamic modulus test, while two flat end LVDTs are used for the resilient modulus test. The instrumented specimen is conditioned at target temperature (at least two hours) in a separate chamber and then installed for testing in a UTM-130 machine with a temperature chamber. A dummy sample is used to control the surface and core temperature of a sample.

4 TEST RESULTS

The dynamic modulus test is conducted at three target temperatures (5, 21, 40 °C) and seven frequencies (10, 5, 2, 1, 0.5, 0.2, 0.1 Hz) on two asphalt mixtures (Ab11 and Agb11). Similarly, the resilient modulus test is conducted at five temperatures (5, 10, 21, 30, and 40 °C) and different loading times. The loading times are selected to match the frequency used for the dynamic modulus test. The dynamic and resilient moduli test results are shown in Figure 2 and Figure 3. As expected, both dynamic and resilient moduli decrease as temperature increases and frequency reduced. It is important to note that the M_r value is highly dependent on the magnitude of the applied load and selected loading time. Hence, the pulse load is selected based on the estimated stiffness at target temperature and frequency. In this study, ten conditioning cycles are applied at each frequency, and the last five load pulses are used to estimate the M_r value. A tuning test is conducted to estimate the initial modulus for dynamic modulus at each test temperature. The coefficient of variance (%CV) for the last five loading pulses is generally less than 10% in all measurements at different loading times and temperatures.

To compare E^* and the M_r , the loading time or frequency should be equivalent in both tests (i.e., $\omega = 1/t$ or $f = 1/2\pi t$). The ratio of E^* to M_r is computed (i.e., $E = \kappa M_r$ where κ is a ratio) at the same frequency and temperature. The average κ values are 1.27 and 1.12 for Ab11 and Agb11 asphalt concrete mixtures, respectively. As shown in Figure 4, the ratio (κ) is

dependent on temperature, frequency, and asphalt type. It is observed that κ increases as temperature and frequency increase.

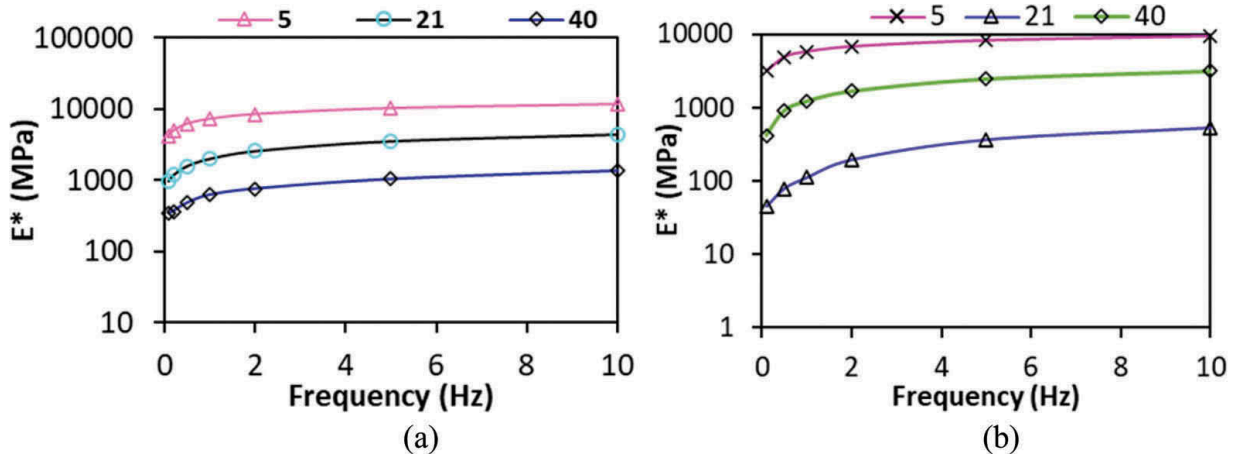


Figure 2. Dynamic Modulus (E^*) test results (a) Ab11 (b) Agb11.

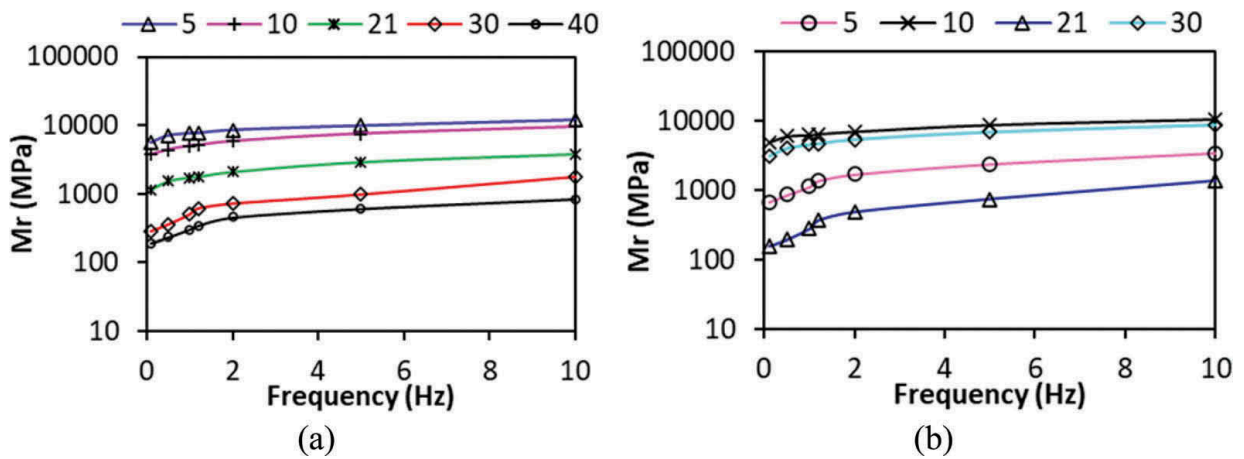


Figure 3. Resilient Modulus (M_r) test results (a) Ab11 (b) Agb11.

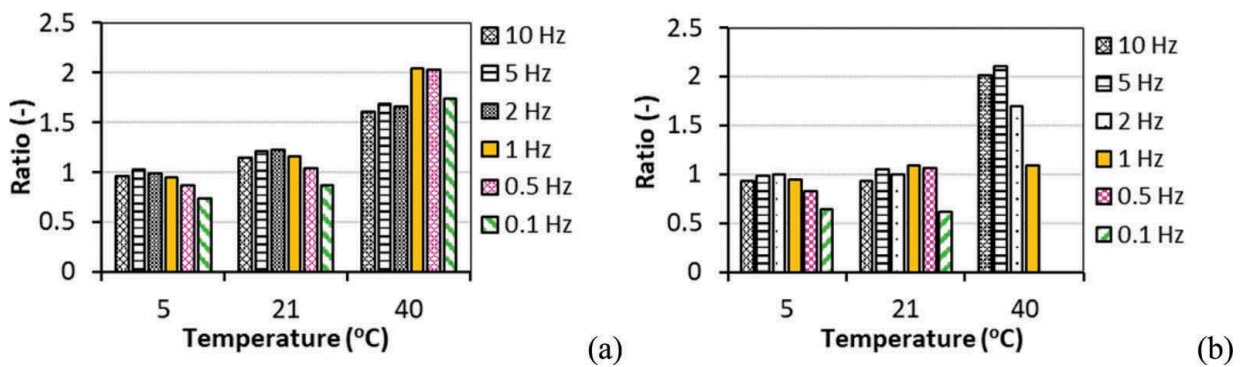


Figure 4. Dynamic to Resilient Modulus Ratio at same temperature and frequency (a) Ab11 (b) Agb11.

5 COMPARISON BETWEEN DYNAMIC AND RESILIENT MODULI

5.1 Master curve construction for E^* and Mr

The test data are shifted horizontally (along the logarithmic time or frequency axis) to construct a master curve at a reference temperature. In this paper, two different models are used to develop a master curve for dynamic and resilient moduli. The first is the mathematical Sigmoid function (Equation 6) (Pellinen et al., 2002) and the second type is a rheological model referred to as the 2S2P1D model (Equation 7). The 2S2P1D model was developed at the DGCBL laboratory of the ENTPE (Olard and Di Benedetto, 2003, Tiouajni et al., 2011). The model consists of 2 Springs, 2 Parabolic creep elements, and 1 Dashpot in the continuous spectrum.

$$\log|E^*| = \delta + \frac{(\alpha - \delta)}{1 + \exp(\eta - \gamma \log f_R)} \quad (6)$$

where $|E^*|$ - the dynamic modulus; δ , α - the minimum and maximum logarithm dynamic modulus, respectively; η , γ - shape factors; $f_R = f \cdot a_T$ - reduced frequency; a_T - time-temperature shift factor.

$$E_{*2S2P1D}(\omega) = E_{00} + \frac{E_0 - E_{00}}{1 + \delta(i\omega\tau)^{-k} + (i\omega\tau)^{-h} + (i\beta\omega\tau)^{-1}} \quad (7)$$

Where ω - the angular frequency ($\omega = 2\pi f$); δ , k , h - constants such that $0 < k < h < 1$;

E_{00} - static modulus ($\omega \rightarrow 0$); E_0 - the glassy modulus ($\omega \rightarrow +\infty$); η - the Newtonian viscosity of the dashpot [$\eta = (E_0 - E_{00})\beta\tau$]; β - a constant that depends on the viscosity of the dashpot; τ - the characteristic time [$\tau = a_T \tau_0$] where τ_0 is determined at a reference temperature.

The shift factors and master curves presented in this paper are all at 21°C reference temperature, and modeling constants are determined by nonlinear optimization using the solver function in Microsoft Excel. As shown in Figure 5 and Figure 6, both the sigmoid and the 2S2P1D models accurately fit a smooth dynamic modulus master curve for both mixtures (Ab11 and Agb11). However, the rheological 2S2P1D model has difficulty producing a smooth resilient modulus master curve. On the other hand, the sigmoid function has shown a good fit for the measured Mr data. The dynamic modulus master curve is generally bigger

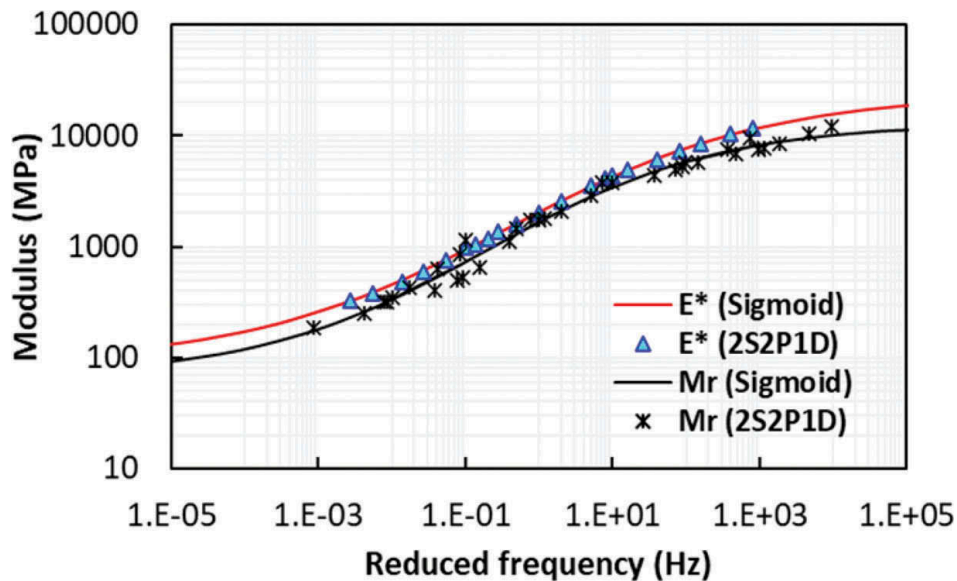


Figure 5. Dynamic modulus (E^*) and Resilient Modulus (Mr) Master Curves (Ab11).

than the resilient modulus at the same temperature and frequency due to the rest period in the resilient modulus test (i.e., recovered strain is larger than strain amplitude in dynamic modulus) (Loulizi et al., 2006). However, this conclusion is not always the case. As shown in Figure 6, the Mr curve is above the E* at low frequency (less 1Hz) and below the E* curve at high frequencies for the Agb11 asphalt concrete. The corresponding time-temperature shift factors are shown in Figure 7.

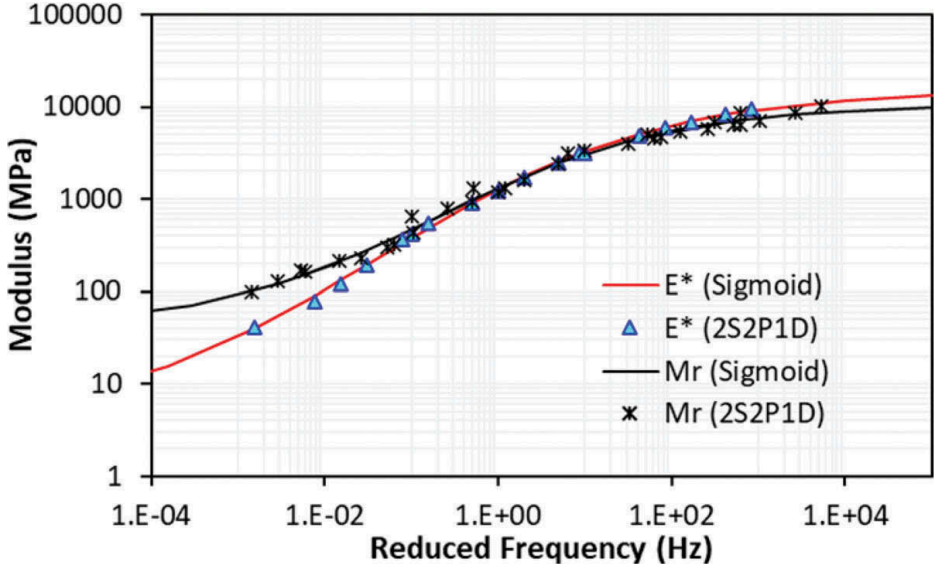


Figure 6. Dynamic modulus (E*) and Resilient Modulus (Mr) Master Curves (Agb11).

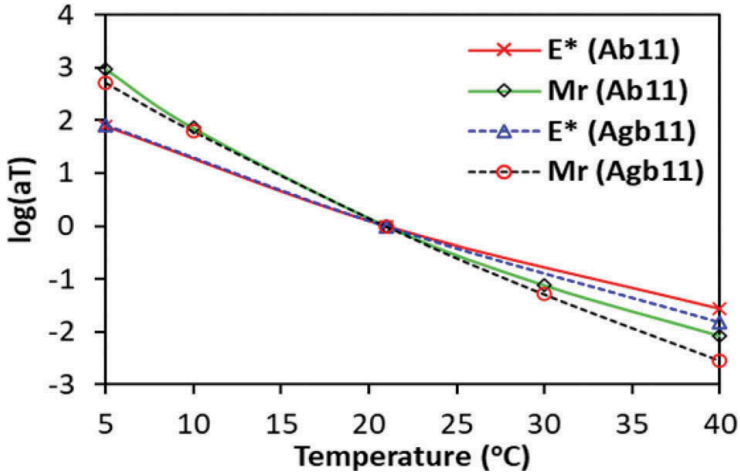


Figure 7. Temperature shift factors.

5.2 Storage dynamic modulus (E') vs. resilient modulus (Mr)

During the deformation of a viscoelastic body, part of the total work of deformation is dissipated as heat through viscous losses, but the remainder of the deformational energy is stored elastically (Tschoegl, 1989). The dissipated energy per unit volume (J/m³ per cycle) due to viscous effects is the loss modulus. The ratio of loss ($\Delta W = \pi \sigma_0 \epsilon_0 \sin \phi$) to maximum stored ($W = \frac{\sigma_0 \epsilon_0}{2}$) energy per cycle (also called specific loss) is given in Equation 8.

$$\frac{\Delta W}{W} = \frac{\pi \sigma_o \varepsilon_o \sin \varphi}{\frac{\sigma_o \varepsilon_o}{2}} = 2\pi \sin \varphi \quad (8)$$

Where σ_o , ε_o , φ – stress amplitude, strain amplitude, and phase angle, respectively. Note that the specific loss is independent of the stress and strain amplitude.

The storage modulus (E') is the relevant and crucial quantity used to compute the time-domain viscoelastic properties (compliance and relaxation modulus) of asphalt concrete. As Mr is a time-domain test, it is imperative to compare the two moduli at similar conditions. The average ratios ($\kappa = E'/Mr$) are found to be 1.12 and 0.84 for Ab11 and Agb11, respectively. Figure 8 (a and b) shows the E' and Mr master curves for both specimens, and Figure 9 presents the comparison. One can observe the changes in Figure 5 and Figure 6, and Figure 8. For the Ab11 mixture, E' is very close to Mr at intermediate frequencies (0.1 to 10 Hz or the experimental window) while it barely changes from E^* at low and high reduced frequencies. For Agb11, the reduced frequency where E^* is equal to Mr (about 1.2 Hz) has shifted to the right (about 10 Hz) for E' and Mr curves.

The loss ratio of Ab11 and Agb11 is presented in Figure 10. A mixture with a softer binder (Agb11) has more energy loss than the stiffer mixture (Ab11), as expected. The maximum energy loss has occurred around the intermediate frequency. Furthermore, the bell-shaped energy loss curve indicates the thermo-rheological simplicity of the tested materials.

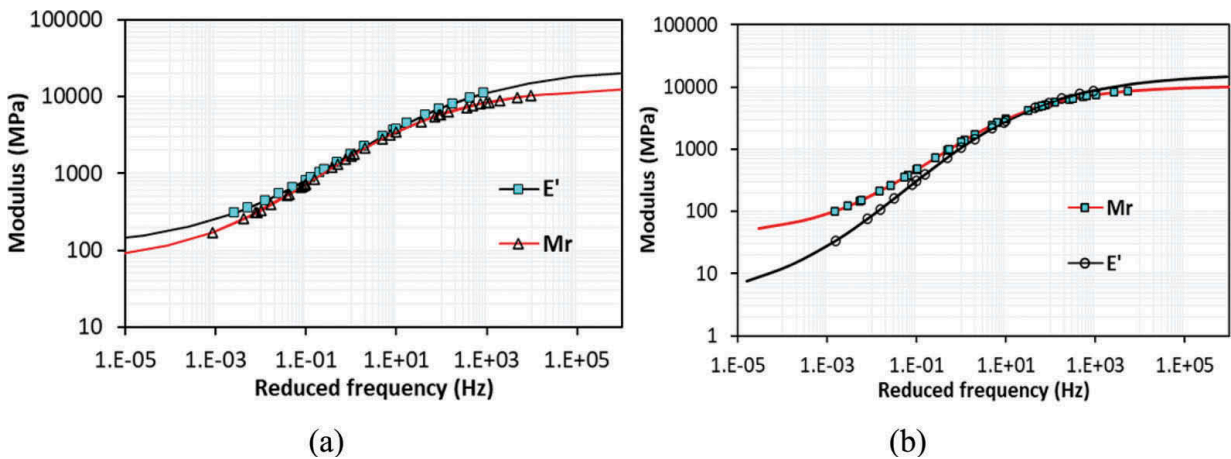


Figure 8. Master curves for E' and Mr using Sigmoid function (a) Ab11 (b) Agb11.

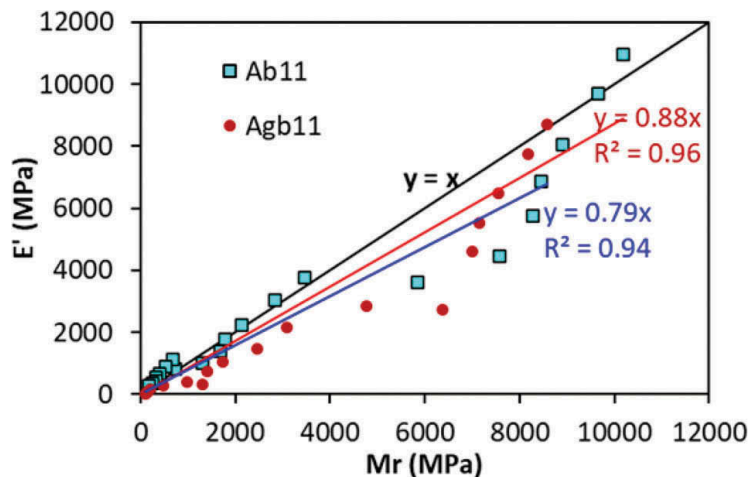


Figure 9. E' versus Mr for Ab11 and Agb11.

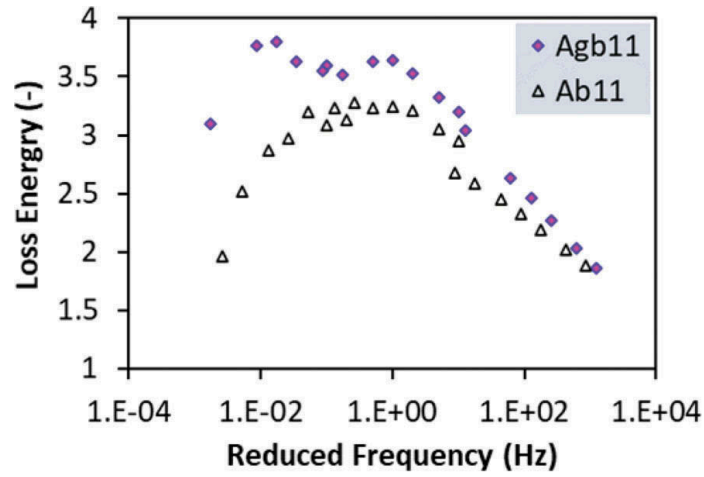


Figure 10. Energy loss for Ab11 and Agb11 mixtures.

5.3 Relaxation modulus ($E(t)$) vs. resilient modulus (Mr)

Although the frequency domain dynamic modulus data can give sufficient information about asphalt concrete's viscoelastic properties, the time domain relaxation modulus and creep compliance are usually used in performance prediction. The generalized Maxwell model (GM) in parallel is used to obtain relaxation modulus, $E(t)$. The one-dimensional $E(t)$ takes the following Prony form.

$$E(t) = E_{\infty} + \sum_{m=1}^M E_m \left(e^{(-t/\rho_m)} \right) \quad (9)$$

Where E_{∞} - Long-term (equilibrium) modulus; E_m - components of the relaxation modulus; ρ_m - components of relaxation time; and M - the total number of the Maxwell elements (one Maxwell element is composed of one elastic spring and one viscous dashpot connected in series).

The Prony coefficients are determined by the least-squares method from dynamic storage modulus (E'). A good fit is obtained by optimizing eight Prony coefficients (E_m and ρ_m). As can be seen from Figure 5, Figure 8, and Figure 11, the Mr curve is less than the E' and $E(t)$ master curves. The E' vs. Mr and $E(t)$ vs. Mr curves have the same goodness of fit except the x-axis domain is frequency and time, respectively.

Finally, although IDT is more of a quality control test, vital physical properties can be extracted. The virtues of IDT (such as simplicity, economy, repeatability, versatility) are the advantages for industrial applications over the companion dynamic modulus test. Mr alone cannot explain the viscoelastic property of asphalt concrete. Therefore, it is envisaged that advanced analyses should be undertaken by correlating with E^* to deduce the fundamental properties (such as relaxation and compliance moduli) from already collected and stored IDT test data.

6 CONCLUSION

This paper presents comparative analyses between dynamic modulus (E^*) and Indirect Tensile Resilient modulus (Mr) in linear viscoelastic range. Two different asphalt mixes are used for the investigation. The time-temperature superposition principle is used to construct E^* and Mr master curves using sigmoid and 2S2P1D models. Based on the analyses and observations presented in this study, the following conclusions can be drawn.

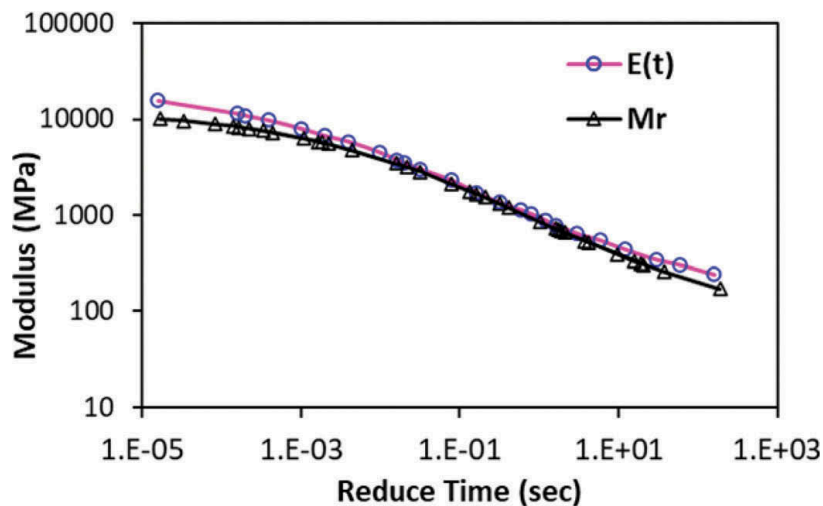


Figure 11. Master curves for $E(t)$ and M_r for Ab11.

- The thermo-rheological simplicity of two asphalt concrete mixtures (Ab11 and Agb11) is investigated using the time-temperature superposition principle.
- An S-shaped master curve is developed using the sigmoid and the 2S2P1D functions for both resilient and dynamic moduli test data. Unlike the sigmoid function, the rheological 2S2P1D model showed some waviness to reflect a smooth M_r master curve. This could be related to the model's inherent sinusoidal nature and is suitable for the harmonic stress-strain evolution.
- Comparison between the three quantities (i.e., E^* , E' , and M_r) is performed at the same temperature and frequency. The average ratios between E^* and M_r are found to be 1.27 for Ab11 and 1.12 for Agb11 mixes. Similarly, reduced average ratios of 1.12 and 0.84 are found between E' and M_r due to the deduction loss modulus. It is recognized that the ratios of E^* and M_r is dependent on several factors like mixe type, temperature, frequency, etc.
- The time-domain relaxation modulus ($E(t)$) master curve is constructed using the Prony method. Almost identical goodness of fit (96%) is found like the E' master curve. Generally, the comparison of time-domain quantities of E^* with M_r is reasonable and practical.
- In addition, a material database is obtained for Ab11 and Agb11 mixtures at wide frequencies and temperatures that can be utilized for the Norwegian pavement management system.
- This work is a preliminary study comparing M_r with E^* for asphalt concrete by developing master curves in both the time and frequency domain. More advance vertical shifting models are needed with more datasets.

REFERENCES

- Bennert, T., Haas, E. & Wass, E. 2018. *Indirect Tensile Test (IDT) to Determine Asphalt Mixture Performance Indicators During Quality Control Testing In New Jersey*. Transportation Research Record: Journal Of The Transportation Research Board, 2672, 394–403.
- Gayte, P., Di Benedetto, H., Sauzéat, C. & Nguyen, Q. T. 2016. *Influence Of Transient Effects For Analysis Of Complex Modulus Tests On Bituminous Mixtures*. Road Materials And Pavement Design, 17, 271–289.
- Lacroix, A., Khandan, A. A. M. & Kim, Y. R. 2007. *Predicting The Resilient Modulus Of Asphalt Concrete From The Dynamic Modulus*. Transportation Research Record: Journal Of The Transportation Research Board, 2001, 132–140.

- Levenberg, E. & Uzan, J. 2004. *Triaxial Small-Strain Viscoelastic-Viscoplastic Modeling Of Asphalt Aggregate Mixes*. *Mechanics Of Time-Dependent Materials*, 8, 365–384.
- Loulizi, A., Flintsch, G. W., Al-Qadi, I. L. & Mokarem, D. 2006. *Comparing Resilient Modulus And Dynamic Modulus Of Hot-Mix Asphalt As Material Properties For Flexible Pavement Design*. *Transportation Research Record: Journal Of The Transportation Research Board*, 1970, 161–170.
- Nguyen, M. L., Sauzéat, C., Di Benedetto, H. & Tapsoba, N. 2013. *Validation Of The Time–Temperature Superposition Principle For Crack Propagation In Bituminous Mixtures*. *Materials And Structures*, 46, 1075–1087.
- Olard, F. & Di Benedetto, H. 2003. *General “2S2P1D” Model And Relation Between The Linear Viscoelastic Behaviours Of Bituminous Binders And Mixes*. *Road Materials And Pavement Design*, 4, 185–224.
- Pellinen, T. K., Witzczak, M. W. & Bonaquist, R. F. *Asphalt Mix Master Curve Construction Using Sigmoidal Fitting Function With Non-Linear Least Squares Optimization*. *Recent Advances In Materials Characterization And Modeling Of Pavement Systems*, 2002. 83–101.
- Ping, W. V. & Xiao, Y. 2008. *Empirical Correlation Of Indirect Tension Resilient Modulus And Complex Modulus Test Results For Asphalt Concrete Mixtures*. *Road Materials And Pavement Design*, 9, 177–200.
- Schwartz, C. W., Gibson, N. & Schapery, R. A. 2002. *Time-Temperature Superposition For Asphalt Concrete At Large Compressive Strains*. *Transportation Research Record: Journal Of The Transportation Research Board*, 1789, 101–112.
- Tiouajni, S., Di Benedetto, H., Sauzéat, C. & Pouget, S. 2011. *Approximation Of Linear Viscoelastic Model In The 3 Dimensional Case With Mechanical Analogues Of Finite Size*. *Road Materials And Pavement Design*, 12, 897–930.
- Tschoegl, N. W. 1989. *Energy Storage And Dissipation In A Linear Viscoelastic Material*. In: TSCHOEGL, N. W. (Ed.) *The Phenomenological Theory Of Linear Viscoelastic Behavior: An Introduction*. Berlin, Heidelberg: Springer Berlin Heidelberg.
- Williams, M. L., Landel, R. F. & Ferry, J. D. 1955. *The Temperature Dependence Of Relaxation Mechanisms In Amorphous Polymers And Other Glass-Forming Liquids*. *Journal Of The American Chemical Society*, 77, 3701–3707.
- Yun, T., Underwood, B. S. & Kim, Y. R. 2010. *Time-Temperature Superposition For HMA With Growing Damage And Permanent Strain In Confined Tension And Compression*. *Journal Of Materials In Civil Engineering*, 22, 415–422.
- Yusoff, N. I. M., Chailleux, E. & Airey, G. D. 2011. *A Comparative Study Of The Influence Of Shift Factor Equations On Master Curve Construction*. *International Journal Of Pavement Research And Technology*, 4, P. 324–336.
- Zhao, Y. & Richard Kim, Y. 2003. *Time–Temperature Superposition For Asphalt Mixtures With Growing Damage And Permanent Deformation In Compression*. *Transportation Research Record: Journal Of The Transportation Research Board*, 1832, 161–172.

Paper D

Permanent deformation and fatigue damage interaction in asphalt concrete using energy approach

Mequanent Mulugeta Alamnie, Ephrem Taddesse and Inge Hoff. Eleventh International Conference on the Bearing Capacity of Roads, Railways and Airfields, Vol.3, 2022:118-127. doi:[10.1201/9781003222910-12](https://doi.org/10.1201/9781003222910-12)

Permanent deformation and fatigue damage interaction in asphalt concrete using energy approach

M. Alamnie & E. Taddesse

Department of Engineering Sciences, Civil and Structural Engineering, University of Agder, Grimstad, Norway

I. Hoff

Department of Civil and Transport Engineering, Norwegian University of Science and Technology, Trondheim, Norway

ABSTRACT: The interaction of fatigue and permanent deformation is very complex phenomenon and little attempt is made on this topic. This paper presents an investigation on the interaction of the two damages using the energy approach. Laboratory tests were conducted for both fatigue and permanent deformation on two different asphalt concrete in a sequential test procedure. A new failure criterion is proposed based on the dissipated energy ratio (DER). The proposed criterion for permanent deformation gives more damage indicator (inflection points) than the conventional flow number/strain rate criterion. The sequential test procedure is also found economical that can be standardized. From the study, strain hardening (pre-deformed) accelerates fatigue cracking susceptible. Similarly, high fatigued samples are more prone to permanent deformation than new samples. The energy approach is convenient for potential coupling of fatigue and permanent deformation interactions.

Keywords: Permanent deformation, fatigue, dissipated energy ratio, sequential test

1 INTRODUCTION

As asphalt concrete pavement is subjected to repetitive loads, different damage modes develop over its lifetime. Fatigue cracking and permanent deformation are the two dominant pavement damage mechanisms. One of the distinguishing features of fatigue and permanent deformation is the loading mode. In fatigue damage, cracks grow perpendicular to the tensile loading direction, whereas in permanent deformation, wing cracks can develop parallel to the load direction (Dyskin et al., 2003). The influence of temperature is another crucial factor in distinctive damage evolution. Fatigue is critical at intermediate and low temperatures. On the other hand, permanent deformation is high-temperature damage. At elevated temperatures, the critical energy threshold that causes fatigue cracking increases (or the mixture relaxes faster). Consequently, more energy is needed to initiate crack (Onifade et al., 2015, Sangpetngam et al., 2003). On the other hand, plastic flow and aggregate re-orientation dominate at high temperatures. Traditionally, bottom-up cracking of the asphalt concrete layer was the primary fatigue damage mechanism. However, experimental and field observations showed that top-down cracking due to tire compression is also the mechanism for fatigue damage (Pellinen et al., 2004, Roque et al., 2004). Crack initiation in compression occurs when the viscoplastic strain hardening reaches saturation at the flow number (FN).

The damages in asphalt concrete evolve through energy dissipation due to viscous flow leading to *fatigue cracking* and plastic flow for *permanent deformation* (Widyatmoko et al., 1999), and some part of the energy is transferred into heat (Di Benedetto et al., 2011). The energy dissipation caused material ductility exhaustion, hardening, and viscoplastic flow. Different energy-based failure criteria were proposed using the classic energy balance principle (Ghuzlan and Carpenter, 2000, Anderson et al., 2001, Shen et al., 2006, Korsunsky et al., 2007). The existing models treat fatigue and permanent deformation damage independently, and the complex interaction between the two damage modes is still not well researched. One of the limitations is the lack of an integrated testing protocol for fatigue-permanent deformation interaction. Some attempts can be found in literature, such as an Indirect Tension (IDT) testing for deformation and fracture (Bahadori et al., 2015) and a haversine loading waveform in fatigue tests (Liu et al., 2020, Gupta and Atul Narayan, 2019). The haversine load is used because it can be decomposed into pure creep (for permanent deformation part) and pure sinusoidal (fatigue part) components. However, the creep-recovery behavior cannot be captured with such approaches.

Moreover, field and laboratory observations have shown that fatigue cracking accompany permanent deformation (rutting) (Lundstrom et al., 2007, Pellinen et al., 2004). In addition, the same load causes both damages, and strain-hardening and cracking can develop simultaneously at intermediate temperatures. Therefore, the independent treatment of the two damages is an oversimplification and far from the actual condition. The pavement is more susceptible to fatigue cracking in the cold seasons, and micro-cracks can initiate. These pre-existing cracks can significantly accelerate the permanent deformation at high pavement temperatures in hot seasons. The inverse is true that viscoplastic strain hardened during the hot season is more susceptible to fatigue cracking in cold seasons. Both damages are critical at intermediate temperatures. Hence, the independent treatment of the two damages sets clear limitations for the mechanistic pavement design.

In this paper, an attempt is made to investigate the effect of fatigue on permanent deformation and vice versa using an energy approach. Several asphalt concrete samples were tested for fatigue (F) and permanent deformation (PD) in a Sequential Test (ST) procedure. The tests were performed in two different orders: the F-PD and PD-F sequences. A new energy-based failure criterion is proposed and validated using experimental data from two different asphalt mixtures.

2 ENERGY-BASED MODELS

The dissipated energy in a cyclic load is the area under the stress-strain hysteresis loop. In a cyclic creep-recovery test, material hardening grows, irrecoverable viscoplastic strain accumulates, and the hysteresis loops shift horizontally (Figure 1a). On the other hand, the idealized hysteresis loop in the cyclic fatigue test causes stiffness reduction and phase angle increment with negligible viscoplastic strain (hysteresis loops do not shift horizontally) (Figure 1b). Nevertheless, the stress-strain hysteresis in simultaneous damage conditions could evolve in a complex manner due to hardening-softening, healing, etc. The dissipated energy (DE) is expressed by the following integral, where $\sigma(t)$ is the stress function and $\frac{\partial \varepsilon(\tau)}{\partial \tau}$ is the strain rate.

$$DE = \int \sigma(t) \frac{\partial \varepsilon(\tau)}{\partial \tau} d\tau \quad (1)$$

The DE in fatigue and permanent deformation damages can be computed using the appropriate stress and strain rate functions in Equation 1.

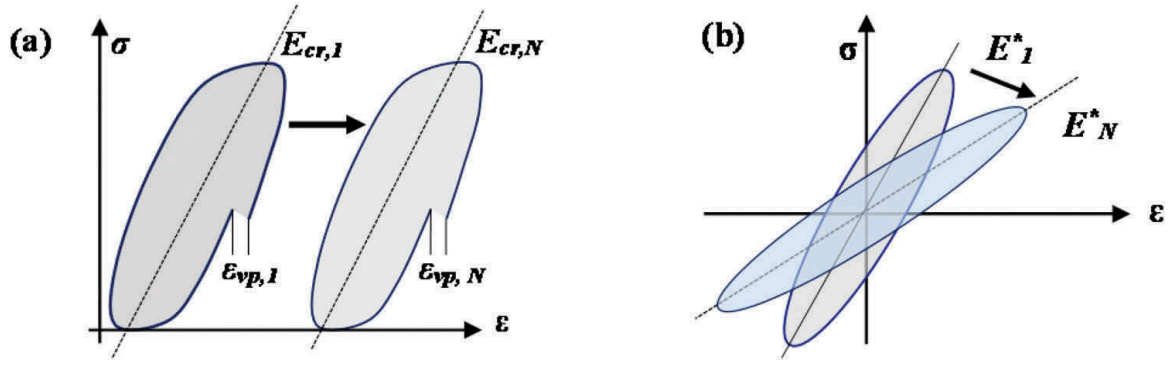


Figure 1. Schematic – stress-strain hysteresis loops (a) creep-recovery (b) tension-compression fatigue.

2.1 Fatigue failure criterion

For a strain-controlled fatigue test with sinusoidal strain wave, the dissipated energy due to fatigue (DE_f) is obtained by substituting the sinusoidal stress ($\sigma_s = \sigma_i \sin \omega t$) and strain ($\varepsilon_s = \varepsilon_i \sin(\omega t - \varphi_i)$) signals into Equation 1 and integrating (σ_i , ε_i , ω and φ_i – stress amplitude, strain amplitude, angular frequency, and phase angle measured at cycle, i).

$$DE_f = 2\pi\sigma_i\varepsilon_i \sin(\varphi_i) \quad (2)$$

The dissipated energy ratio (DER) criterion is used (Ghuzlan and Carpenter, 2000) as a damage indicator.

$$DER = n \times \frac{DE_1}{DE_n} \quad (3)$$

Where DE_1 –dissipated energy at initial cycle, DE_n – dissipated energy at n^{th} load cycle. For a sinusoidal loading, the DER can be expressed as,

$$DER = n \times \frac{\pi E^*_1 \varepsilon_1^2 \sin \varphi_1}{\pi E^*_n \varepsilon_n^2 \sin \varphi_n} \quad (4)$$

For a test in controlled-strain mode, $\varepsilon_1 = \varepsilon_n$ and with approximation $\frac{\sin \varphi_1}{\sin \varphi_n} \approx \frac{\varphi_1}{\varphi_n}$, then DER is found as;

$$DER = \left(\frac{n}{E^*_n} \right) \left(\frac{E^*_1 \sin \varphi_1}{\sin \varphi_n} \right) = n \left(\frac{E^*_1}{E^*_n} \right) \left(\frac{\varphi_1}{\varphi_n} \right) \quad (5)$$

2.2 Permanent deformation failure criterion

The flow number (FN) has been used as a general failure criterion for permanent deformation (Biligiri et al., 2007). Flow number is a cycle where the viscoplastic strain rate start ascending (or the second derivative of the strain function changes from negative to a positive value, i.e., $\varepsilon''_{vp} > 0$). The well-known Francken model (Francken and Clauwaert, 1987) is used to fit the permanent deformation test data (where A, B, C, D – are model coefficients, N – number of cycles).

$$\varepsilon_{vp} = AN^B + C(e^{DN} - 1) \quad (6)$$

$$\varepsilon'_{vp} = ABN^{B-1} + CDe^{DN} \quad (7)$$

The dissipated energy due to permanent deformation (DE_{pd}) is obtained by substituting a haversine stress pulse $\sigma_h = \sigma_0 \sin^2\left(\frac{\omega t}{2}\right)$ where σ_0 is stress amplitude and strain rate (Equation 7) into Equation 1.

$$DE_{PD} = \frac{\pi \sigma_0}{\omega} \frac{\varepsilon_{vp}}{2} \quad (8)$$

The permanent deformation failure criterion using DER takes the following form.

$$DER_{PD} = n \frac{DE_{PD1}}{DE_{PDN}} = n \frac{AB + CDe^D}{ABN^{B-1} + CDe^{DN}} \quad (9)$$

n is current cycle number, DE_{PD1} is dissipated energy at the first cycle. The quantity $AB + CDe^D$ is a material constant dependent on compressive stress level, temperature, and initial damage of the material. The exponent component (CDe^D) is found very small compared to the first part and can be approximated as $K \cong AB$. The denominator ($ABN^{B-1} + CDe^{DN}$) is the strain rate (ε_{vp}). Thus, the DER (for $0 < K < 1$) is expressed as;

$$DER_{PD} = n \left(\frac{k}{\varepsilon_{vp}} \right) \quad (10)$$

3 TEST METHOD

3.1 Materials

Two different asphalt mixtures (AB11 and SKA11) sampled from asphalt mixing plants were used for tests in this research. The cylindrical specimens (150 mm by 180 mm height) were produced using a gyratory compactor, and the final specimens (100 mm diameter by 150 mm height) were produced by coring and cutting. In Table 1, the aggregate gradation of the mixtures is given where AB11 mixture contains a polymer-modified binder (PMB 65/105-60) and SKA11 is made of a 70/100 neat binder.

Table 1. Aggregate gradation.

Mix	Sieve size [mm]							Content [%]
	16	11.2	8	4	2	0.25	0.063	
	Percent Passing [%]							
AB11	100	95	70	48	36	15.5	10	5.6
SKA11	100	91.2	53.6	35.7	21.7	12.8	8.4	5.83

3.2 Test procedure

A Sequential Test (ST) procedure is suggested in this paper. In this procedure, fatigue and permanent deformation tests were conducted sequentially on the same specimen. The sequences are referred as PD-F and F-PD sequences (F – for fatigue, PD – for permanent deformation), as shown in Figure 2. In the PD-F sequence, permanent deformation test is conducted first with in the steady-state region and the same sample is tested in Tension-compression fatigue test. Similarly, for F-PD sequence, the new sample is tested in Tension-compression fatigue first and then under-went permanent deformation test. The test parameters are summarized in Table 2.

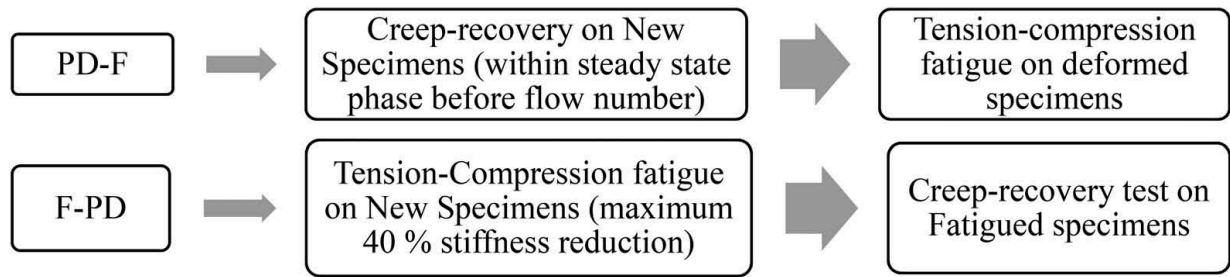


Figure 2. Sequential Test Procedure.

Table 2. Main characterization tests, parameters, and conditions.

Test	Temperature (°C)	Load waveform	Mode	Frequency/Time
T-C fatigue	10, 15, 21, 30	Sinusoidal	Control-strain (at 100, 150, 200, 300, 400 $\mu\epsilon$)	10 Hz
Creep-recovery	21, 30, 40	Haversine	Control-stress (0.5 to 2 MPa)	Loading/rest time: 0.4 /1.6 sec

4 RESULTS AND DISCUSSION

Several asphalt concrete specimens were tested in tension-compression fatigue and cyclic creep-recovery to investigate the interaction of fatigue and permanent deformation damages according to the sequential test procedure. The first part of the tests in the sequential procedure was conducted to induce the respective pre-damage on the specimen. For example, in the F-PD procedure, the fatigue part of the test is performed to induce a certain level of fatigue cracking (maximum of 40 % stiffness reduction) on the specimen. Then fatigued specimens are tested for permanent deformation until failure. The same is true for the PD-F procedure, where the first part of the test (i.e., PD) is conducted to induce a sufficient level of strain hardening to the specimen before the flow number (within the steady-state region not to failure). Then PD specimens were tested in T-C fatigue until failure.

4.1 The F-PD procedure

In the F-PD sequence, the specimens were tested in T-C fatigue in a controlled-strain mode at temperatures of 10, 15, 21, and 30 °C and at different on-specimen target strains (150, 200, 300, 400 $\mu\epsilon$). The maximum percentage of stiffness reduction during fatigue was no more than 40 %. Then the fatigued specimens were conditioned and tested at 30 and 40 °C in a controlled-stress creep-recovery test. Examples of test results in the F-PD sequence are shown in Figure 3. As can be seen (Figure 3 a and b), samples with high fatigue damage (high on-specimen strain like 400 $\mu\epsilon$) at 10 °C have a rapid rate of permanent deformation and a small flow number (FN). However, samples fatigued at 21 and 30 °C have little effect on the permanent deformation growth. This property is related to the need of high energy to initial fatigue cracking at elevated temperatures due to viscosity.

The flow number (FN) is a classic permanent deformation failure criterion for asphalt concrete. It marks the commencement of the tertiary stage, which is characterized by a high rate of deformation and micro-crack formation. The proposed DER criterion (Equation 10) gives an additional inflection point using the DER curve. It is referred to as the peak value (PV). As shown in Figure 4, four distinct creep stages can be visualized using the DER criterion; (I) An increasing rate in the first stage, (II) a steady-state

increase in the secondary stage, (III) increment at a decreasing rate in the third stage, and (IV) descending phase after the peak point in the fourth stage. The tertiary (III) phase is dominated by micro-crack formation and propagation, resulting in macro-crack formation at PV. It is believed that the PV indicates the formation of macro-cracks and unstable deformation. The DER starts descending rapidly in the fourth stage due to excessive deformation or high energy dissipation. For the F-PD sequence (samples with pre-existing cracks due to fatigue), wing cracks can grow parallel to the load direction. At PV, the accumulated wing cracks and micro-cracks coalesce and form macro-cracks. Therefore, the FN in the DER curve corresponds to a cycle where the steady-state DER start decreasing or the dissipated energy starts increasing. Moreover, Figure 5 shows that fatigued samples have higher DE or lower DER value than new samples. Since the fatigue test is conducted at lower temperatures, healing can occur during the rest period and during conditioning at a higher temperature (40 °C) for permanent deformation.

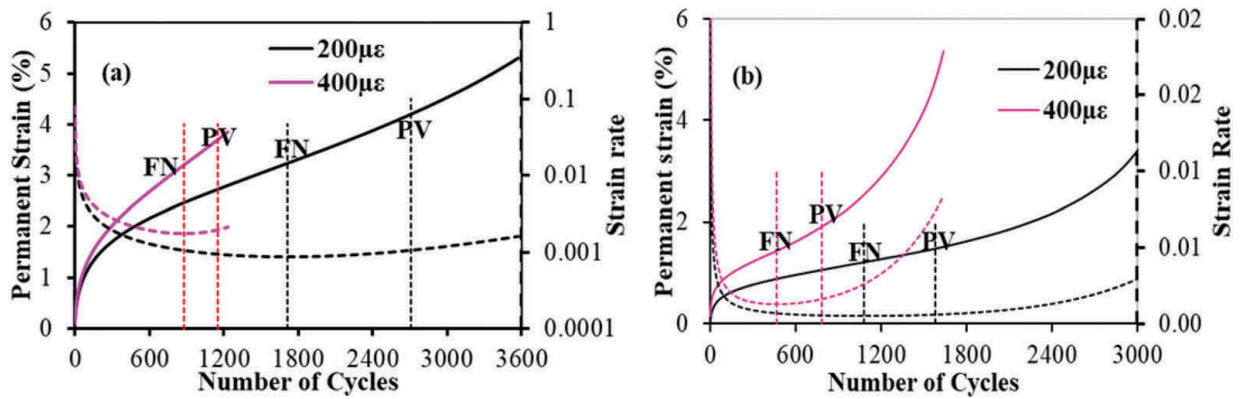


Figure 3. Permanent deformation of fatigued samples (F-PD) at 10°C and 200 and 400 µε target strain (a) AB11 - PD at 30°C, $\sigma = 2\text{MPa}$ (b) SKA11 - PD at 40°C, $\sigma = 0.65\text{MPa}$.

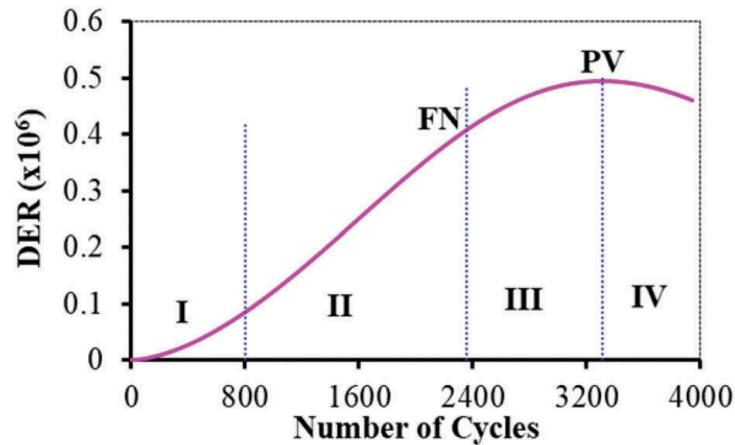


Figure 4. The typical four phases of DER Curve (F-PD - Fatigued at 10°C and 300µε, PD - 30°C and $\sigma = 2\text{MPa}$).

Furthermore, the proposed failure criterion is verified using test data on a new specimen with confinement and a longer recovery period of 16 sec (Figure 6). Confinement played a role in the energy dissipation evolution, and DE is directly proportional to axial stress and temperature. The DER shows the level of damage (viscoplastic) of the sample more clearly than the DE quantity. Large DER means the material is less damaged, and the decreasing rate of DER indicates micro-crack is initiated and flow number identified.

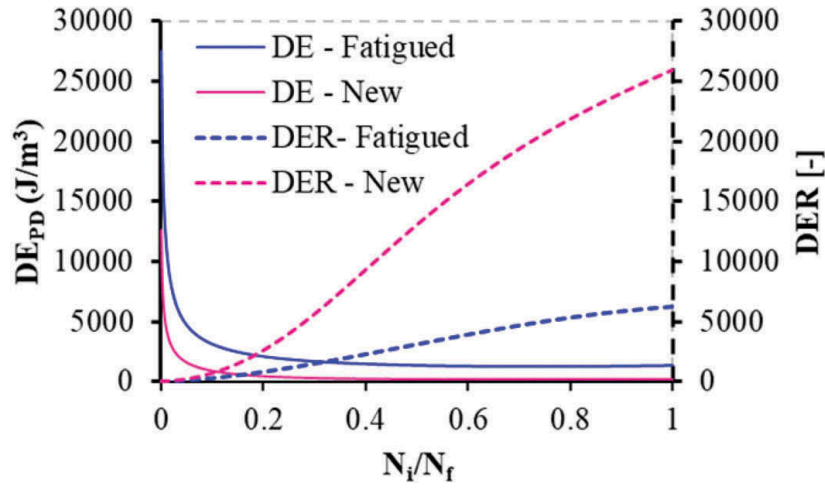


Figure 5. DE and DER for Permanent deformation (at $\sigma = 0.5\text{MPa}$, 40°C) on new and fatigued (10°C and $150\mu\epsilon$) samples.

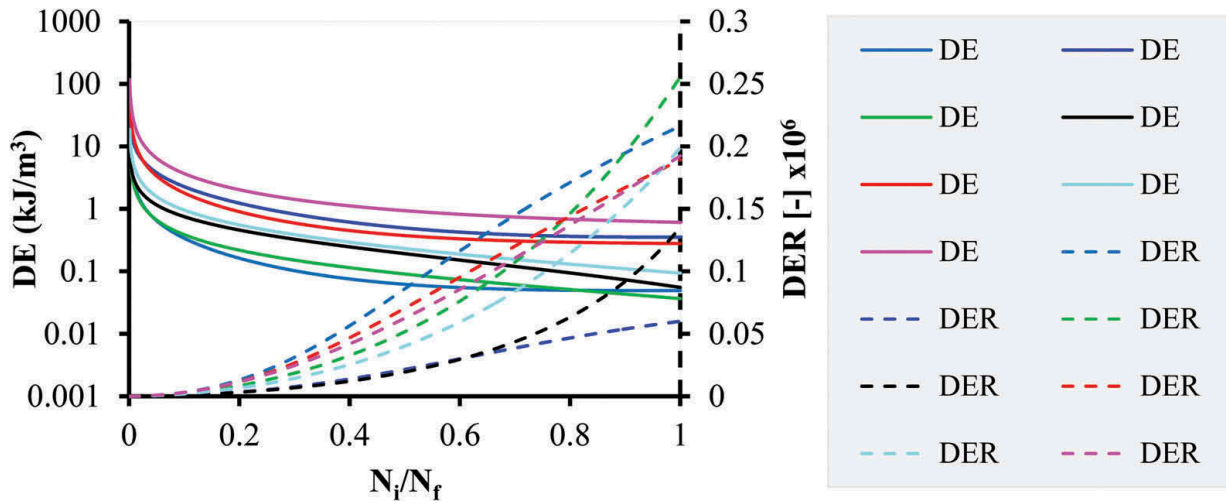


Figure 6. DE and DER due to permanent deformation with confinement on new specimens (at different axial stresses and temperatures) – AB11.

4.2 The PD-F procedure

In the PD-F procedure, permanent deformation is induced on new specimens and the deformed specimen undergoes tension-compression fatigue. Figure 7 (a and b) shows that strain hardening due to permanent deformation increases asphalt concrete's apparent dynamic modulus (stiffness). This increase in stiffness makes the mixtures prone to rapid fatigue damage rate (D).

$$D = 1 - \frac{E_i^*}{E_o^*} \quad (11)$$

where E_i^* is dynamic modulus at cycle i , and E_o^* is the initial dynamic modulus. Hence, the effect of strain hardening has a crucial role in the fatigue damage evolution. In most cases, permanent deformation can accumulate before visible fatigue cracks are seen during pavement service life. In such conditions, the PD-F sequence is a realistic and accurate way to investigate the fatigue life of asphalt concrete mixtures experimentally. However, fatigue cracks can also develop before permanent deformation, especially in cold climates, due to thermal cracking as well as fatigue cracking at intermediate temperatures.

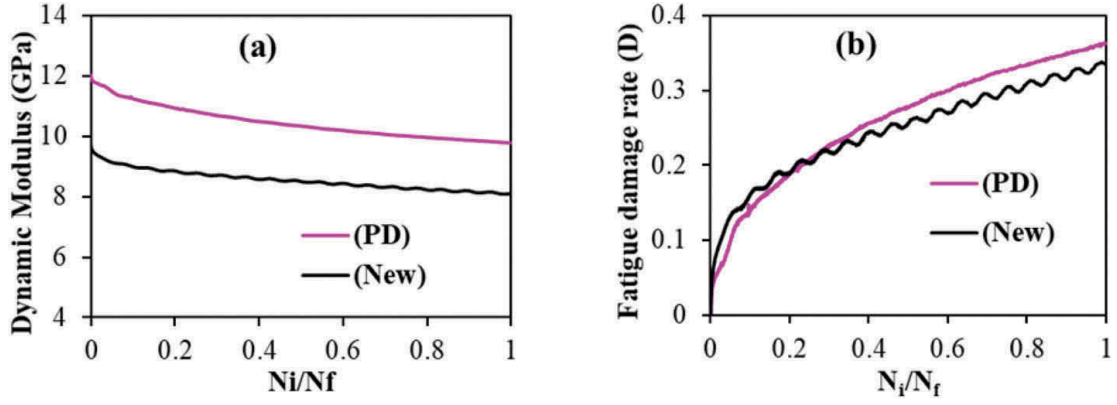


Figure 7. T-C fatigue at 10 °C and 150 $\mu\epsilon$ on new and deformed SKA11 samples (PD at 40°C, $\sigma = 0.65\text{MPa}$) (a) apparent dynamic modulus (b) damage rate, D.

4.3 Coupling the dissipated energy

The total dissipated energy (DE_T) on a specimen tested according to the sequential tests (F-PD and PD-F) can be approximated by the linear sum of dissipated energy. Thus, DE_T is expressed by adding Equation 2 and Equation 8 as follows.

$$DE_T = 2\pi\sigma_i\epsilon_i\sin(\varphi_i) + \frac{\pi}{\omega} \frac{\sigma_0}{2} \epsilon_{vp}^g \quad (12)$$

It is also important to underline that some creep deformation can be accumulated during fatigue tests that contribute to the hardening of the specimen. However, the amount of creep energy dissipation during cyclic fatigue tests is insignificant compared to that of cyclic.

Examples of dissipated energies during fatigue (DE_F), permanent deformation (DE_{PD}) and total dissipated energy (DE_T) are shown in Figure 8. The DEs in permanent deformation damage are cumulative sum upto the flow number $DE_{PD} = \sum_i^{FN} DE_i$. The fatigue dissipated energy (DE_F) is dependent on the target strain, temperature and initial level of hardening (deformation) as shown in Table 3. Generally, DE_F decreases as temperature increases due to viscoplastic heat loss instead of viscoplastic flow (deformation) at higher temperatures.

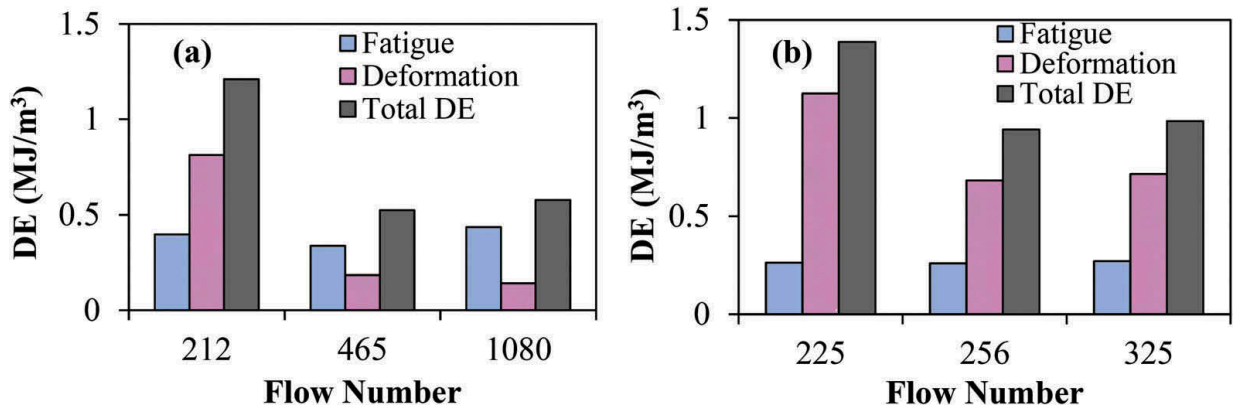


Figure 8. Dissipated energies (DE_F , DE_{PD} , DE_{Tot}) for fatigued SKA11 samples (PD at 40°C, $\sigma = 0.65\text{MPa}$) (a) 10 °C (b) 15 °C .

Table 3. Cumulative Dissipated Eenergy [J/m^3] during fatigue test on new SKA11 samples.

Strain [$\mu\epsilon$]	Fatigue test Temperature [$^{\circ}C$]		
	10	15	21
150	1.97E+05	-	1.7E+05
200	3.68E+05	6.74E+05	2.4E+05
300	7.91E+05	5.54E+05	2.3E+05
400	8.00E+05	1.65E+06	-

4.4 Summary

Permanent deformation and fatigue cracking are the most dominant pavement damages. These damages have been studied independently. There is also an assumption that permanent deformation occurs before fatigue cracking develops. However, such an assumption depends on the climatic condition and mixture properties. For instance, top-down cracks can develop in stiff and thick pavements due to tire compression before permanent deformation accumulates and the pre-existing crack can accelerate permanent deformation in later life of the pavement. The study presented in this paper indicates that fatigue and permanent deformation pre-damages have a significant role in the evolution of permanent deformation and fatigue cracking, respectively. Moreover, the sequential test procedure can be standardized to investigate the interaction between the two damages for a more realistic performance prediction. The F-PD procedure is more deterministic and easy to control the desired level of fatigue damage. However, the PD-F sequence should be conducted with care in order not to break the sample beyond the steady-state zone. The energy approach applied in this paper is simple and convenient to analyze the interaction of fatigue and permanent deformation.

5 CONCLUSION

The interaction of fatigue and permanent deformation is a very complex phenomenon and little attempt is made on asphalt concrete. In this paper, an investigation is made on the effect of fatigue on permanent deformation and vice versa in a sequential test procedure using an energy approach. The main findings are summarized as follows.

- The energy approach is convenient to analyze the interaction between permanent deformation and fatigue cracking.
- New failure criterion based on the dissipated energy ratio (DER) is proposed. The criterion is more comprehensive than the classic flow number (strain rate) for permanent deformation damage.
- The post flow number micro-crack growth rate can be visualized easily, and the macro-crack formation can be seen at the peak point of DER curve.
- It is observed that permanently deformed samples are more susceptible to fatigue cracking than new samples because of strain hardening. Fatigue damage at high temperatures (21 and 30 $^{\circ}C$) has a marginal effect on permanent deformation.
- The proposed sequential test method can make significant saving for both testing and material production.

REFERENCES

- Anderson, D. A., Le Hir, Y. M., Marasteanu, M. O., Planche, J.-P., Martin, D. & Gauthier, G. 2001. Evaluation Of Fatigue Criteria For Asphalt Binders. *Transportation Research Record: Journal Of The Transportation Research Board*, 1766, 48–56.

- Bahadori, A., Mansourkhaki, A. & Ameri, M. 2015. A Phenomenological Fatigue Performance Model Of Asphalt Mixtures Based On Fracture Energy Density. *Journal Of Testing And Evaluation*, 43, 133–139.
- Biligiri, K. P., Kaloush, K. E., Mamlouk, M. S. & Witzczak, M. W. 2007. Rational Modeling Of Tertiary Flow For Asphalt Mixtures. *Transportation Research Record: Journal Of The Transportation Research Board*, 2001, 63–72.
- Di Benedetto, H., Nguyen, Q. T. & Sauzéat, C. 2011. Nonlinearity, Heating, Fatigue And Thixotropy During Cyclic Loading Of Asphalt Mixtures. *Road Materials And Pavement Design*, 12, 129–158.
- Dyskin, A. V., Sahouryeh, E., Jewell, R. J., Joer, H. & Ustinov, K. B. 2003. Influence Of Shape And Locations Of Initial 3-D Cracks On Their Growth In Uniaxial Compression. *Engineering Fracture Mechanics*, 70, 2115–2136.
- Francken, L. & Clauwaert, C. Characterization And Structural Assessment Of Bound Materials For Flexible Road Structures. Sixth International Conference, Structural Design Of Asphalt Pavements, 1987 Ann Arbor, Michigan University. Michigan University.
- Ghuzlan, K. A. & Carpenter, S. H. 2000. Energy-Derived, Damage-Based Failure Criterion For Fatigue Testing. *Transportation Research Record: Journal Of The Transportation Research Board*, 1723, 141–149.
- Gupta, R. & Atul Narayan, S. P. 2019. Tensile Creep Of Asphalt Concrete In Repeated Loading Tests And Its Effect On Energy Dissipation. *International Journal Of Pavement Engineering*, 1–13.
- Korsunsky, A. M., Dini, D., Dunne, F. P. E. & Walsh, M. J. 2007. Comparative Assessment Of Dissipated Energy And Other Fatigue Criteria. *International Journal Of Fatigue*, 29, 1990–1995.
- Liu, H., Yang, X., Jiang, L., Lv, S., Huang, T. & Yang, Y. 2020. Fatigue-Creep Damage Interaction Model Of Asphalt Mixture Under The Semi-Sine Cycle Loading. *Construction And Building Materials*, 251, 119070.
- Lundstrom, R., Ekblad, J., Isacson, U. & Karlsson, R. 2007. Fatigue Modeling As Related To Flexible Pavement Design. *Road Materials And Pavement Design*, 8, 165–205.
- Onifade, I., Birgisson, B. & Balieu, R. 2015. Energy-Based Damage And Fracture Framework For Viscoelastic Asphalt Concrete. *Engineering Fracture Mechanics*, 145, 67–85.
- Pellinen, T. K., Christensen, D. W., Rowe, G. M. & Sharrock, M. 2004. Fatigue-Transfer Functions: How Do They Compare? *Transportation Research Record: Journal Of The Transportation Research Board*, 1896, 77–87.
- Roque, R., Birgisson, B., Drakos, C. & Dietrich, B. 2004. Development And Field Evaluation Of Energy-Based Criteria For Top-Down Cracking Performance Of Hot Mix Asphalt (With Discussion). *Journal Of The Association Of Asphalt Paving Technologists*, 73.
- Sangpetngam, B., Birgisson, B. & Roque, R. 2003. Development Of Efficient Crack Growth Simulator Based On Hot-Mix Asphalt Fracture Mechanics. *Transportation Research Record: Journal Of The Transportation Research Board*, 1832, 105–112.
- Shen, S., Airey, G. D., Carpenter, S. H. & Huang, H. 2006. A Dissipated Energy Approach To Fatigue Evaluation. *Road Materials And Pavement Design*, 7, 47–69.
- Widyatmoko, I., Ellis, C. & Read, J. M. 1999. Energy Dissipation And The Deformation Resistance Of Bituminous Mixtures. *Materials And Structures*, 32, 218–223.

Paper E

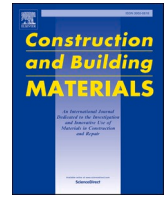
A study on Permanent Deformation and Fatigue Damage Interaction in Asphalt Concrete

Mequanent Mulugeta Alamnie, Ephrem Taddesse and Inge Hoff. Construction and Building Materials, 407 (133473), 2023. doi:[10.1016/j.conbuildmat.2023.133473](https://doi.org/10.1016/j.conbuildmat.2023.133473)



Contents lists available at ScienceDirect

Construction and Building Materials

journal homepage: www.elsevier.com/locate/conbuildmat

A study on permanent deformation and fatigue damage interaction in asphalt concrete

Mequanent Mulugeta Alamnie^{a,*}, Ephrem Taddesse^a, Inge Hoff^b^a Department of Engineering Sciences, University of Agder, Grimstad 4879, Norway^b Department of Civil and Environmental Engineering, Norwegian University of Science and Technology, Trondheim 7491, Norway

ARTICLE INFO

Keywords:

Permanent Deformation
Fatigue
Sequential Test
Dissipated Energy
Continuum damage
Flow Number

ABSTRACT

The dominant load-induced damages, permanent deformation (PD) and fatigue cracking (F), are traditionally predicted separately by taking temperature as a variable of departure. This paper presents an experimental study of the two damages and interaction using sequential test procedure (STP) based on 'sequential damage'. The STP is conducted in PD-F and F-PD sequences on each specimen using a creep-recovery and cyclic fatigue tests. The effect of strain hardening on fatigue cracking is studied in the PD-F sequence, and the impact of fatigue cracking on permanent deformation is explored using the F-PD sequence. First, the shear deformation in tertiary stage of creep recovery is investigated using the dissipated energy ratio criterion and a new fourth creep phase is obtained. Following the PD-F sequence, strain-hardening is found a significant accelerator of fatigue damage rate, particularly on aged and laboratory produced mixes. The fatigue tests without considering the strain-hardening effect underestimate fatigue damage rate. In the F-PD sequence, the effect of pre-existing crack (up to 40% modulus reduction) on permanent deformation is found marginal. The sequential test and damage approach is an effective way to analyze interaction between damage modes and evaluate asphalt mixtures.

1. Introduction

Asphaltic concrete is a crucial pavement material with a viscoelastic and viscoplastic behavior under different strain levels and temperature conditions. Pavement structures are typically exposed to high magnitude, complex mechanical, and environmental loads. The complex tire-pavement interface stress and environmental factors caused different modes of damage in asphalt pavements. The damage on the pavement is manifested in the form of energy dissipation, material ductility exhaustion, cracking, hardening, and viscoplastic flow. Among the different damage modes, permanent deformation and fatigue cracking are the two dominant damage mechanisms. At the material level, the constituents of asphalt mixture (aggregates, binder, and air voids) and confinement have significant effect on the respective damage mechanisms [1,2].

Permanent deformation (or rutting) in asphalt layer is caused by the accumulation of non-recoverable (viscoplastic) strain under repeated traffic loading, mainly at elevated temperatures. At structural level, permanent deformation is related to three mechanisms: (1) viscoplastic deformation in the asphalt layer (densification and shear flow), (2) the sub-structural (subbase and subgrade) settlement, and (3) studded tire

abrasion in the wheel path [3–5]. At the mixture level, the permanent strain is accumulated because of microstructure changes in the asphalt mixture matrix under a creep-recovery cycle. A strain hardening-relaxation phenomenon is one of the behaviors of asphalt concrete. The merits of considering the hardening-relaxation behavior is to consider the load history effect in the model and to capture a variable hardening rate at each loading cycle [6–8]. However, the permanent deformation modeling is heavily relayed on the data from a standard repeated creep-recovery test. The accumulated permanent strain at the end of each creep-recovery cycle is described in three distinct stages: *primary*, *secondary* and *tertiary* [9,10]. The primary creep stage is characterized by a rapid deformation at a decreasing rate (volumetric densification), and the secondary stage (steady state) has a constant viscoplastic strain rate. The viscoplastic strain hardening reaches saturation at the flow number and the tertiary creep commences with a rapid shear deformation [11]. At the maximum strain hardening saturation, the extra energy is consumed to initiate microcracks (viscodamage) and an increase in phase angle [12].

Fatigue damage, on the other hand, is a stiffness deterioration mechanism due to the formation and propagation of cracks under cyclic stress- or strain-control load. Several fatigue test protocols were

* Corresponding author.

E-mail address: mequanent.m.alamnie@uia.no (M.M. Alamnie).

attempted such as the indirect tensile, beam bending, and axial loading scenarios [13,14]. The traditional fatigue design criterion was based on the critical tensile strain at the bottom of the asphalt layer and the crack propagates bottom-up (BUC). The BUC is mainly due to structural problems not load-related. Studies showed that load related fatigue cracks started at or near the pavement surface and propagated downwards, that is, top-down cracking (TDC). Although researchers have reached different conclusions regarding the causes and locations of TDC, it is believed that TDC is caused by high radial tensile stress at the surface and longitudinal cracks in wheel paths [15–18]. Furthermore, experimental and field observations showed that TDC is critical in medium and thick asphalt layers, and BUC is dominant in thin pavements. It is also argued that the BUC appears as disintegrated zones (cannot reach the surface), and can conjoined and coalesce with TDC [19]. Furthermore, differential stiffness in the surface and base layers of asphalt pavement, and rutting of substructure layers can cause significant tensile stresses at the surface and bottom of asphalt pavement layer that leads to both TDC and BUC. This means design based on tensile strain at the bottom of asphalt layer overestimates fatigue life.

Nevertheless, an interaction of permanent deformation and fatigue cracking (TDC or BUC) in asphalt concrete has never been studied in detail and little is known about the simultaneous damage evolution. Current fatigue and permanent deformation models (both energy- or continuum- based) are based the assumption of mutually independent (non-associated) damage evolution. Temperature is often taken as a boundary thermodynamic variable between fatigue and permanent deformation. This is because asphalt relaxes faster at high temperature and become fatigue cracking resistant, and the stiffness (elasticity) increase at low temperature where permanent deformation is insignificant [20]. This distinction can be accurate in a controlled test at fixed temperature. However, the interaction between the two main damages is inevitable in actual pavement due to the reasons: (1) pavement temperature varies significantly in a day let alone over seasons, (2) the same load causes both damages, (3) as a viscoelastic-viscoplastic material, pure cracking never happen and plastic deformation around localized regions of cracks also evolves simultaneously, regardless of the temperature [21]. Hence, pure cracking and pure permanent deformation is unlikely by varying the temperature or loading level. Based on field observations, surface deformation along the wheel path causes longitudinal surface cracking inside or just outside of wheel-path [16,17,22]. Furthermore, as a three-phase material, the air voids are the most important components of asphalt mixture morphology, and about 4% void content is generally provided to prevent early rutting failure. The air voids can be considered as multitude of distributed pre-existing cracks [23]. For example, air void contents of 4% and 7% corresponds to pre-existing crack size of 0.65 mm and 0.79 mm, respectively [24]. When external load is applied, stress concentrates around the pre-existing flaws (air voids), and wing cracks initiate and propagate parallel to the load direction. Thus, the air voids can act as point of crack initiation due to tension–tension or tension–compression load and viscodamage cracking due to compression [25]. These observations are testimonial for the association of fatigue cracking and the accompanying permanent deformation.

This paper is focused on the experimental study of permanent deformation and fatigue damage, and the effect of one damage evolution on another. The interaction between the two damage modes is analyzed by following a sequential test procedure in two orders [26]: (1) the permanent deformation – fatigue (PD-F) damage sequence, (2) the fatigue – permanent deformation (F-PD) sequence. The PD-F sequence is to incorporate pre-deformation or strain hardening on fatigue response and the F-PD sequence is to simulate the fatigue damage development prior to permanent deformation in certain cases. In cold climate regions (seasons) and thick pavements, fatigue can develop without or prior to viscoplastic deformation. Then, fatigue cracked pavements can then undergo permanent deformation due to phase angle increment. Seven asphalt concrete mixtures were tested and analyzed in this study and the

viscoelastic, viscoplastic and damage responses were studied using uniaxial dynamic modulus, repeated creep-recovery, and uniaxial fatigue tests.

2. Viscoelastic, viscoplastic and damage modeling

2.1. Viscoelastic model

Asphalt concrete behaves in linear viscoelastic manner at specific strain levels [27,28]. The strain limits for linear viscoelastic response limit was assumed different values in the ranges between 50 to 150 micro-strains. The dynamic (complex) modulus $|E^*|$ is a fundamental material property using to analyze the viscoelastic response of asphalt concrete. It is expressed in a complex number form that represents the viscous and elastic components of modulus. The frequency-, stress- and temperature-dependent properties of asphalt concrete can be characterized by constructing a dynamic modulus master curve [29]. The true stress–strain constitutive equation cannot be expressed using the dynamic modulus, which contains an imaginary component. The relaxation function $E(t)$ is used to define the fundamental stress–strain constitutive relationship using true viscoelastic strain ϵ^{ve} or pseudo strain ϵ_i^R and pseudo stiffness (C).

$$\sigma^{ve} = \int_0^t E(t-\tau) \frac{\partial \epsilon^{ve}}{\partial \tau} d\tau \quad (1)$$

$$\sigma = C \epsilon_i^R = C \left(\frac{1}{E_R} \int_0^t E(t-\tau) \frac{\partial \epsilon^{ve}}{\partial \tau} d\tau \right) \quad (2)$$

where E_R is reference modulus (in unit modulus).

Asphalt concrete is a rate dependent material, and the viscoelastic properties are not adequate to fully characterize its responses beyond the viscoelastic stress limit (σ^{ve}) under different modes of loading.

2.2. Viscoplastic model

Viscoplasticity is the response beyond linearity limit where a rate-dependent viscoplastic strain is accumulated under repetitive loadings. In a creep-recovery test with rest period, the viscoplastic strain is conventionally determined by the additive decomposition of total strain or from experiment measurement of the nonrecoverable strain. Luo et al. [30] applied the decomposition technique for direction tension mode in a pseudo strain space. As a viscoelastic-viscoplastic material, a true separation between the viscoelastic (ϵ^{ve}) and viscoplastic (ϵ^{vp}) strain is difficult with short rest period using a haversine loading pulse [31]. A coupled viscoelastic-viscoplastic analysis is the accurate way to model permanent deformation. Several research have been conducted on the viscoplastic evolution inspired by the phenomenological, microscopic or macroscopic responses of viscoplastic strain due to external loads [32]. However, most of the existing modeling approaches are focused on prediction of permanent strain data from the creep-recovery test using empirical and mechanistic-empirical equations [33]. The classic uniaxial viscoplastic flow rate (strain-hardening) model assumes a power law in viscoplasticity [34,35].

$$\dot{\epsilon}_{vp} = \frac{g(\sigma)}{\lambda} \quad (3)$$

where $g(\sigma)$ is stress function, $\lambda = G \epsilon_{vp}^p$ is viscosity parameter approximated by a power form, G and p are model coefficients. Power-based models can approximate the secondary or steady-state creep strain with good accuracy. However, power function has inherent limitation to fit viscoplastic strain in the tertiary stage (viscodamage phase). Several other empirical and mechanistic-empirical models were proposed for all creep phases [10,11]. The Francken model is the most widely applied

three-stage model, such as in AASHTO standard. The model takes the following form.

$$\varepsilon_{vp} = AN^B + C(e^{DN} - 1) \quad (4)$$

where A , B , C and D are coefficients and N is the number cycles. In the model, parameter 'B' is the rate of strain hardening in the secondary stage and C indicates the start of tertiary stage (or flow number). Such type of models overrides the mechanistic and microscopic aspects of viscoplasticity and relied on the quality of creep-recovery test data, rest period between creep cycles and other control variables like temperature, confinement, axial stress magnitude, and mixture properties.

2.3. The continuum damage model

Viscoelastic continuum damage (VECD) theory is widely applied for asphalt concrete, which is derived based on Schapery's elastic-viscoelastic correspondence principle and work potential theory [36,37]. The theory utilizes internal state variable (S) to model damage. The damage variable (S) represents microstructural changes that leads to a reduction in effective stiffness due to cracking. The damage rate is defined using the maximum pseudo strain energy (W^R) and damage coefficient α as follows.

$$\frac{dS}{dt} = \left(-\frac{\partial W^R}{\partial S} \right)^\alpha \quad (5)$$

$$W^R = \frac{1}{2} \sigma \varepsilon_i^R = \frac{1}{2} C(S) (\varepsilon_i^R)^2 \quad (6)$$

$$C(S) = \frac{\sigma}{\varepsilon_i^R} \quad (7)$$

The parameter α is a unique material property related to viscoelastic damage evolution [38], which is dependent on the maximum slope (m_o) of relaxation modulus curve ($\alpha = \frac{1}{m_o} + 1$ for controlled-strain fatigue test). The detail formulation of simplified VECD (S-VECD) model is presented in previous studies [39–42]. The accumulated damage after one load cycle (ΔS) takes the following form.

$$\Delta S = \left[-\frac{DMR}{2} (\varepsilon_{a,i}^R)^2 (C_i^* - C_{i+1}^*) \right]^{\frac{\alpha}{1-\alpha}} (\Delta t_R)^{\frac{1}{1-\alpha}} \quad (8)$$

$$\varepsilon_{a,i}^R = \frac{(\beta + 1)}{2} \varepsilon_{pp} \quad (9)$$

$$DMR = \frac{|E^*|_{\text{fingerprint}}}{|E^*|_{LVE}} \quad (10)$$

$$\Delta t_R = \frac{1}{\alpha_T} \left[\frac{\Delta N}{10} \right] \quad (11)$$

The C - S relationship (Eqn (8)) combines the effects of strain level, temperature, sample variability, and frequency.

where, DMR is the dynamic modulus ratio used to normalize specimen-to-specimen variation,

E_{LVE}^* is dynamic modulus from linear viscoelastic test,

$|E^*|_{\text{fingerprint}}$ is fingerprint dynamic modulus),

$\varepsilon_{a,i}^R$ is the pseudo strain amplitude,

$\beta = \frac{\sigma_{mean}}{\sigma_{pp}}$ is a load form factor,

ε_{pp} and σ_{pp} are peak-to-peak strain stress amplitudes (respectively),

σ_{mean} mean stress,

Δt_R is a reduced time of a cycle,

ΔN is the number of load cycles between two successive strain amplitudes.

2.4. Energy approach

Dissipated energy (DE) in a cyclic load is the area under the stress-strain hysteresis loop (or the work done per cycle), which is expressed by the following integral.

$$DE = \int_0^{\tau} \sigma(t) \frac{\partial \varepsilon(\tau)}{\partial \tau} d\tau \quad (12)$$

The energy expended due to applied sinusoidal, creep or creep-recovery type of loadings can be formulated by substituting the appropriate strain rate and stress functions in Eqn (12). For a controlled-strain cyclic fatigue test with a sinusoidal stress $\sigma(t) = \sigma_o \sin(\omega t + \varphi_i)$ and strain $\varepsilon(t) = \varepsilon_o \sin(\omega t)$ functions, the dissipated energy takes the following form.

$$DE_F = \pi E_i^* \varepsilon_i^2 \sin(\varphi_i) \quad (13)$$

E_i^* is the apparent dynamic modulus at i^{th} cycle, φ_i is the phase angle, ε_o is target strain amplitude. The dissipated energy was computed by decomposing into elastic, viscous and viscoplastic (if any) stress-strain components [21,43]. Masad et al. [43] have identified three dissipated pseudo strain energy (DPSE) components: (1) energy dissipated due to increase in the apparent phase angle and the hysteresis loop, (2) dissipated energy related to permanent deformation (viscoplastic strain) and (3) change in pseudo stiffness due to damage. They also concluded that the second component of dissipated energy is less than 5 % of the change of dissipated energy between an idealized hysteresis loop and a hysteresis area with some creep-recovery strain. On the other hand, the dissipated energy due to creep (i.e., constant strain rate) is $DE_{Creep} = \sigma_o^* \varepsilon_{cr}$. For creep-recovery permanent deformation (DE_{PD}), creep damage accumulates only during the creep phase of a creep-recovery cycle. Thus DE_{PD} is expressed using the Francken model as follows.

$$DE_{PD} \cong \sigma_o (AN^B + CD(e^{DN} - 1)) = \sigma_o^* \varepsilon_{vp} \quad (14)$$

The dissipated energy ratio (DER) criteria were proposed as failure indicator for asphalt concrete [44–46]. The common one is expressed as follows.

$$DER = n \left(\frac{DE_1}{DE_n} \right) \quad (15)$$

where DE_1 and DE_n are the dissipated energies at the first and the n^{th} load cycle. The DER for a controlled-strain (ε_o) cyclic fatigue (DER_F) and for creep-recovery permanent deformation (DER_{PD}) can be expressed as follows.

$$DER_F = n \times \frac{\pi E_1^* \varepsilon_1^2 \sin \varphi_1}{\pi E_n^* \varepsilon_n^2 \sin \varphi_n} \approx n \left(\frac{E_1}{E_n} \right) \left(\frac{\varphi_1}{\varphi_n} \right) \quad (16)$$

$$DER_{PD} = N \left(\frac{A + C(e^D - 1)}{AN^B + CD(e^{DN} - 1)} \right) = N \left(\frac{K}{\varepsilon_{vp}} \right) \quad (17)$$

where $K = A + C(e^D - 1)$ is constant, which is dependent on stress level, initial deformation, and tertiary stage shear failure rate (C and D).

3. Test Methods, and material

3.1. Materials

In this study, seven asphalt concrete mixtures were evaluated for testing. Four of the mixtures were collected from two asphalt mix production plants in Norway (denoted as P1 and P2). The mixtures are asphalt concrete (AC) and stone mastic asphalt (SMA) mixtures, as shown in Table 1. Moreover, two mixes were produced in the laboratory (designated as AC-L and SMA-L). The AC-P1 mixture is pure binder and the AC-P1-X is a polymer modified mixture. Similarly, the SMA-P2

Table 1
Tested asphalt mixtures compositions (aggregate gradation and binder properties).

Mix Type	Sieve size (mm)							Binder Content (%)	Binder Grade (at 25 °C)
	16	11.2	8	4	2	0.25	0.063		
Percent passing (%)									
<i>Plant-Produced mixtures (P1 and P2)</i>									
AC-P1	100	95	75	47.5	33.5	11.5	8	5.6	70/100
AC-P1-X	100	95	70	48	36	15.5	7	5.8	PMB 65/105-60
SMA-P1	100	94	56	36	27	16	10.5	5.83	70/100
SMA-P2	100	92	58	37	23	13	9	5.95	"
SMA-P2-X	100	91.2	53.6	35.7	21.7	12.8	8.4	5.83	"
<i>Laboratory-Produced mixtures (L)</i>									
AC-L	100	95	70	47.5	33.5	12.5	7.5	5.1	70/100
SMA-L	100	95	55.5	37.5	26	16	11	5.3	"

mixtures were sampled at different times from mixing plant 2, denoted as SMA-P2 and SMA-P2-X. Two of the mixtures, AC-P1-X and SMA-P2-X are one year older (aged) than the other mixtures. The samples were stored up to one year at room temperature. All mixtures have a nominal maximum aggregate size (NMAS) of 11 mm with pure binder except a polymer modified (PMB) for AC-P1-X.

3.2. Test methods

Cylindrical test specimens of size about 180 mm height and 150 mm diameter were produced using a gyratory compactor according to Superpave gyratory compaction procedure. The final test specimens were fabricated by coring and cutting to 150 mm height and 100 mm diameter. The IPC global universal testing machine (UTM-130) was used for testing according to the test parameters given in Table 2.

Three main types of tests were conducted to characterize asphalt mixture’s viscoelastic, viscoplastic and fatigue responses. The tests are: (1) the dynamic modulus test to determine linear viscoelastic characteristics (AASHTO T378 2017), (2) a controlled-strain uniaxial fatigue test (AASHTO TP-107 2017) in both tension-tension and tension-compression modes, and (3) cyclic creep-recovery tests (EN 12697-25 2016 and AASHTO T378 2017).

3.2.1. Sequential test approach

Inspired by the sequential creep and fatigue damage evolution in researches by [47,48], the sequential test was proposed in this study to investigate the effects of permanent deformation on fatigue damage evolution and vice versa [26]. To simulate the effect of one damage mode on the other, the test campaign is performed in two sequences on each test specimen – the PD-F and F-PD sequences. The permanent deformation – fatigue (PD-F) is intended to capture the early life

Table 2
Summary of test parameters, controls, and variables.

	Test Types Dynamic modulus	Creep- recovery	Uniaxial Fatigue
Test Standard	AASHTO T378	EN 12697-25	AASHTO TP107
Specimen size (height to diameter ratio)	1.5	1.5	1.5
Number of duplicates	4	3	2
Temperature, °C	-10, 5, 10, 21, 40	30, 40, 50	10, 15, 21, 30
Frequency, Hz	20, 10, 5, 2, 1, 0.5, 0.2, 0.1	-	10
Control mode	Control strain (µε): 50	Control stress (MPa): 0.5 to 2	Target strain (µε): 100, 150, 200, 300, 400
Loading (rest) time, s	-	0.1 (0.9)	-
Pulse (Confinement)	Sinusoidal (Uniaxial)	Haversine (Uniaxial and triaxial)	Sinusoidal (Uniaxial)

permanent deformation (hardening) before fatigue started. In other words, permanent deformation is a short- and fatigue is a long- term (in ranges of 10⁶ cycles) damage after aging. In most cases, except thermal cracking, viscoplastic strain accumulates before fatigue cracking initiates, and permanent deformation is believed to be the cause of surface cracking in pavement [16]. In the PD-F sequence, virgin specimens are tested in a creep-recovery test within the steady-state stage well before flow number (FN) commences i.e., N < FN. Then, the pre-deformed (strain-hardened) specimens are tested in uniaxial fatigue at low temperatures until failure.

The fatigue – permanent deformation (F-PD) sequences is proposed to simulate the effect of preexisting fatigue cracking on permanent deformation mechanism of asphalt concrete. In this sequence, new specimens are first tested in the uniaxial fatigue test (in tension-compression T-C or tension-tension T-T modes) in controlled-strain modes at low and intermediate temperatures (not more than 40 % of initial stiffness reduction). A 50 % initial modulus reduction due to fatigue cracking has been considered as failure indicator in asphalt concrete [13,49]. Then, the pre-fatigued specimens are tested in creep-recovery tests at elevated temperatures.

The nondestructive fingerprint dynamic modulus test was performed before the fatigue damage tests. The overall testing process is illustrated in Fig. 1, and the ball and socket joint system for uniaxial cyclic fatigue test scheme is shown in Fig. 2. A plastic steel putty epoxy was used to glue the top and bottom tension platens.

4. Results and discussions

4.1. Dynamic modulus test

The dynamic modulus master curve is fitted using a sigmoid function and the WLF [50] time-temperature shift factor α_T through the least square optimization technique.

$$\log|E^*| = \delta + \frac{(\alpha - \delta)}{1 + \exp(\eta - \gamma \log f_R)} \tag{18}$$

$$\log(\alpha_T) = -\frac{C_1(T - T_0)}{C_2 + T - T_0} \tag{19}$$

where δ, α, η and γ are coefficients; f_R is reduced frequency (= α_T × f); C₁ and C₂ are WLF constants. The dynamic modulus master curves of the tested mixtures are constructed at 21 °C reference temperature. As shown in Fig. 3, laboratory-produced (AC-L, SMA-L) and aged (AC-P1-X, SMA-P2-X) mixtures have low dynamic modulus (stiffness) at high temperatures. This implies that the mixtures are more susceptible to permanent deformation than unaged and plant-produced mixtures. It is possible to verify deformability using the ratio of dissipated (loss) to the maximum stored energy per cycle (2πsinφ, where φ is phase angle) given in Table 3. High energy loss corresponds to high phase angle and deformability potential.

On the other hand, the dynamic modulus at low temperatures and

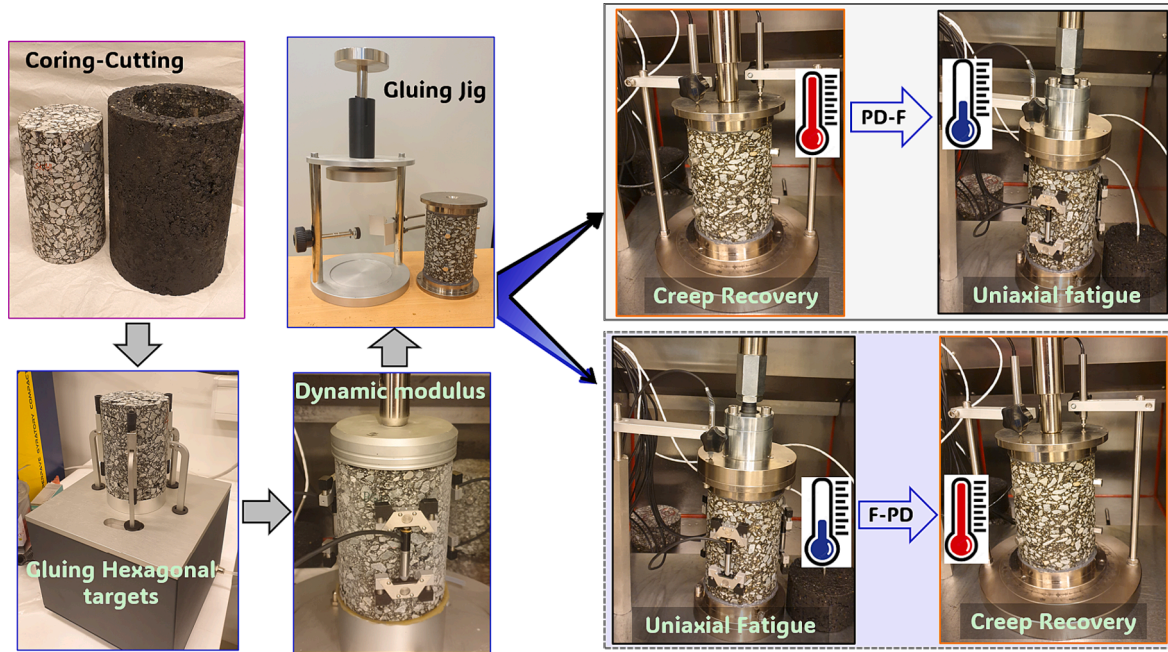


Fig. 1. Overall process testing specimen instrumentation and test sequences (dynamic modulus, creep recovery, and uniaxial fatigue tests).

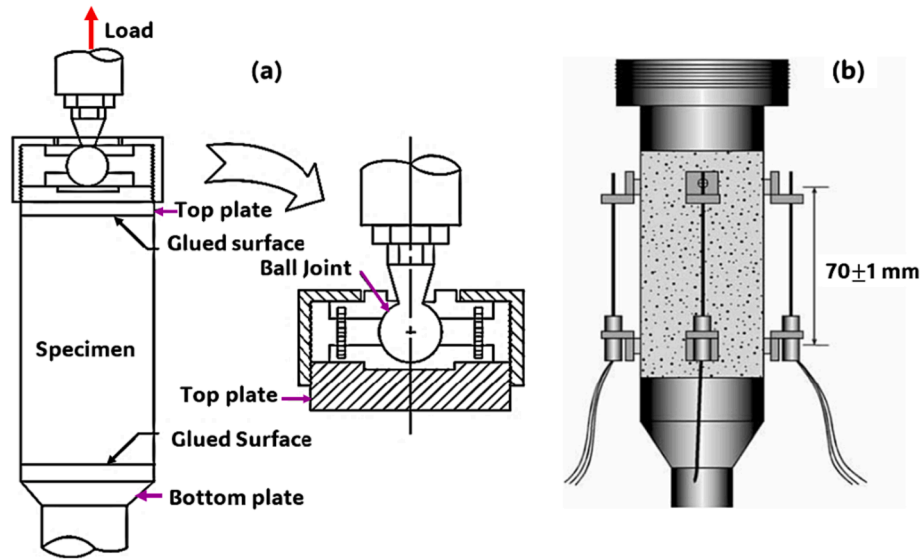


Fig. 2. Schematic of fatigue test configuration (a) locking ball joint (b) gauge point.

high frequencies corresponds to fatigue properties of mixtures. To better understand the fatigue response of the materials, the relaxation modulus curve is often used instead of dynamic modulus curve which contains the loss modulus component ($E'' = E^* \sin \phi$). Fatigue damage is the deterioration of the storage modulus due to increase in loss modulus or phase angle. For this reason, the time-domain relaxation modulus $E(t)$ is often used to describe viscoelastic responses than the frequency-domain dynamic modulus. The relaxation modulus is obtained from the storage modulus (E') data using the analytical Prony method. The relaxation modulus is expressed using the Generalized Maxwell (GM) model in discrete form as follows.

$$E(t) = E_\infty + \sum_{i=1}^M E_i \left(e^{-t/\rho_i} \right) \quad (20)$$

where E_∞ is long-term (equilibrium) modulus; E_i and ρ_i are relaxation

modulus and relaxation time, respectively; and M is the total of number of GM elements. A total of 12 Prony series coefficients were found sufficient to fit the relaxation modulus curve using a pre-smoothened storage modulus data (Fig. 4). The pre-smoothing is done using a sigmoid-type continuous function to remove outliers in the storage modulus data [29]. The log-log ratio of the relaxation modulus – time curve is the slope, such that, the maximum slope is $m_o = \max \left\{ \frac{\Delta \log(E(t))}{\Delta \log(t)} \right\}$. It has been established that the maximum slope is related to the viscoelastic damage rate (α), which is expressed for strain-controlled tests as $\alpha = \frac{1}{m_o} + 1$ [38]. The viscoelastic damage rate is found dependent on confining stress for triaxial test scenarios [29]. As given in Table 3, laboratory-produced mixtures (AC-L and SMA-L) have the maximum slope of relaxation modulus which corresponds to minimum damage rate (alpha). This is inline with the possibility that plant-produced mixtures could undergo oxidative aging [51] and hardening

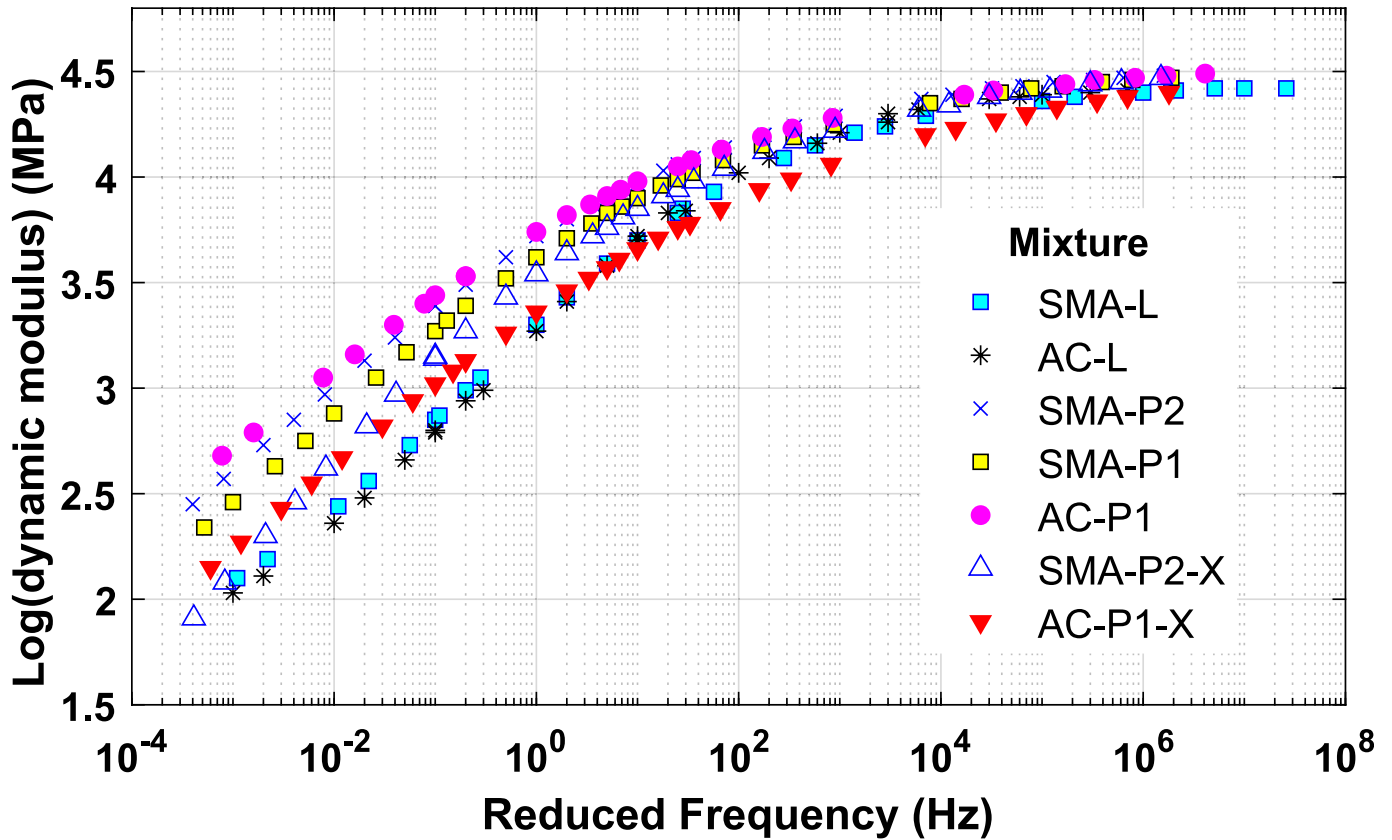


Fig. 3. Dynamic modulus master curves (reference temperature at 21 °C).

Table 3

Loss modulus ratio and relaxation modulus-related variables (long-term relaxation modulus and viscoelastic damage parameter).

	AC-L	SMA-L	AC-P1	SMA-P1	SMA-P2	AC-P1-X	SMA-P2-X
Maximum loss ratio ($2\pi\sin\phi$)	4.09	4.08	3.61	3.831	3.76	3.84	4.25
E_{∞} (MPa)	61.92	87.88	172.48	101.74	127.12	72.20	38.78
Maximum Slope (m_0)	0.70	0.69	0.52	0.59	0.53	0.50	0.65
Alpha (α)	2.43	2.45	2.91	2.69	2.90	3.02	2.54

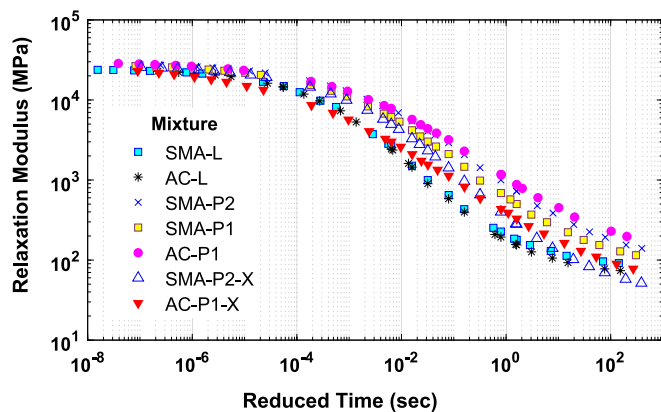


Fig. 4. Relaxation modulus master curves (reference temperature at 21 °C).

phenomena due to re-heating the loose mixture sample for gyratory compaction.

4.2. Cyclic creep-recovery test

Permanent deformation damage response of asphalt concrete is highly stress and stress-path dependent [29,52]. Stress sensitivity increases with temperature for both viscoelastic and viscoplastic responses. The creep-recovery response of asphalt concrete was explained using the strain rate in the three creep phases. In a typical asphalt mixture, the strain rate decreases in the primary stage, constant rate (steady state) in the secondary stage, and rapidly increases in the tertiary stage. The rate in the steady-state stage is the most important property to assess the performance of asphalt concrete because of the strain hardening. The tertiary stage commences with the formation of micro-cracks at the maximum saturation of strain-hardening, the flow number (FN). The FN can be identified when the second derivative of the Francken model (Eqn (4)) changes from negative to positive. After the flow number, shear failure starts at constant volume. The first part of the equation (AN^B) is the power function to fit the primary and secondary stages and the viscodamage part is fitted using ($C(e^{DN} - 1)$). The coefficient 'B' is the rate of strain in the secondary stage or the rate of hardening.

Furthermore, triaxial creep-recovery tests are selected in lieu of the uniaxial to simulate the actual field confinement. The realistic confining pressure in pavements is thought to be between 100 and 200 kPa, depending on the mixture type. The confining- and axial stress-dependent responses of asphalt concrete can be seen in Fig. 5 (a to d). The axial stress increases the rate of deformation, while confinement retards the strain rate and increases in the viscosity (λ) thus extends the flow number.

4.2.1. Four-stage permanent deformation criterion

From a mechanistic viewpoint, the classic flow number failure criterion is only an indicator for the initiation of shear deformation (viscodamage) and could not give the full history of viscoplastic damage evolution. In actual practice, pavements can be in-service after micro cracks initiated at the flow number, that is, from micro-crack initiation at FN to the formation of macro cracking. In this phase, the micro cracks accumulate, grow, and coalesce to cause macro cracks. Therefore, it is worth investigating the remaining life of pavement from maximum hardening saturation to the formation of macro crack, which is referred to as *shear endurance life (SEL)*. To estimate the life between FN and the macro crack formation a new formulation is proposed. Note that using the conventional strain rate method, it was not possible to identify the cycle number where macro-cracks started. The dissipated energy approach is applied to formulate a fourth creep phase in the tertiary creep stage and to calculate the shear endurance life, *SEL*. The cycle number at the macro-crack formation need to be revealed, which is denoted as N_{PV} . Thus, SEL is expressed as

$$SEL = N_{PV} - FN \tag{21}$$

The dissipated energy criterion DER_{pd} from Equation (17) is applied to

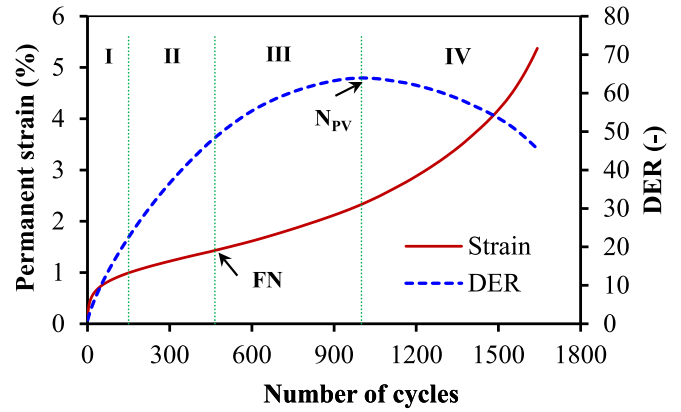


Fig. 6. Four-stage permanent deformation evolution – SMA-P2-X (T = 40 °C, $\sigma_d = 650kPa$).

find a peak point (cycle number) in the tertiary creep stage where the macro-crack started. As shown in Fig. 6, it is possible to reveal additional fourth creep phase in the tertiary creep stage using the dissipated energy ratio method.

The peak value of the DER curve (N_{PV}) is believed to be the point of macro-crack formation that corresponds to excessive energy dissipation. At this point, the shear endurance limit is reached, and the sample can carry no more external load. As the FN marks the start of micro-crack initiation, and the N_{PV} marks the formation of macro-cracks and the commencement of the fourth creep stage. The DER curve starts descending in the fourth stage due to excessive energy dissipation, which leads to loss of integrity or collapse. In the above expression (Eqn

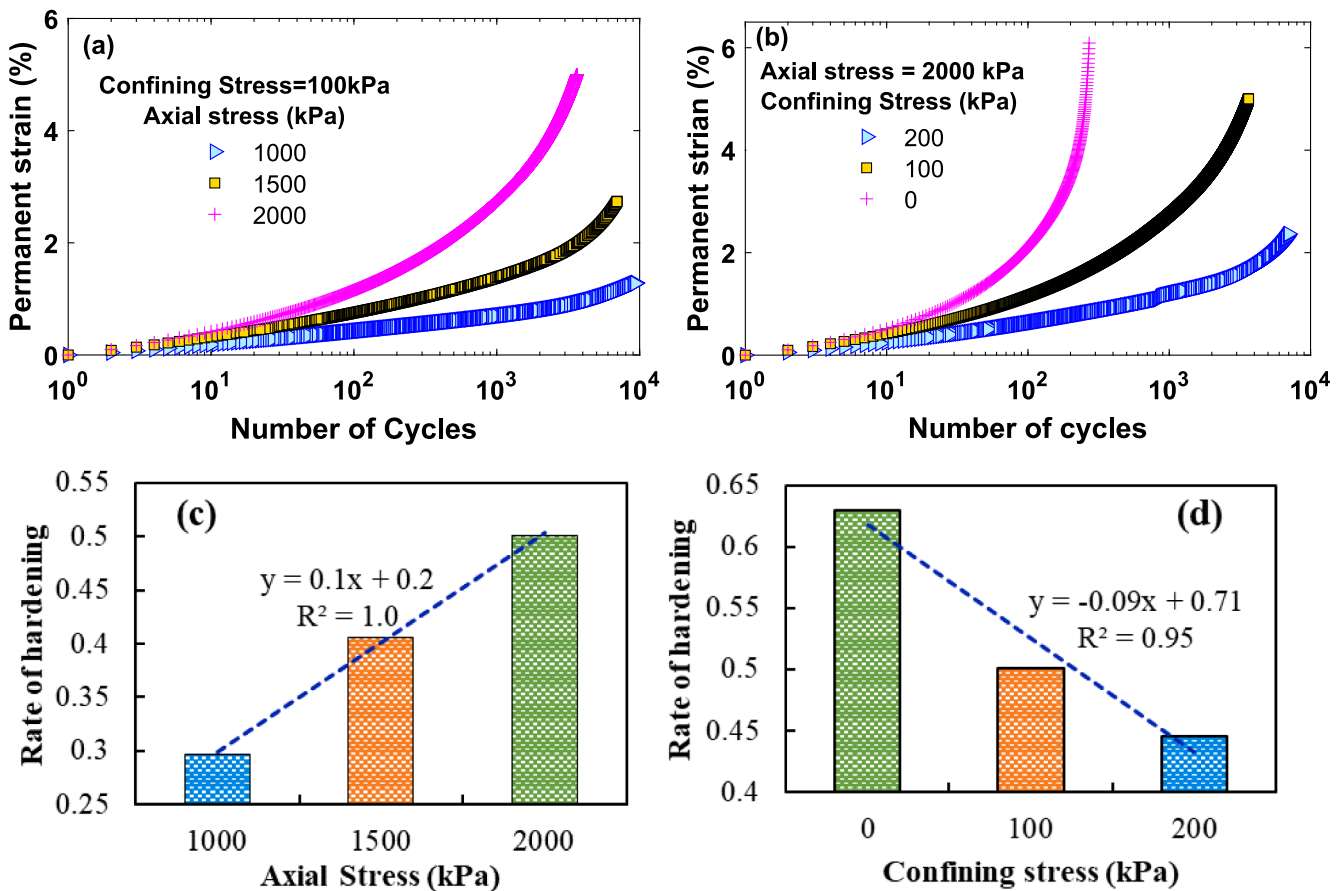


Fig. 5. Effect of stress on permanent deformation and hardening rate – (AC-P1 at 50 °C).

(21)), the corresponding permanent strains at peak point (ϵ_{PV}) and flow number (ϵ_{FN}) can be used to express the shear endurance life, $\epsilon_{SEL} = \epsilon_{PV} - \epsilon_{FN}$.

An example is presented to illustrate the relation using aged specimen (SMA-P2-X). As shown in Fig. 7, a positive correlation is found between flow number and SEL and N_{PV} with good accuracy. High flow number means a long shear endurance life before macro-crack formation. The correlation between the number of cycles in Fig. 7(a) has shown better relationship than using the corresponding strain quantities in Fig. 7(b).

Similar correlation can be seen for other six mixtures tested at different temperatures, and axial stress levels. The result presented in Fig. 8 is for the AC-P1-X mixture. The data points in the Fig. 8 represents the SEL and N_{PV} of tested samples at two different temperatures (30 °C and 40 °C), three axial stresses (0.65, 1.5 and 2 MPa), and new and pre-fatigued samples. Regardless of initial conditions, the correlation between the flow number and the peak value is found in agreement, but the shear endurance life (SEL) has shown slightly weak correlation. This implies that the shear deformation (viscodamage) phase is dependent on stress, temperature, and initial conditions of the specimen.

Furthermore, the deformability rates (ϵ_{FN}/FN , ϵ_{PV}/N_{PV} and ϵ_{SEL}/SEL) are used to assess the viscoplastic deformation rates of different mixtures. Fig. 9 shows the good correlation between the deformability rate and the flow number. The data points in the figure corresponds to flow numbers and permanent strain at maximum saturation for different AC-P1-X and SMA-P2-X duplicate samples tested at different temperatures (30 and 40 °C), and deviatoric stresses (from 0.5 to 2 MPa). Regardless of the differences with testing parameters, the deformability rate can be approximated with a power relationship.

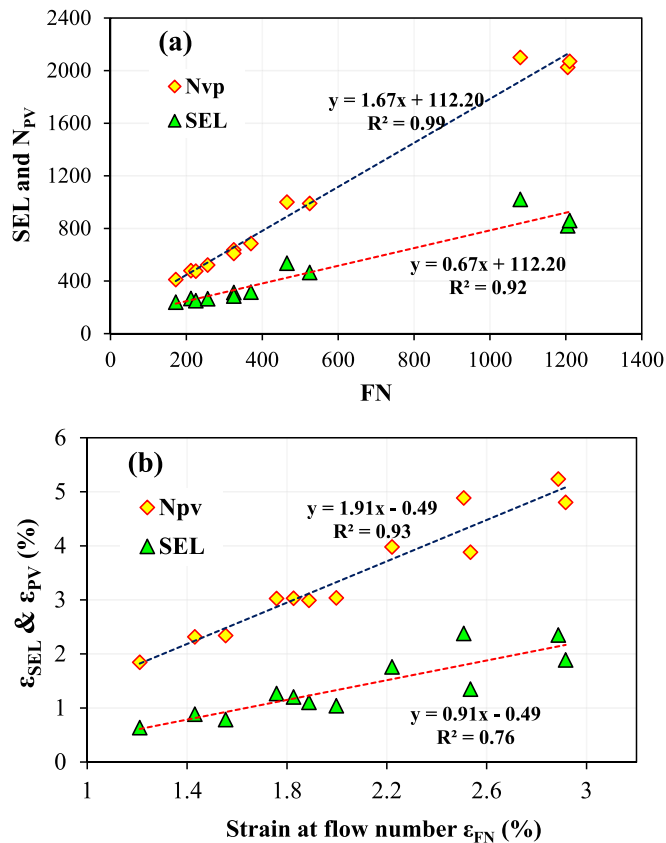


Fig. 7. Correlation between (a) cycle numbers (b) strains components – SMA-P2-X (T = 40 °C).

4.3. Uniaxial fatigue test

Uniaxial fatigue tests were conducted on different asphalt concrete mixtures on new and strain-hardened specimens according to test parameters given in Table 2. Fatigue tests are recommended between 5 and 15 °C, mostly at 10 °C [44]. Typical fatigue damage response is described using dynamic modulus deterioration curve which evolved in three stages, as shown in Fig. 10, a rapid reduction in the first phase, steady state in the second stage and a rapid reduction in the third stage.

As discussed in Section 2.3, the viscoelastic continuum damage model is the most comprehensive fatigue damage constitutive model that considers time-temperatures factor, rate of relaxation module change, factor for specimen-to-specimen variation and pseudo stiffness deterioration. Therefore, the damage characteristic curves (C – S) are constructed to characterize the pseudo stiffness deterioration (C) due to damage (S). The 50 % pseudo stiffness reduction is considered as fatigue failure point. The C-S relationship relates the temperature dependent viscoelastic damage quantity with the pseudo stiffness deterioration. As shown Fig. 11, laboratory-produced and aged specimens have shown rapid damage rate compared to that of plant produced specimens. The C – S curve can be used to classify different mixtures. However, the comparison based on the C-S curve can be misleading. For example, from rheological viewpoint, the damage rate (alpha) is smaller for laboratory and aged samples (Table 3). Several factors such as initial void (pre-flaw) can influence the damage rate. Moreover, the damage rate of the tested mixtures is consistent with the slope of relaxation modulus or the viscoelastic damage parameter (alpha).

Furthermore, the dissipated energy ratio, $DER_F = n \times \left(\frac{E_d}{E_i}\right) \left(\frac{\phi_d}{\phi_i}\right)$ is used to characterized the rate of damage accumulation for different fatigue tests. For the control-strain fatigue tests, the effect of target on-specimen strain is an important factor for damage rate. Fig. 12 shows examples of specimens fatigued for about 16 % to 40 % reduction of initial modulus. It is found that the DER_F curve is dependent on temperature and on-specimen control strain ($\mu\epsilon$). Specimens with high damage have lower rate of DER at low temperatures. As temperature increases, DER_F decreases or fatigue resistance increases.

5. The interaction of fatigue and permanent deformation

5.1. The PD-F sequence

5.1.1. The effect of strain hardening on fatigue damage

The rational of the PD-F sequence is the assumption that permanent deformation evolves before ductility exhaustion and significant fatigue cracking in asphalt concrete, as discussed in Section 3.2.1. For instance, new pavements are more likely to undergone volumetric densification (deformation) before fatigue cracking initiates. This is due to the reason that high energy is required to initial fatigue cracking due to the fast relaxation and viscous properties of new asphalt pavements. Therefore, initial strain-hardening of the asphalt concrete can have a direct consequence on the fatigue damage rate of serviceable pavements. To investigate this scenario, asphalt concrete samples are pre-deformed in steady-state stage at 40 or 50 °C and the same sample is tested in uniaxial fatigue part of the PD-F sequential test at 10 °C and 10 Hz in tension-tension or tension-compression mode.

The objective of the PD-F test sequence is to investigate the effect of strain hardening on the fatigue damage rate of asphalt concrete mixtures. Considering the pre-deformation (strain hardening) effect during fatigue test is believed as a more realistic way of damage sequence when actual pavement is considered. In the PD part, volumetric deformation evolves (air void reduction), and the viscous nature of asphalt concrete is reduced, making the material prone to fatigue cracking. Thus, strain hardening can cause an increase in the ‘nominal stiffness’ of the specimen and accelerates fatigue damage. After a certain level of hardening (aging), both fatigue and permanent deformation damages can develop

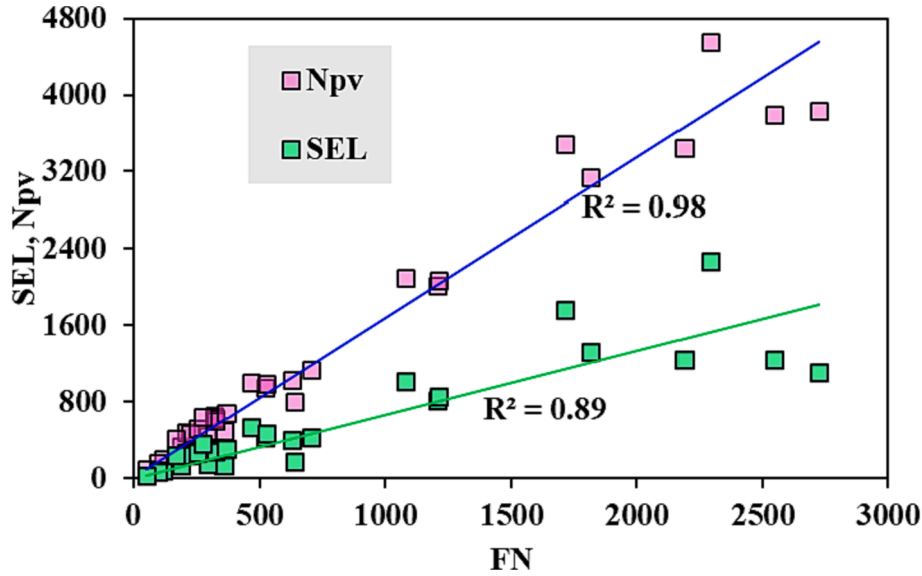


Fig. 8. Correlation between FN, N_{pv} and SEL – AC-P1-X.

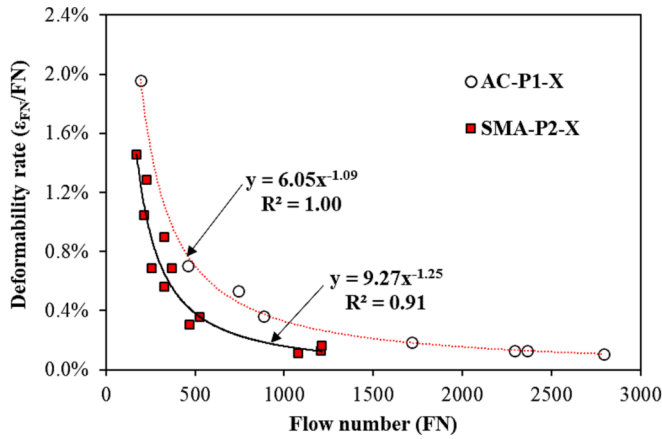


Fig. 9. Deformability rate ($\frac{\epsilon_{FN}}{FN}$) versus flow number for different mixtures.

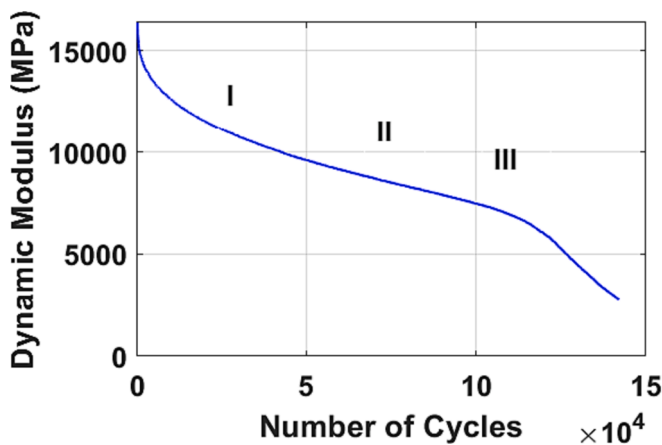


Fig. 10. Typical fatigue damage test ($T = 10\text{ }^\circ\text{C}$ and $300\text{ }\mu\text{e}$) – SMA-P2.

simultaneously.

The viscoelastic continuum damage (VECD) approach is applied to quantify the fatigue damage evolution. The damage characteristic curve is fitted using the expression $C = 1 - as^b$, where parameter b is the slope

of $\log C - \log S$ curve. As shown in Fig. 13, the strain hardening (PD) accelerates fatigue damage rate in the PD-F test sequence. It is evident that pre-deformed samples have shown high fatigue damage rate and energy dissipation than undeformed (new) samples. The results are consistent for the new and aged tested specimens.

Moreover, Fig. 14 (a) demonstrates that the rate of pseudo stiffness deterioration or parameter 'b' in $C = 1 - as^b$ is used to visualize pseudo stiffness deterioration rate. This agrees with the relaxation modulus rate (maximum slope and alpha) (Fig. 4 and Table 3). Alternatively, the dissipated energy quantity can also be used to explain the PD-F interaction of fatigue and permanent deformation. As shown in Fig. 14 (b), for the same amount of pseudo stiffness reduction, the amount of cumulative dissipated energy needed is greater for new samples than the pre-deformed ones. This means the number of cycles required to cause a 50 % of pseudo stiffness reduction are smaller for pre-deformed (strain hardened) samples than the new (undeformed) specimens. In other words, the amount of energy expended on new samples is much higher than the pre-deformed samples to cause failure. Thus, both the dissipated energy and continuum damage approaches yield similar conclusions (Fig. 14 a and b).

The cumulative damage variable (S) at 50 % pseudo stiffness reduction and the dissipated energy quantity (DE_F) give some comparable regression and good correlation, as shown in Fig. 15. The correlation could be perfect linear. However, the damage (S) is the aggregate of all internal state variables including any viscoplastic deformation and viscous while the DE_F is the energy expended due to an assumed pure sinusoidal load only.

5.2. The F-PD sequence

5.2.1. The effect of pre-fatigue cracking on permanent deformation

As discussed in Section 3.2.1, the objective of the F-PD sequence test is to investigate the effect of pre-existing fatigue crack on the permanent deformation responses of different asphalt concrete mixtures. First, the fatigue part of the F-PD sequence is conducted at 10 Hz frequency and 10 °C temperature to induce a certain extent of fatigue cracking (maximum of 40 % dynamic modulus reduction). Then, the same pre-fatigued specimen is test in a creep-recovery permanent deformation test at higher temperature (30, 40 and 50 °C) until failure. The fatigue part of the F-PD test sequence is intended only to cause initial cracks not to fail the sample in a controlled-strain test prior to creep-recovery test. It is possible that viscoplastic deformation can develop during the

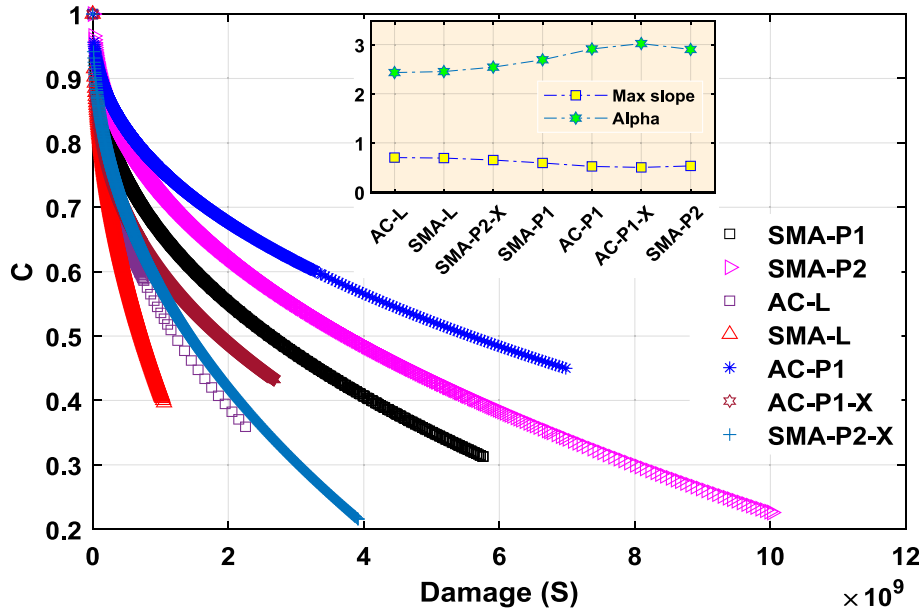


Fig. 11. Fatigue damage characteristics ($T = 10\text{ }^\circ\text{C}$ and Target strain = $300\text{ }\mu\epsilon$).

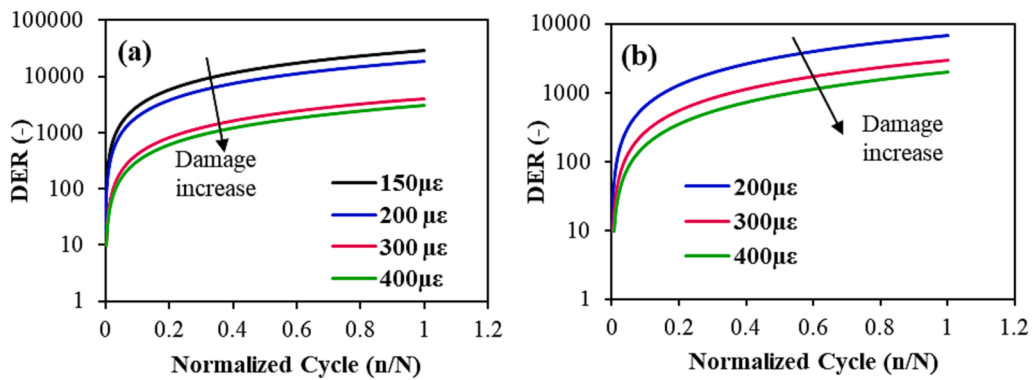


Fig. 12. DER_F for T-C fatigue test at different control-strain (SMA-P2-X) (a) $10\text{ }^\circ\text{C}$ (b) $15\text{ }^\circ\text{C}$.

fatigue part of the tests. However, it is highly dependent on the fatigue test temperature and target on-specimen strain amplitude. It is found that a tension–compression fatigue test at $10\text{ }^\circ\text{C}$ caused no more than 0.08 % creep strain. Thus, the corresponding dissipated energy due to the creep strain is insignificant compared to the cyclic fatigue part [43].

The effect of pre-existing cracking on permanent deformation in the F-PD sequence is analyzed using the strain rate in the steady-state stage, flow number and the expended energy. The dissipated energy and hardening rate are strongly dependent on the deviatoric stress. High deviatoric stress result in high dissipation, rapid creep rate, and small flow number. First, the deformation (hardening rate) is studied with respect to the energy quantities in the F-PD sequence. It can be seen in Fig. 16 (a) that the strain hardening (parameter ‘B’ in Francken model) is positively proportional with the dissipated energy due to creep-recovery deformation (where DE_{PD} is the cumulative energy up to flow number). However, the rate of strain hardening has a negative correlation with the dissipated energy due to fatigue (DE_F) in the F-PD sequence (Fig. 16 b). In addition, the effect of pre-fatigue on permanent deformation is analyzed by correlating the flow number and respected expended energies in fatigue and permanent deformation damages (DE_F and DE_{PD}).

It is also found that neither DE_F nor DE_{PD} energy quantities are consistent with the flow number, as shown in Fig. 17. The expended energies are dependent on mixture type and temperature. In Fig. 17a,

the DE_{PD} at $30\text{ }^\circ\text{C}$ shows an increasing trend for AC-P1-X mixture. On the other hand, it has a decreasing relation for the SMA-P2-X at $40\text{ }^\circ\text{C}$ with respect to flow number (Fig. 17b). The DE_{PD} is high for a small flow number, that is, deformation rate is high due to rapid permanent deformation at higher temperature (Fig. 17b). It should be emphasized here that comparison based on energy dissipation quantity alone is difficult and could give misleading conclusions. It also varies from specimen to specimen, initial voids, and pre-fatigue damage. Several phenomena can be the reasons for the inconsistency of the effect of fatigue on the subsequent permanent deformation damage. Firstly, the PD part of F-PD test is performed at higher temperatures ($30, 40$ and $50\text{ }^\circ\text{C}$) and some of the initial fatigue cracks (at $10\text{ }^\circ\text{C}$) can heal during the rest period and temperature conditioning period for the creep-recovery tests. However, energy dissipation is irreversible regardless of the sample’s apparent (damage) state or the healing potential. Secondly, the tension–compression or tension–tension cyclic fatigue test using cylindrical specimens requires large loading cycle to cause significant cracks (the 50 % stiffness reduction is only an approximate failure criteria). Therefore, 20 to 40 % stiffness reduction in fatigue tests has little impact on the subsequent permanent deformation damage. The third reason could be related to potential hardening or post compaction during the tension–compression fatigue test phase. This compaction can improve deformation resistance. Thus, based on this study, the effect of small pre-crack on the permanent deformation (F-PD sequence) is found marginal.

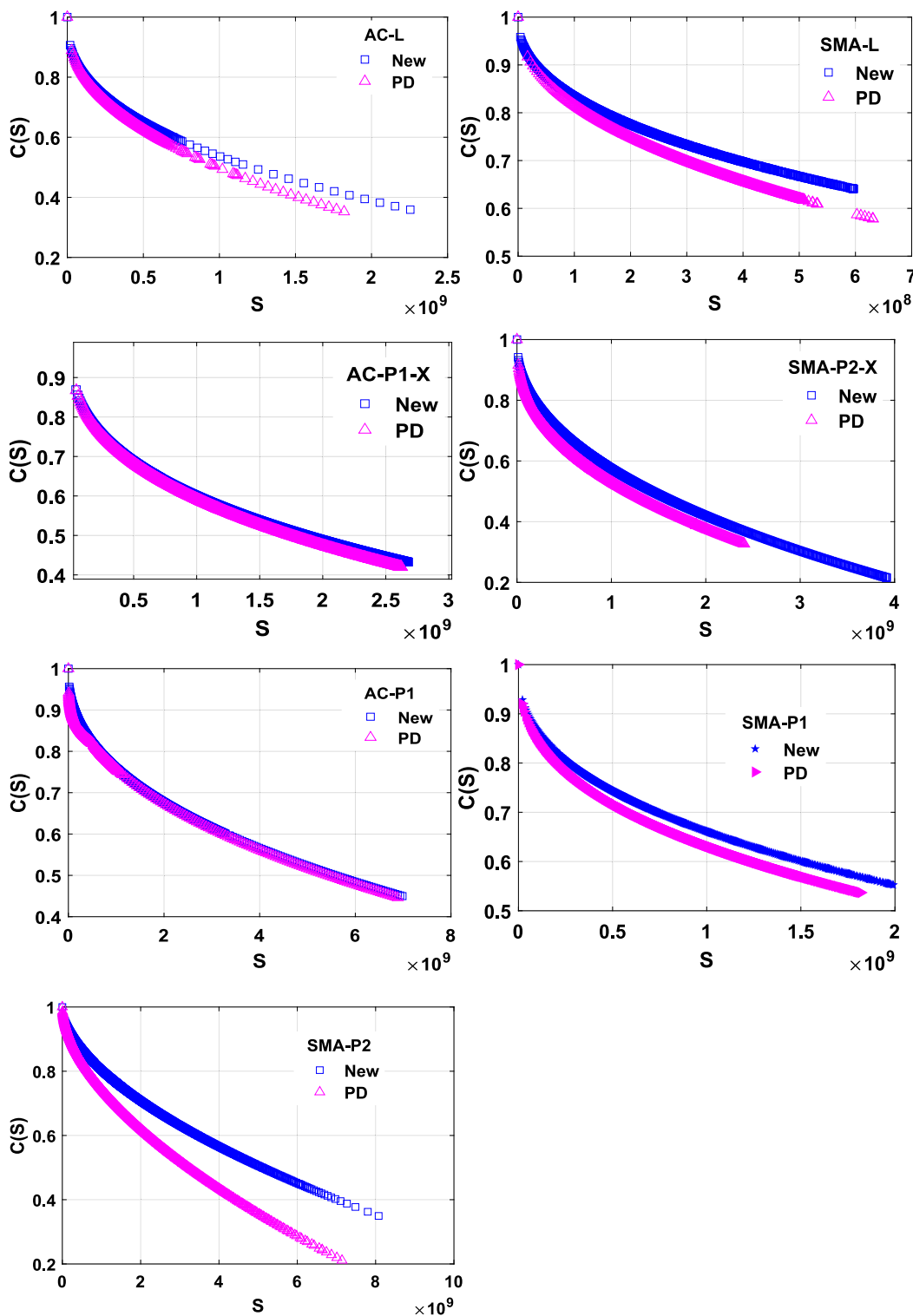


Fig. 13. PD-F sequence - fatigue damage characteristics ($T = 10\text{ }^{\circ}\text{C}$ and target strain $300\text{ }\mu\epsilon$) of new and per-deformed (PD) asphalt mixtures.

5.3. Total dissipated energy

Based on the sequential procedure, the total dissipated energy (DE_T) can be the discrete sum of expended energies on each test specimen. A simple linear summation can be assumed ($DE_T = DE_{PD} + DE_F$). Different behaviors of asphalt concrete such as hardening relaxation, healing, aging etc., can significantly affect the interaction between fatigue and permanent deformation in both the PD-F and F-PD sequences. The effect of temperature and role of material type is also crucial for energy

dissipation. The magnitude of DE_F is found much smaller than the DE_{PD} for both the F-PD and PD-F sequences (Fig. 17). This can be due to the reason that the fatigue test is conducted in strain-controlled mode and the expended energy per cycle DE_F is much smaller than DE_{PD} . On the other hand, the DE_{PD} is a stress-controlled test at high temperature. Thus, DE_T decreases as the flow number increases for the same amount of fatigue damage (DE_F). Fig. 18 shows the total expended energy for the F-PD sequence. The mixtures AC-P1-X and SMA-P2-X are used to explain the F-PD test sequence. The fatigue part is tested at $10\text{ }^{\circ}\text{C}$, and the PD

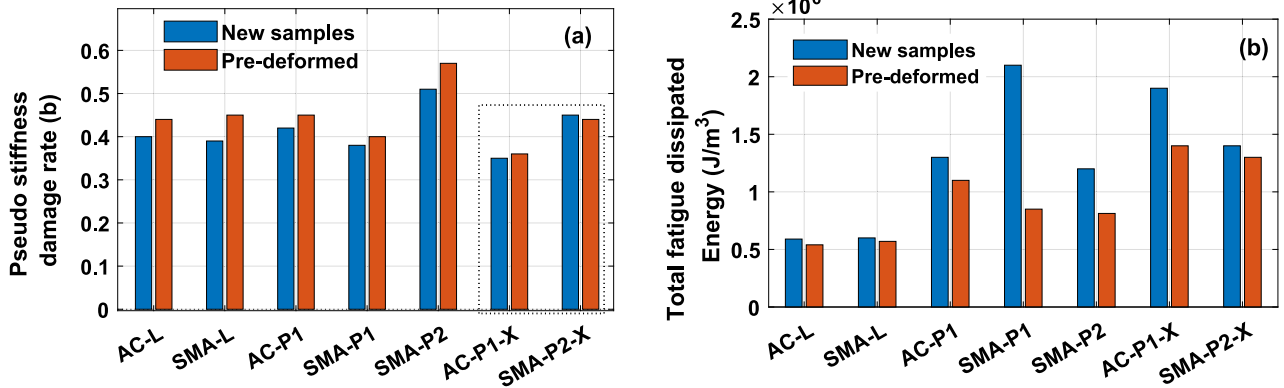


Fig. 14. Effect of pre-deformation on fatigue damage responses (a) parameter *b* (b) total fatigue dissipated energy until failure (50% pseudo stiffness).

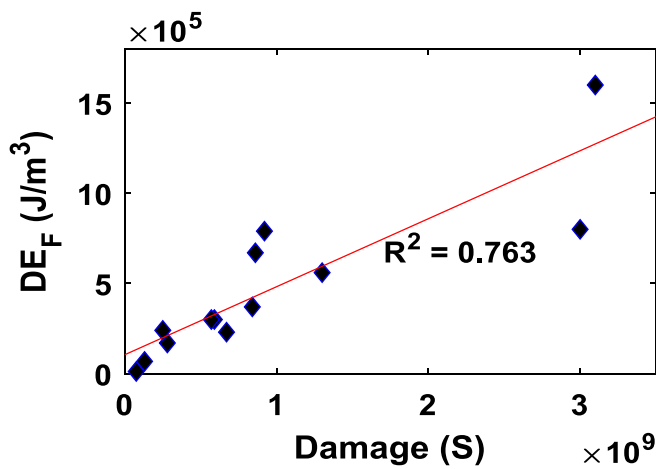


Fig. 15. Damage variable *S* and dissipated energy DE_F on new samples – AC-P1-X. Note: the data points are for different samples tested at different controlled-strain levels.

part is at 30 °C and 40 °C for fatigue and permanent deformation. Based on a simple additive of energies, inconsistency with respect to the flow number is observed (Fig. 18). The dissipation rate is defined as the ratio of total dissipated energy to the corresponding flow number ($\frac{DE_F}{FN}$) and indicate a descending pattern with flow number for both mixtures, as shown in Fig. 18 (a and b). It should be underlined that the total dissipation energy is dependent on sequence and the damage interaction will affect the total dissipated energy in a nonlinear manner both in the F-PD and PD-F sequences. Hence, the total dissipated energies in the two

sequences (DE_{F-PD} and DE_{PD-F}) will be different.

5.4. Discussion

The mechanistic prediction of damage in asphalt pavement has been the focus of study in last recent decades. Asphalt concrete is exposed to cyclic load from traffic and undergo a creep-recovery process in its service life, and two main damage evolve in the form of stiffness deterioration (fatigue cracking) and viscoplastic strain (permanent deformation). From the literature study, it is evident that the interaction between these two dominant damage modes was not presented in detailed. However, field observations have shown the mutual progression of the two damage on the pavement surface along the longitudinal wheel path.

In this study, the experimental investigation of seven different asphalt mixtures is conducted by testing each specimen for fatigue and then for permanent deformation at low and high temperatures respectively and vice versa. The sequential test procedure is proposed to introduce the effect of pre-cracking on the permanent deformation response (in the F-PD sequence) and strain-hardening on the fatigue cracking (in the PD-F sequence). Here, temperature is considered as a factor in the sequential damage and for the testing. Most standard laboratory tests utilize gyratory compacted samples for fatigue and permanent deformation due the difficulty of getting field cored samples longer than 40- or 50-mm for fatigue and permanent deformation tests. The sequential test approach can be used to resolve and investigate the influence of pre-fatigue on deformation and vice versa using longer sample sizes. Thus, the consideration of strain hardening in fatigue test and the pre-cracking in permanent deformation is a reasonable way to characterize interaction between the two damages and try to simulate the field condition.

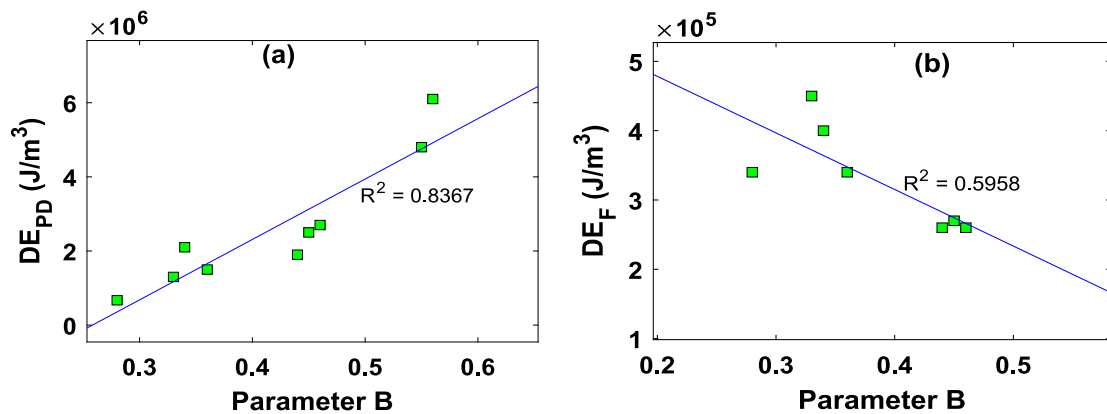


Fig. 16. Effect of pre-fatigue damage on permanent deformation rate – the F-PD sequence (a) DE_{PD} of pre-fatigued samples (b) initial DE_F of samples used for PD test.

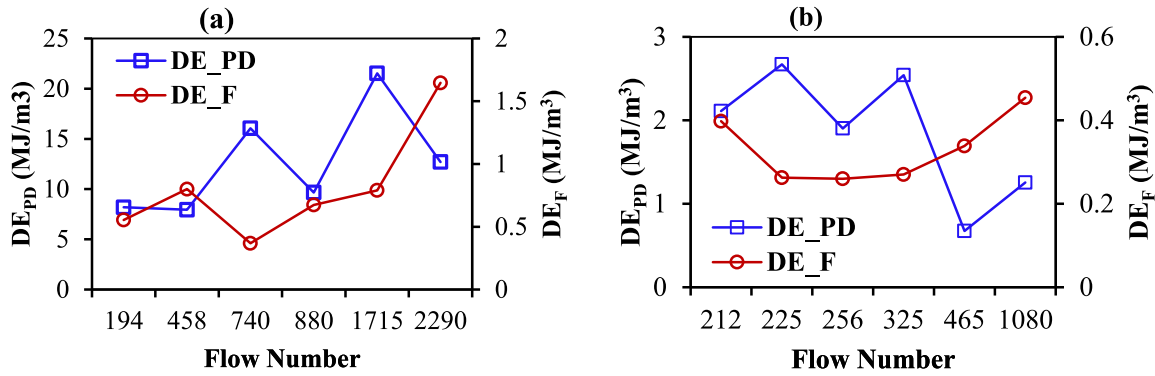


Fig. 17. Dissipated energies of pre-fatigued samples in F-PD sequence: (a) AC-P1-X fatigue at 10 °C and PD at 30 °C and 2 MPa (b) SMA-P2-X fatigue at 10 °C and PD at 40 °C, 0.65 MPa.

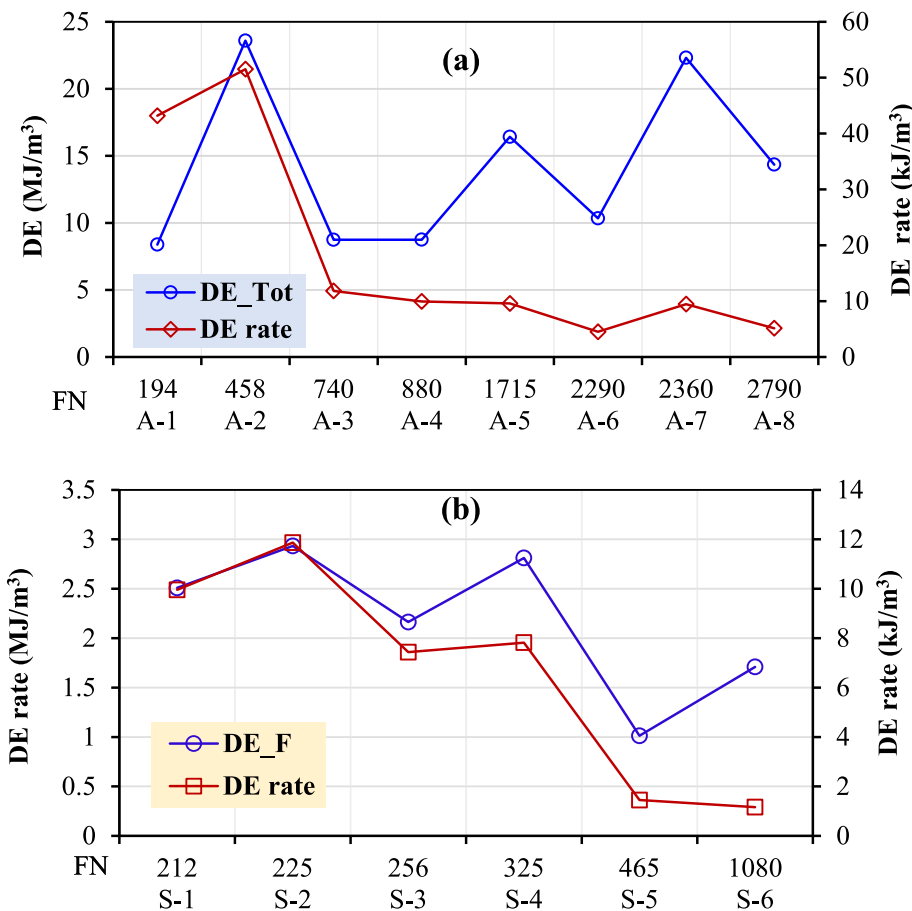


Fig. 18. Correlation of total dissipated energy and flow numbers in F-PD sequence (a) AC-P1-X, PD at 30 °C (b) SMA-P2-X, PD at 40 °C.

First, the linear viscoelastic responses of mixes are analyzed using dynamic modulus test and the time-temperature superposition principle. The respective damages are quantified using the energy and continuum approaches. In the energy approach, the total dissipated energy is computed by assuming a simple linear addition of expended energies on each specimen tested in F-PD and PD-F sequences. The discreteness of energy per cycle is an advantage for simplicity but can be inefficient to consider the microstructural changes in a continuous time history. The interaction between deformation and fatigue damages is believed to be a complex phenomenon due to the thermo-piezo-rheological, healing, hardening-relaxation behaviors of asphaltic materials. The continuum method is the most comprehensive method for the time-dependent (history) of damage evolution and has the advantage of damage

coupling in continua.

From experimental observation and analyses, the PD-F sequence is more plausible and suitable for experimentation, and the continuum method is applied conveniently to model the fatigue part of the sequence (section 5.1.1). In most pavements, permanent deformation expected before fatigue cracking initiation. The PD part of test in the PD-F sequence should be performed with attention so that the specimen will not fail beyond steady-state stage or flow number. Some asphalt mixes may not have all the three distinct creep phases. Therefore, the PD part of PD-F sequence needs careful consideration so that only strain hardening is induced not micro-cracks in the specimen. On the other hand, the F-PD sequence is observed to be challenging to quantify the effect of fatigue cracking on the permanent deformation due to

relaxation and healing effects at high temperature during conditioning.

Furthermore, the sequential test approach offers saving in both material and sample preparation time. A single specimen is utilized for three tests i.e., dynamic modulus, fatigue, and creep-recovery (depending on either the F-PD or PD-F sequence). A framework can be developed and standardized to investigate the sequential test procedure for various levels of pre-deformation or pre-crack as a function of material properties, temperature, stress and strain levels, etc. In general, the study explored the interaction of fatigue and permanent deformation damages and verified the proposed test procedure and models using extensive test data from seven asphalt mixtures produced in laboratory and mixes collected from asphalt production plants.

6. Conclusion

The focus of this study is the experimental investigation of permanent deformation and fatigue damage of asphalt concrete mixes using repeated creep-recovery and uniaxial fatigue tests, respectively. The interaction between the two damage was explored using the energy and continuum approaches on seven asphalt mixes.

- A new permanent deformation failure criterion is proposed using the dissipated energy ratio (DER) and validated using different new and aged asphalt concrete samples. A new post flow number creep phase is found in the shear deformation stage that marks the formation of macro-cracks at the end of shear endurance limit.
- A sequential test procedure (STP) is proposed to investigate the interaction between fatigue (F) and permanent deformation (PD) damage in two orders – *the F-PD and PD-F sequences*. The sequential damage assumption is found simple and effective approach to characterize damage interaction using the existing conventional test protocols.
- The PD-F sequence has shown that permanent deformation (*strain hardening*) is the cause high fatigue damage rate, which agrees with the literature and field observations. The finding ascertains that the fatigue test using new samples can overestimate fatigue life of asphalt mixtures.
- In the F-PD sequence, the effect of pre-fatigue cracking up to 40 % initial stiffness at low or intermediate temperatures is found marginal on permanent deformation at 30 °C and 40 °C. Healing and relaxation are the likely reasons for this phenomenon.
- Aged and laboratory mixed samples are found prone to high fatigue damage, and the effect of strain hardening on fatigue is highly pronounced on stone mastic asphalt (SMA).
- The energy method is simple and straightforward, but the discreteness of energy quantity can be the limitation for accurate characterization of damage in continua. A nonlinear interactive damage model should be considered for accurate time-history characterization of fatigue-permanent deformation interaction.

CRedit authorship contribution statement

Mequanent Mulugeta Alammie: Conceptualization, Methodology, Data curation, Writing – original draft, Visualization. **Ephrem Tadesse:** Conceptualization, Supervision, Writing – review & editing. **Inge Hoff:** Conceptualization, Supervision, Writing – review & editing.

Declaration of Competing Interest

The authors declare the following financial interests/personal relationships which may be considered as potential competing interests: Mequanent Mulugeta Alammie reports financial support was provided by University of Agder Department of Engineering sciences.

Data availability

Data will be made available on request.

References

- [1] M. Zaumanis, L.D. Poulikakos, M.N. Partl, Performance-based design of asphalt mixtures and review of key parameters, *Materials & Design* 141 (2018) 185–201.
- [2] N. Roy, A. Veeraragavan, J.M. Krishnan, Influence of confinement pressure and air voids on the repeated creep and recovery of asphalt concrete mixtures, *International Journal of Pavement Engineering* 17 (2) (2016) 133–147.
- [3] D. Perraton, H. Di Benedetto, C. Sauzéat, C. De La Roche, W. Bankowski, M. Partl, J. Grenfell, Rutting of bituminous mixtures: wheel tracking tests campaign analysis, *Materials and Structures* 44 (5) (2011) 969–986.
- [4] J. Lundberg, S. Janhäll, M. Gustafsson, S. Erlingsson, Calibration of the swedish studded tyre abrasion wear prediction model with implication for the NORTRIP road dust emission model, *International Journal of Pavement Engineering* (2019) 1–15.
- [5] H. Di Benedetto, T. Gabet, J. Grenfell, D. Perraton, C. Sauzéat, D. Bodin, *Mechanical testing of bituminous mixtures*, Springer, Netherlands, 2013, pp. 143–256.
- [6] M.M. Karimi, N. Tabatabaee, B. Jahangiri, M.K. Darabi, Constitutive modeling of hardening-relaxation response of asphalt concrete in cyclic compressive loading, *Construction and Building Materials* 137 (2017) 169–184.
- [7] V. Subramanian, M.N. Guddati, Y. Richard Kim, A viscoplastic model for rate-dependent hardening for asphalt concrete in compression, *Mechanics of Materials* 59 (2013) 142–159.
- [8] M.K. Darabi, R.K. Abu Al-Rub, E.A. Masad, C.-W. Huang, D.N. Little, A modified viscoplastic model to predict the permanent deformation of asphaltic materials under cyclic-compression loading at high temperatures, *International Journal of Plasticity* 35 (2012) 100–134.
- [9] F. Zhou, T. Scullion, Discussion: Three stages of permanent deformation curve and rutting model, *International Journal of Pavement Engineering* 3 (4) (2002) 251–260.
- [10] H. Fang, Q. Liu, L. Mo, B. Javilla, B. Shu, S. Wu, Characterization of three-stage rutting development of asphalt mixtures, *Construction and Building Materials* 154 (2017) 340–348.
- [11] M. Ameri, A.H. Sheikhmotevali, A. Fasihpour, Evaluation and comparison of flow number calculation methods, *Road Materials and Pavement Design* 15 (1) (2014) 182–206.
- [12] Y. Zhang, R. Luo, R.L. Lytton, Characterizing permanent deformation and fracture of asphalt mixtures by using compressive dynamic modulus tests, *Journal of Materials in Civil Engineering* 24 (7) (2012) 898–906.
- [13] M. Gajewski, W. Bańkowski, A.C. Pronk, Evaluation of fatigue life of high modulus asphalt concrete with use of three different definitions, *International Journal of Pavement Engineering* 21 (14) (2020) 1717–1728.
- [14] S. Son, I.M. Said, I.L. Al-Qadi, Fracture properties of asphalt concrete under various displacement conditions and temperatures, *Construction and Building Materials* 222 (2019) 332–341.
- [15] M. Ling, X. Luo, Y. Chen, F. Gu, R.L. Lytton, Mechanistic-empirical models for top-down cracking initiation of asphalt pavements, *International Journal of Pavement Engineering* (2018) 1–10.
- [16] E.F. de Freitas, P. Pereira, L. Picado-Santos, A.T. Papagiannakis, Effect of construction quality, temperature, and rutting on initiation of Top-Down cracking, *Transportation Research Record* 1929 (1) (2005) 174–182.
- [17] L. Ann Myers, R. Roque, B. Birgisson, Propagation mechanisms for Surface-Initiated longitudinal wheelpath cracks, *Transportation Research Record* 1778 (1) (2001) 113–122.
- [18] X. Luo, F. Gu, M. Ling, R.L. Lytton, Review of mechanistic-empirical modeling of top-down cracking in asphalt pavements, *Construction and Building Materials* 191 (2018) 1053–1070.
- [19] S. Mun, M.N. Guddati, Y.R. Kim, Fatigue cracking mechanisms in asphalt pavements with viscoelastic continuum damage Finite-Element program, *Transportation Research Record: Journal of the Transportation Research Board* 1896 (1) (2004) 96–106.
- [20] I. Onifade, B. Birgisson, R. Balieu, Energy-based damage and fracture framework for viscoelastic asphalt concrete, *Engineering Fracture Mechanics* 145 (2015) 67–85.
- [21] X. Luo, R. Luo, R.L. Lytton, Characterization of fatigue damage in asphalt mixtures using pseudostrain energy, *Journal of Materials in Civil Engineering* 25 (2) (2013) 208–218.
- [22] T. Svasdisant, M. Schorsch, G.Y. Baladi, S. Pinyosunun, Mechanistic analysis of Top-Down cracks in asphalt pavements, *Transportation Research Record: Journal of the Transportation Research Board* 1809 (1) (2002) 126–136.
- [23] X. Luo, R. Luo, R.L. Lytton, Energy-based mechanistic approach for damage characterization of pre-flawed visco-elasto-plastic materials, *Mechanics of Materials* 70 (2014) 18–32.
- [24] Y. Zhang, X. Luo, R. Luo, R.L. Lytton, Crack initiation in asphalt mixtures under external compressive loads, *Construction and Building Materials* 72 (2014) 94–103.
- [25] M.K. Darabi, R.K. Abu Al-Rub, E.A. Masad, C.-W. Huang, D.N. Little, A thermo-viscoelastic-viscoplastic-viscodamage constitutive model for asphaltic materials, *International Journal of Solids and Structures* 48 (1) (2011) 191–207.

- [26] M. Alamnie, E. Tadesse, I. Hoff, Permanent deformation and fatigue damage interaction in asphalt concrete using energy approach, *Eleventh International Conference on the Bearing Capacity of Roads, Railways and Airfields*, Volume 3 (2022) 118–127.
- [27] E. Levenberg, J. Uzan, Triaxial Small-Strain Viscoelastic-Viscoplastic modeling of asphalt aggregate mixes, *Mechanics of Time-Dependent Materials* 8 (4) (2004) 365–384.
- [28] A. Graziani, F. Cardone, A. Virgili, F. Canestrari, Linear viscoelastic characterisation of bituminous mixtures using random stress excitations, *Road Materials and Pavement Design* 20 (sup1) (2019) S390–S408.
- [29] M.M. Alamnie, E. Tadesse, I. Hoff, Thermo-piezo-rheological characterization of asphalt concrete, *Construction and Building Materials* 329 (2022), 127106.
- [30] R. Luo, H. Liu, Y. Zhang, Characterization of linear viscoelastic, nonlinear viscoelastic and damage stages of asphalt mixtures, *Construction and Building Materials* 125 (2016) 72–80.
- [31] W. Cao, Y.R. Kim, A viscoplastic model for the confined permanent deformation of asphalt concrete in compression, *Mechanics of Materials* 92 (2016) 235–247.
- [32] J. Zhang, Z. Fan, K. Fang, J. Pei, L. Xu, Development and validation of nonlinear viscoelastic damage (NLVED) model for three-stage permanent deformation of asphalt concrete, *Construction and Building Materials* 102 (2016) 384–392.
- [33] M.M. Alamnie, E. Tadesse, I. Hoff, Advances in permanent deformation modeling of asphalt concrete—A review, *Materials* 15 (10) (2022) 3480.
- [34] R.A. Schapery, Nonlinear viscoelastic and viscoplastic constitutive equations with growing damage, *International Journal of Fracture* 97 (1/4) (1999) 33–66.
- [35] N.H. Gibson, C.W. Schwartz, R.A. Schapery, M.W. Witzczak, Viscoelastic, viscoplastic, and damage modeling of asphalt concrete in unconfined compression, *Transportation Research Record: Journal of the Transportation Research Board* 1860 (1) (2003) 3–15.
- [36] R.A. Schapery, Correspondence principles and a generalized J integral for large deformation and fracture analysis of viscoelastic media, *International Journal of Fracture* 25 (3) (1984) 195–223.
- [37] R. Schapery, A theory of mechanical behavior of elastic media with growing damage and other changes in structure, *Journal of the Mechanics and Physics of Solids* 38 (2) (1990) 215–253.
- [38] H.-J. Lee, J.S. Daniel, Y.R. Kim, Continuum damage Mechanics-Based fatigue model of asphalt concrete, *Journal of Materials in Civil Engineering* 12 (2) (2000) 105–112.
- [39] B.S. Underwood, C. Baek, Y.R. Kim, Simplified viscoelastic continuum damage model as platform for asphalt concrete fatigue analysis, *Transportation Research Record: Journal of the Transportation Research Board* 2296 (1) (2012) 36–45.
- [40] Y.R. Kim, M.N. Guddati, B.S. Underwood, T.Y. Yun, V. Subramanian, S. Savadatti, Development of a multiaxial viscoelastoplastic continuum damage model for asphalt mixtures, in: C. North Carolina State University. Dept. of Civil, E. Environmental (Eds.) *Federal Highway Administration*, 2009.
- [41] B.S. Underwood, Y.R. Kim, M.N. Guddati, Improved calculation method of damage parameter in viscoelastic continuum damage model, *International Journal of Pavement Engineering* 11 (6) (2010) 459–476.
- [42] J.S. Daniel, Y.R. Kim, Development of a simplified fatigue test and analysis procedure using a viscoelastic, continuum damage model (with discussion), *Journal of the Association of Asphalt Paving Technologists* 71 (2002).
- [43] E. Masad, V.T.F. Castelo Branco, D.N. Little, R. Lytton, A unified method for the analysis of controlled-strain and controlled-stress fatigue testing, *International Journal of Pavement Engineering* 9 (4) (2008) 233–246.
- [44] S. Shen, G.D. Airey, S.H. Carpenter, H. Huang, A dissipated energy approach to fatigue evaluation, *Road Materials and Pavement Design* 7 (1) (2006) 47–69.
- [45] K.A. Ghuzlan, S.H. Carpenter, Energy-Derived, Damage-Based failure criterion for fatigue testing, *Transportation Research Record: Journal of the Transportation Research Board* 1723 (1) (2000) 141–149.
- [46] M. Shadman, H. Ziari, Laboratory evaluation of fatigue life characteristics of polymer modified porous asphalt: A dissipated energy approach, *Construction and Building Materials* 138 (2017) 434–440.
- [47] J. Lemaitre, A. Plumtree, Application of damage concepts to predict Creep-Fatigue failures, *Journal of Engineering Materials and Technology* 101 (3) (1979) 284–292.
- [48] R.P. Skelton, D. Gandy, Creep – fatigue damage accumulation and interaction diagram based on metallographic interpretation of mechanisms, *Materials at High Temperatures* 25 (1) (2008) 27–54.
- [49] H. Di Benedetto, C. De La Roche, H. Baaj, A. Pronk, R. Lundström, Fatigue of bituminous mixtures, *Materials and Structures* 37 (3) (2004) 202–216.
- [50] M.L. Williams, R.F. Landel, J.D. Ferry, The temperature dependence of relaxation mechanisms in amorphous polymers and other glass-forming liquids, *Journal of the American Chemical Society* 77 (14) (1955) 3701–3707.
- [51] E. Rahmani, M.K. Darabi, D.N. Little, E.A. Masad, Constitutive modeling of coupled aging-viscoelastic response of asphalt concrete, *Construction and Building Materials* 131 (2017) 1–15.
- [52] J. Blanc, T. Gabet, P. Hornych, J.-M. Piau, H. Di Benedetto, Cyclic triaxial tests on bituminous mixtures, *Road Materials and Pavement Design* 16 (1) (2014) 46–69.

Paper F

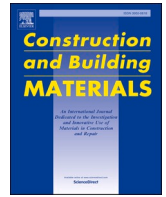
Comparative study of indirect tensile test and uniaxial compression test on asphalt mixtures: Dynamic modulus and stress-strain state

Hao Chen, Mequanent Mulugeta Alamnie, Diego Maria Barbieri, Xuemei Zhang, Gang Liu, Inge Hoff. Construction and Building Materials, 366 (130187), 2023. doi: [10.1016/j.conbuildmat.2022.130187](https://doi.org/10.1016/j.conbuildmat.2022.130187)



Contents lists available at ScienceDirect

Construction and Building Materials

journal homepage: www.elsevier.com/locate/conbuildmat

Comparative study of indirect tensile test and uniaxial compression test on asphalt mixtures: Dynamic modulus and stress-strain state

Hao Chen^{a,*}, Mequanent Mulugeta Alamnie^b, Diego Maria Barbieri^{a,c}, Xuemei Zhang^a, Gang Liu^d, Inge Hoff^a

^a Department of Civil and Environmental Engineering, Norwegian University of Science and Technology, Trondheim 7491, Norway

^b Department of Engineering Sciences, University of Agder, Grimstad 4879, Norway

^c Department of Mechanical and Structural Engineering and Materials Science, University of Stavanger, Stavanger 4021, Norway

^d School of Materials Science and Engineering, Wuhan University of Technology, Wuhan 430070, China

ARTICLE INFO

Keywords:

Indirect tensile test
Uniaxial compression test
Asphalt mixture
Master curve
Dynamic modulus
Stress–strain state

ABSTRACT

Dynamic modulus is an essential parameter for the performance characterisation of asphalt materials for performance prediction and pavement design. The Indirect Tensile (IDT) test and the Uniaxial Compression (UC) test are both well-known experiments performed in the laboratory to characterise the dynamic modulus of asphalt mixtures over a range of temperatures and loading frequencies. A considerable amount of research has investigated the difference between two test modes, while few studies analysed the fundamental difference in stress–strain distributions for the two test setups. This work aims at comparing the effect of the two test methods on dynamic modulus of asphalt mixtures, as well as stress–strain state. For these purposes, two types of mixtures commonly employed to build road surface layers, namely Asphalt Concrete (AC) and Stone Mastic Asphalt (SMA), were created and tested. The specimens were prepared with a gyratory compactor. The master curves of dynamic modulus and the stress–strain states obtained from the two testing procedures were compared. The dynamic modulus and phase angle results are almost identical for medium frequency and temperature, whereas the results exhibit significant discrepancies for lower and higher frequency values. AC 11 and SMA 11 mixtures show differences in comparison between the two tests. Moreover, the strains measured by the IDT test are variable and the strains obtained from the UC test stabilise around 40 $\mu\epsilon$. Similarly, both tests have poor strain control at 40 °C. The values of normalised stresses measured by the IDT test are approximately 3.26 and 2.34 times greater than the ones measured by the UC test for AC 11 and SMA 11 mixtures, respectively. In general, the results of the mechanical characterisation of the asphalt mixtures conducted using both tests are similar. The IDT test has the advantage of sample size for sample preparation methods in both laboratory and field, and the UC test has a better deformation control at low and medium temperatures.

1. Introduction

In the development of pavement design, the Mechanistic-Empirical (ME) pavement design approach applicable to various materials and environmental conditions has been gradually adopted to replace previous empirical design approaches [1,2]. The mechanical characterisation of road construction materials is necessary to predict the response of the structure according to the ME pavement design. When it comes to asphalt materials, the dynamic modulus is an essential parameter for engineering computations [3]. The dynamic modulus of asphalt

mixtures mainly depends on the temperature and the loading time due to its viscoelastic properties [4–6]. The Uniaxial Compression (UC) test, which can be conducted at different temperatures and frequencies with a dynamic loading form, is the standard test method for the determination of dynamic modulus of asphalt mixture in the ME pavement design guide [7]. The dynamic modulus is calculated by dividing the peak-to-peak stress by the peak-to-peak strain for the asphalt mixture subjected to a sinusoidal load. Afterwards, the dynamic modulus master curve is constructed according to the time–temperature superposition principle [8] to predict the dynamic modulus of asphalt mixture over a

* Corresponding author.

E-mail addresses: hao.chen@ntnu.no (H. Chen), mequanent.m.alamnie@uia.no (M.M. Alamnie), diegomb271@gmail.com (D.M. Barbieri), xuemei.zhang@ntnu.no (X. Zhang), liug@whut.edu.cn (G. Liu), inge.hoff@ntnu.no (I. Hoff).

<https://doi.org/10.1016/j.conbuildmat.2022.130187>

Received 10 October 2022; Received in revised form 25 November 2022; Accepted 20 December 2022

Available online 26 December 2022

0950-0618/© 2022 The Author(s). Published by Elsevier Ltd. This is an open access article under the CC BY license (<http://creativecommons.org/licenses/by/4.0/>).

Table 1
Physical properties of bitumen 70/100.

Physical property	Unit	Bitumen 70/100	Test standard
Penetration at 25 °C	0.1 mm	92	EN 1426:2015 [22]
Softening point (Ring and Ball)	°C	46.0	EN 1427:2015 [23]

Table 2
Resistance to wear and fragmentation of crushed rock aggregates.

Property	Value	Requirements for AADT > 15 000	Test standard
Micro-Deval coefficient	14.2	≤ 20	EN 1097-1:2011 [24]
Los Angeles value	18.2	≤ 15	EN 1097-2:2020 [25]

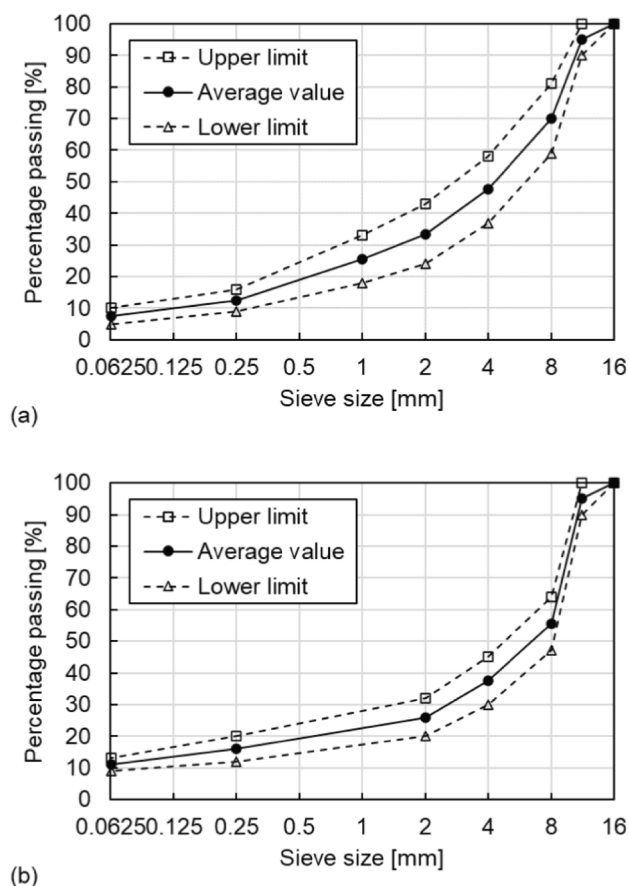


Fig. 1. Grading curves of (a) AC 11 and (b) SMA 11.

Table 3
OBC and voids characteristics of AC 11 and SMA 11.

Asphalt mixture	OBC [%]	Void characteristic (EN 12697-8:2018 [29])			
		V_a [%]	Standard deviation	VFB [%]	Standard deviation
AC 11	5.1 %	3.8 %	0.2 %	77.0 %	1.3 %
SMA 11	5.3 %	4.0 %	0.3 %	77.1 %	1.6 %

wide frequency range. This test method is widely used not only for traditional materials but also for innovative and recycled construction resources [9–11].

The dynamic modulus can be tested on samples produced in the laboratory or from samples cored from a real pavement. However, the thickness of the core sample extracted from the existing pavement is often less than the required height of the UC test. Differently, the Indirect Tensile (IDT) test determines the dynamic modulus according to a biaxial stress state on a thinner specimen [12]. Compared with UC test, the IDT test is largely used thanks to the easiness of operation (e.g., smaller samples) and its suitability to characterise core road samples. Even though the IDT test is commonly used for the evaluation of resilient modulus, strength and fatigue of asphalt mixture, it has been also performed to assess the dynamic modulus. Zaumanis et al. [13] conducted IDT investigation to determine the dynamic modulus of 100 % recycled asphalt mixtures while appraising the suitability of the IDT setup to characterise highly recycled asphalt mixtures. Mollenhauer et al. [14] obtained the stiffness of asphalt mixtures by conducting IDT tests to develop a German ME pavement design. Zhang et al. [15] have adopted the IDT test to compare the change in dynamic modulus of asphalt mixture before and after chemical ageing. The Norwegian Public Roads Administration (NPRA) is currently developing a ME pavement design system and, therefore, needs the creation of a database defining the dynamic modulus for the asphalt mixtures employed in the Nordics pavements [16].

Although both IDT and UC tests can measure the dynamic modulus of asphalt materials, their results show some discrepancies due to the different stress–strain states and test conditions [17]. Understanding these differences is important to select the correct material characterisation testing and to define the pavement design system more accurately. Kim et al. [18] developed an analytical solution to assess the dynamic modulus from the IDT test. In this regard, twelve asphalt mixtures used in North Carolina were tested according to both IDT and UC procedures. The results displayed a little discrepancy in the dynamic modulus master curves. However, Qin et al. [19] found some differences between the two tests in dynamic modulus, phase angle, and shift factor. The dynamic modulus and shift factor measured using the UC test were higher than the corresponding values obtained using the IDT test. As very few studies shed light on the differences between the IDT and the UC testing procedures from the perspective of stress–strain states for Norwegian asphalt mixtures, this work addresses this gap as well as delves into the fundamental difference in stress–strain distributions for the two test setups and provides guidance on test methods for the development of Norwegian ME pavement design.

In this study, Asphalt Concrete (AC) and Stone Mastic Asphalt (SMA) mixtures were characterised as they were commonly used for surfacing road pavements. The mixtures were compressed using a gyratory compactor and the samples were drilled and cut according to the testing requirements. The IDT and UC tests were conducted in the laboratories of the Norwegian University of Science and Technology (NTNU) and the University of Agder (UiA), respectively. The master curves were constructed based on the ME pavement design guide and shift factor function defined by the Williams-Landel-Ferry (WLF) equation. The differences in the values of dynamic modulus, phase angle, shift factor as well as the discrepancies in the stress–strain states for the two tests were analysed.

2. Materials and test methods

2.1. Materials

The bituminous binder employed was type 70/100, which is the most used in Norwegian asphalt pavements. Crushed rocks having magmatic and metamorphic origin as well as limestone filler were used as aggregates [20,21]. The main physical properties of the binder are given in Table 1. The resistance of aggregates to wear and fragmentation is

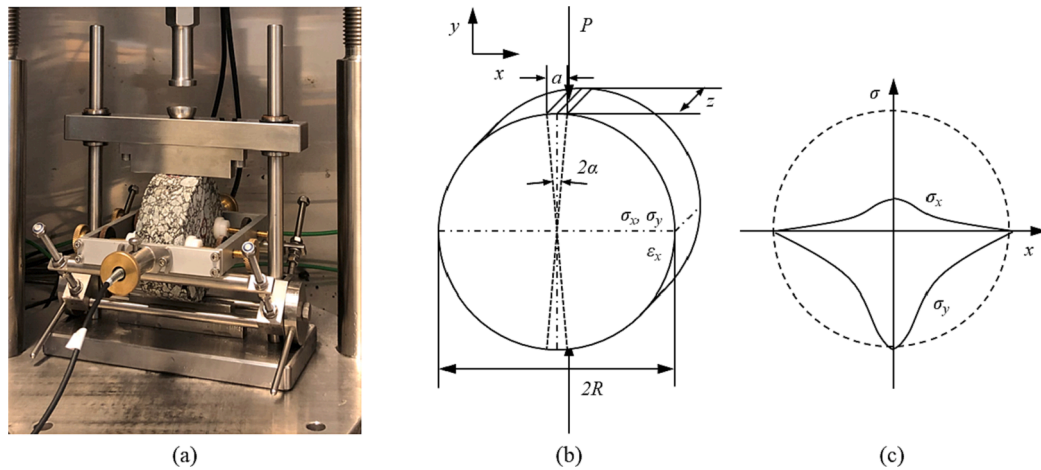


Fig. 2. (a) IDT test setup using UTM, (b) scheme of IDT test specimen subjected to a vertical load and (c) stress distribution.

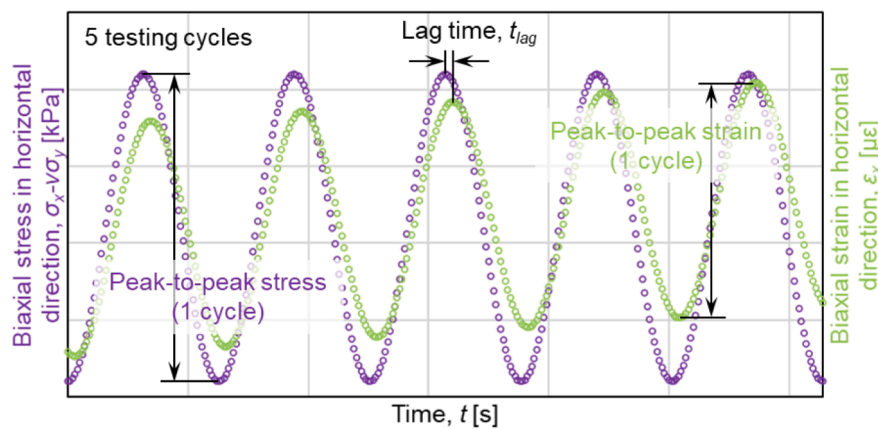


Fig. 3. Schematic trend of stress and strain for IDT test.

specified in Table 2, which fulfils the Norwegian requirements of AC and SMA mixtures with an Annual Average Daily Traffic (AADT) higher than 15 000.

2.2. Sample preparation

Sample preparation is very important for the results from laboratory testing of asphalt and special care was taken to produce samples as homogeneous as possible to compare the two testing methods without any bias from the sample preparation.

The particle size distributions are given in Fig. 1 and the average gradation curves are selected to prepare the tested samples. The Optimum Binder Content (OBC) was determined by the Marshall mixture design. The asphalt mixture specimens were prepared in the laboratory of NTNU using a gyratory compactor (ICT-150RB produced by Invelop Oy, Savonlinna, Finland). The compaction pressure was 620 kPa, and the gyratory angle was set to 17 mrad (0.97°) [26]. The 100 and 115 design gyrations were applied for the AC 11 and SMA 11, respectively [27]. Asphalt cylinders with a diameter of 150 mm and a height of 180 mm were thus obtained; afterwards, IDT specimens (diameter = 100 mm, height = 40 mm) and UC specimens (diameter = 100 mm, height = 150 mm) were drilled and cut. The OBC and the void characteristics including the Air Voids Content (V_a) and the Voids Filled with Binder (VFB) are shown in Table 3, which fulfil the corresponding requirements [28]. Four replicate samples were created for each asphalt mixture type.

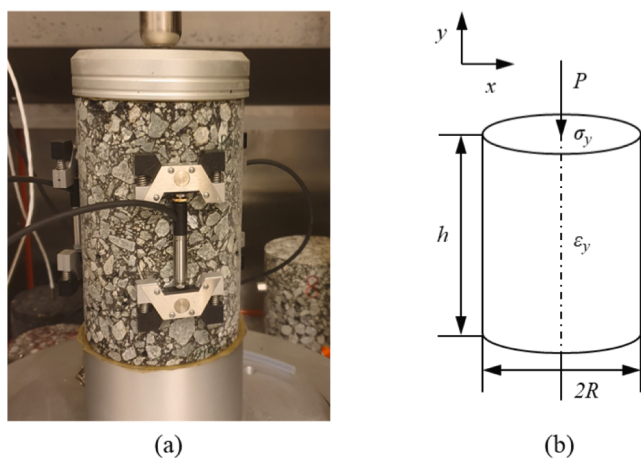


Fig. 4. (a) UC test setup using UTM-130 and (b) scheme of UC specimen subjected to a vertical load.

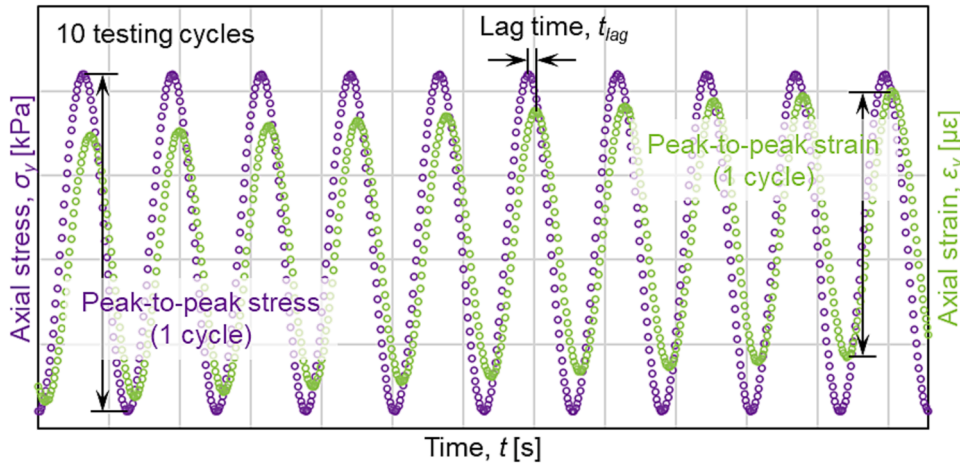


Fig. 5. Schematic trend of stress and strain for UC test.

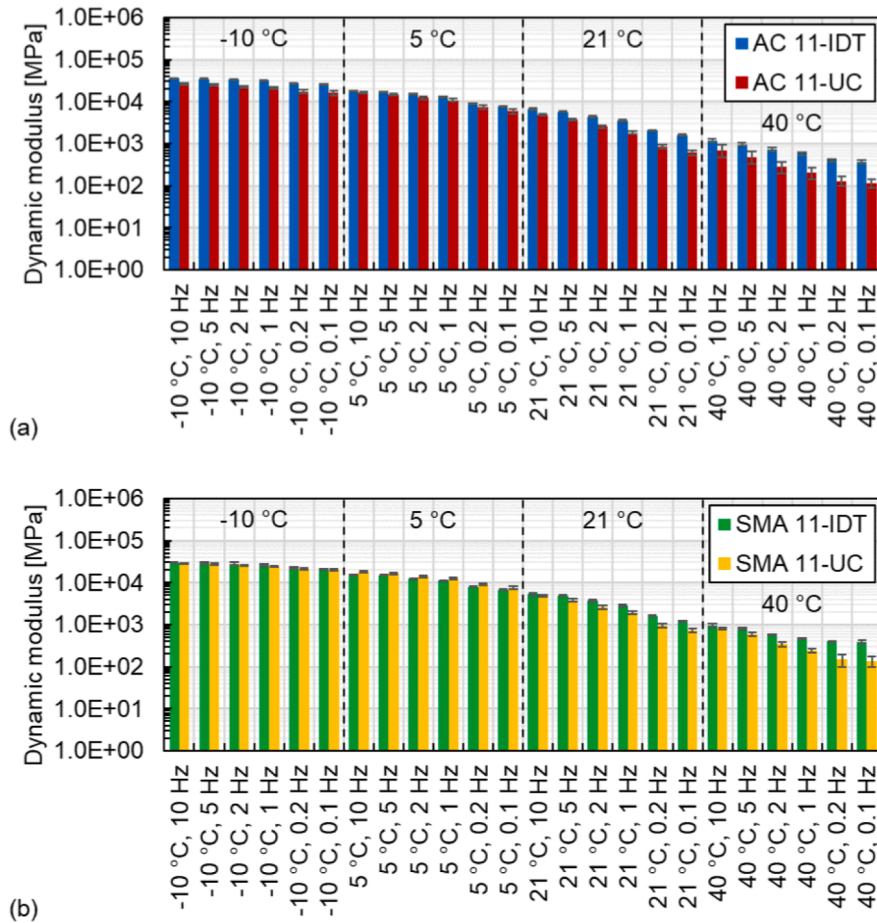


Fig. 6. Dynamic modulus results: (a) AC 11 and (b) SMA 11.

A total of 16 samples were tested and they were denominated as AC 11-IDT, AC 11-UC, SMA 11-IDT and SMA 11-UC.

2.3. Dynamic modulus tests

2.3.1. Indirect tensile test

The cyclic IDT test was performed by a servo-pneumatic Universal Testing Machine (UTM) produced by Cooper Technology exerting a controlled harmonic sinusoidal load with a haversine wave. Two Linear

Variable Differential Transformers (LVDT) were used on both sides in the horizontal direction. The test was conducted in accordance with EN 12697-26 [30] at frequencies of 10, 5, 2, 1, 0.2 and 0.1 Hz and the temperatures of -10, 5, 21 and 40 °C to obtain a broad and continuous dynamic modulus master curve for measured values. The applied loads were adjusted to keep the initial horizontal strain amplitude in a range between 50 με to 100 με for every testing temperature and frequency. The IDT test is regarded as a stress-strain dual control test.

The scheme of the IDT test is shown in Fig. 2; the x and y axes are

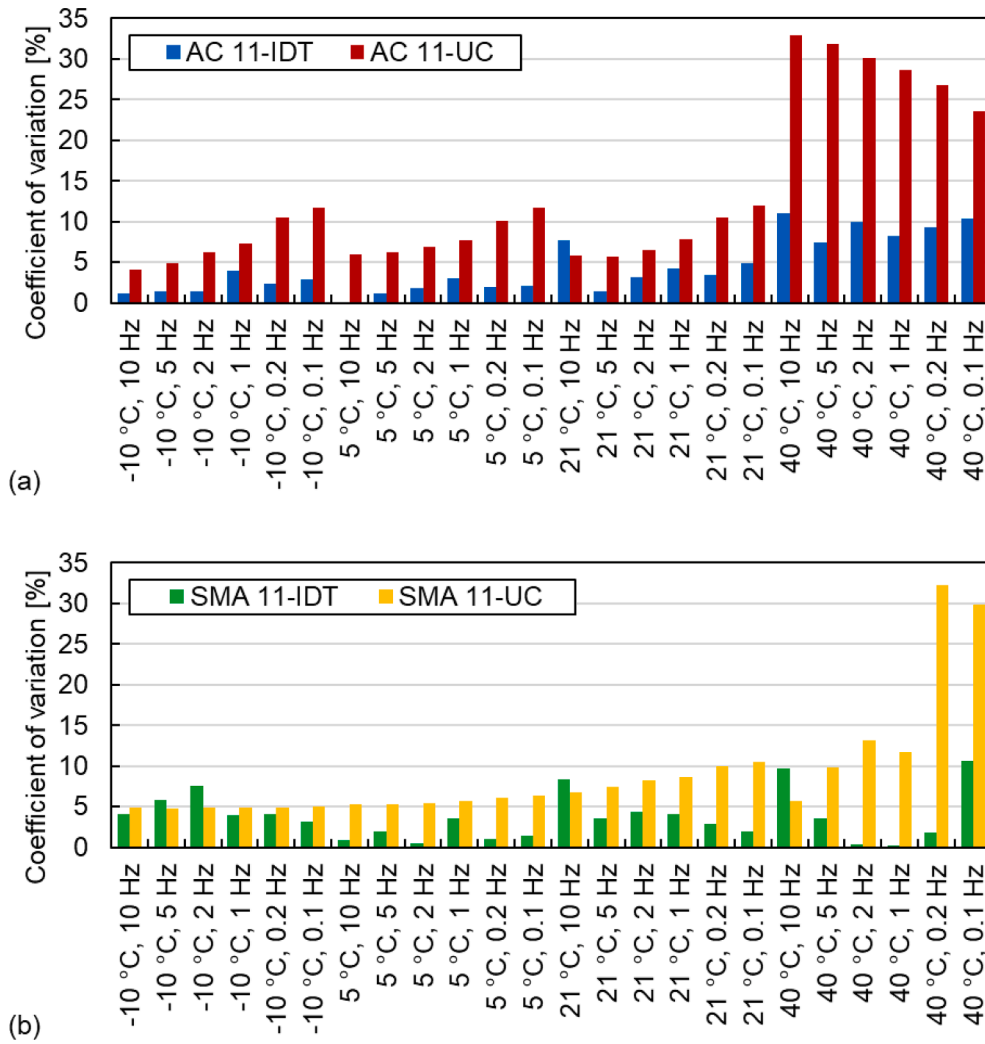


Fig. 7. Coefficient of variation of dynamic modulus results: (a) AC 11 and (b) SMA 11.

defined as the horizontal and vertical direction, respectively. Based on the linear viscoelastic solution the stress and strain in the horizontal direction of the IDT test specimen are used to calculate the dynamic modulus [18]. The stress distribution is presented in Fig. 2(c). The coordinate axis between the position in the horizontal direction and the stress at this position was established. The IDT test specimen was applied a vertical harmonic sinusoidal load, P , which can be expressed as shown in Eq. (1). Along the horizontal diameter of the IDT specimen the horizontal stress, $\sigma_x(x)$, and the vertical stress, $\sigma_y(x)$, can be evaluated as defined by Eq. (2) and Eq. (3), respectively [31–33].

$$P = P_0 \cdot e^{i\omega t} = P_0 [\cos(\omega t) + i \sin(\omega t)] \quad (1)$$

$$\sigma_x(x) = \frac{2P}{\pi a z} \left[\frac{(1 - x^2/R^2) \sin 2\alpha}{1 + 2(x^2/R^2) \cos 2\alpha + x^4/R^4} - \tan^{-1} \left(\frac{1 - x^2/R^2}{1 + x^2/R^2} \tan \alpha \right) \right] \quad (2)$$

$$= \frac{2P}{\pi a z} [f(x) - g(x)]$$

$$\sigma_y(x) = \frac{2P}{\pi a z} \left[\frac{(1 - x^2/R^2) \sin 2\alpha}{1 + 2(x^2/R^2) \cos 2\alpha + x^4/R^4} + \tan^{-1} \left(\frac{1 - x^2/R^2}{1 + x^2/R^2} \tan \alpha \right) \right] \quad (3)$$

$$= -\frac{2P}{\pi a z} [f(x) + g(x)]$$

where x is the distance from the origin along the abscissa, P_0 is the

amplitude of the sinusoidal load, ω is the angular frequency of the sinusoidal load, t is time, a is the loading strip width, z is the thickness of the sample and R is the radius of the sample. The horizontal strain, $\epsilon_x(x, t)$, is expressed:

$$\epsilon_x(x, t) = \frac{1}{E^*} [\sigma_x(x) - \nu \sigma_y(x)] \quad (4)$$

$$= \frac{2P_0}{E^* \pi a z} e^{i(\omega t - \varphi)} [(\nu + 1)f(x) + (\nu - 1)g(x)]$$

where E^* is the dynamic modulus, φ is the phase angle and ν is the Poisson's ratio. The total deformation between $-R$ and R at the horizontal central axis, $\Delta H(t)$, is given:

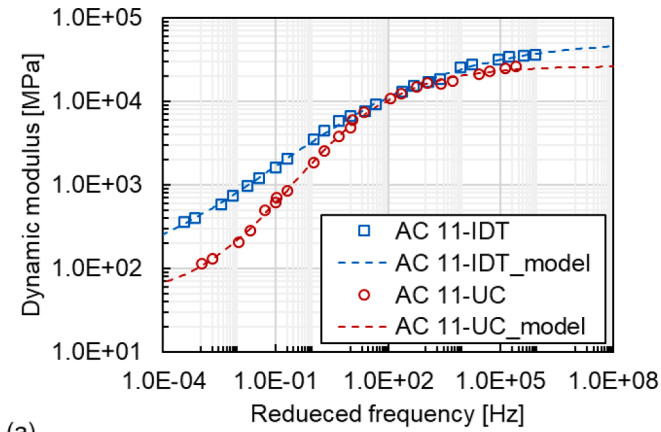
$$\Delta H(t) = \int_{-R}^R \epsilon_x(x, t) dx \quad (5)$$

$$= \frac{2P_0}{E^* \pi a z} e^{i(\omega t - \varphi)} \left[(\nu + 1) \int_{-R}^R f(x) dx + (\nu - 1) \int_{-R}^R g(x) dx \right]$$

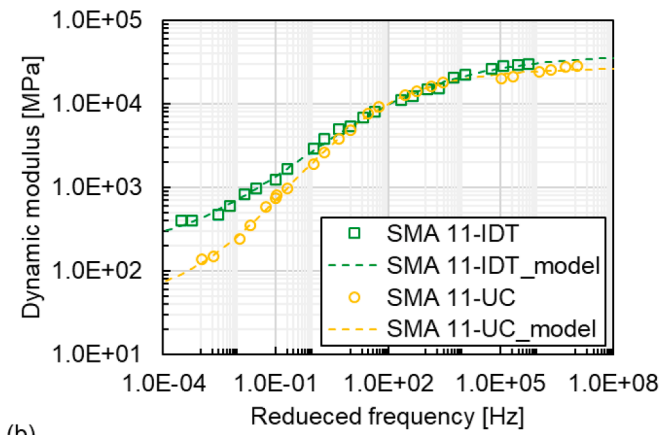
$$= \frac{2P_0}{E^* \pi a z} e^{i(\omega t - \varphi)} A$$

Therefore, in the IDT mode, the dynamic modulus from the horizontal deformation can be expressed as:

$$E^* = |E^*| \cdot e^{i\varphi} = \frac{2P_0 \sin(\omega t - \varphi)}{\pi a z \Delta H(t)} A \quad (6)$$



(a)



(b)

Fig. 8. Master curves of dynamic modulus: (a) AC 11 and (b) SMA 11.

Table 4

The fitting parameters and statistical parameters of the dynamic modulus master curves for asphalt mixtures.

Fitting parameter		AC 11-IDT	SMA 11-IDT	AC 11-UC	SMA 11-UC
Sigmoidal function	δ	1.755	2.152	1.594	1.575
	α	2.974	2.431	2.823	2.847
	β	-0.382	-0.106	-0.385	-0.432
	γ	0.413	0.504	0.701	0.650
	C_1	33.802	49.893	19.297	11.018
WLF equation	C_2	243.539	356.001	166.369	87.622
	<i>Goodness of fit statistics</i>				
S_e		724.649	673.983	798.555	1098.795
S_y		12566.958	10345.098	8937.466	10067.358
S_e/S_y		0.058	0.065	0.089	0.109
R^2		0.997	0.996	0.992	0.988

where $|E^*|$ is the norm of the dynamic modulus.

The schematic trend of the stress–strain state for the IDT test is shown in Fig. 3. In the IDT test mode, the value of biaxial stress and strain in the horizontal direction were recorded. The peak-to-peak stress and strain of the specified five cycles per test condition according to EN 12697-26 [30] are used to determine the dynamic modulus. For the cyclic IDT test, the vertical load and the peak-to-peak deformation were recorded to calculate the dynamic modulus based on Eq. (6). The test data is analysed to obtain the dynamic modulus of the IDT test specimen under a certain test condition. The strain response lags to the stress due to the viscoelastic behaviour of asphalt materials, as shown in Fig. 3. The phase angle is to describe the lag of the strain response, which is equal to the lag time, t_{lag} , multiplied by the angular frequency. The stress and

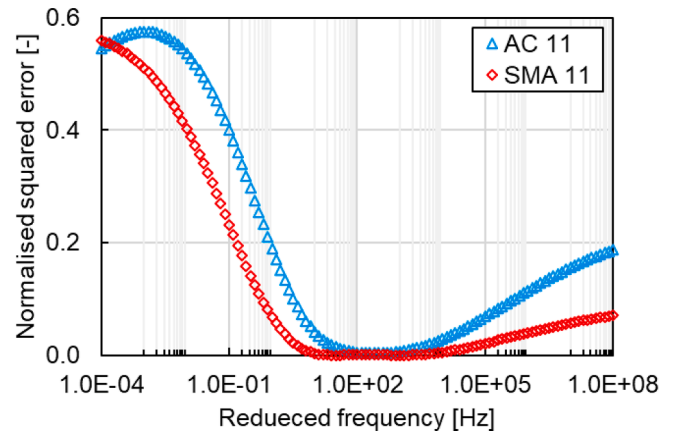


Fig. 9. NSE of dynamic modulus between two test modes for AC 11 and SMA 11.

strain as a function of the time are expressed in Eq. (7) and Eq. (8).

$$\varepsilon(t) = \varepsilon_0 \sin(\omega t) \quad (7)$$

$$\sigma(t) = \sigma_0 \sin(\omega t - \varphi) \quad (8)$$

where σ_0 is the stress amplitude, and ε_0 is the strain amplitude.

2.3.2. Uniaxial compression test

The UC test was performed using the servo-hydraulic UTM (UTM-130) manufactured by IPC global®. The machine is capable of exerting sinusoidal axial load over a wide range of frequencies. Three LVDT with 70 mm gauge lengths installed at 120° apart were used. The test was conducted in accordance with AASHTO T378-17 [34] at the same test conditions as the IDT test. The UC dynamic modulus test was performed in a controlled-strain mode with a target strain of 50 $\mu\epsilon$ or less.

The illustration of the UC test is shown in Fig. 4. Differently from the IDT test, the UC test determines the dynamic modulus uniaxially as it measures the vertical stress, $\sigma_y(t)$, and strain, $\varepsilon_y(t)$, along the direction of the applied load as shown in Fig. 5., which is expressed as follows.

$$E^* = |E^*| \cdot e^{i\varphi} = \frac{\sigma_y(t)}{\varepsilon_y(t)} = \frac{\sigma_0 \sin(\omega t - \varphi)}{\varepsilon_0 \sin(\omega t)} \quad (9)$$

In the UC test, the value of axial stress and strain were recorded. The mean value of stiffness from the 10 testing cycles determined the dynamic modulus of the UC test specimen at a certain test condition. As the same as the IDT test, the phase angle can be determined by the lag time between stress and strain.

2.4. Master curve construction

The master curve was constructed by fitting the experimental test data of dynamic modulus according to the sigmoidal function described in the ME pavement design guide was selected as expressed in Eq. (10) and Eq. (11). The WLF equation given in Eq. (12) was used to describe the relationship between shift factor and temperature above the glass transition temperature (T_g) [35].

$$\log(|E^*|) = \delta + \frac{\alpha}{1 + e^{\beta - \gamma(\log f_r)}} \quad (10)$$

$$\log(f_r) = \log(f) + \log[\alpha(T)] \quad (11)$$

where f_r is the frequency at the reference temperature, T_r , T is the test temperature, $\alpha(T)$ is the shift factor, δ , α , β and γ are the fitting parameters.

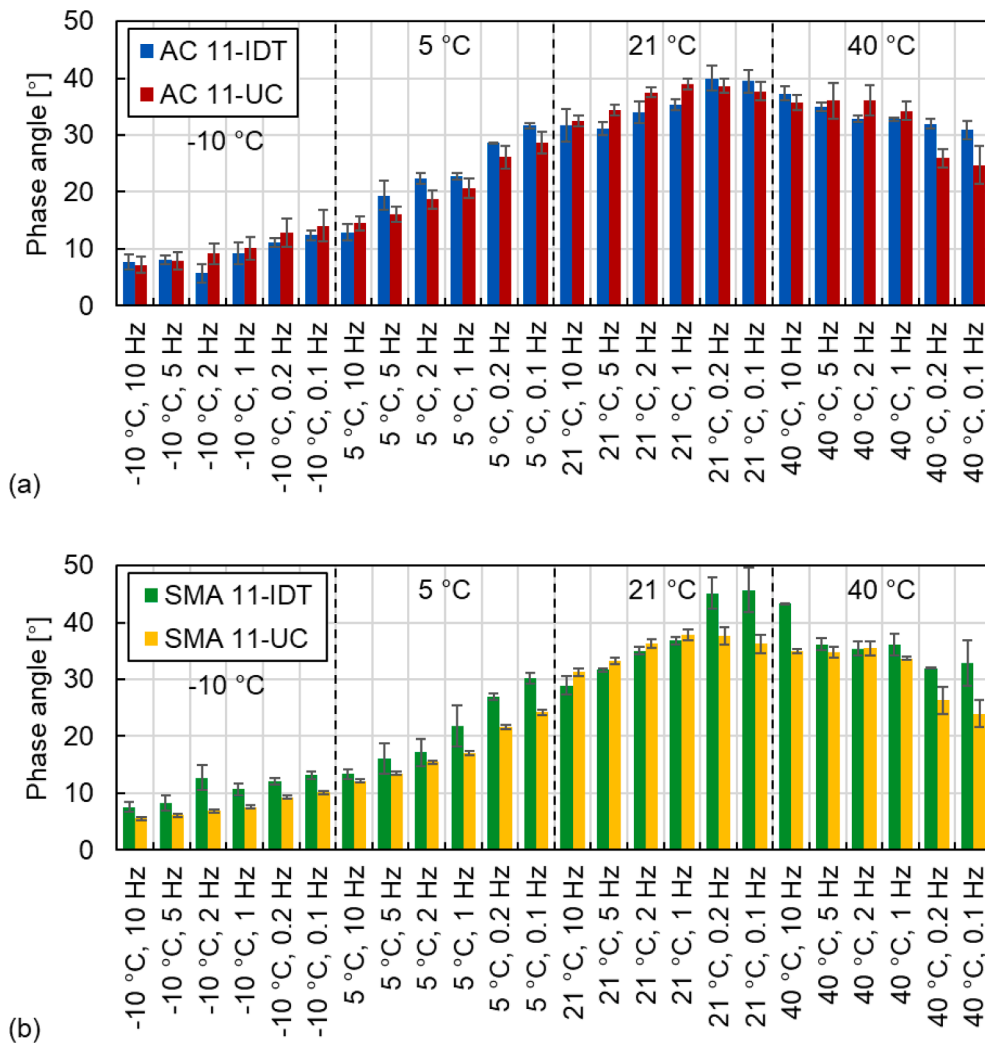


Fig. 10. Phase angle results: (a) AC 11 and (b) SMA 11.

$$\log[\alpha(T)] = \frac{-C_1(T - T_r)}{C_2 + (T - T_r)} \tag{12}$$

where C_1 and C_2 are the fitting parameters. The reference temperature of master curve construction for both tests was the same at 21 °C.

The phase angle master curve was constructed through the Lorentzian equation, denoted as Eq. (13) [36,37]:

$$\varphi = \frac{k_p \cdot k_g^2}{[\log(f_r) - k_c]^2 + k_g^2} \tag{13}$$

where φ is the phase angle, k_p is the peak value, k_g is the growth rate and k_c is the critical point. The master curves of both tests were constructed using the Solver add-in tool in Microsoft Excel. The non-linear least squares regression was performed to fit the test data based on the sigmoidal function, WLF equation and Lorentzian equation [38,39].

3. Results and discussion

3.1. Master curve of dynamic modulus and phase angle

3.1.1. Dynamic modulus

The dynamic modulus results of the IDT and the UC tests are shown in Fig. 6. Fig. 6(a) displays that the dynamic moduli of AC 11 mixtures measured by both tests are similar at 5 °C and there are some differences

at higher and lower temperatures. The dynamic moduli of SMA 11 mixtures obtained by two tests are similar at low temperatures (-10 and 5 °C) and different at higher temperatures. The CoV of the dynamic modulus results are given in Fig. 7. The CoV of AC 11-IDT, AC 11-UC, SMA 11-IDT and SMA 11-UC are smaller at -10, 5, 21 °C, which are around 10 % or less. The CoV of AC 11-IDT, SMA 11-IDT and SMA 11-UC are bigger at 40 °C, which is up to 30 %. This indicates that the dynamic modulus test has a smaller variation at low temperatures and a bigger variation at high temperatures. Furthermore, the CoV of SMA 11 mixtures are lower than the ones of AC 11 mixtures, which displays that the grading type of mixtures has an influence on the test variation.

To compare the two test methods under a wider range of conditions, dynamic modulus master curves of asphalt mixtures are constructed. The dynamic modulus master curves of AC 11-IDT, SMA 11-IDT, AC 11-UC and SMA 11-UC are presented in Fig. 8. The fitting parameters and the goodness of fit statistics [40], including the standard error of estimation (S_e), the standard error of deviation (S_y), the standard error ratio (S_e/S_y) and the coefficients of determination (R^2), are given in Table 4. All master curves have good fits. The R^2 of dynamic modulus are over 0.988. Both R^2 of dynamic modulus for AC 11-IDT and SMA 11-IDT are bigger than the R^2 values of AC 11-UC and SMA 11-UC. Meanwhile, both the S_e/S_y of dynamic modulus for AC 11-IDT and SMA 11-IDT are smaller than the S_e/S_y of AC 11-UC and SMA 11-UC. These outcomes

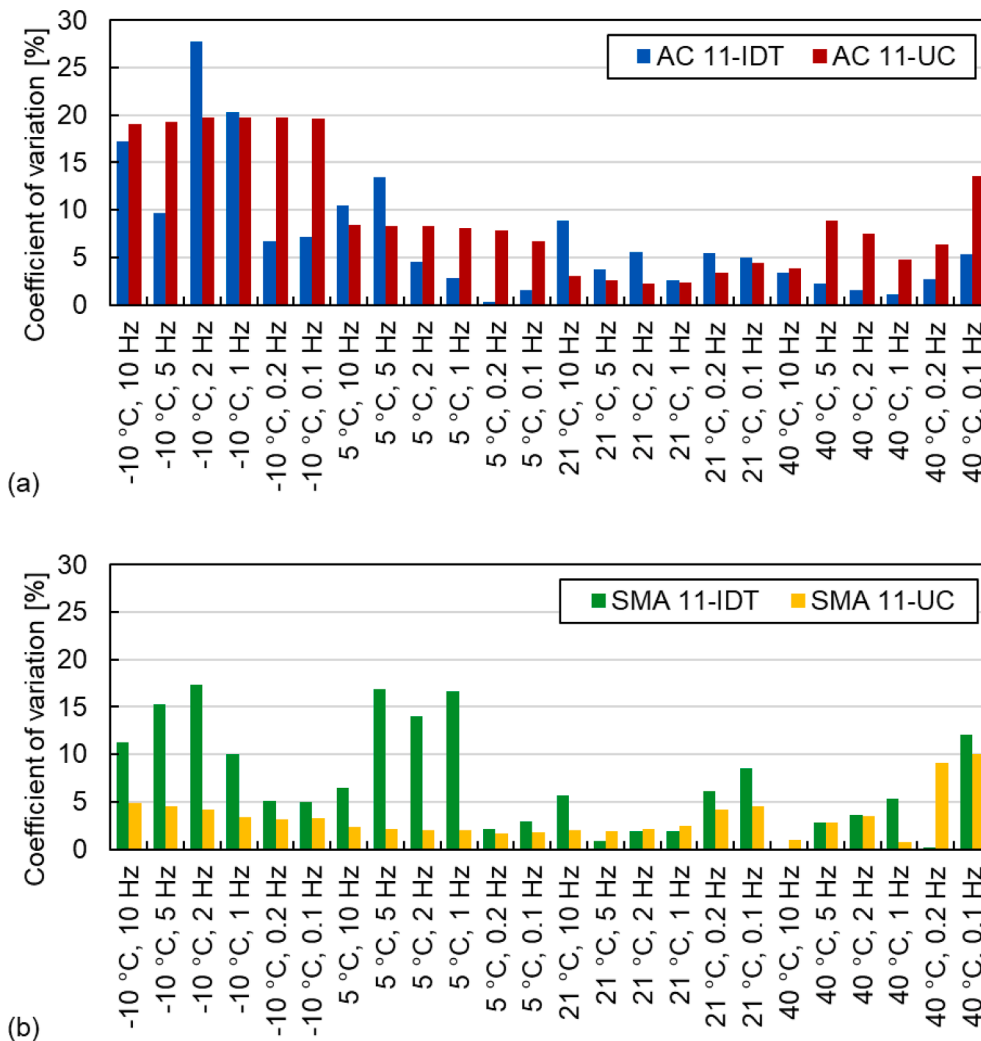


Fig. 11. Coefficient of variation of phase angle results: (a) AC 11 and (b) SMA 11.

indicate that the dynamic modulus master curves have a better fit for IDT test data. Furthermore, it can be observed from Fig. 8 that the dynamic moduli obtained by the two tests are relatively consistent in the frequency range from 10 Hz to 10⁴ Hz. When the frequency is higher than 10⁴ Hz or lower than 10 Hz, the dynamic moduli display differences. Compared with SMA 11, two tests induce a more severe difference in dynamic modulus at both higher and lower frequencies for AC 11. This result indicates that AC 11 structure tends to expand the difference in dynamic modulus caused by the two tests compared to SMA 11 structure.

As all the dynamic modulus master curves of the four asphalt mixtures have a good fit, the dynamic modulus predicted by the master curves at each frequency is compared by the Normalized Squared Error (NSE) following Eq. (14). The smaller the NSE value, the more consistent the two test results.

$$NSE = \frac{(|E^*|_{IDT} - |E^*|_{UC})^2}{|E^*|_{IDT}^2} \quad (14)$$

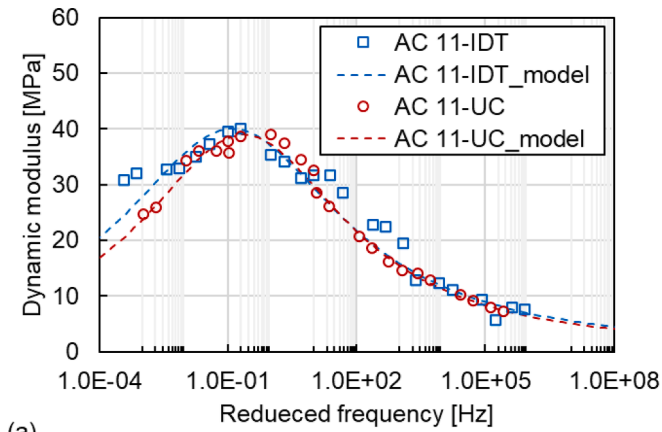
where $|E^*|_{IDT}$ is the dynamic modulus obtained by the IDT test, $|E^*|_{UC}$ is the dynamic modulus obtained by the UC test. The NSE between two tests of AC 11 and SMA 11 is illustrated in Fig. 9. The dynamic moduli obtained by the two tests are considered relatively consistent with a NSE less than 0.005.

As presented in Fig. 9, the dynamic moduli obtained from both tests

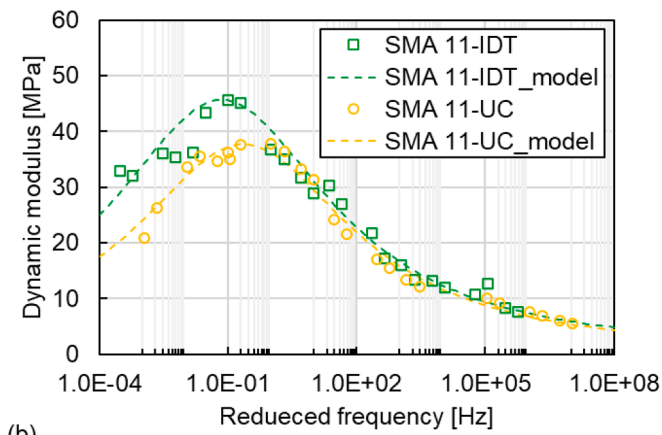
for the AC 11 are consistent in the frequency range from 10² Hz to 10³ Hz. The dynamic modulus evaluated from both tests for the SMA 11 is consistent in the frequency range from 10 Hz to 10⁴ Hz. Meanwhile, the NSE of the two mixtures increase gradually with the increase of the frequency over 10⁴ Hz or decrease of the frequency less than 10 Hz. The NSE of SMA 11 is smaller than that of the NSE of AC 11. These results indicate that the dynamic moduli of asphalt mixtures measured by the two tests are almost the same in the reduced frequency range from 10 Hz to 10⁴ Hz. On the contrary, differences are found at high and low frequencies (temperatures) where the dynamic moduli measured by the IDT test are greater than those obtained with UC test. Fig. 9 shows that the NSE of the two mixtures is large at extreme frequencies, particularly at very low reduced frequencies. This might be connected to the various stress-strain responses of the specimens under the two test modes at relatively high temperatures. The difference in NSE between the two asphalt mixtures might be caused by the distinct physical structures. Comparing with AC 11 mixture, SMA 11 has an embedded structure between large size aggregates and its dynamic modulus is less affected by temperature [41].

3.1.2. Phase angle

Fig. 10 presents the phase angle results of the IDT test and the UC test. The phase angles obtained by both tests are similar at 21 °C for AC 11 and SMA 11 mixtures. The differences in phase angles between the



(a)



(b)

Fig. 12. Master curves of phase angle: (a) AC 11 and (b) SMA 11.

Table 5

The fitting parameters and statistical parameters of the phase angle master curves for asphalt mixtures.

Fitting parameter		AC 11-IDT	SMA 11-IDT	AC 11-UC	SMA 11-UC
Lorentzian equation	k_p	40.006	45.656	38.960	37.745
	k_g	3.167	3.141	2.946	3.114
	k_c	-0.910	-1.154	-0.639	-0.653
<i>Goodness of fit statistics</i>					
S_e		2.961	2.661	1.299	1.611
S_y		11.358	12.273	11.223	11.934
S_e/S_y		0.261	0.217	0.116	0.135
R^2		0.932	0.953	0.987	0.982

two tests occur at higher and lower temperatures. The CoV of phase angle results are smaller at 21 °C as shown in Fig. 11, which indicates that the two test modes are stable at 21 °C leading to fewer result differences of both tests in the properties of the same materials.

Similar to the dynamic modulus, phase angle master curves are constructed to compare the differences between the two test methods over a wider range of conditions. The phase angle master curves of AC 11-IDT, SMA 11-IDT, AC 11-UC and SMA 11-UC are presented in Fig. 12. The fitting parameters and the goodness of fit statistics are given in Table 5. The statistical parameters of phase angle for the two tests are different from the ones of dynamic modulus. Both R^2 of phase angle for AC 11-IDT and SMA 11-IDT are smaller than R^2 of AC 11-UC and SMA 11-UC shown in Table 5. Both S_e/S_y of phase angle for AC 11-IDT and SMA 11-IDT exceed S_e/S_y of AC 11-UC and SMA 11-UC. Thus, the phase

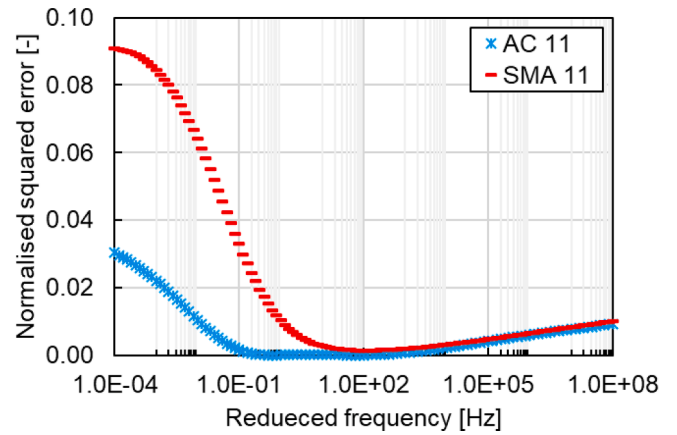
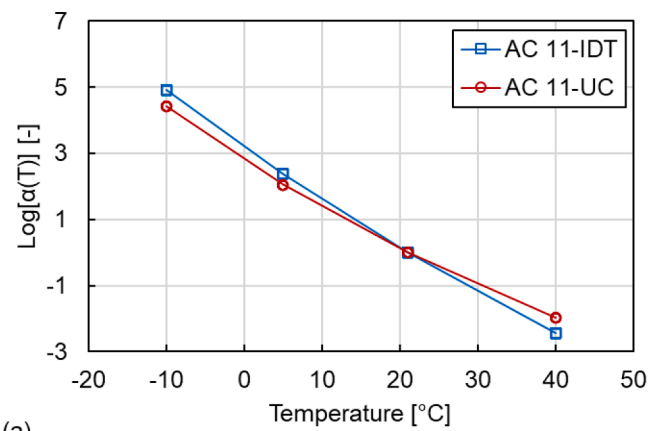
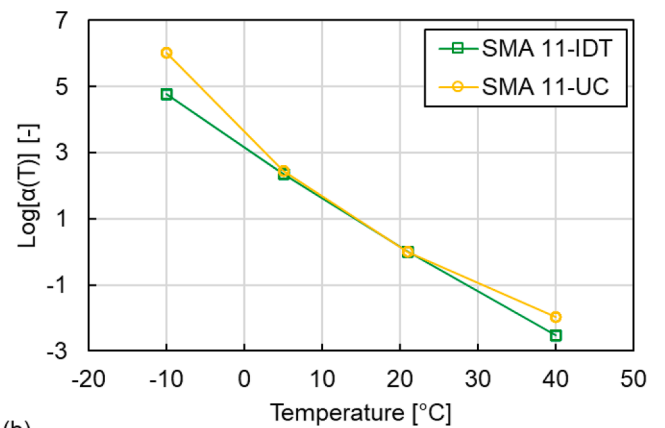


Fig. 13. NSE of phase angle between two test modes for AC 11 and SMA 11.



(a)



(b)

Fig. 14. Shift factors for specimens: (a) AC 11 and (b) SMA 11.

angle master curves of the UC test data have a better fit than that of the IDT test data. As shown in Fig. 12, the phase angle master curves for both tests are similar at high frequencies and show differences at lower frequencies. This difference is more severe for the SMA 11 mixtures than for the AC 11 mixtures.

The NSE of the phase angle is calculated from the Lorentzian equation and is also utilised to compare the phase angle at each frequency as similar to the comparison of dynamic modulus. Fig. 13 presents the NSE of phase angle for AC 11 and SMA 11. A smaller NSE value is obtained at a higher frequency and a bigger NSE value emerged at a lower

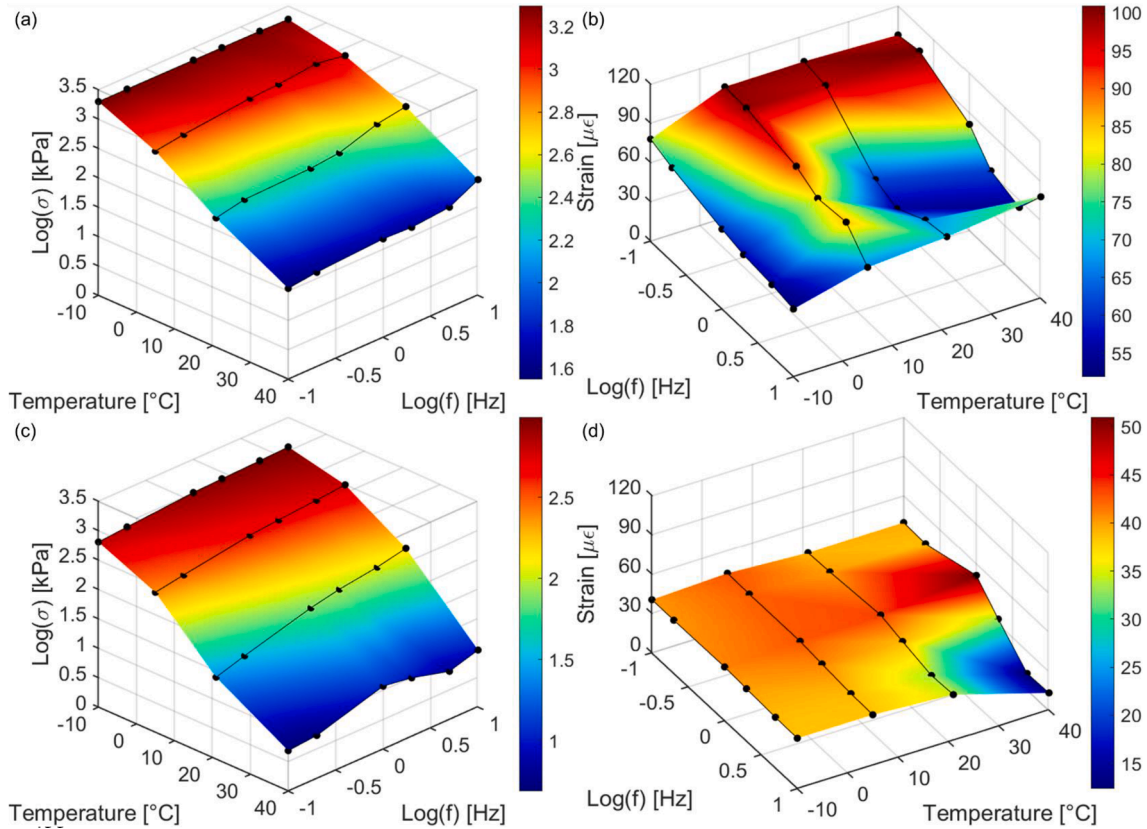


Fig. 15. Stress–strain states of AC 11 in IDT test and UC test at various conditions: (a) AC 11-IDT stress, (b) AC 11-IDT strain, (c) AC 11-UC stress and (d) AC 11-UC strain.

frequency. Meanwhile, the *NSE* of AC 11 is less than 0.005 in the range of 0.1 Hz to 10^5 Hz, showing the consistency of the phase angle of the two tests in this range. For the SMA 11 mixtures, the consistent range of phase angles from 10 Hz to 10^5 Hz for both tests is smaller than the range for the AC 11 mixtures. Furthermore, the *NSE* values of SMA 11 mixtures are bigger than the ones of AC 11 mixtures in the low frequency range. This phenomenon indicates that the difference in phase angle between the two test methods is larger for SMA 11 mixtures than for AC 11 mixtures. Besides, the phase angle of the IDT test is larger than that of the UC test, which is consistent with Kim’s research [18]. The horizontal phase angles of the IDT test are generally higher than the phase angles determined from the UC test. The averaged phase angles from horizontal direction and vertical direction are close to the values from the UC test. It can be interpreted that the IDT test only considers the phase angle in the horizontal direction.

3.1.3. Shift factor

The results of the shift factor are also investigated, as shown in Fig. 14. The shift factor reflects how far the measured values have moved relative to the dynamic modulus at the reference temperature, resulting in an impact on the modelling values of the master curves. In terms of AC 11 mixtures, the slope of the shift factor of AC 11-IDT is higher than the one of AC 11-UC, which means that the curve of AC 11-IDT is shifted more in the construction of the master curve than that of AC 11-UC. However, for the SMA 11 mixtures, the measured values of SMA 11-UC move more at high frequencies relative to SMA 11-IDT. When the measured values are higher, moving more distance to high and low frequencies widens the difference, reflecting that the difference in dynamic modulus of the two test methods is greater for the AC 11 mixtures

than for the SMA 11 mixtures. This result reveals that the structure of the tested asphalt mixture has a great impact on the results obtained with the two test procedures. The SMA mixtures with the embedded structure are less affected by the test than the AC mixtures with the dense structure.

3.2. Comparison of stress–strain state

3.2.1. Stress–strain response

The stress–strain states are obtained based on Section 2.3. The stress amplitude of the IDT test is expressed in Eq. (15). The stress amplitude of the UC test and the strain amplitudes of the two tests can be obtained from the testing programs.

$$\begin{aligned} \sigma_0 &= \sigma_{0x} - \nu\sigma_{0y} \\ &= \frac{2P_0}{\pi a z} (\sin 2\alpha - \alpha) - \nu \left[-\frac{2P_0}{\pi a z} (\sin 2\alpha + \alpha) \right] \\ &\approx \frac{P_0}{\pi R z} + \nu \frac{3P_0}{\pi R z} \end{aligned} \tag{15}$$

The stress–strain states of AC 11 mixtures for the two tests are represented in Fig. 15 at various temperature and frequency conditions. Fig. 16 shows the *CoV* of the stress and strain results. As shown in Fig. 15 (a, c), the stresses of both test modes for AC 11 decrease as the temperature increases. This is explained that both test modes control the strain in a certain range to ensure that the tested asphalt mixture is in the linear viscoelastic range. The increase in temperature causes the softening of the asphalt mixture yet the strain range does not change. The strains of two tests for AC 11 are shown in Fig. 15(b, d). It is observed

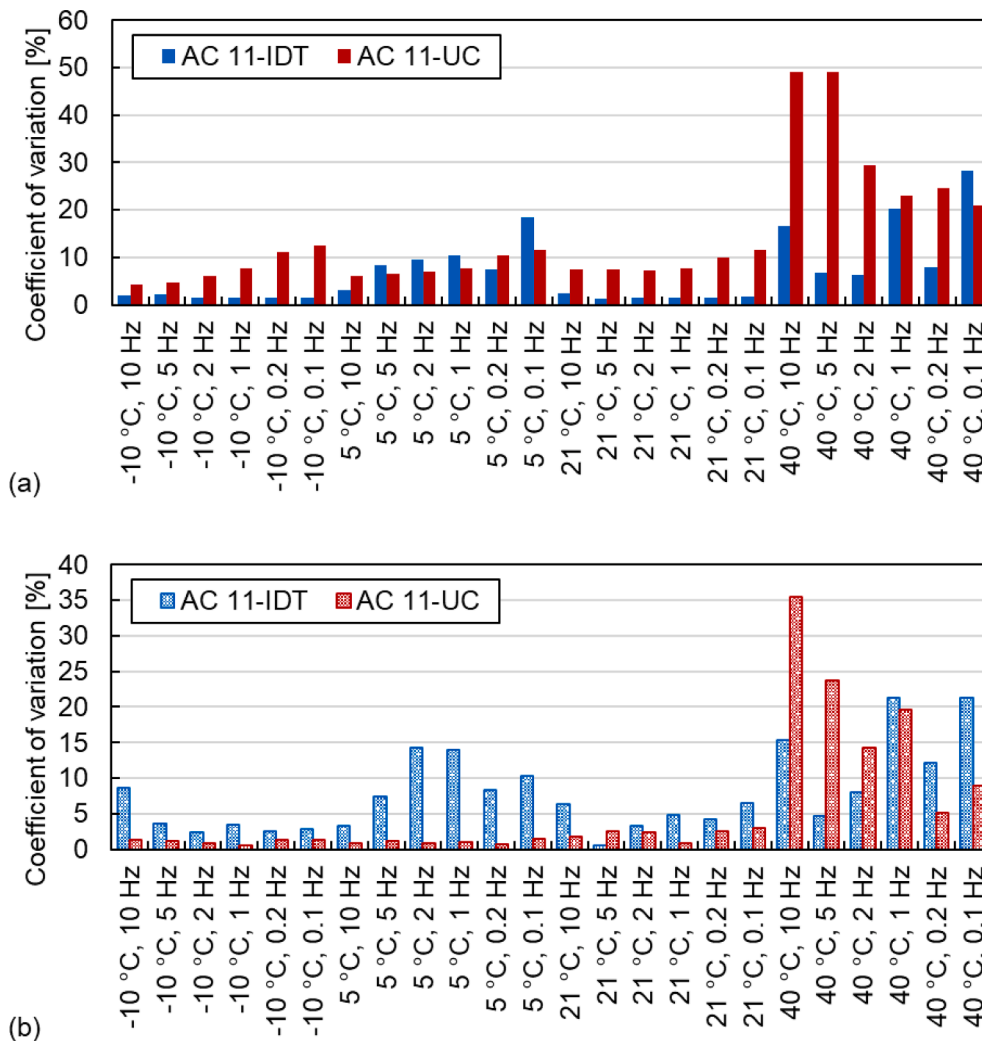


Fig. 16. Coefficient of variation of stress and strain results of AC 11 mixtures: (a) stress and (b) strain.

that the strains of the UC test are maintained around 40 $\mu\epsilon$ at all temperatures except for 40 °C. However, the strains of the IDT test are not stable at a certain value with the temperature changing, and there is no intuitive changing trend between the strain and the temperature. This indicates that the UC test controls the strain better than the IDT test and the strains of both tests are varied at the high temperatures.

Fig. 15 also shows the changes in stress and strain with the frequency. At low temperatures, the stresses measured for both tests are maintained at a relatively constant stress level as the frequency changes. The stresses are gradually affected by frequency as the temperature increases. For high temperatures, the stress values fluctuate more with various frequencies for both tests. The variation in the trends of strain and stress with frequency for the IDT test is similar, while the strain in the UC test is stable at an average of 40 $\mu\epsilon$. When it comes to the changes in strains, the UC test has better deformation control than the IDT test. However, both approaches do not control the deformation well at high temperatures due to the viscous properties of the asphalt mixture at high temperatures. The change in the stress–strain state with temperature and frequency can be explained by considering the viscoelastic behaviour of asphalt materials. At low temperatures, the elastic component plays a major role; therefore, the dynamic modulus does not change much with frequency, and the stress and strain are stable. At high

temperatures, the viscous component plays a more important role, and the dynamic modulus as well as the stress–strain state are highly related to temperature values. It is worth noting that the strain value measured during the IDT test at a high temperature and low frequency is close to the upper limit. Therefore, it is difficult to ensure that the asphalt material specimen is within the linear viscoelastic range at high temperatures when investigated with the IDT test.

Fig. 16 indicates that the CoV of stress and strain results for AC 11 mixtures are small at -10, 5, 21 °C and high at 40 °C, which is consistent with the CoV of dynamic modulus results. This result further reflects that the mechanical properties of asphalt mixtures are more stably determined at low and medium temperatures by both two test modes. The larger variations occur at high temperatures.

The stress–strain states measured for SMA 11 mixtures and their CoV are shown in Fig. 17 and Fig. 18, respectively. The trend of stress–strain states for SMA 11 is similar to the one for AC 11, indicating the major relevance of the viscoelastic properties of asphalt materials. However, there are still some distinctions between the two asphalt mixtures. At low temperatures, the stress of the SMA 11 is larger than that of the AC 11 except for 10 Hz in the IDT test. The strain of the SMA 11 is bigger than that of the AC 11 except for 10 Hz in the IDT test. Meanwhile, the stresses of the UC test grow slowly with the increase in frequency, and

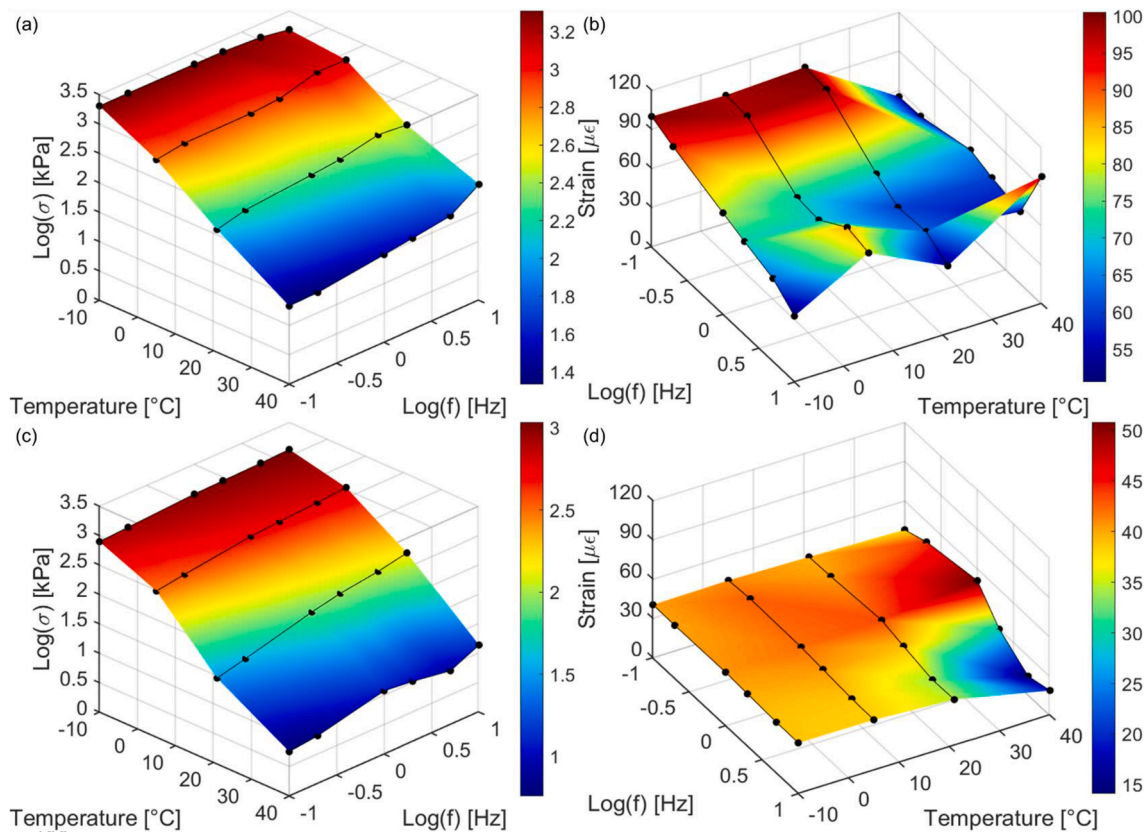


Fig. 17. Stress–strain states of SMA 11 in IDT test and UC test at various conditions: (a) SMA 11-IDT stress, (b) SMA 11-IDT strain, (c) SMA 11-UC stress and (d) SMA 11-UC strain.

the strains remain around 40 $\mu\epsilon$ for both AC 11 and SMA 11. Thus, this finding illustrates that the UC test has better control of stress and strain than the IDT test. Comparing the results depicted in Fig. 15(a, c) and Fig. 17(a, c) for high temperatures, the IDT test stress values measured for the SMA 11 samples are smaller than the ones for the AC 11 specimens. At 40 °C, the stress values of the SMA 11 in the IDT test decrease on average by about 15 % relative to the AC 11. However, the stress of the SMA 11 is almost the same as that of the AC 11 in the UC test at 40 °C. The trends of the strain values measured for both SMA 11 and AC 11 asphalt mixtures are similar at high temperatures.

The CoV of stress and strain results for SMA 11 mixtures have a similar trend to that for AC 11 mixtures as presented in Fig. 18. It is worth finding that the CoV of the UC test strain is very small at -10, 5, 21 °C and is relatively large at 40 °C for both asphalt mixtures. This reflects that the UC test has a very stable control on strain at -10, 5, 21 °C and controls strain unstably at high temperatures.

3.2.2. Normalised stress and strain

As the different modes of control strain for the two tests, the stress and the strain are normalised by dividing by the maximum value method for comparison. The normalised stresses at every temperature are used to reflect the changing trend of the stress. The exponential formulations used to fit the experimental values of mean stress and temperature are shown in Fig. 19. The high R^2 values validate the reliability of the relationship. The normalised stresses at -10 °C are similar for both tests and the difference occurs at high temperatures. At 40 °C, the values of normalised stresses measured by the IDT test are approximately 3.26 and 2.34 times greater than the ones measured by the UC test for AC 11

and SMA 11 mixtures, respectively. Compared with UC test, the results indicate that the stress level of the IDT test is higher and the difference between the two tests of AC 11 is greater than that of SMA 11 in terms of stress.

The relationship between normalised strain and temperature is shown in Fig. 20. At -10 °C, the normalized strain of the UC test has a stable value of around 0.8, which corresponded to 40 $\mu\epsilon$. The strain difference with frequencies increases gradually with the increase in temperature. At 40 °C, the strains of the UC test at six frequencies are quite different. The normalised strain of the IDT test shows large deviations at all four test temperatures. The strain deviation under different frequencies of the IDT test is greater than that of the UC test at -10, 5 and 21 °C and smaller than that of the UC test at 40 °C. The results indicate that the changing trend of strain with temperature for the UC test is smaller than that of the IDT test at low and medium temperatures, while higher at high temperatures. This result demonstrates a better control over strain of the UC test at low and medium temperatures, which is consistent with the CoV of strain results.

3.3. Comparison between IDT test and UC test

The main features of the IDT test and UC test setups and result trends are summarised in Table 6. Due to the smaller dimension (weight) of the test specimen dimension (weight) the IDT test is more convenient for testing field core samples and for sample preparation in the laboratory, e.g., making plate samples and core and cut from them. The biaxial stress of the IDT test involves Poisson’s ratio. In this test, the stress–strain response in horizontal direction is only considered and Poisson’s ratio is

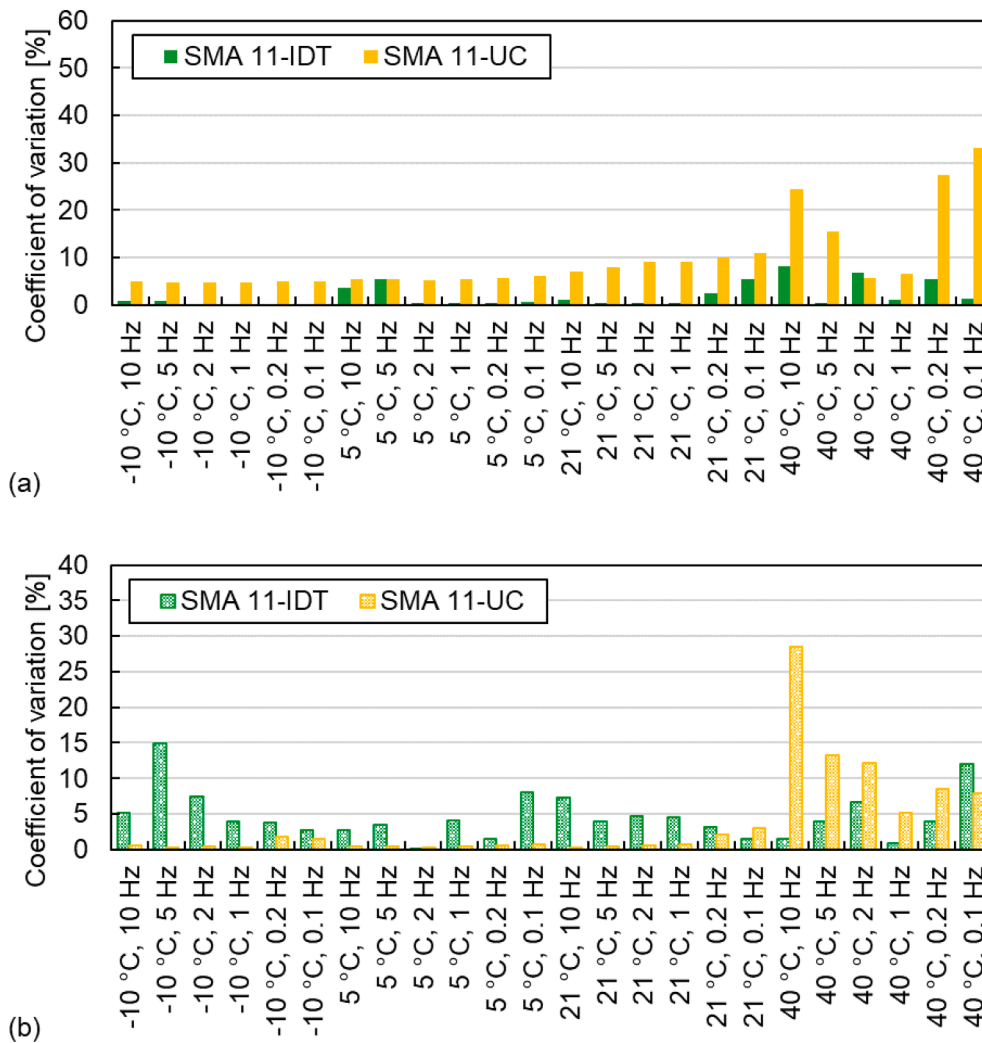


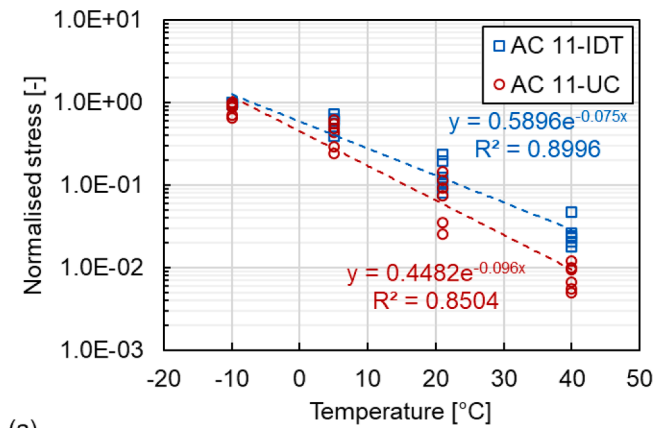
Fig. 18. Coefficient of variation of stress and strain results of SMA 11 mixtures: (a) stress and (b) strain.

selected as a constant value of 0.35 according to the standard (EN 12697–26). Differently from IDT test, the UC test takes account into stresses in a single direction (vertical direction) less affected by Poisson’s ratio. Moreover, the UC test employs confining pressure, which can better simulate real service conditions of road pavement [42]. However, the UC test needs more time to condition temperature due to the larger size of the sample. Nevertheless, both IDT test and UC test can work well at intermediate temperatures. Considering the dynamic moduli, the results from the two tests are almost identical for intermediate frequency and temperature ranges, and slightly different at extreme temperatures. Regarding the phase angle, the UC test results are more accurate than IDT test results. Besides, the stress–strain states for IDT test and UC test are different. This is due to the different force forms and strain control modes of the two tests. The biaxial and uniaxial loads are applied to the IDT and UC tests, respectively. The initial strain of IDT test is controlled manually, while the strain of UC test is controlled by the software in the whole test procedure. Furthermore, the greater number of analysed cycles for the UC test also reflects better stability than the IDT test. Therefore, the UC test shows better deformation control at low and medium temperatures.

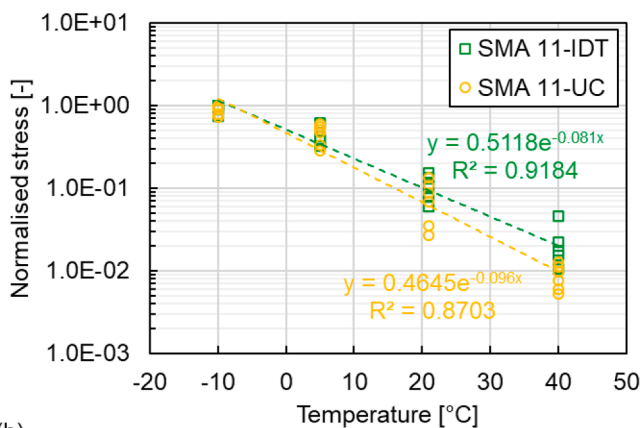
4. Conclusions

This study compares the two standard laboratory tests used for the mechanical characterisation of bituminous asphalt, namely Indirect Tensile (IDT) test and Uniaxial Compression (UC). The performance of two mixtures commonly employed for road surfacing, Asphalt Concrete (AC) and Stone Mastic Asphalt (SMA), are compared in terms of dynamic modulus, phase angle, shift factor and stress–strain state. Based on the attained results, the conclusions are drawn as follows:

- The dynamic moduli measured using both tests at medium frequency (temperature) range are the same. Moreover, the values obtained from IDT test are higher than the ones assessed by UC test at extreme frequencies (temperatures). The different mesoscopic structures of the asphalt mixture can account for the discrepancies in the results attained with the two test methods. The difference in dynamic modulus of SMA mixtures measured by both tests is smaller than that of AC mixtures.
- Compared with IDT test, the phase angle master curve has a better fit for UC test and has lower values.
- The shift factor of SMA 11-UC is bigger than that of SMA 11-IDT at low temperatures, which is different from the situation for AC 11

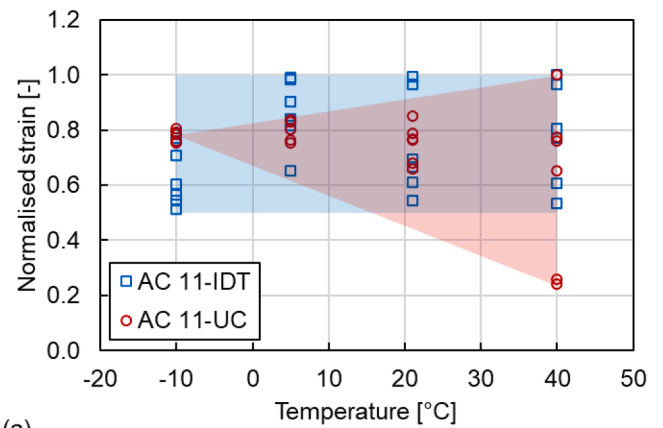


(a)

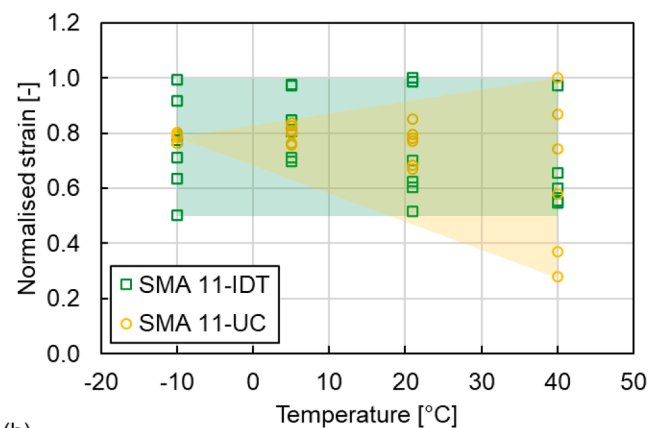


(b)

Fig. 19. Relationship between normalised stress and temperature: (a) AC 11 and (b) SMA 11.



(a)



(b)

Fig. 20. Relationship between normalised strain and temperature: (a) AC 11 and (b) SMA 11.

mixtures. The measured dynamic modulus and the shifting situation cause a smaller difference between the two test methods in modelling dynamic modulus for the SMA 11 mixtures.

- The stress level pertaining to the IDT test is bigger than the one achieved during UC test. The IDT test strain values are various at all four test temperatures. Although the variation of strain obtained from the UC test is based on the frequency largens as the temperature increases, the stress-strain states are stable at low and medium temperatures, showing a better strain control than the IDT test.
- The coefficients of variation of dynamic modulus, stress and strain results are small at -10, 5, 21 °C and higher at 40 °C indicating that both test modes are more stable for testing the mechanical properties of asphalt mixtures at low and medium temperatures. The phase angle results only show small variations at 21 °C.

In general, both tests can be used to properly characterise the dynamic modulus of asphalt materials. The IDT test can be efficiently used for the characterisation of road surfaces built in cold regions. Moreover, the IDT test plays an important role when it comes to the mechanical characterisation of existing asphalt pavements since the dimensions of the field samples normally meet the size requirements. The UC test controls strain better for low and medium temperature ranges compared with IDT test, resulting in more accurate results. A confining pressure can be applied for UC test, which better simulates real field conditions. For Norwegian conditions as a basis for practical design, the IDT test seems to be the best choice due to easier/more realistic sample

preparation and to compare with field cored samples.

The comparison between IDT and UC modes in dynamic modulus tests for AC 11 and SMA 11 mixtures was focused on in this study. Further studies involving more types of asphalt mixtures are recommended to investigate the effect of materials on the difference between the two test modes and fully understand the two modes of dynamic modulus tests. Moreover, the connection of the IDT and UC tests under extreme environmental conditions will be established to develop the wide application of the IDT test in ME pavement design.

5. Data availability

Data will be made available on request.

CRediT authorship contribution statement

Hao Chen: Conceptualization, Methodology, Software, Formal analysis, Investigation, Data curation, Writing – original draft. **Mequanent Mulugeta Alamnie:** Conceptualization, Methodology, Investigation, Data curation, Writing – review & editing. **Diego Maria Barbieri:** Investigation, Writing – review & editing. **Xuemei Zhang:** Investigation, Writing – review & editing. **Gang Liu:** Methodology, Writing – review & editing, Supervision. **Inge Hoff:** Resources, Writing – review & editing, Supervision.

Table 6
Summarised comparison between IDT test and UC test.

Item	IDT test	UC test
Standard	EN 12697–26:2018	AASHTO T378-17
Cylindrical specimen dimension	Diameter Thickness (height)	100 mm 150 mm
Conditioning temperature time	≥ 4 h (Better for low temperature)	–10 °C ~ Overnight 5 °C ~ 4 h or Overnight 21 °C ~ 3 h 40 °C ~ 2 h (Suitable for intermediate and high temperature)
Test temperature (this study)	–10 °C, 5 °C, 21 °C, 40 °C	
Test frequency (this study)	10 Hz, 5 Hz, 2 Hz, 1 Hz, 0.2 Hz, 0.1 Hz	
Applied load	Harmonic sinusoidal load	
Load control mode	Controlled stress-strain	Controlled strain
Number of analysed cycles	5 cycles	10 cycles
Dynamic modulus	$f_r: 10^4 \sim 11$ AC 10 Hz CoV SMA 11 CoV $f_r: 10 \sim 10^4$ AC 11 Hz CoV SMA 11 CoV $f_r: 10^4 \sim 10^8$ AC 11 Hz CoV SMA 11 CoV S_e/S_y AC 11 SMA 11 R^2 AC 11 SMA 11 $f_r: 10^4 \sim 11$ AC 10 Hz CoV SMA 11 CoV $f_r: 10 \sim 10^4$ AC 11 Hz CoV SMA 11 CoV $f_r: 10^4 \sim 10^8$ AC 11 Hz CoV SMA 11 CoV S_e/S_y AC 11 SMA 11 R^2 AC 11 SMA 11	255 ~ 6379 MPa 67 ~ 5072 MPa 1.4 % ~ 11.0 % 292 ~ 5341 MPa 74 ~ 5028 MPa 0.2 % ~ 10.6 % 6379 ~ 24329 MPa 5072 ~ 20224 MPa 0.1 % ~ 7.7 % 5341 ~ 21066 MPa 5028 ~ 19546 MPa 0.5 % ~ 8.3 % 24329 ~ 45411 MPa 1.1 % ~ 3.9 % 21066 ~ 35123 MPa 4.0 % ~ 7.5 % 0.058 0.065 0.109 0.997 0.992 0.996 0.988 20 ~ 40° 17 ~ 39° 1.0 % ~ 5.5 % 25 ~ 46° 18 ~ 38° 0.1 % ~ 12.1 % 0.8 % ~ 10.0 % 12 ~ 29° 11 ~ 30° 0.3 % ~ 13.4 % 3.0 % ~ 19.8 % 12 ~ 31° 12 ~ 29° 2.1 % ~ 16.9 % 1.7 % ~ 2.4 % 4 ~ 12° 4 ~ 11° 9.7 % ~ 27.8 % 19.0 % ~ 19.7 % 4 ~ 11° 5 ~ 12° 4 ~ 11° 10.1 % ~ 17.4 % 3.1 % ~ 4.9 % 0.261 0.116 0.135 0.135 0.932 0.987 0.982 0.982 2.4 ~ 4.9 2.0 ~ 4.4 2.3 ~ 4.8 2.5 ~ 6.0
Shift factor	$T < T_r$	2.4 ~ 4.9 2.0 ~ 4.4 2.3 ~ 4.8 2.5 ~ 6.0

Table 6 (continued)

Item	IDT test	UC test
Stress	$T \geq T_r$ AC 11 SMA 11	–2.4 ~ 0 –2.0 ~ 0
	Direction	Horizontal and vertical (biaxial)
	$T < T_r$ AC 11 CoV SMA 11 CoV	766 ~ 1982 kPa 240 ~ 987 kPa 1.5 % ~ 18.4 % 4.3 % ~ 12.5 % 665 ~ 2047 kPa 306 ~ 1087 kPa 0.1 % ~ 5.5 % 4.7 % ~ 6.2 %
	$T \geq T_r$ AC 11 CoV SMA 11 CoV	35 ~ 468 kPa 5 ~ 143 kPa 1.2 % ~ 28.3 % 7.3 % ~ 49.2 % 22 ~ 310 kPa 6 ~ 146 kPa 0.3 % ~ 8.3 % 5.6 % ~ 33.2 %
	Direction	Horizontal Vertical
	$T < T_r$ AC 11 CoV SMA 11 CoV	52 ~ 100 µε 38 ~ 43 µε 2.3 % ~ 14.3 % 0.6 % ~ 1.5 % 51 ~ 100 µε 38 ~ 43 µε 0.1 % ~ 14.9 % 0.3 % ~ 1.8 % 0.5 % ~ 21.3 % 0.8 % ~ 35.5 % 52 ~ 101 µε 14 ~ 51 µε 0.8 % ~ 11.9 % 0.3 % ~ 28.5 %
	$T \geq T_r$ AC 11 CoV SMA 11 CoV	54 ~ 101 µε 12 ~ 51 µε 0.5 % ~ 21.3 % 0.8 % ~ 35.5 % 52 ~ 101 µε 14 ~ 51 µε 0.8 % ~ 11.9 % 0.3 % ~ 28.5 %

Declaration of Competing Interest

The authors declare that they have no known competing financial interests or personal relationships that could have appeared to influence the work reported in this paper.

Data availability

Data will be made available on request.

Acknowledgements

This research work was supported by the VegDim project of the Norwegian Public Roads Administration. The financial support provided by China Scholarship Council (No. 201806950077) and Department of Civil and Environmental Engineering, Norwegian University of Science and Technology (No. K-649105) is highly acknowledged. The support kindly provided by the laboratory technicians Bent Lervik and Jan Erik Molde is greatly acknowledged.

References

- [1] Y.H. Huang, Pavement analysis and design, Pearson Prentice, Hall Upper Saddle River, NJ, 2004.
- [2] A. Maji, A. Das, Reliability considerations of bituminous pavement design by mechanistic-empirical approach, Int. J. Pavement Eng. 9 (1) (2008) 19–31.
- [3] Nchrp, Guide for Mechanistic-Empirical Design of New and Rehabilitated Pavement Structures, NCHRP 1–37A Part 2 Design Inputs Chapter 2 Material Characterization, Transportation Research Board, Washington, D.C., 2004.
- [4] D. Lesueur, J.F. Gerard, P. Claudy, J.M. Letoffe, J.P. Planche, D. Martin, A structure-related model to describe asphalt linear viscoelasticity, J. Rheol. 40 (5) (1996) 813–836.
- [5] D.D. Li, M.L. Greenfield, Viscosity, relaxation time, and dynamics within a model asphalt of larger molecules, J. Chem. Phys. 140 (3) (2014), 034507.
- [6] X. Zhang, H. Chen, D.M. Barbieri, B. Lou, I. Hoff, The classification and reutilisation of recycled asphalt pavement binder: Norwegian case study, Case Stud. Constr. Mater. 17 (2022) e01491.
- [7] T. Officials, AASHTO Guide for Design of Pavement Structures, AASHTO (1993).

- [8] C.W. Schwartz, N. Gibson, R.A. Schapery, Time-temperature superposition for asphalt concrete at large compressive strains, *Transp. Res. Rec.* 1789 (1) (2002) 101–112.
- [9] H. Yao, Z. You, L. Li, C.H. Lee, D. Wingard, Y.K. Yap, X. Shi, S.W. Goh, Rheological properties and chemical bonding of asphalt modified with nanosilica, *J. Mater. Civ. Eng.* 25 (11) (2013) 1619–1630.
- [10] T. Chen, Y. Luan, T. Ma, J. Zhu, X. Huang, S. Ma, Mechanical and microstructural characteristics of different interfaces in cold recycled mixture containing cement and asphalt emulsion, *J. Clean. Prod.* 258 (2020), 120674.
- [11] J. Zhu, T. Ma, J. Fan, Z. Fang, T. Chen, Y. Zhou, Experimental study of high modulus asphalt mixture containing reclaimed asphalt pavement, *J. Clean. Prod.* 263 (2020), 121447.
- [12] D.W. Christensen, R.F. Bonaquist, Evaluation of indirect tensile test (IDT) procedures for low-temperature performance of hot mix asphalt, *Transp. Res. Board* (2004).
- [13] M. Zaumanis, M.C. Cavalli, L.D. Poulidakos, How not to design 100% recycled asphalt mixture using performance-based tests, *Road Mater. Pavement Des.* 21 (6) (2020) 1634–1646.
- [14] K. Mollenhauer, P. Plachkova-Dzhurova, Categories for stiffness and fatigue based on cyclic indirect tensile tests and their applicability in construction contracts. 6th Euraspilat & Eurobitumen Congress, 2016.
- [15] X. Zhang, H. Chen, D.M. Barbieri, I. Hoff, Laboratory Evaluation of Mechanical Properties of Asphalt Mixtures Exposed to Sodium Chloride, 03611981221082579, *Transp. Res. Rec.* (2022).
- [16] R.G. Saba, Analytical Design of Pavement Structures, NPRA reports, Norway, (2019).
- [17] H. Cheng, Y. Wang, L. Liu, L. Sun, Y. Zhang, R. Yang, Estimating tensile and compressive moduli of asphalt mixture from indirect tensile and four-point bending tests, *ASCE J. Mater. Civ. Eng.* 33 (1) (2021) 04020402.
- [18] Y.R. Kim, Y. Seo, M. King, M. Momen, Dynamic modulus testing of asphalt concrete in indirect tension mode, *Transp. Res. Rec.* 1891 (1) (2004) 163–173.
- [19] X. Qin, L. Ma, H. Wang, Comparison analysis of dynamic modulus of asphalt mixture: indirect tension and uniaxial compression test, *Transportmetrica A* 15 (1) (2019) 165–178.
- [20] D. Barbieri, I. Hoff, H. Mork, Laboratory investigation on unbound materials used in a highway with premature damage, *Bearing capacity of Roads, Railways and Airfields*, CRC Press, 2017, pp. 101–108.
- [21] D.M. Barbieri, I. Hoff, M.B.E. Mørk, Mechanical assessment of crushed rocks derived from tunnelling operations, in: *Civil Infrastructures Confronting Severe Weathers and Climate Changes Conference*, Springer, 2018, pp. 225–241.
- [22] CEN, EN 1426:2015 Bitumen and bituminous binders Determination of needle penetration, Brussels, Belgium, (2015).
- [23] CEN, EN 1427:2015 Bitumen and bituminous binders Determination of the softening point Ring and Ball method, Brussels, Belgium, (2015).
- [24] CEN, EN 1097-1:2011 Tests for mechanical and physical properties of aggregates Part 1: Determination of the resistance to wear (micro-Deval), Brussels, Belgium, (2011).
- [25] CEN, EN 1097-2:2020 Tests for mechanical and physical properties of aggregates Part 2: Methods for the determination of resistance to fragmentation, Brussels, Belgium, (2020).
- [26] CEN, EN 12697-31:2019 Bituminous mixtures Test methods Part 31: Specimen preparation by gyratory compactor, Brussels, Belgium, (2019).
- [27] M.M. Alammie, E. Taddesse, I. Hoff, Thermo-piezo-rheological characterization of asphalt concrete, *Constr. Build. Mater.* 329 (2022), 127106.
- [28] R.E. Asbjørn Arnevik, Nils Sigurd Uthus, Joralf Aurstad, Jostein Aksnes, Torbjørn Jørgensen, Guidelines asphalt 2019, NPRA reports, Norway, (2019).
- [29] CEN, EN 12697-8:2018 Bituminous mixtures Test methods Part 8: Determination of void characteristics of bituminous specimens, Brussels, Belgium, (2018).
- [30] CEN, EN 12697-26:2018 Bituminous mixtures Test methods Part 26: Stiffness, Brussels, Belgium, (2018).
- [31] G. Cerni, E. Bocci, F. Cardone, A. Corradini, Correlation between asphalt mixture stiffness determined through static and dynamic indirect tensile tests, *Arab. J. Sci. Eng.* 42 (3) (2017) 1295–1303.
- [32] F. Olard, F. Noël, F. Loup, Modulus testing in indirect tension mode, *Road Mater. Pavement Des.* 7 (4) (2006) 543–554.
- [33] P. Ghasemi, S. Lin, D.K. Rollins, R.C. Williams, Predicting dynamic modulus of asphalt mixture using data obtained from indirect tension mode of testing, arXiv preprint arXiv:1905.06810 (2019).
- [34] AASHTO, T 378-17 Standard Method of Test for Determination the Dynamic Modulus and Flow Number for Asphalt Mixtures Using the Asphalt Mixture Performance Tester (AMPT), Washington, D.C., (2017).
- [35] M.L. Williams, R.F. Landel, J.D. Ferry, The temperature dependence of relaxation mechanisms in amorphous polymers and other glass-forming liquids, *J. Am. Chem. Soc.* 77 (14) (1955) 3701–3707.
- [36] R. Nemati, E.V. Dave, Nominal property based predictive models for asphalt mixture complex modulus (dynamic modulus and phase angle), *Constr. Build. Mater.* 158 (2018) 308–319.
- [37] A.R. Archilla, J.P. Corrales-Azofeifa, J.P. Aguiar-Moya, Comprehensive Model for the Prediction of the Phase Angle Master Curve of Asphalt Concrete Mixes, in: *RILEM International Symposium on Bituminous Materials*, Springer, 2020, pp. 473–479.
- [38] T.K. Pellinen, M.W. Witzczak, R.F. Bonaquist, Asphalt mix master curve construction using sigmoidal fitting function with non-linear least squares optimization, Recent advances in materials characterization and modeling of pavement systems (2004) 83-101.
- [39] H. Chen, D.M. Barbieri, X. Zhang, I. Hoff, Reliability of Calculation of Dynamic Modulus for Asphalt Mixtures Using Different Master Curve Models and Shift Factor Equations, *Materials* 15 (12) (2022) 4325.
- [40] M.W. Witzczak, Simple performance test for superpave mix design, Transportation Research Board (2002).
- [41] I.M. Asi, Laboratory comparison study for the use of stone matrix asphalt in hot weather climates, *Constr. Build. Mater.* 20 (10) (2006) 982–989.
- [42] H.L. Von Quintus, J. Rauhut, T. Kennedy, Comparisons of asphalt concrete stiffness as measured by various testing techniques (with discussion), Association of Asphalt Paving Technologists Proceedings, (1982).